

STUDY OF ZERO-GRAVITY, VAPOR/LIQUID SEPARATORS

R. C. Mitchell, V. Hudson, J. A. Stark, and R. C. White
General Dynamics Convair

GPO PRICE \$ _____

CFSTI PRICE(S) \$ _____

GDC-DDB65-009

January 1966

Hard copy (HC) \$4.00

Microfiche (MF) 1.00

ff 653 July 65

Prepared Under

Contract NAS 8-20146

N66-22825

FACILITY FORM 602

(ACCESSION NUMBER)	(THRU)
<u>46 290</u>	<u>1</u>
(PAGES)	(CODE)
<u>CR-71624</u>	<u>28</u>
(NASA CR OR TMX OR AD NUMBER)	(CATEGORY)

GENERAL DYNAMICS
Convair Division

STUDY OF ZERO-GRAVITY, VAPOR/LIQUID SEPARATORS

R. C. Mitchell, V. Hudson, J. A. Stark, and R. C. White
General Dynamics Convair

GDC-DDB65-009

January 1966

Prepared Under

Contract NAS 8-20146

GENERAL DYNAMICS
Convair Division

FOREWORD

This report was prepared by General Dynamics Convair under contract NAS 8-20146, "Study of Zero-Gravity, Vapor/Liquid Separators" for the George C. Marshall Space Flight Center of the National Aeronautics and Space Administration. The work was administered under the technical direction of the Propulsion & Vehicle Engineering Laboratory, George C. Marshall Space Flight Center with Mr. C. D. Arnett (Mailing Symbol R-P&VE-PTF) acting as project manager.

In addition to the project leader, Dr. R. C. Mitchell, the following Convair personnel contributed to the study: Messrs. J. C. Ballinger, J. R. Burt, V. Hudson, J. S. Nuding, D. S. Oesterle, A. T. Parker, J. N. Sharmahd, J. A. Stark, J. W. Streetman, J. Sterrett, W. M. Tsunoda, R. C. White, and G. B. Wood.

SUMMARY

The need for venting cryogenic propellant storage tanks while coasting in space under zero or low acceleration became a real one in the late 1950's, when the development of advanced space vehicles capable of engine restarts was begun. It is desirable to vent vapor only, because venting of liquid propellant imposes a severe weight penalty on a vehicle. This is difficult, since a simple vent tube cannot be used under low acceleration conditions because the vapor/liquid distribution in the tank can shift easily with small disturbing forces.

This report presents the results of a study of various ways of separating vapor from liquid in a low-acceleration field in order to permit venting of vapor. Four primary methods of separation were studied:

- a. Heat Exchange — where the vent fluid is throttled to a low pressure and temperature and allowed to exchange heat with the tank fluid in order to vaporize any liquid initially present in the vent stream.
- b. Mechanical Separation — employing a rotating element imparting centrifugal forces to the fluid to separate the gas from the liquid.
- c. Dielectrophoresis — utilizing the forces caused by a non-uniform electric field acting upon a dielectric fluid, such as hydrogen. Both total liquid control and separator devices were considered.
- d. Surface Tension — utilizing fluid surface forces to orient the liquid in a tank, employing baffles or screens, or to effect a separation in a vent separator device.

Other separation methods including fluid rotation, a "hydrogen sublimator", and magnetic positioning were considered, but were not studied in detail or included in the predesign comparisons with the four methods listed above.

Predesign data were generated for separation systems employing heat exchange, mechanical separation, dielectrophoresis, and surface tension as applied to three vehicle/mission cases: 1) the S-IVB stage with continuous venting during a 4-1/2-hour coast, one engine restart, and retention of the existing settling rockets; 2) the S-IVB stage without constraints; and 3) a cryogenic service module (CSM) with a multiple-restart, 205-hour mission. These predesigns were compared using the criteria of payload weight penalty, system complexity, current feasibility, availability of design data, performance of system in 100-percent liquid, and estimated system failure rates. The comparisons were made for liquid hydrogen with tank pressure of 20 psia; maximum vent rate of 1260 lb/hr for the S-IVB and 1 lb/hr for the CSM; average vent rate of 667 lb/hr for the S-IVB and 0.5 lb/hr for the CSM; and design fluid inlet quality of 0.1 for the S-IVB and 0.00138 for the CSM. The

predesigns for Cases 1 and 2 were identical since it was concluded that retention of the settling rockets is desirable to prevent wetting of the forward dome, which would result in a considerable increase in external heat load. It was found that the dielectrophoretic and surface tension devices were consistently poorer than either the mechanical or heat exchange separator systems on all of the selection criteria. The latter two systems were competitive with each other on many of the criteria, but the heat exchange system was judged to be the most promising one for the three vehicle/mission cases considered in this study.

More detailed studies of the heat exchange type of system were then made, using the S-IVB hydrogen tank as a typical application. A conceptual feasibility design was developed (see Figure 11-1), incorporating the most nearly optimum design and operating features which were determined. Some of these features are summarized below:

- a. The "heat exchange system" consists of a flow regulator valve through which the incoming vent-side fluid is expanded to a lower temperature and pressure, a heat exchanger in which the cooled vent stream exchanges heat with the warmer tank fluid, and a turbine through which the vent stream leaving the exchanger is further expanded to supply power to drive the pump that circulates tank-side fluid through the exchanger and within the tank. After leaving the turbine the vent stream flows through a control valve sensing tank pressure and finally to small thrusters where it is used to supply settling thrust to the stage during coast periods.
- b. The heat exchanger is a compact, finned-surface, counterflow exchanger with a single pass on each of the vent and tank sides.
- c. There is a common location for the vent- and tank-side inlets.
- d. The vent stream exchanger exit temperature and pressure are 37° R and 6 psia, respectively.
- e. The system should be located in the forward dome region of the tank, and suspended from the existing manhole cover, if possible.

The designed system was sized for a tank pressure of 20 psia, maximum vent rate of 1260 lb/hr, and inlet fluid quality of zero (100-percent liquid). The total hardware weight of this system, including ducting and valves, is estimated to be 113 pounds. The weight of vented propellant required to maintain constant tank pressure during a 4-1/2-hour coast period would be about 28 pounds less than would be required if 20-psia saturated vapor were vented. Therefore, the net system effect would be a payload decrease of 66 pounds, referred to the idealized base case of venting saturated 20-psia vapor without a vent separator system.

Preliminary analysis of the system operation during start-up indicated that no loss of liquid should occur with the recommended design feature of providing a common inlet location for the hot and cold streams.

The results of parametric analyses are presented, showing the effects of variations in tank pressure, inlet fluid quality, overall system pressure drop, and vent flow rate upon system design or the performance of a fixed design.

A recommended test program is presented that would prove the workability of the selected heat exchange system and provide the information needed for final optimization and production design. The primary categories requiring further work before an optimum system can be fully developed are:

- a. Heat transfer and flow distribution data for hydrogen under low-acceleration conditions.
- b. Transient response and control characteristics of the system, particularly during start-up and sudden changes in inlet fluid quality.
- c. Tank mixing characteristics and requirements under low acceleration.
- d. Development and performance tests.

The testing requirements are primarily to provide the information needed for accurate design and to prove out the final design. There is no apparent reason to doubt that a successful heat exchange venting system can be developed. To verify the analysis, however, a sub-scale demonstration test is recommended as the logical next step.

TABLE OF CONTENTS

<u>Section</u>		<u>Page</u>
1	INTRODUCTION	1-1
2	HEAT EXCHANGER VENT SYSTEM	2-1
	2.1 State of the Art	2-1
	2.2 Predesign Data	2-3
	2.3 Conclusions	2-9
3	MECHANICAL VAPOR/LIQUID SEPARATORS	3-1
	3.1 State of the Art	3-1
	3.2 Predesign Data	3-5
	3.3 Conclusions	3-11
4	DIELECTROPHORETIC SYSTEMS	4-1
	4.1 Introduction	4-1
	4.2 Total Fluid Control	4-2
	4.3 Dielectrophoretic Liquid/Vapor Separators	4-8
	4.4 Failures in Dielectrophoretic Systems	4-17
5	VENTING BY MEANS OF SURFACE TENSION	5-1
	5.1 Introduction	5-1
	5.2 Venting by Means of Total Fluid Orientation	5-2
	5.3 Separators	5-4
6	OTHER SEPARATION METHODS	6-1
	6.1 Fluid Rotation	6-1
	6.2 Hydrogen Sublimator	6-3
	6.3 Magnetic Positioning	6-4
7	COMPARISON OF SEPARATORS	7-1
	7.1 Description of Vehicle/Mission Cases	7-1
	7.2 Selection Criteria and Their Evaluation	7-1
	7.3 Section of Most-Promising Separator	7-11
8	STUDY OF HYDROGEN HEAT TRANSFER DATA	8-1
	8.1 Survey of Existing Information	8-1
	8.2 Recommended Data	8-16
	8.3 Heat Exchanger System Sizing Procedures	8-21

TABLE OF CONTENTS, Contd

<u>Section</u>	<u>Page</u>
9	TRADE-OFF STUDIES FOR HEAT EXCHANGE VENT SYSTEM . . . 9-1
	9.1 Inlet Locations 9-1
	9.2 Available Thrust From Vented Hydrogen Gas 9-3
	9.3 Optimum System Operating Conditions 9-5
10	TRANSIENT BEHAVIOR OF HEAT EXCHANGE SYSTEM 10-1
	10.1 Turbine/Pump Acceleration 10-1
	10.2 Heat Exchanger Outlet Condition at Start-up 10-3
	10.3 Conclusions 10-10
11	CONCEPTUAL FEASIBILITY DESIGN OF HEAT EXCHANGE SYSTEM 11-1
	11.1 Description of Components 11-1
	11.2 System Hardware Weight 11-6
12	PARAMETRIC ANALYSIS AND OTHER VARIATIONS OF HEAT EXCHANGE SYSTEM 12-1
	12.1 Parametric Analysis 12-1
	12.2 Effect of Combining the Heat Exchanger and Mechanical Separator Systems 12-10
	12.3 Effect of Adding Partial Reliquefaction Cycle to Mechanical Separator 12-32
13	TEST PROGRAM FOR HEAT EXCHANGE SYSTEM 13-1
	13.1 Test Requirements 13-1
	13.2 Concept Feasibility Demonstration 13-2
	13.3 Exploratory and Component Tests 13-4
	13.4 Tank Mixing Tests 13-13
	13.5 Development and Performance Tests 13-15
	13.6 Test Sequence and Integration 13-18
14	CONCLUSIONS AND RECOMMENDATIONS 14-1
15	REFERENCES 15-1
<u>Appendix</u>	
A	HYDROGEN PROPERTIES A-1
B	HEAT EXCHANGER PREDESIGN CALCULATIONS B-1
	B.1 General Procedure B-1
	B.2 S-IVB Pre-design Calculations B-2
	B.3 Heat Exchanger Sizing, Cryogenic Service Module B-22

TABLE OF CONTENTS, Contd

<u>Appendix</u>	<u>Page</u>
C	MECHANICAL SEPARATOR PREDESIGN CALCULATIONS C-1
C.1	Separation Criteria C-1
C.2	Power Required to Separate C-6
C.3	Development of Predesign Data for the S-IVB Continuous Vent Case C-7
C.4	Cryogenic Service Module Predesign Calculations C-18
D	CALCULATION OF FRICTIONAL PRESSURE DROP FOR TWO- PHASE FLOW D-1
E	CALCULATION OF SEPARATION SYSTEM EFFECT ON PAYLOAD WEIGHT E-1
E.1	Vent Rate Required to Maintain Tank at Constant Pressure E-1
E.2	Method of Calculating Payload Weight Change E-3
F	TURBINE ANALYSIS F-1

LIST OF ILLUSTRATIONS

<u>Figure</u>	<u>Title</u>	<u>Page</u>
2-1	Heat Exchanger Vent System	2-2
2-2	Heat Exchanger Vent System Schematic, S-IVB Case	2-4
2-3	Heat Exchanger Core, S-IVB Case	2-5
2-4	Heat Exchanger Vent, Cryogenic Service Module	2-9
3-1	Convair and Janitrol Zero-g Separators	3-2
3-2	Mechanical Separator Flow Schematics	3-3
3-3	Electric-Motor-Driven Vapor/Liquid Separator	3-6
4-1	Cryogenic Service Module Hydrogen Tank	4-9
4-2	Weights of Electrodes and Electrode Supports for the S-IVB Hydrogen Tank, Total Fluid Control Concept	4-10
4-3	Electrostatic Field Separator, S-IVB Hydrogen Tank	4-12
4-4	Pressure Drop in Passages Versus Mass Flow Rate (Pure Vapor Flow), S-IVB Hydrogen Tank Dielectrophoretic Separator	4-14
4-5	Required Voltage Between Electrodes Versus Inlet Vapor Flow Rate Into Separator for Various Inlet Qualities (Faraday Gap = 0.01 ft), S-IVB Hydrogen Tank Dielectrophoretic Separator	4-15
4-6	Electrostatic Field Separator, Cryogenic Service Module Hydrogen and Oxygen Tanks	4-16
5-1	Schematic Diagram of Surface Tension Separator System	5-5
5-2	Summary of Surface Tension Separator Predesign for Mission/ Vehicle Cases I and II	5-9
5-3	Summary of Surface Tension Separator for Mission/Vehicle Case III	5-10
6-1	Vortex Tube Vapor/Liquid Separator Concept	6-1
6-2	Required Pump Input Power Versus Chamber Diameter for Vortex Tube Vapor/Liquid Separator	6-2
7-1	Vehicle and Mission Ground Rules Common to Both Cases I and II	7-2
7-2	Vehicle and Mission Ground Rules for Case III, Cryogenic Service Module	7-3

LIST OF ILLUSTRATIONS, Contd

<u>Figure</u>	<u>Title</u>	<u>Page</u>
8-1	Typical Pool Boiling Curve	8-3
8-2	Experimental Nucleate Pool Boiling of Hydrogen at ~1 Atmosphere Compared with the Predictive Correlation of Kutateladze	8-6
8-3	Comparison of Pool Boiling Correlations for Hydrogen at 0.8- Atmosphere Pressure	8-7
8-4	Forced Convection Boiling - Constant q/A	8-8
8-5	Forced Convection Boiling, Constant Tube Temperature	8-9
8-6	Procedures for Estimation of Heat Transfer With Forced- Convection Surface Boiling	8-10
8-7	Transition From Forced Convection to Boiling	8-12
8-8	Forced Convection Boiling Heat Transfer Correlation	8-13
8-9	Forced Convection Boiling Heat Transfer Data Selection	8-17
8-10	Multiplier for Adjusting 1-Atmosphere Kutateladze Correlation to Other Pressures	8-18
8-11	Single-Phase Heat Transfer and Friction Data	8-20
8-12	Heat Exchanger and System Flow Processes	8-22
8-13	Heat Transfer Surface Effectiveness Versus Film Coefficient	8-24
9-1	Theoretical Specific Impulse Versus Nozzle Pressure for Para-Hydrogen	9-4
9-2	Payload Loss Versus Heat Exchanger Outlet Temperature for Various Exchanger Design Conditions	9-7
9-3	Payload Decrease Versus Heat Exchanger Pressure for Two Values of Exchanger Hot-Side Mass Flux, G_H	9-9
9-4	Available and Required Turbine Output Power Versus Turbine Upstream Pressure	9-10
9-5	Payload Decrease Versus Vent-Side Exchanger Outlet Temper- ature for Set of Conditions Chosen From Trade-off Studies	9-11
10-1	Turbine/Pump Start-up Speed Versus Time From Rest	10-4
10-2	Heat Exchanger Specific Heat Versus Temperature	10-6
11-1	Heat Exchanger Vent System Feasibility Design	11-2

LIST OF ILLUSTRATIONS, Contd

<u>Figure</u>	<u>Title</u>	<u>Page</u>
11-2	Typical Heat Exchanger Construction	11-4
12-1	Effect of Tank Pressure Variation Upon Heat Exchanger Vent System	12-2
12-2	Effect of Inlet Fluid Quality Upon Performance of Fixed System Design	12-4
12-3	System Designs at Various Vent Exit Temperatures for 0.5 Inlet Quality to System	12-5
12-4	Optimum Design Vent Stream Exchanger Exit Temperature for Two Average Fluid Inlet Qualities During Operation	12-6
12-5	System Total Weight Penalty Versus Design Inlet Fluid Quality for Approximately Constant Pump Output Power of 0.25 Horsepower	12-8
12-6	Decrease in Payload Weight and Corresponding Exchanger Pressure Versus Vent System Pressure Drop Between Tank and Outlet of Turbine	12-9
12-7	Effect of Vent Rate on Vent System Weight	12-11
12-8	Required Exchanger Area Versus Exchanger Pressure	12-12
12-9	Required Exchanger Hot-Side Heat Transfer Area Versus Vent Stream Exchanger Exit Temperature for 100-Percent Liquid Inlet Fluid	12-13
12-10	Required Exchanger Area and Turbine Power for 8.5-psia Exchanger Pressure	12-14
12-11	Payload Decrease Versus Vent Stream Exchanger Exit Temperature for 8.5-psia Exchanger Pressure	12-15
12-12	Heat Exchanger Mechanical Separator Schematic	12-18
12-13	Separator-Pump-Turbine Combination	12-18
12-14	Performance of Turbine-Driven Combination Separator and Pump	12-21
12-15	Combination Mechanical Separator and Heat Exchanger	12-26
12-16	Hydrogen Partial-Reliquefaction Cycle	12-32
12-17	Available Payload Weight Decrease Versus Total Coast Time Comparison for Vapor/Liquid Separation and Separation Plus Partial Reliquefaction	12-35

LIST OF ILLUSTRATIONS, Contd

<u>Figure</u>	<u>Title</u>	<u>Page</u>
13-1	Concept Feasibility Test Schematic	13-5
13-2	Heat Exchanger Test	13-7
13-3	Heat Exchange Test Measurements and Layout	13-8
13-4	Flow Distribution Tests	13-10
13-5	Expected Typical Gravity Dependence	13-12
13-6	Pump and Header Test	13-17
A-1	Density Versus Temperature of Liquid Para-Hydrogen and Saturated Equilibrium Hydrogen Vapor	A-1
A-2	Vapor Pressure and Latent Heat of Vaporization Versus Temperature for Para-Hydrogen	A-2
A-3	Heat Capacity of Hydrogen Liquid and Vapor Versus Temperature	A-3
A-4	Prandtl Number and Viscosity of Saturated Gaseous Hydrogen	A-4
A-5	Viscosity of Liquid Hydrogen Versus Temperature	A-5
A-6	Thermal Conductivity of Liquid Para-Hydrogen or Normal Hydrogen Versus Temperature	A-6
A-7	Thermal Conductivity of Gaseous Para-Hydrogen Versus Temperature	A-7
B-1	Turbine-Pump Performance for S-IVB Heat Exchanger System Predesign	B-3
B-2	Density Versus Pressure for Constant Enthalpy Flashing Flow Across a Restriction	B-18
B-3	Integrated $\Delta p\rho$ for Constant Enthalpy Flashing Flow Across a Restriction	B-19
C-1	Reynolds Number Versus Gas Velocity for Various Liquid Drop Diameters	C-4
C-2	Inlet Gas Velocity Versus Separated-Drop Diameter as a Function of Separator Speed and Radius	C-5
C-3	Required Separator Speed Versus Separated-Drop Diameter for Various Wheel Radii	C-8
C-4	Inlet Gas Velocity Versus Separator Diameter and Flow Area for Vent Gas Flow Rates of 0.35 lb/sec and 0.06 lb/sec	C-9

LIST OF ILLUSTRATIONS, Contd

<u>Figure</u>	<u>Title</u>	<u>Page</u>
C-5	Required Separator Horsepower Versus Separator Speed for Various Wheel Radii · · · · ·	C-10
C-6	Motor Operating Characteristics · · · · ·	C-12
C-7	Turbine-Driven Separator Performance Curves · · · · ·	C-16
C-8	Turbine Performance Curve · · · · ·	C-17
D-1	Φ_{Ltt} and Φ_{Vtt} Versus $\sqrt{\chi_{tt}}$ · · · · ·	D-3
F-1	Impulse Stage Velocity Diagram · · · · ·	F-1
F-2	Turbine Bucket Velocity Loss Parameter · · · · ·	F-3

LIST OF TABLES

<u>Table</u>	<u>Title</u>	<u>Page</u>
2-1	Heat Exchanger Predesign Data Summary, S-IVB Case	2-6
2-2	Heat Exchanger Predesign Data, Cryogenic Service Module LH ₂ Tank	2-10
3-1	Mechanical Vapor/Liquid Separator (Electric-Motor Driven)	3-7
3-2	Mechanical Vapor/Liquid Separator (Turbine Driven)	3-7
3-3	Operating and Failure Mode Characteristics, S-IVB Motor- Driven Unit	3-9
3-4	Mechanical Vapor/Liquid Separator (Electric-Motor Driven)	3-10
3-5	Mechanical Vapor/Liquid Separator (Electric-Motor Driven)	3-10
7-1	Case I and II Hydrogen Separation Systems Weight Summary	7-5
7-2	Case III Hydrogen Separation Systems Weight Summary	7-6
7-3	Case I and II Component Failure Rates and System Failures Per Mission	7-7
7-4	Case III Component Failure Rates and System Failures Per Mission	7-8
7-5	Comparison of Zero-g, Vapor/Liquid Hydrogen Separation Systems for Cases I and II (S-IVB)	7-9
7-6	Comparison of Zero-g, Vapor/Liquid Hydrogen Separation Systems for Case III (CSM)	7-10
11-1	Summary of Design Information and Conditions for Heat Exchange Feasibility Design	11-3
11-2	Summary of Component Weight Estimates for Conceptual Feasibility Design System	11-7
12-1	Weight Summary -- Heat Exchanger, Mechanical Separator, and Combinations of Both	12-16
12-2	Comparison Data - Effect of Partial Reliquefaction of H ₂ Vent Gas	12-34
E-1	Exchange Ratios	E-4

NOMENCLATURE

a	acceleration
A	area; A_c free flow area; A_D , projected area subject to drag force; A_f , fin area; A_s , heat transfer surface area; A_{fr} , heat exchanger total flow area
AF	area fraction
B	flow stream heat capacity rate = $\dot{W} C_P$
c_s	velocity of sound
C	capacitance
C_D	drag coefficient = $\frac{8 F_D}{\pi \rho_L D_B^2 u_B^2}$ (spherical bubble)
C_P	heat capacity at constant pressure
C_S	heat capacity of saturated vapor at saturation temperature and pressure
C_v	loss coefficient for flow restriction
D	diameter; D_L , droplet diameter
E	electrical voltage
E_x	heat exchanger effectiveness
f	fanning friction factor $\equiv \frac{(\text{head loss}) D g_c}{2 L u^2}$
F	force (or thrust)
G	mass velocity per unit flow area
g_c	gravitational conversion factor to maintain dimensional equivalence in Newton's law: $F = ma/g_c$ when F is expressed in lbf, m in lbm, and a in ft/sec ² ; equal to 32.174 lbm-ft/lbf-sec ² .

g_o	"standard" gravitational acceleration = 32.174 ft/sec^2
h	specific enthalpy (enthalpy per unit weight)
h_f	heat transfer film coefficient; h_c , coefficient for cold-side film; h_{fc} , coefficient for forced convection
h_s	change in enthalpy for isentropic expansion
H	fluid head
i	electrical current
I	moment of inertia
I_{sp}	specific impulse; I_{spv} = specific impulse in vacuum
J	dimensionless parameter = $(h/GC_P)(N_{PR})^{2/3}$
k	thermal conductivity
K	dielectric constant in Section 4; porous material permeability in Section 5.
L	length
m	mass
\dot{m}	mass flow rate
M	Mach number
MW	molecular weight
n	number
n_s	specific speed
N	rotational speed in revolutions per unit time

N_B	Bond number = $\frac{(\rho_L - \rho_V) a r^2}{\sigma}$
N_{NU}	Nusselt number = $\frac{hL}{k}$, where L is a characteristic length
N_{PR}	Prandtl number = $\frac{C_P \mu}{k}$
N_{ST}	Stanton number = $\frac{h}{C_P u \rho}$
p	absolute pressure
P	power
q	heat flow rate (e. g., Btu/hr)
Q	volumetric flow rate
r	radius or radius of curvature
R	universal gas constant = 1.987 Btu/hr-mole-°R = 1544. ft-lbf/lb-mole-°R
Re	Reynolds number $\equiv \frac{uD\rho}{\mu} = \frac{DG}{\mu}$
\bar{R}_H	hydraulic radius = $\frac{\text{cross-sectional flow area}}{\text{wetted perimeter}}$
s	specific entropy (entropy per unit weight)
S	entropy
S_s	shear stress
t	time
T	absolute temperature
T_{fl}	fluid temperature

T_s	temperature of saturated fluid
T_w	wall temperature
u	velocity; u_b , turbine bucket tip velocity; u_o turbine nozzle velocity
U	overall heat transfer coefficient; U_u or U_c overall coefficient based upon hot or cold-side area
U_x	internal energy
v	specific volume
V	volume
VF	volume fraction
W	weight
W_H	weight of vent system hardware
W_{PL}	available payload weight
W_V	weight of vented propellant
\dot{W}	weight flow rate
x	distance, defined as used
X	quality \equiv weight fraction of vapor in vapor/liquid mixture
Y	volume fraction of vapor in vapor/liquid mixture
<u>Greek</u>	
α	angular acceleration
β	angle
β_E	ratio of total heat transfer area on one side of plate-fin exchanger to the free volume between the plates on that side.

f	film
F	fin
H	hot side
i	in or inside
L	liquid
m	mean
o	original, outside, out
sg	saturated gas
T	total
t	turbine
u	upstream
v	vent or valve
V	vapor
Ω	out or outside

Superscripts

—	average
---	---------

γ	isentropic exponent $\equiv \left(\frac{\partial p}{\partial \rho} \right)_s$
ϵ	dielectric permeability; ϵ_0 = dielectric permeability of pure vacuum = 8.85×10^{-12} farads/meter
η	efficiency
η_0	heat exchanger surface effectiveness
θ	angle
λ	heat of vaporization
μ	viscosity
ξ	pressure loss coefficient
ρ	density
σ	surface tension
σ_x	ratio of free flow area to total frontal area
τ	torque
ψ	turbine velocity ratio
ω	angular velocity

Subscripts

b	turbine bucket
B	bubble
c	cold side
C	centrifugal
d	downstream
D	drag
e	exchanger

SECTION 1

INTRODUCTION

The need for venting cryogenic propellant storage tanks while coasting in space under zero or low acceleration became a real one in the late 1950's, when advanced space vehicles capable of engine restarts began to be developed.

A cryogenic propellant tank in space absorbs heat, thereby vaporizing some of the already-saturated liquid and tending to increase the tank pressure. The rate of heat addition and, therefore, tank pressure rise can be decreased by insulating the tank, but even with very heavy thermal protection systems some energy will be transmitted to the propellant. The storage tank must either be strong enough to withstand the resulting pressure rise, or some means must be provided to relieve the tank pressure. The only method of relieving tank pressure employed in practice has been venting of propellant, hopefully vapor only.

Venting can be very simply accomplished on the earth's surface because the liquid and vapor always occupy known positions within the tank and a simple vent pipe can be employed. This is not practical under low-gravity conditions because the vapor/liquid distribution in the tank can shift easily with small disturbing forces. Swalley, et al (Reference 1-1), discuss a number of sources of such disturbing forces.

- a. Sloshing induced during the ascent flight could be one of the major sources of energy in the propellant at injection into orbit.
- b. During ground hold and ascent, environmental heating will cause thermal convective patterns to form in the liquid, with the hot fluid rising to the top of the liquid due to buoyancy forces and spreading across the surface. If the acceleration is suddenly reduced, as at injection, it is believed that the liquid streamlines will continue vertically instead of continuing to bend over at the liquid surface.
- c. Termination of propellant draining from the tank could cause disturbances associated with valve closure or change in direction of fluid momentum near the tank outlet.
- d. The tank sidewalls and lower bulkheads will be deflected during boost flight. At injection into orbit the structure will try to return to its undeflected position and, in the process, transmit some of its stored energy to the liquid.
- e. Although liquids have low compressibilities, the amount of energy stored in the hydrogen because of the hydrostatic head may have a significant effect on the propellant behavior at injection.

- f. During orbital coast several other types of disturbances may contribute to fluid motion, such as: aerodynamic drag, gravity gradient, solar pressure, attitude control operation, or crew movements.

Settling rockets have been used in current venting applications, but have two undesirable features: they affect vehicle guidance and control, and are excessively heavy for very high acceleration levels or coast times. It is important, therefore, to study ways of separating vapor from a two-phase mixture of cryogenic propellant in order to insure venting of vapor only.

This study has considered a number of possible separation systems including ones employing heat exchange, mechanical separation, dielectrophoresis, surface tension, and liquid or tank rotation. Three vehicle/mission cases (see pp. 7-2 and 7-3) were used as typical applications of the previous separation methods: Case I was the S-IVB stage with continuous venting during a 4 1/2-hour coast, one engine restart, and retention of the existing settling rockets; Case II was the S-IVB stage without constraints; and Case III was a cryogenic service module with a multiple-restart, 205-hour mission. Information was gathered and analyses made to generate predesigned separator systems representative of each of the separation phenomena, and the information is summarized in Sections 2 through 6 of this report. The predesign separator systems for hydrogen were compared, as discussed in Section 7, and the heat exchange venting system selected as the most promising one for the three vehicle/mission cases used here. The remainder of the report is devoted primarily to more detailed work related to the heat exchange venting system.

Section 8 summarizes the results of a comprehensive survey of existing hydrogen heat transfer data, gives recommended data that were used in all heat transfer calculations given in subsequent sections, and outlines the heat exchanger sizing procedure used in the trade-off studies, parametric analyses, and design work.

A number of trade-off studies are discussed in Section 9. They are not intended to represent a complete optimization of a heat exchange system, but to give a basis for decisions about system components and desirable operating conditions. One of the choices made was to recommend a turbine-driven pump rather than one with an electric motor drive. Therefore, because of the possible start-up questions about such a "boot-strap" system, the preliminary transient analysis of Section 10 was made, resulting in the conclusion that the vent-side and tank-side inlet streams should be common to avoid the most adverse combination of inlet qualities (i. e. , liquid on the vent side and vapor on the tank side). With this provision, however, it was predicted that there would be no problems with start-up.

Section 11 shows the results of a conceptual feasibility design system for the S-IVB hydrogen tank. Its variations in performance with changes in operating conditions are shown in Section 12. Also in Section 12 are parametric results for variations in design conditions, a comparison of combination heat-exchange/mechanical-separator vent systems with the separate heat exchange or mechanical separator systems, and a comparison of combination partial reliquefaction/mechanical-separator and vent systems with a mechanical separator system alone.

Finally, Section 13 outlines a test program that would demonstrate the workability of the recommended type of venting system and generate the information needed for final system optimization and design.

SECTION 2

HEAT EXCHANGER VENT SYSTEM

2.1 STATE OF THE ART. The heat exchanger system is designed to operate with either gas or liquid and is therefore independent of the local fluid quality. Basically, the vent fluid is throttled to a low pressure and temperature and allowed to exchange heat with the tank fluid before being vented overboard. Assuming a sufficient amount of heat transfer to evaporate all of the liquid originally present in the vent fluid and sufficient heat transfer on the tank side to condense the equivalent quantity of gas, the net effect on the tank pressure is the same as for all-gas venting. A schematic and a T-S diagram of the basic concept are shown in Figure 2-1.

There have been a number of reports published covering analysis and testing of the basic system concept. The steady-state performance of the system has been demonstrated under 1-g using Freon-12 (Reference 2-1) and hydrogen (References 2-2 and 2-3); the hydrogen flow rates ranged from 0.07 lb/hr to 6.4 lb/hr. The testing performed at Beech Aircraft (Reference 2-3) included cycling of the system heat exchanger inlet from gas to liquid and vice versa. Only gas was observed at the heat exchanger outlet; however, it was felt that due to the location of the liquid detection devices a true indication of whether or not liquid occurred at the exit was not obtained. The testing did point out the need for highly refined techniques when using LH₂ since the very low temperatures involve high possibility of extraneous heat leakage.

This testing was performed using fixed throttling valves sized for gas or liquid with heat transfer on the tank side by natural convection. In actual low-g operation, a single valve is desirable for controlling the throttling process when the inlet can be alternately gas and/or liquid. If a fixed throttling device were used, the flow rate when operating with liquid inlet would be approximately seven times that with a gas inlet, and since the valve would need to be sized for the gas case and the heat exchanger for the liquid case, the heat exchanger would need to be large enough to evaporate approximately seven times the nominal rate required. Both Air Research (Reference 2-4) and Beech (Reference 2-3) have proposed the use of a pressure regulator to control the pressure in the heat exchanger and provide for throttling of the vent fluid. If the heat exchanger were designed for low pressure drop and a fairly high outlet temperature then fluid conditions out of the heat exchanger would be fairly constant, regardless of the condition of the inlet fluid, and flow control could be accurately maintained downstream of the heat exchanger by a valve sensing tank pressure.

Recently, testing has been accomplished at Convair, under a company-funded program, on a system using a downstream-pressure-regulator as a throttling valve with a fixed restriction downstream of the heat exchanger (Reference 2-5). The test fluid was Freon-12. The system inlet was cycled from gas to liquid and vice versa with no observable transient loss of liquid, even with the system adjusted for essentially saturated

gas outflow (no superheat) at stabilized conditions. The vent flow rate remained essentially constant for a constant tank heating rate regardless of the inlet fluid condition (gas or liquid) during cycling. A standard regulating valve was used for the tests. It was concluded that no serious problems need be expected in a flight system with respect to this component.

A further consideration for system operation at low-g is the heat transfer requirement on the tank side. For the g levels and vent rates normally involved, it is estimated that relying on natural convection heat transfer will require very large heat exchangers. It has been proposed to increase the tank-side heat transfer by using a turbine-driven pump to circulate tank-side fluid through a plate-fin type of exchanger, using the vent gas from the exchanger outlet to drive the turbine (Reference 2-4).

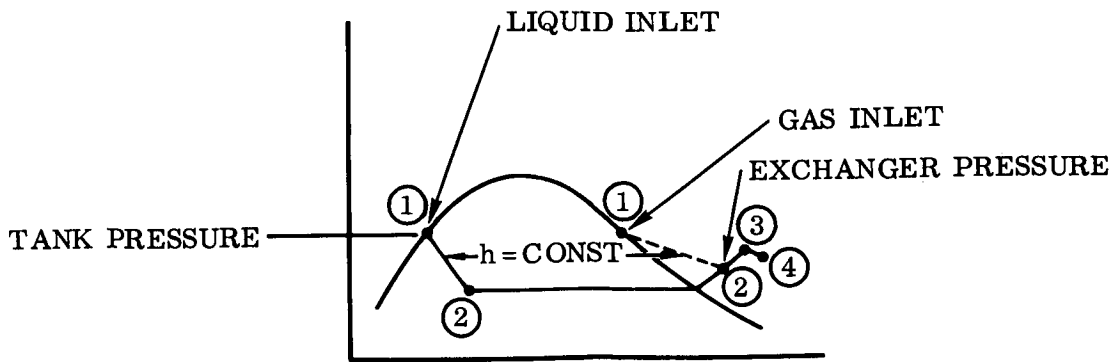
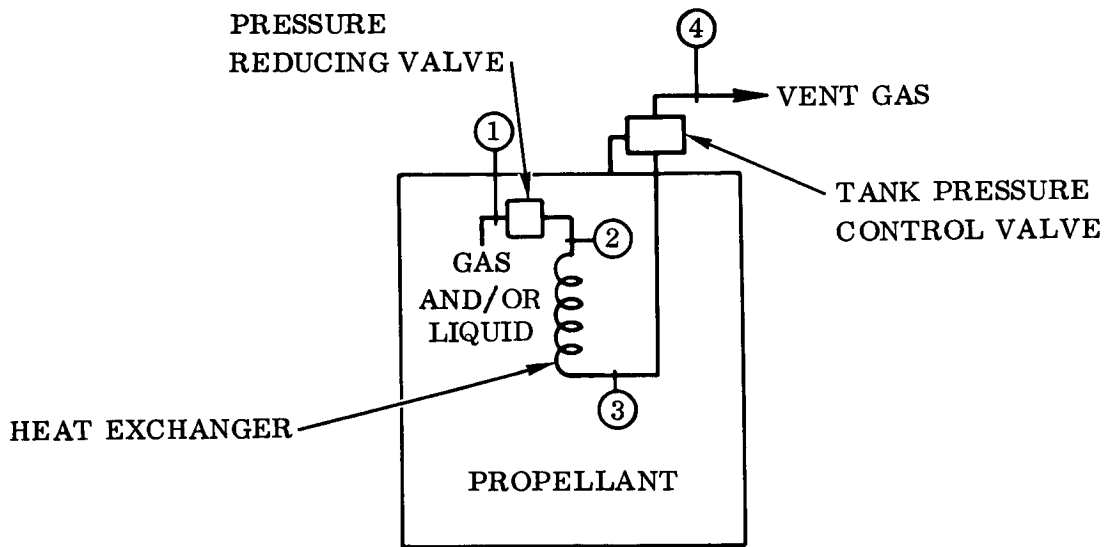


Figure 2-1. Heat Exchanger Vent System

Conclusions on the present state of the art are that

- a. The feasibility of the basic heat exchanger vent system concept has been demonstrated.
- b. Operation of the system with hydrogen at low-g needs further evaluation with respect to heat transfer and system transients resulting from venting initiation with liquid hydrogen at the inlet or sudden changes in the vent inlet quality, when a vent-gas-driven turbine is employed for fluid circulation.

2.2 PREDESIGN DATA. During the course of the overall study several heat exchanger concepts were considered; each iteration included a higher level of refinement. The data presented in this section represent the initial analysis that was developed for comparison purposes only. Subsequent sections refine the results given.

From a review of the available literature and the requirements of the S-IVB and Cryogenic Service Module a system model consisting of the following components was chosen for the present analysis.

- a. Heat exchanger.
- b. Circulating pump to circulate sufficient tank fluid over the heat exchanger to provide the necessary heat transfer.
- c. Pump drive, which can be a turbine using the vent gas or an auxiliary power source such as an electric motor.
- d. Throttling regulator to reduce the vent fluid pressure and temperature and provide a fairly constant pressure in the heat exchanger for gas and/or liquid inlet conditions.
- e. Tank pressure control valve, which can be an on/off relief device sensing tank pressure or a continuous regulating vent device sensing tank pressure.

Predesign data and a discussion of the analysis are presented in the following paragraphs for the three basic vehicle cases described in Paragraph 7.1.

2.2.1 Case I (S-IVB, Continuous Vent). The system schematic is shown in Figure 2-2. The heat exchanger core is described in Figure 2-3. Weight and performance data of the predesigned system used in the comparisons of Section 7 are presented in Table 2-1.

In the analysis it is assumed that the heat exchanger is mounted in the ullage space in such a manner as to prevent additional wetting of the forward dome. Ullage fluid is taken into the hot side of the exchanger and discharged toward the liquid surface.

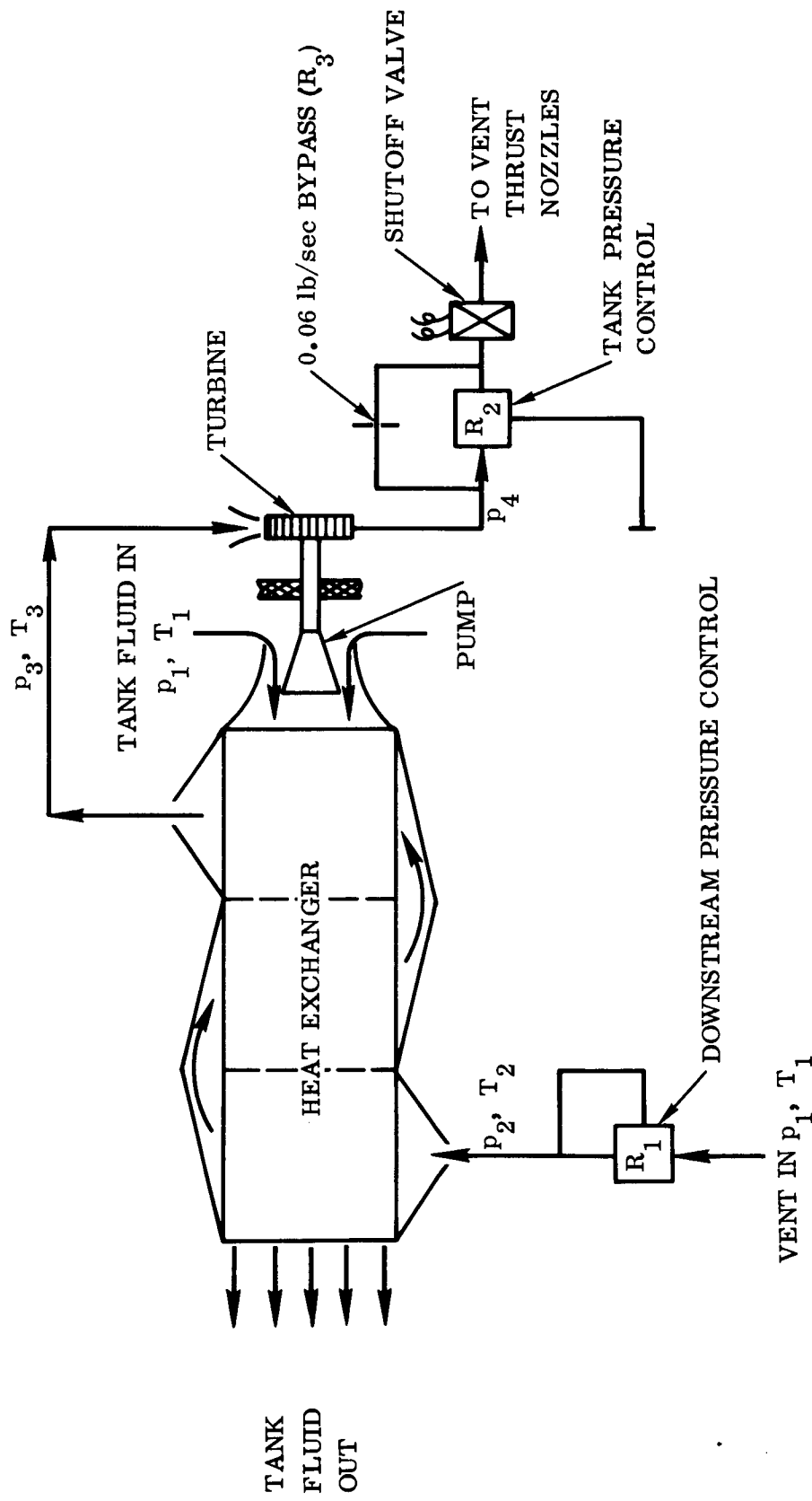


Figure 2-2. Heat Exchanger Vent System Schematic, S-IVB Case

14 CHANNELS HOT SIDE
 13 CHANNELS COLD SIDE
 3 PASSES ON COLD SIDE
 17.8-3/8W WAVY FIN
 SURFACES BOTH SIDES
 PER TABLE 9-3 OF
 REFERENCE 2-6

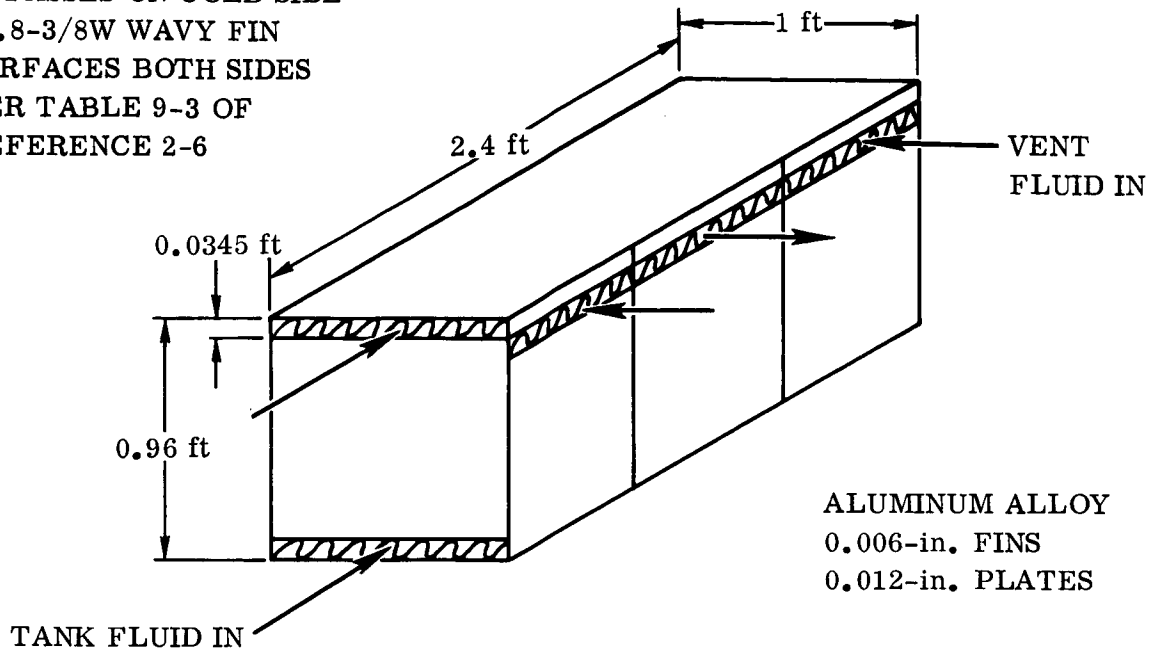


Figure 2-3. Heat Exchanger Core, S-IVB Case

The exchanger is assumed to be of the "compact" plate-fin type, and the sizing and performance analysis is based on the methods outlined in Reference 2-6. A high-efficiency fin surface is desired, and a wavy type with 17.8 fins per inch and other fin characteristics given in Table 9-3 of Reference 2-6 is assumed. The wavy fins have high efficiency and are fairly easy to fabricate.

A rough estimate was made of the use of a coiled-tube heat exchanger without positive mixing, assuming natural convection heat transfer at $2 \times 10^{-5}g$. Although such a system would be quite simple as compared with one including a pump and turbine, its estimated weight was approximately 1600 pounds; therefore, it was not considered further in this study.

It is recognized that the heat exchange surface and configuration chosen for this initial phase of the study are not necessarily optimum. In addition to variations in surface geometry there are many factors that affect the final heat exchanger size. For example, there is a trade-off between heat exchanger size and the tank fluid circulation (pump power) and the amount of superheat of the vent fluid. Also, lower heat exchanger pressures give higher heat transfer efficiency, in that there is an increased temperature potential across the exchanger. An attempt was not made in this section to completely optimize the heat exchange system and the data presented are for a representa-

Table 2-1. Heat Exchanger Predesign Data Summary, S-IVB Case

COMPONENT	DESCRIPTION	WEIGHT (lb)
Heat Exchanger	Plate-Fin Type	80
Pump	Nominal 6-in. Diameter, 12000 rpm @ 5000 lb/hr Saturated GH ₂ @ 20 psia $\Delta p = 34.6 \text{ lb/ft}^2$	9
Turbine	Nominal 6-in. Diameter Impulse - Subsonic Flow 12000 rpm, bhp = 1.3 hp @ 0.35 lb/sec Flow	6
Throttling Pressure Regulator	5-psia Outlet with 20-psia Inlet, Operation with GH ₂ and/or LH ₂ , 2 in.	6
Tank - Pressure Regulator	6-in. Diameter	12
Shutoff Valve	Electrically Operated	4
Total Fixed Weight		117 lb

System Performance

Subscripts refer to stations shown in Figure 2-2.

$$\begin{aligned}
 p_1 &= 20 \text{ psia} & T_1 &= 38.5^\circ\text{R} \\
 p_2 &= 5 \text{ psia} & T_2 &= 31^\circ\text{R}
 \end{aligned}$$

VENT SIDE					TANK SIDE				
Inlet Fluid Condition	Flow Rate (lb/hr)	p_3 psia	T_3 °R	p_4 psia	Inlet Fluid Condition	Flow Rate (lb/hr)	Δp psi	Pump- Turbine (bhp)	* $\Delta \dot{W}$ Vent (lb/hr)
Saturated LH ₂	1,260	4.9	34.1	4	Saturated GH ₂	5,000	0.24	1.3	+37.3
Saturated LH ₂	1,260	4.9	36.3	4	Saturated LH ₂	46,000	0.6	0.7	- 7.2
Saturated LH ₂	216	≈ 5	≈ 38.5	≈ 4.95	Saturated GH ₂	725	0.009	0.0068	- 8.5

*Refers to additional (+) or reduced (-) vent flow required to account for vent conditions different from saturated gas at 20 psia.

tive system suitable for predesign comparisons. The effect of variations of the major system parameters are presented in subsequent paragraphs.

Since tank-side pressure drop does directly affect the required circulating pump power, the heat exchanger design was restricted to a single pass on the tank (hot) side. A complete summary of the basic assumptions made in the present analysis is given below.

Heat Exchanger Assumptions

- a. Sizing is based on a vent flow of 1260 lb/hr with saturated LH_2 at 20 psia at the inlet to the throttling valve, and the outlet of the exchanger at 5 psia and $4 \pm 1^\circ \text{F}$ superheat. This amount of superheat at 5 psia gives a vent enthalpy comparable to that of saturated gas at 20-psia tank pressure, and allows efficient turbine operation. Also, heat exchanger pressure of 5 psia with an estimated turbine pressure drop of 1 psia gives a reasonable pressure available for the vent thrust nozzles.
- b. For sizing purposes, the tank (hot) side fluid is assumed to be saturated GH_2 at 20 psia.
- c. For saturated gas on the hot side, the heat transfer coefficient is based on an assumption of all-gas flow at constant saturation temperature of 38.4°R . The amount of gas condensed is determined and a minimum gas velocity maintained sufficient to prevent a buildup of liquid condensate on the heat transfer surface.
- d. The vent-side heat transfer coefficient in the boiling region is taken as the sum of that calculated for liquid forced convection (assuming all fluid is liquid) and that determined from pool boiling data are taken from Figure 9 of Reference 2-8.
- e. All forced-convection heat transfer coefficients for both gas and liquid are determined from Figure 8-11, which represents a replot and extrapolation of the data of Figure 10-67 of Reference 2-6.
- f. The vent-side pressure drop through the exchanger is maintained at 0.1 psi maximum.
- g. Based on standard heat exchanger design practice the total heat exchanger weight, including headers and mounting provisions, is taken as 1.43 times the basic core weight.
- h. The fins are 0.006-inch soft aluminum alloy. The plates are 0.012-inch hard aluminum alloy.
- i. The heat transfer surface effectiveness, η_o , is determined from Equation 2-3 of Reference 2-6. Values of η_o are plotted as a function of h_f in Paragraph 8.3, Figure 8-13.

Circulating Pump Assumptions

- a. The pump efficiency at the design point, including bearing and seal losses, is 60 percent.
- b. The pump is an axial-flow type with vanes similar to the inducer of the Centaur boost pump, allowing operation in saturated hydrogen.
- c. To determine the pump load variation from design with changes in speed and operating fluid, it is assumed that 10 percent of the total pump power at the design point is consumed by bearings and seals, and that this portion is independent of the operating fluid and proportional to the square of the speed. The remaining 90 percent of the pump power is proportional to fluid density at constant speed and proportional to the cube of the speed at constant density. These assumptions can be derived from standard pump laws where a fixed downstream restriction exists (Reference 2-9).

Turbine Assumptions

- a. The vent-gas-driven turbine is a full-admission, impulse, single-stage type.
- b. The efficiency versus the bucket-velocity/nozzle-velocity ratio is the same as assumed for the mechanical separator turbine case and is shown in Figure C-8.

For use in the comparisons of Section 7, nominal operation of the system is assumed to be with the same fluid conditions at the vent inlet as at the hot-side inlet. For this condition the worst operating case will be with 100-percent liquid at the inlets, for which the resulting average vent rate is 7 lb/hr less than the base case of 20-psia saturated vapor vent. (See Table 2-1.)

The detailed analysis is presented in Appendix B.

2.2.2 Case II (S-IVB). Indications are that a significant increase in the amount of heat transferred to the tank will occur if the forward dome is wetted. Also, the venting of a superheated gas from the ullage results in high vent efficiency (low vent-rate-to-tank-heating-rate ratio). Therefore, it appears advantageous to use vent-gas settling rockets in this case, and the same data have been used for the Case II heat exchange system as were used for Case I. (See Table 2-1.) To justify the wetting of the forward dome by complete circulation of the tank fluid, which would likely occur with the heat exchanger system operating without settling rockets, it would be necessary to know more closely the actual conditions provided by the settling rockets and the effect on heat transfer.

2.2.3 Case III (Cryogenic Service Module). Here no settling forces of significance are assumed available from the vent gas, since the vent rates are extremely low. It is assumed that for effective operation of the heat exchanger system the tank fluid con-

tents must be mixed and significant accumulation of hot fluid prevented from causing inefficient system operation and/or tank overpressure.

For comparison purposes, the same fluid velocities and mixing energies are assumed as were determined for the mixing portion of the mechanical separator (Paragraph C.4). This assumption results in an external power requirement to the mixer motor of 1.34×10^{-3} horsepower, with an increase in required vent rate of 0.018 lb/hr.

The heat exchanger is a coil of tubing as shown in Figure 2-4, with an average fluid velocity on the outside of 0.1 fps and a vent flow rate of 1 lb/hr. The system weight data are given in Table 2-2. An electric motor is used to drive the mixer. It is theoretically possible to use the vent-gas flow to drive the mixer; however, the flow rates are very low and the practical equipment limitations relatively unexplored. Therefore, the use of a vent-gas-driven turbine was not considered for the initial system comparisons.

Detailed sizing and performance calculations are presented in Appendix B.

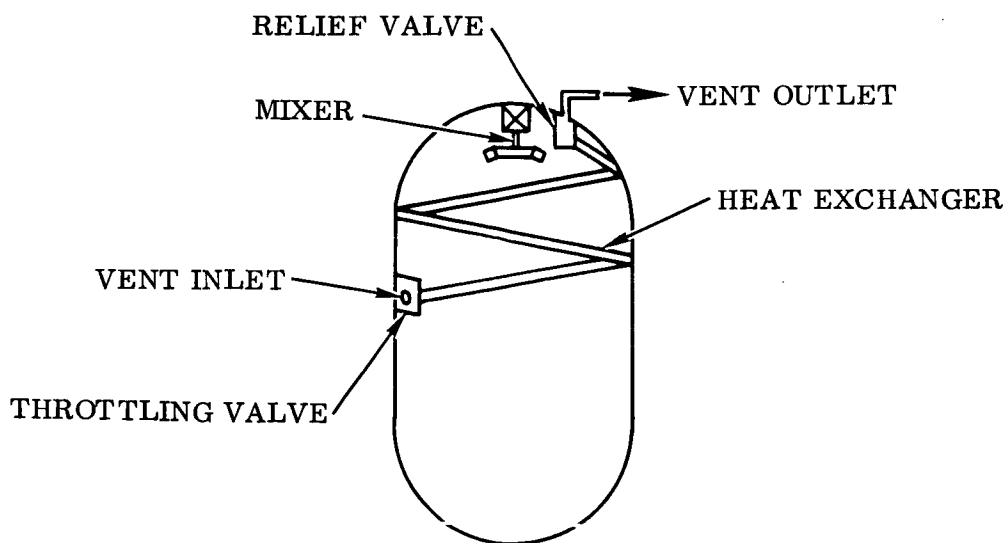


Figure 2-4. Heat Exchanger Vent, Cryogenic Service Module

2.3 CONCLUSIONS. The following conclusions are drawn from the data generated.

- a. System performance during transient operation is a major unknown in the present analysis. At initiation of the vent cycle there is essentially no hot-side fluid flow and relatively low heat transfer to the initial vent fluid. As venting progresses the turbine-pump will increase the hot-side flow and the system will "bootstrap" to steady-state operation. For the vent inlet submerged in liquid, it is possible that some liquid will be lost during start-up. The heat sink of the exchanger will tend to vaporize some of the initial liquid; however, the heat capacity of the aluminum

at LH₂ temperatures can be quite low. This start-up condition is analyzed in Section 10 for the final S-IVB heat exchanger design.

Also, the overall response of the regulators, heat exchanger, and turbine-pump will be important in determining overshooting and/or undershooting of the tank pressure during normal operations and under conditions of phase changes of the hot- or cold-side fluids.

Further analysis should be done in the controls area, perhaps including an analog simulation. Final answers, however, can only be obtained from testing. Many of the answers could be obtained from testing at 1-g using Freon-type fluids for initial response tests, and finally hydrogen in a complete system test.

- b. Another unknown in the analysis is a complete knowledge of boiling and condensing heat transfer coefficients for hydrogen under low-g conditions. Boiling heat transfer data do exist; however, there is a fairly wide spread in the data. The data do appear to show that acceleration level does not significantly affect the boiling heat transfer. Condensing heat transfer data at low-g are completely lacking. It should be noted that a more accurate knowledge of the heat transfer coefficients would allow a more accurate optimization of the system. However, it is felt that by making conservative assumptions the present knowledge is sufficient to design a unit that will work.

Table 2-2. Heat Exchanger Predesign Data, Cryogenic Service Module LH₂ Tank

COMPONENT	DESCRIPTION	WEIGHT (lb)
Heat Exchanger	1/2 in. × 70 ft × 0.02-in. Wall Al Alloy Tubing	3.7
Electric Motor	2.68 × 10 ⁻⁴ hp Output @ 12,000 rpm 1.34 × 10 ⁻³ hp Input	1
Mixer	- - -	1.5
Throttling Regulator	1/4-in. Port Size	1.5
Relief Valve	1/4-in. Port Size, Positive Shutoff	1.3
Power Supply	Apollo Fuel Cell	0.4
Total Fixed Weight		9.4 lb

Δ vent rate due to external power into the tank from the electric motor is 0.018 lb/hr.

SECTION 3

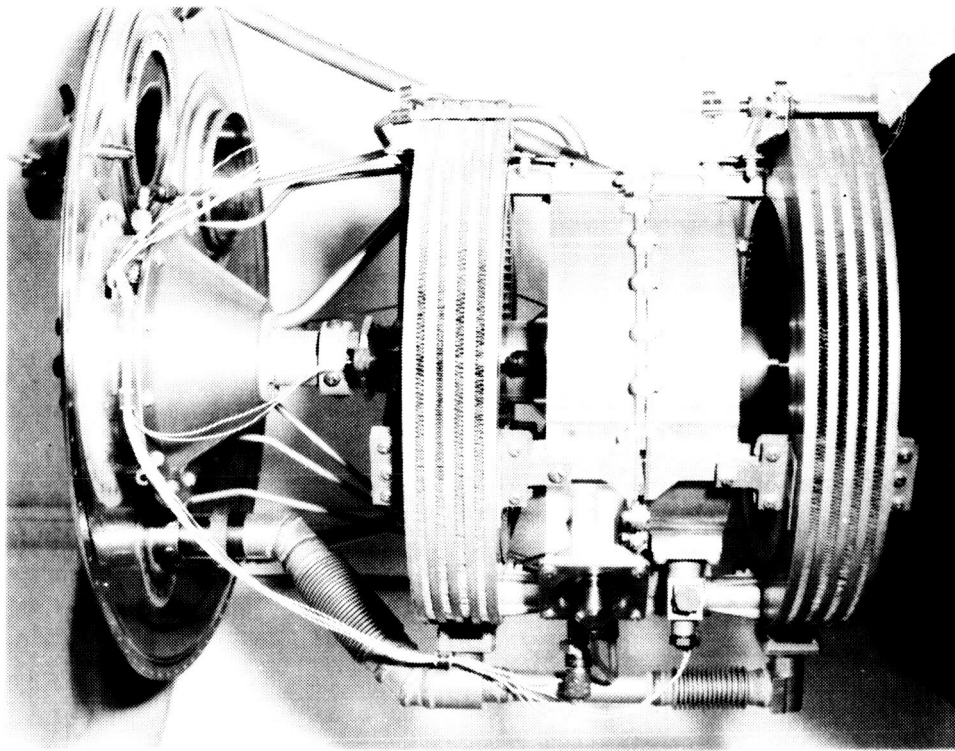
MECHANICAL VAPOR/LIQUID SEPARATORS

3.1 STATE OF THE ART. The mechanical or dynamic method of vapor/liquid separation relies on the difference in density of the vapor and the liquid to promote separation. The mechanical devices considered here employ a rotating separator to create an artificial g field such that centrifugal forces separate the liquid from the gas, and the gas is then vented overboard. Such devices have been designed, built, and tested. Current designs are for use with LH₂ although similar units could be designed for use with LO₂. Testing has been accomplished using air/water, GN₂/LN₂, and GH₂/LH₂ as the test mediums. Testing to date has been primarily under 1-g conditions. Some qualitative data have been obtained from aircraft zero-g testing. A major lack of knowledge exists with respect to the performance of units completely submerged and operating in LH₂. Separator units have been built by General Dynamics Convair, Janitrol, and Pesco. A discussion of each of these units and the data available follows.

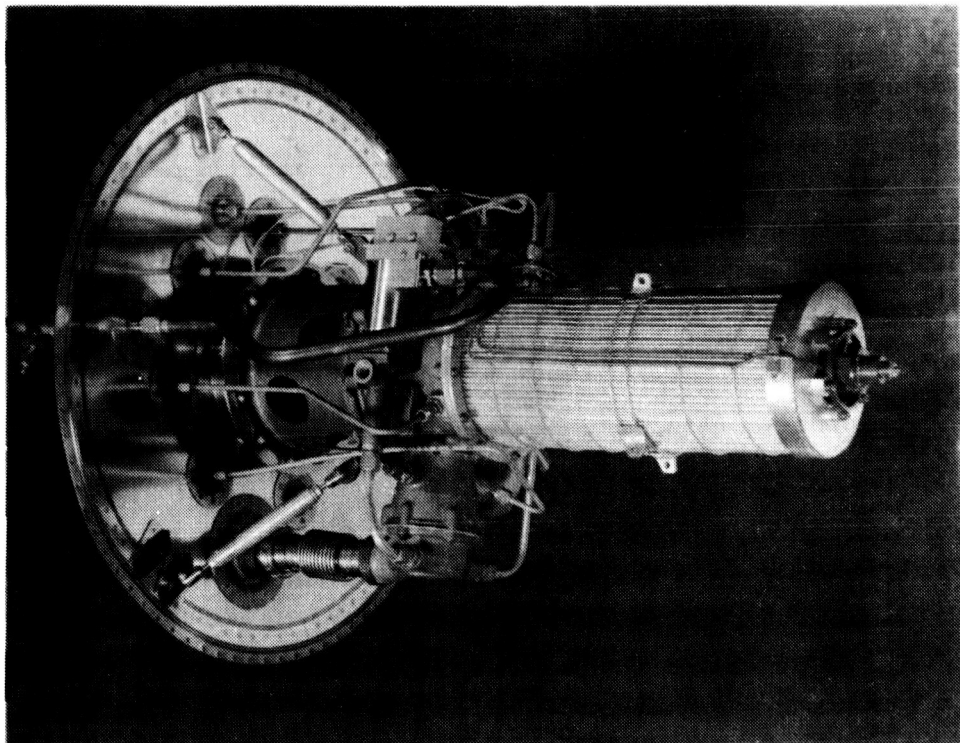
3.1.1 Convair Separator. The unit built and tested by Convair is shown in Figure 3-1. A simple flow schematic is shown in Figure 3-2.

The design utilizes a rotating wheel to provide a vortexing of the fluid within the tank along with centrifugal action to separate gas from the liquid. Gas enters the separator through radial holes located in the periphery of the rotating wheel, expands through a turbine, passes through a heat exchanger, and then is vented overboard. The turbine is used to drive the rotating wheel. The heat exchanger is utilized to remove heat from the fluid in the tank in order to improve overall system efficiency.

Development testing of the unit is covered in Reference 3-1. Problem areas encountered in early testing of the unit were excessive bearing and face seal friction and leakage through face seals and static valve seats. The bearing problems were primarily due to warpage of the bearing mounting structure at the LH₂ temperatures, causing binding and overheating. This problem was solved by the use of a more stable mounting structure and slightly greater clearances on the bearing mounting case. The face seal problem was solved by greater attention to alignment and lapping of the carbon face seal as assembled. The static seal leakages were reduced to within acceptable limits by proper attention to alignment and lapping of the Kel-F seats used in the small shutoff valves. The unit utilizes two counter-rotating wheels in order to reduce the torque effect on the vehicle. The flow capacity of the unit is 100 lb/hr of gaseous hydrogen at a tank pressure of 21 psia, the nominal operating speed in hydrogen is 9000 rpm, and the weight is approximately 25 pounds. A typical heat exchanger exit condition is superheated gas at 39°R and 4.5 psia, with a 21-psia GH₂/LH₂ mixture at the separator inlet.



CONVAIR SEPARATOR



JANITROL SEPARATOR

Figure 3-1. Convair and Janitrol Zero-g Separators

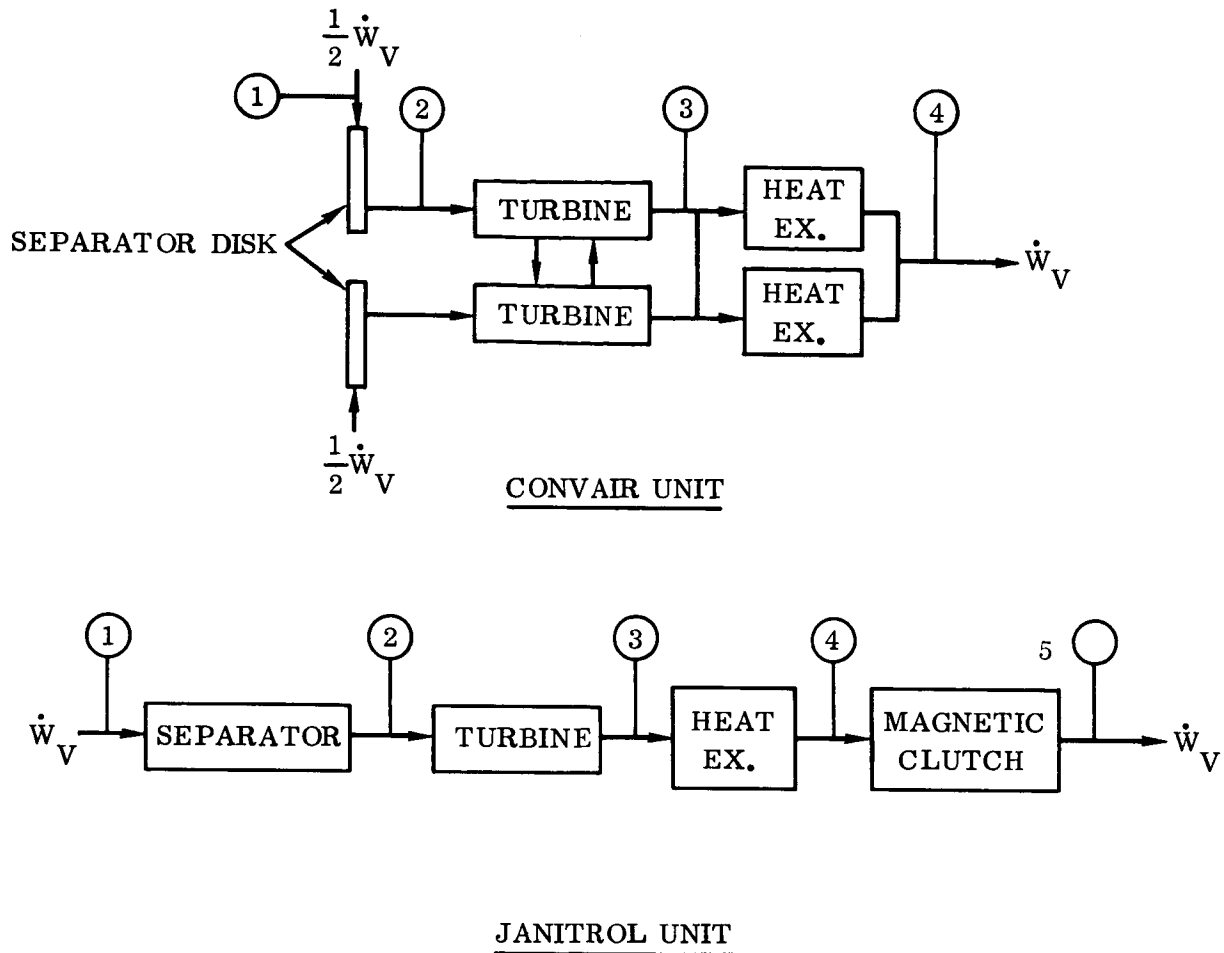


Figure 3-2. Mechanical Separator Flow Schematics

Testing was accomplished in water/nitrogen, LN_2/GN_2 , and LH_2/GH_2 environments. Liquid was sprayed on the unit to simulate a liquid/gas mixture at the unit. Test results are contained in References 3-1 through 3-4.

3.1.2 Janitrol Separator. The unit is shown in Figure 3-1. A simple flow schematic is shown in Figure 3-2. The Janitrol unit differs from the Convair unit in that a rotating tube is used instead of a disk and the turbine is connected to the rotating separator through a magnetic clutch. Vent gas is ducted through the clutch to improve efficiency by removal of excess heat.

Testing of this unit was accomplished with water and with LH_2/GH_2 . The primary problems with the unit were bearing failures and leakage. The unit uses hydrodynamic journal type bearings. Bearing operation was unstable under the loading conditions imposed, when operating with LH_2 . The problem was reduced by bearing redesign and better mounting. Also, the heat exchanger appears to be excessively restrictive of tank fluid circulation. Labyrinth type sealing used at the bearings resulted in approximately 4000-scim external leakage. Flow rate of the unit is approximately 80 lb/hr

of GH_2 . The unit weight is approximately 20 pounds. The nominal operating speeds in hydrogen of the separator and turbine are 4500 rpm and 9000 rpm respectively. A typical heat exchanger exit condition is 35°R at 5 psia with 25-psia two-phase hydrogen inlet. The effect of the heat exchanger on the vent fluid condition was negligible. Development and test data history of the unit is given in References 3-5 and 3-6.

3.1.3 Pesco Separator. The Saturn S-IVB vehicle as originally conceived required the use of a vapor/liquid separator. The original design criteria were for an on/off venting system requiring high vent flow (short vent duration) of 6 lb/sec of hydrogen gas with inlet conditions of 38 psia and -417°F saturated hydrogen gas. The Pesco unit utilizes a low-pressure-drop turbine driven by vent gas. No heat exchanger is used. Original operating requirements were weight 15 pounds, separation efficiency 100 percent at inlet mixtures up to 99-percent liquid by weight, and pressure drop 2 psi maximum. A unit was built and tested using air and water, but testing has not been done with cryogenic fluids. The water test data indicate that the unit can achieve 99-percent separation efficiency at inlet qualities only up to 75-percent liquid by weight with a pressure drop of 3 psi across the turbine separator combination. The actual weight of the unit is estimated at about 20 pounds. A motor-driven unit has been proposed for operation with the S-IVB continuous vent system where a low positive acceleration is applied to the vehicle by the vent gas. This unit would only be required to vent 0.35 lb/sec maximum. The design operating speed of the Pesco unit is approximately 2000 rpm. The unit represents an efficient design with low inlet gas velocities when operating with the 0.35 lb/sec vent rate.

3.1.4 Conclusions

- a. Mechanical separation units can perform liquid/vapor separation under low acceleration conditions, and are within the state-of-the-art.
- b. Liquid loss during start-up, especially in a nearly full tank, can be significant, and auxiliary power might be provided to obtain a fluid vortex prior to opening the vent. More testing and analysis is needed in connection with the liquid start-up problem.
- c. The use of a low-pressure-drop turbine appears advantageous since the flow is subsonic and efficiency of operation is not as greatly affected by changes in the operating fluid.
- d. A large inlet flow area with low gas velocity across the separator disk, resulting in lower required separation speeds and lower power consumption, is a desirable feature of the Pesco unit.
- e. The General Dynamics Convair configuration with respect to bearings and seals is fairly well developed for operation at LH_2 temperatures.

3.2 PREDESIGN DATA. Data are generated for the three basic vehicle cases described in Section 7.

Analysis of the mechanical or dynamic-type fluid separation system indicated the critical or worst design case to be when the liquid at the separator inlet is in the form of very small drops. In this case separation occurs when the centrifugal forces imparted to the liquid by the separator are greater than the drag forces exerted by the gas flowing into the unit. As the drop size decreases the chance of liquid entrainment increases. For high separation efficiency, the design should have low gas velocities into the separator and inlet configurations of a nature to promote coalescence of small drops of liquid into larger drops as centrifugal energy is being added to the liquid. A separator inlet with large flow area and curved vanes fills this criterion and has been used in the initial predesigns. Predesigns developed for the system comparisons are summarized in the following paragraphs for each vehicle case.

3.2.1 Case I (S-IVB, Continuous Vent). Both an electric-motor-driven separator and a turbine-driven unit were considered. Both designs rely on the S-IVB settling rockets to prevent large masses of 100-percent liquid at the unit inlets and are based on achieving essentially 100-percent separation with a 10-percent quality (90-percent liquid) at the unit, for a vent flow-rate range of 0.06 to 0.35 lb/sec. Detailed design packaging was not optimized for the purposes of this predesign. The motor-driven unit, sketched in Figure 3-3, is designed for a maximum pressure drop of 1 psi, and it is assumed that operation is initiated at the start of the coast period and prior to actual venting in order to ensure gas at the unit at the time of venting. During periods of complete liquid inundation, some liquid will be lost; however, the motor-driven unit is designed to operate at essentially full speed under such conditions and should quickly clear itself.

The turbine-driven unit will operate at significantly reduced speeds when in liquid and the amount of liquid loss could be appreciable. However, more needs to be known about the tank fluid dynamics under the low-g coast conditions before a reasonable estimate can be made of the actual liquid losses.

The power added to the tank fluid by the electric motor and the energy removed from the vent fluid by the turbine are accounted for by calculating their effects upon vent flow rate. The design data for the motor-driven unit are summarized in Table 3-1 and those for the turbine-driven unit in Table 3-2. The operating cycle and possible failure modes and consequences associated with each component are listed in Table 3-3 for the motor-driven unit and are, in general, characteristic of the turbine-driven unit also.

3.2.2 Case II (S-IVB). For the vent flow rates of the S-IVB vehicle, it appears advantageous to make use of the vent gas to apply an acceleration to help maintain the mechanical separator free of liquid. Also, it appears advantageous from an overall heat transfer standpoint to settle the propellants as much as possible to prevent

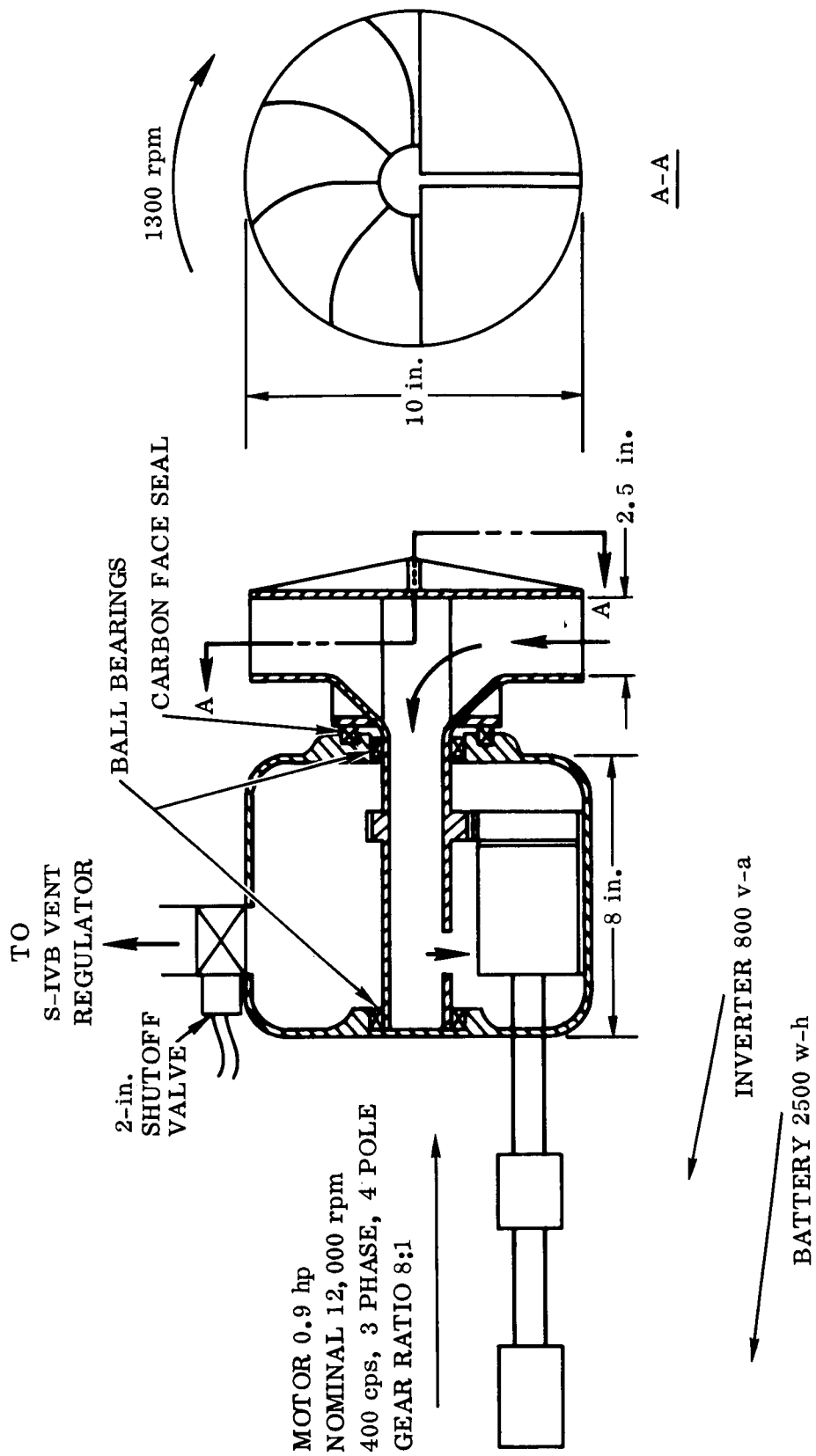


Figure 3-3. Electric-Motor-Driven Vapor/Liquid Separator

Table 3-1. Mechanical Vapor/Liquid Separator (Electric-Motor Driven)

S-IVB VEHICLE WITH CONTINUOUS VENTING AND VENT GAS SETTling

COMPONENT	DESCRIPTION	NOMINAL POWER RATING	WEIGHT (lb)
Separator Assembly	Al Alloy	0.39 HP @ 1300 rpm	12.8
Motor Gearing	400 cycle, 4 pole, 3-phase induction, 8:1 ratio, 95% efficiency	Motor bhp = 0.885 @ 11,650 rpm	10
Battery	Ag - Zn	2500 w-hr	50
Inverter	400 cycle	800-v-a inverter	32
Controls	On Switch (Redundant)	_____	1
Valves	2-in. -Diam, Solenoid Operated Shutoff	_____	3

Total Fixed Weight _ _ _ _ _ 108.8 lb

External Power to Tank 420 watts average, $\Delta \dot{W}_{vent}^* = 0.002 \text{ lb/sec}$,

$$\dot{W}_T = 0.352 \text{ to } 0.062 \text{ lb/sec}$$

* Represents the increase in vent requirement due to electrical power into the propellant tank when operation is in 90-percent liquid by weight.

Table 3-2. Mechanical Vapor/Liquid Separator (Turbine Driven)

S-IVB VEHICLE WITH CONTINUOUS VENTING AND VENT GAS SETTling

COMPONENT	DESCRIPTION	NOMINAL POWER RATING	WEIGHT (lb)
Separator Assembly	Al Alloy	0.39 hp @ 1300 rpm 0.35 lb/sec flow	13.1
Turbine	10-in. -Diam Al Alloy	0.56 hp @ 1480 rpm 0.35 lb/sec flow $\Delta p = 2.5 \text{ psi}$	2
Valves	2-in. -Diam, Solenoid-Operated Shutoff	_____	3

Total Fixed Weight _ _ _ _ _ 18.1 lb

$$\Delta \dot{W}_{vent} = 0.0021 \text{ to } 0.00001 \text{ lb/sec}$$

$$\dot{W}_T = 0.3521 \text{ to } 0.06001 \text{ lb/sec}$$

wetting of the forward dome. If continuous venting were not required, a motor-load sensing device could be used that would shut off the vent flow when the separator became inundated with liquid. This method would be an advantage in preventing the loss of liquid; however, shutting down the vent thrust would increase the possibility of extended periods of inundation and shutdown that could allow an excessive increase in tank pressure. Therefore, the use of a continuous vent thrust is also assumed for the Case II vehicle, and the predesign will be identical to that developed for Case I and summarized in Tables 3-1 through 3-3.

3.2.3 Case III (Cryogenic Service Module)

3.2.3.1 LH₂ Tank. No settling forces of significance are assumed available due to the extremely low vent rates. Design of the separator is, therefore, based on the assumption that a gas/liquid mixture exists at the unit corresponding to the average existing in the tank. The basic configuration is the same as for the S-IVB unit shown in Figure 3-3. In determining power requirements, it is assumed that there is the requirement to maintain continuous mixing of the entire propellant tank in addition to the normal separation requirement. An electric-motor drive is used. A preliminary analysis indicates that the use of a vent gas turbine would be theoretically feasible; however, a detailed analysis would be required to determine actual hardware requirements and feasibility since units operating at the extremely low continuous flow rates of the present case have not been built. Also, the liquid loss during start-up would probably be significant for cyclic operation and difficult to predict; therefore, data are not presented for a turbine-driven unit. The electric-motor-driven unit is assumed to be started prior to actual venting in order to ensure gas at the separator at initiation of venting. Design is based on an initial propellant tank ullage volume of 5 percent. The unit is sized for the maximum heating rate of 189 Btu/hr and is designed for on/off operation; i. e., at heating rates lower than 189 Btu/hr, the venting would occur in a cyclic on/off mode with tank pressure varying between pre-set limits. Design data developed for the initial phase of the study are summarized in Table 3-4. Possible failure modes are similar to those described for the S-IVB system.

3.2.3.2 LO₂ Tank. The same basic assumptions are made for the LO₂ tank vent unit as for the hydrogen tank unit except that the maximum heating rate is 90 Btu/hr for the LO₂ tank. Design data for the oxygen unit are presented in Table 3-5. The failure modes and consequences are the same as for the hydrogen case, except that an additional mode of failure is possible with an electric motor operating in an oxygen environment. Motor windings operating in such an environment are sealed, and if the sealing were to fail, the motor would probably burn with subsequent separator stalling and loss of liquid from the tank.

Table 3-3. Operating and Failure Mode Characteristics, S-IVB Mechanical Motor-Driven Unit

COMPONENT	OPERATING CYCLE	FAILURE MODES	CONSEQUENCES
Separator Pump	4-1/2 hrs continuous	<ol style="list-style-type: none"> 1. Unit completely surrounded with liquid. 2. Excessive friction of bearings or seals causing stalling. 	<ol style="list-style-type: none"> 1, 2. Loss of liquid with reduction in vehicle Δu proportional to the amount of liquid lost.
Gearing	4-1/2 hrs continuous	Binding causing shut-down or reduction in speed.	Loss of liquid with reduction in vehicle Δu proportional to the amount of liquid lost.
Motor	4-1/2 hrs continuous	Failure to operate at required speed.	Loss of liquid with reduction in vehicle Δu proportional to the amount of liquid lost.
Inverter	4-1/2 hrs continuous	Failure to operate at proper output.	Loss of liquid with reduction in vehicle Δu proportional to the amount of liquid lost.
Battery	4-1/2 hrs continuous	Failure to operate at proper output.	Loss of liquid with reduction in vehicle Δu proportional to the amount of liquid lost.
Switch	One operation at initiation of coast	<ol style="list-style-type: none"> 1. Failure to start separator. 2. Starts prematurely. 	<ol style="list-style-type: none"> 1. Loss of liquid with reduction in vehicle Δu proportional to the amount of liquid lost. 2. Available power is consumed prior to termination of coast.
Shutoff Valve	One operation at initiation of venting	<ol style="list-style-type: none"> 1. Failure to open. 2. Opens prematurely. 	<ol style="list-style-type: none"> 1. Tank overpressure. 2. Loss of liquid. Also, possible loss of tank pressure during firing.

Table 3-4. Mechanical Vapor/Liquid Separator (Electric-Motor Driven)

CRYOGENIC SERVICE MODULE LH₂ TANK WITH ON/OFF VENTING AND NO SETTLING

COMPONENT	DESCRIPTION	NOMINAL POWER RATING	WEIGHT (lb)
Separator & Mixer Assembly	4-in.-Diam Al Alloy	5.88×10^{-4} hp @ 302 rpm	4.5
Motor and Gearing	400 cycle, 4 pole, 3-phase induction, 40:1 ratio	Input 2.94×10^{-3} hp, Output 5.88×10^{-4} hp @ 302 rpm	1
Fuel Cell	Fuel Cell Reactants and Tank	—————	0.4
Valves	1/4-in. Nominal On/Off Pressure Relief Valve	—————	1.3
Total Fixed Weight — — — —			7.2 lb
External Power to Tank 2.195 watts		$\Delta \dot{W}_{vent} = 0.0396$ lb/hr	

Table 3-5. Mechanical Vapor/Liquid Separator (Electric-Motor Driven)

CRYOGENIC SERVICE MODULE LO₂ TANK WITH ON/OFF VENTING AND NO SETTLING

COMPONENT	DESCRIPTION	NOMINAL POWER RATING	WEIGHT (lb)
Separator & Mixer Assembly	2-in.-Diam Separator Al Alloy 4-in.-Diam Mixer	1.066×10^{-3} hp @ 230 rpm	4.0
Motor Gearing	400 cycle, 4 pole, 3-phase induction, 48:1 ratio	1.066×10^{-3} hp Output, 5.33×10^{-3} hp Input @ 230 rpm	1
Fuel Cell	Fuel Cell Reactants and Tank	—————	1.86
Inverter	Existing		0
Controls	On/Off Pressure Switch		0.5
Valves	1/4-in. line size On/Off Pressure Relief Valve	—————	0.5
Total Fixed Weight — — — —			8 lb
External Power to Tank 3.98 watts		$\Delta \dot{W}_{vent} = 0.151$ lb/hr	

3.3 CONCLUSIONS. The following conclusions are drawn from the data generated for the three vehicle cases.

- a. The major unknown in the analysis and comparisons of the mechanical type separators is the quality of the fluid that is likely to exist at the vent throughout the coast. Until such data are obtained, it is extremely difficult to evaluate these vent systems, which are extremely inefficient when operating in close to 100-percent liquid. If some liquid loss can be tolerated and potential periods of inundation could be defined, all systems could be compared on the basis of weight and complexity. The mechanical units can be designed for minimum liquid loss by using a load sensing device in conjunction with a shutoff valve to discontinue the venting during periods of liquid inundation. Such a device could be used with the motor-driven separator and with the turbine-driven unit if an auxiliary power source (such as a motor) were used during periods of separator overload. Even with the use of such a device, however, some knowledge of the duration of shutoff would be required to determine whether excursions in tank pressure during shutoff would be within acceptable limits. Also, in the S-IVB case, complete shutoff of the vent would terminate the thrust of the settling rockets, allowing liquid to wet the forward dome of the vehicle. Further hydrodynamic analysis is needed along with testing at 1-g in full tanks of LH₂ and water. Final correlations and verification testing, however, would have to be performed under extended low-g conditions.
- b. For the S-IVB case, the data show that a turbine-driven unit will theoretically operate satisfactorily over the 0.35 to 0.06 lb/sec flow range. However, more detailed analysis, particularly of the turbine design, is needed to insure proper operation at the low-flow rate. Bearing and seal power would not be quite proportional to the cube of the speed as assumed here; i. e., power at the low flow would need to be greater than shown in the present analysis; therefore, turbine sizing would be based on the low-flow case. This would result in greater inefficiencies at the high flows. Also, a closer look at the separation criteria would be needed due to the low separator speeds of the 0.06 lb/sec-flow condition. The main disadvantage in the use of a turbine drive lies with its extremely inefficient operation with LH₂. An auxiliary drive operating during overload periods to allow the unit to clear itself of liquid in a reasonable time could be used.
- c. Determination of start-up times, minimum power, and propeller configuration for the Cryogenic Service Module to ensure gas at the separator is critical and not well defined at the present. Further work needs to be done in this area.
- d. Determination of separation criteria (minimum power and optimum configuration) for different conditions (slug, foam, droplets) of the liquid at the separator needs further analysis and testing in order to completely optimize the separator design.

The detailed calculations and assumptions used to generate the predesigns are presented in Appendix C.

SECTION 4

DIELECTROPHORETIC SYSTEMS

4.1 INTRODUCTION. Ways of designing a vapor vent system for operation under low or zero acceleration may be placed in one of two prime categories: (a) total fluid control or (b) vapor/liquid separation with subsequent venting of vapor. This section describes preliminary concepts of total fluid control methods and liquid/vapor separation methods employing electrostatic fields to orient dielectric fluids such as oxygen or hydrogen in such a way to permit venting of vapor alone.

The following is not a complete review of literature and documents that have been studied in relation to dielectrophoretic means of liquid control, but includes the more significant documents used in the preliminary design of the systems discussed.

H. A. Pohl (Reference 4-1) called attention to the behavior of dielectric fluids in non-uniform electric fields in 1958. While no practical designs are suggested, the paper presents the fundamental behavior of dielectric liquids in the presence of electrical fields. Also in an earlier paper (Reference 4-2), Pohl applied the name of "dielectrophoresis" to this liquid behavior. Dielectrophoresis is defined as the motion of matter caused by polarization effects in a nonuniform electric field. This electrical phenomenon may be used to orient and control a large class of dielectric fluids including cryogenic fluids like hydrogen and oxygen. In brief; if a cryogenic storage vessel contains an array of electrodes (electrostatic condensers) of some given geometric arrangement and if a voltage is impressed across the electrodes, the dielectric liquid will be moved and drawn into the space between the high potential and ground electrodes within the storage tank. This separation of liquid and vapor enables the design of vapor venting systems that minimize inadvertent venting of liquid in a low-gravity space environment.

J. B. Blackmon (References 4-3, 4-4, and 4-5) has published theoretical and experimental work dealing with dielectrophoretic methods of positioning cryogenic liquids. This work is instructive but of itself does not yield desired configurations applicable to the vehicles under study.

During 1964 General Dynamics Convair undertook an analytical study of dielectrophoresis (Reference 4-6) as it might be applied to the Centaur hydrogen tank. Dynatech Corporation contributed to Convair some theoretical calculations and some configurations applicable to the Centaur tank (References 4-7 and 4-8). These configurations are proprietary to Dynatech and of themselves are not applicable directly to the vehicle or tank configurations under study.

During 1963-64, under contract to the Air Force Aero-Propulsion Laboratory, Dyna-tech Corporation conducted an experimental and theoretical study of total fluid control methods (Reference 4-9). This technical report discusses theory, presents practical design equations, and substantiates theory with model tests.

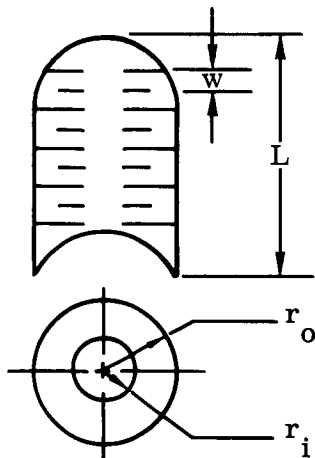
All of the current literature obtained during this study deals with the total fluid control concept, rather than liquid-separator devices, per se. The former can be accomplished by any one of a variety of capacitor configurations within a given tank, e.g., a concentric condenser geometry where the ground and high-potential electrodes are concentrically located about the longitudinal axis of essentially cylindrical tanks, or plate condensers with the plates spaced along the longitudinal axis and at right angles to it. No significant designs of liquid/vapor separator devices employing the dielectrophoretic principle were found.

Reports of small-scale tank tests conducted with a liquid/liquid model at 1g and with liquid/vapor systems in aircraft tests at low acceleration conditions indicate that dielectrophoretic fluid control is possible.

4.2 TOTAL FLUID CONTROL. Two applications were analyzed in a preliminary way to study control of the total fluid in a storage tank.

- a. Cryogenic Service Module hydrogen tank.
- b. S-IVB hydrogen tank.

4.2.1 Basic Design Equations. Consider the case of parallel plate condensers spaced along the longitudinal axis of a tank and at right angles to it.



The average required electric field intensity for the configurations shown in the sketch is given by (Reference 4-9):

$$E^2 = \frac{V^2}{w^2} = \frac{L}{1 - \left(\frac{r_i}{r_o}\right)^2} \left(\frac{\rho_L - \rho_V}{\epsilon_L - \epsilon_V}\right) g \quad (1)$$

where

- E = field intensity, volts/meter
V = voltage between pair of electrodes, volts
w = electrode spacing, meters

- ρ_L = liquid density, kg/m³
 ρ_V = vapor density, kg/m³
 L = liquid height in tank, meters
 r_i = inner radius of electrode, meters
 r_o = outer radius of electrode, meters
 g = local gravitational acceleration, meters/sec²
 ϵ_L = dielectric permeability of liquid hydrogen, farads/meter
 ϵ_V = dielectric permeability of gaseous hydrogen, farads/meter

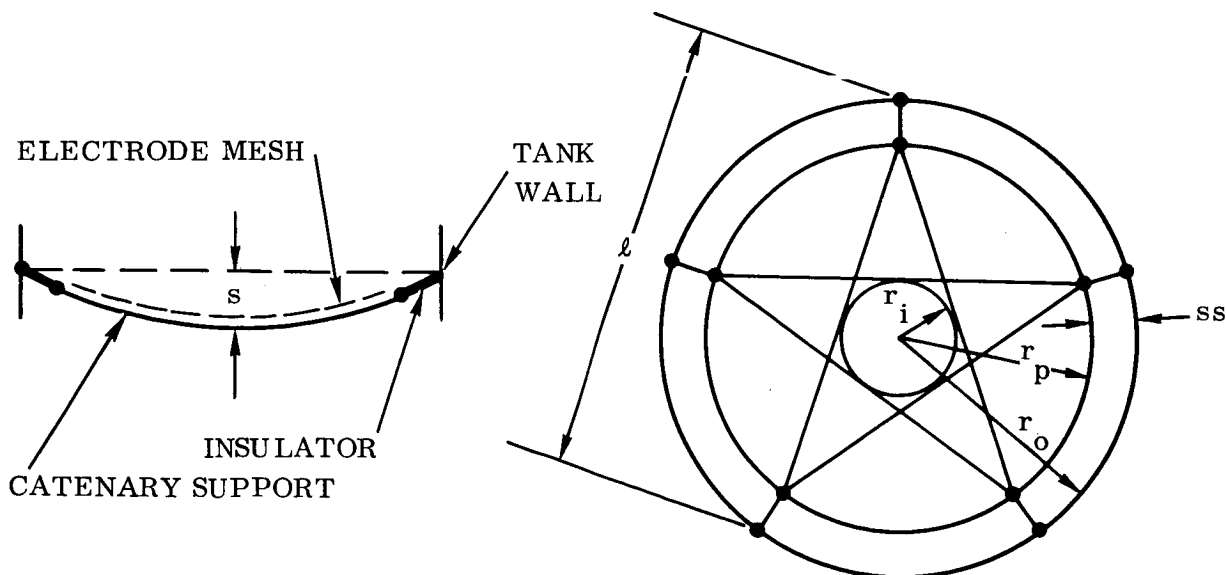
Equation 1 expresses the required field strength as a function of tank geometry, electrode geometry, properties of the fluid to be controlled, and local acceleration conditions.

4.2.1.1 Electrode Weight. Employing the electrode design suggested in Reference 4-9, namely, each electrode consists of two parallel plates of wire screen separated by a small gap, the equation for electrode weight is:

$$\text{Total electrode weight} = 2\pi(r_o^2 - r_i^2) \rho_{sa} n_e \quad (2)$$

where n_e is the number of electrodes and ρ_{sa} is the weight per unit area of wire screen.

4.2.1.2 Electrode Support Weight. An optimal method of electrode wire-mesh screen support within a given tank has not been determined. The catenary method of support suggested in Reference 4-9 was applied to these first preliminary designs, although the catenary is probably not an optimal means of electrode support. For each electrode, five stainless steel tubes are used to support the electrode as shown in the sketch.



With reference to the sketch:

- s = maximum catenary deflection below the horizontal
- l = length of each catenary
- r_o = tank radius
- r_p = outer radius of high-potential electrode
- r_i = electrode inner radius
- ss = insular space between tank and high-potential electrode

In the case of large tanks and high voltages impressed across the electrode, the high-potential electrode must be insulated from the tank wall by suitable nonconducting material. Also the spacing between electrodes (w, previously defined) must be such that for the voltage selected the electrical breakdown value of gaseous hydrogen is not exceeded.

$$ss = \frac{(V)(COF)}{(E_{BRKD})} \quad (3)$$

where

- V = potential between adjacent electrodes
- COF = dimensionless experimental coefficient based on model tanks, on the order of 5.00 (Reference 4-9)
- E_{BRKD} = breakdown field intensity of hydrogen vapor

Since vapor can exist anywhere in the tank electrode system, the voltages selected for design must be below this breakdown value. E_{BRKD} seems to be primarily a function of vapor density, and a careful search was made to establish the experimental range of this parameter. Consultation with Dynatech Corporation and Convair's own perusal of References 4-10 through 4-13 yielded the following range of values of E_{BRKD} for gaseous hydrogen.

$$6000 < E_{BRKD} (20^{\circ}K, 1 \text{ atm}) < 12,000 \text{ kv/foot}$$

In the designs considered and discussed in this study, operating voltages ranged from 50 to 700 kv/foot, all well below E_{BRKD}.

Returning to the catenary weight calculations, the deflection, s, of a parabolic catenary subjected to a distributed load, q, is given by:

$$s = \frac{q l^2}{8H} \quad (4)$$

where

- s = deflection at center, taken as 5 percent of electrode spacing, w
 H = tension in catenary

If the catenaries are fabricated from thin-walled, small-diameter stainless steel tubes, H may be defined as:

$$H = \pi D_c t_c S_c \quad (5)$$

where

- D_c = tube diameter
 t_c = wall thickness of tube
 S_c = allowable stress (taken as 80 percent of yield strength)

Since there are five catenaries per electrode plate, the maximum force on each of five catenaries may be computed as one-fifth of the drag force on each electrode, or

$$l_q = \frac{C_D (\rho_L / 2) u^2 A_e + W_e}{5} + W_c \quad (6)$$

where

- A_e = electrode area
 C_D = electrode screen drag coefficient
 u = slosh velocity

The drag coefficient C_D is uniquely determined as a function of the fraction of area blocked by the selected electrode screen material, FAB, thus

$$C_D = 0.0486 \times 10^{3.12 (\text{FAB})} \quad (7)$$

This relation represents a best fit (Reference 4-9) to experimental data from Mark's Mechanical Engineer's Handbook, Fifth Edition. In turn, FAB is strictly a function of screen geometry and is expressed as

$$\text{FAB} = \frac{(D_1 - D_2) D_1 + D_1 D_2}{(D_1 + D_2)^2} \quad (8)$$

where

- D_1 = screen wire diameter
 D_2 = screen mesh spacing

For the screen assumed in all designs ($D_1 = 0.001$ ft, $D_2 = 0.01$ ft symmetrical) the drag coefficient is 0.17. The maximum slosh velocity within the tank can be calculated by the following expression.

$$u_{\max} = (2\alpha g_o L_T)^{1/2} \quad (9)$$

where

α = disturbance acceleration in g_o (1.6×10^{-2} was used)

L_T = maximum length through which fluid travels

Thus from the equations above, Equation 6 may be written as follows:

$$\ell q = 0.0097 \times 10^{3.12 \text{ (FAB)}} \pi \rho_L \alpha g_o L_T (r_o^2 - r_i^2) + 0.2 W_e + W_c \quad (10)$$

and from Equations 4, 5, and 10 the tubular, catenary support network weight for each electrode can be calculated by:

$$W \text{ (supports for one electrode)} = 5 \pi \ell D_c t_c \rho_c \quad (11)$$

where

ρ_c is the density of the support tubing material.

4.2.1.3 Required Power. The power required to operate the total control systems and to operate the small dielectrophoretic separators was calculated by the methods of Reference 4-9. However the numbers are approximate in that sufficient time was not available to carefully study the inverter/transformer and/or choke/capacitance circuit.

The reactive current for a purely capacitive load is given by:

$$I_{\text{CAP}} = V_{\text{CAP}} 2 \pi f C \quad (12)$$

where

I_{CAP} = current rating, amps

V_{CAP} = voltage impressed across electrode pairs, volts

f = frequency - taken as 300 cps

C = tank electrode (condenser) system capacitance, farads

The capacitance, C , can be calculated by standard relationships.

$$C = KA/4 \pi w (9 \times 10^5), \text{ microfarads} \quad (13)$$

where

- K = dielectric constant of liquid; 1.226 for LH₂ and 1.507 for LO₂
A = area of one condenser plate, cm²
w = distance between ground and high-potential electrodes, cm

The power input to the circuit is

$$P = \frac{I_{CAP} V_{CAP}}{Q} \quad (14)$$

where

Q is the transformer "quality" or "goodness" factor (taken as 174, Reference 4-9).

4.2.2 Predesign Calculations and Results -- Total Fluid Control Concept

4.2.2.1 Cryogenic Service Module. Calculations were made to determine the required number of electrodes for two voltages, namely, 127,500 and 300,000 volts, giving 25 and 10 electrodes required respectively. Using annular circular discs of aluminum wire screen (0.001-ft wire diameter and symmetrical mesh spacing of 0.01 ft) the weights of electrodes alone for the two voltages were 127.5 kv/60 lb and 300 kv/25 lb.

The electrode support system was based on the five catenary per electrode scheme previously mentioned and was highly sensitive to plate spacing since the maximum permissible catenary deflection was fixed at 5 percent of the plate spacing. The results for the two voltages were 127.5 kv/224 lb and 300 kv/36 lb.

The specific power requirement was estimated to be about 1 kw. The weight of the power conversion pack would be of the order of 150 pounds, but could vary considerably depending upon detailed design, which was not possible here.

There is also the question of power pack location. It would be a saving in boiloff weight to locate it outside the tank to prevent adding the considerable energy dissipated in the power hardware to the propellant. However, the mechanical problems of passing very high-voltage electrical cables through a thin-walled cryogenic propellant tank and preventing fluid leakage would require solution before an outside location for the power pack could be planned.

Cyclic orientation of the propellants might be considered, although this would require prior demonstration that the orientation transients and stability problems were small. It was felt to be more reasonable, with the present state-of-the-art, to compare continuous control and venting with the other separators that were also planned for continuous operation. Therefore, cyclic operation was not analyzed.

Figure 4-1 summarizes the weight and performance estimates for the Cryogenic Service Module hydrogen tank total fluid control predesign, using 300 kv across the electrodes, which gave a lower total weight than did the 127.5 kv case.

The possible failure modes, common to both this application and the other total fluid control systems or separator devices, are discussed in Paragraph 4.4.

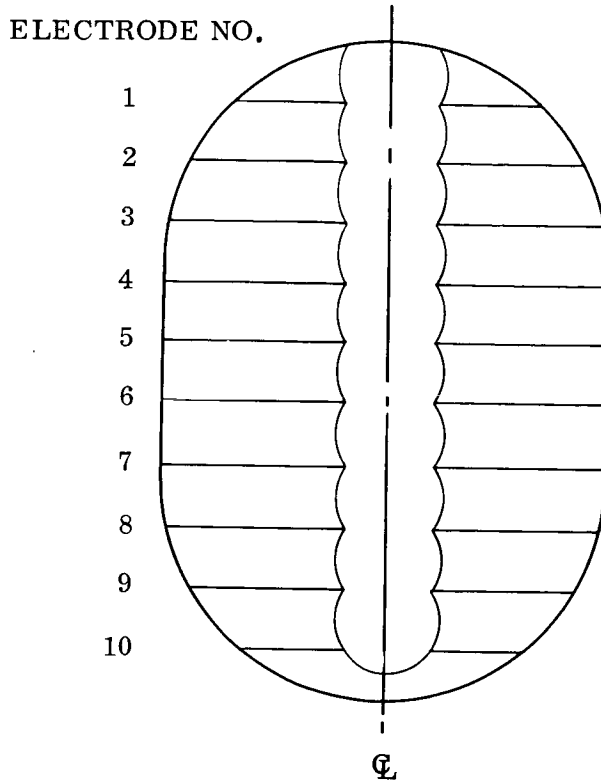
Some of the assumptions and/or unknowns in the predesign are discussed below. The adverse acceleration level chosen for design was $5 \times 10^{-4}g_0$. It is assumed that total orientation of dielectric fluids such as hydrogen or oxygen by means of electrostatic fields is possible, given sufficient electrical field strength. This assumption seems to be fairly well established by model tank tests in laboratory experiments and aircraft tests. However, as far as is known, it has not been demonstrated for either hydrogen or oxygen fluids or for large-scale tanks comparable to those considered in these predesigns. As previously mentioned, there is a question about the location of the power pack, to be determined by whether a satisfactory method of transferring high-voltage power through the tank skin can be developed. The method of supporting the electrodes by catenaries may be inefficient from a weight standpoint, but a detailed study of support methods was beyond the scope of the study. The design and, therefore, weight of the power pack were not determined in detail. However, General Electric Company is now studying this problem at our request and there will be information forthcoming from them. Giannini Controls has produced a converter to supply 100,000 volts for a short (uncooled) duration that weighs only 10 pounds. Dynatech and Ionic Physics, Inc., have a joint project to develop a lightweight power supply package.

4.2.2.2 S-IVB. The results of the predesign calculations on the total fluid control concept for the S-IVB hydrogen tank are outlined below.

The number of electrodes required varied inversely with applied voltage and was (for 100, 200, 300, 400, 500, 600, and 700 kv respectively) 128, 64, 42, 32, 25, 21, and 18. The weights of electrodes and supports as a function of plate voltage are shown in Figure 4-2. These weights are based on electrodes fabricated from aluminum wire screen of 0.001-foot wire diameter and symmetrical mesh spacing of 0.01 foot, an adverse acceleration of $5 \times 10^4 g_0$ for determining field strength, and acceleration of $1.6 \times 10^{-2} g_0$ for sizing the electrode supports.

These weights were sufficiently higher than those for the dielectrophoretic separators or other separator devices that the total fluid control concept for the S-IVB size tank was not pursued further.

4.3 DIELECTROPHORETIC LIQUID/VAPOR SEPARATORS. Descriptions of cryogenic fluid liquid/vapor separators, employing the dielectrophoretic principle, were not found in the literature surveyed. However, a method has been conceived and a configuration established during this study. Some preliminary design configurations have been developed and performance and weights estimated. Three dielectrophoretic separator designs have been evolved, one for the S-IVB tank, one for the Cryogenic



PREDESIGN CONDITIONS:

ADVERSE ACCELERATION (FOR VOLTAGE DETERMINATION) = $5 \times 10^{-4} g_0$

ADVERSE ACCELERATION (FOR DETERMINATION OF SLOSH LOADS ON ELECTRODES) = $1.6 \times 10^{-2} g_0$

FLUID: LH_2 AT 20 psia

RESULTS:

PLATE VOLTAGE DIFFERENCE = 300 kv
 ELECTRODE SPACING = 1.175 ft
 POWER REQUIRED = 1100 watts
 HARDWARE WEIGHT (ASSUMING
 NO CHANGE IN EXISTING VENT
 VALVE OR DUCTING: NOT IN-
 CLUDING BATTERY OR POWER
 SOURCE WEIGHT) = 745 lb

Figure 4-1. Cryogenic Service Module Hydrogen Tank

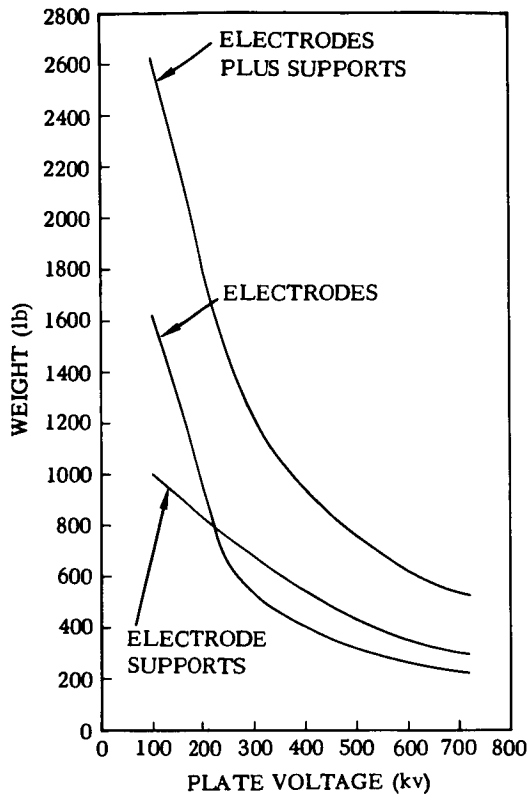


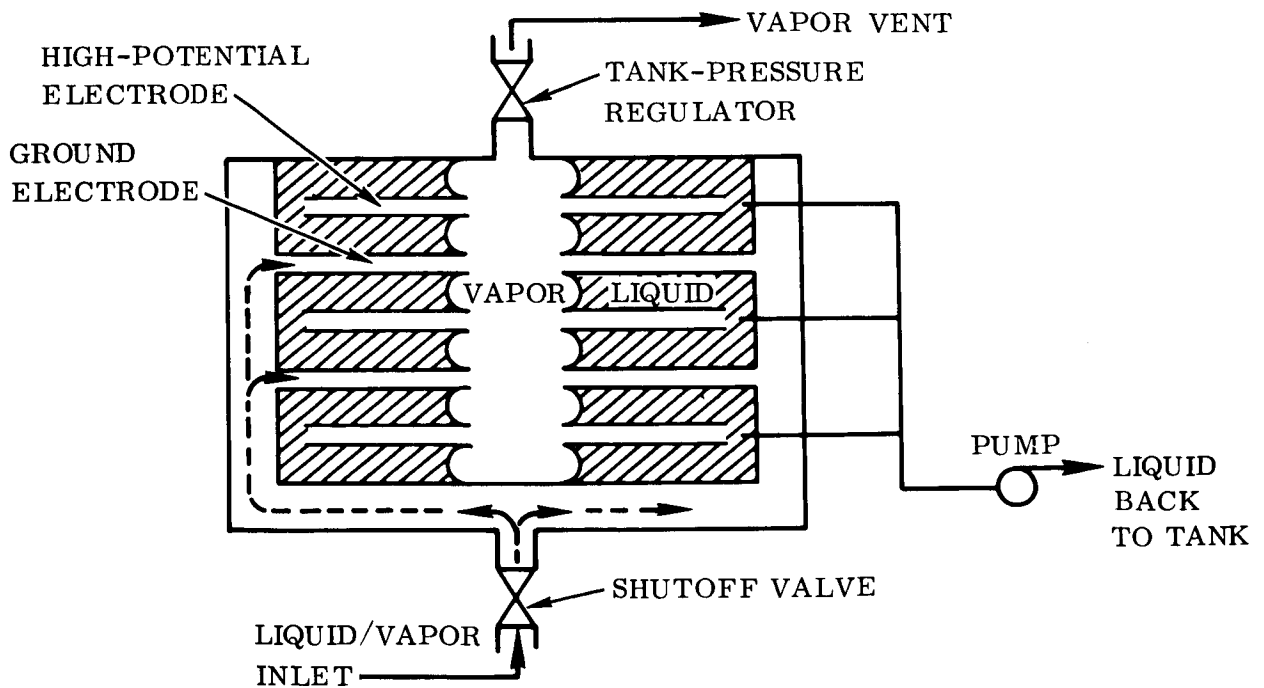
Figure 4-2. Weights of Electrodes and Electrode Supports for the S-IVB Hydrogen Tank, Total Fluid Control Concept

Service Module (CSM) hydrogen tank, and one for the CSM oxygen tank. The principle of operation and basic geometry are the same for all three tank separators; the differences are only in size.

4.3.1 Basic Geometry and Principle of Operation. The conceptual separator design is illustrated by the sketch.

Basically, the separator is a tank within a tank. The inner tank contains parallel electrodes mounted at right angles to the axis of revolution of the cylindrical tank. Essentially, the design is the same as previously described for total fluid control and, as before, within the separator tank the fluid is positioned by an electrostatic field applied between the high-potential and ground electrodes.

Just as in the case of total control, each "electrode" is a pair of wire-mesh screens separated by a small gap, d_f , called the Faraday Gap. This gap is usually of a size similar to the screen mesh spacing.



The inner tank is so arranged and the ground electrodes are so mounted that liquid/vapor mixtures can be circulated from the inlet through the annular passage between the two tanks and enter into the gap between the ground electrodes. The liquid/vapor mixture then flows in parallel through all the ground electrodes toward the center of the tank with removal of liquid from the two-phase mixture. The vapor is removed from the center of the tank and vented through the existing tank vent.

During operation, when voltage is applied between the high-voltage and ground electrodes, the liquid is moved to the region between the electrodes, leaving the Faraday gap free of liquid and forming a passageway for the two-phase vent stream. That the gap is free of liquid in the presence of an electrostatic field is an observed experimental fact (Reference 4-9). It has also been observed that when liquid does penetrate into the Faraday gap it is rapidly absorbed into the liquid column being controlled by the electrostatic field between the electrodes in space w (Reference 4-14). Thus the basic action of the dielectrophoretic separator is one of "stripping" the liquid flowing in the Faraday gap and moving this liquid into the electrostatic field region between electrodes, where it is held in place.

It is obvious that this action would eventually overflow the separator; therefore, a small pump is installed to continuously remove collected liquid and return it to the main tank.

With a reasonable "stripping" efficiency and sufficiently large contact area of all electrodes handling the liquid/vapor mixture, essentially 100-percent vapor should reach the center of the separator and be subsequently vented overboard.

4.3.2 Analytical Design Considerations. There will be a pressure drop between separator inlet and separator core as the vapor/liquid mixture flows through the electrode Faraday gap, causing a pressure force tending to move the liquid column between the electrodes toward the center. Adverse accelerations may cause forces tending to move the controlled liquid from between the plates. If the liquid between the electrodes is removed then liquid will be lost through the vent, and the separator may never again operate successfully. To prevent this, the magnitude of the electrostatic field must be great enough to hold the liquid in place between the electrodes against the two adverse forces listed above.

An equivalent head rise, h , due to the electrostatic field action can be computed by (Reference 4-9):

$$h = \frac{1}{2} \frac{(\epsilon_L - \epsilon_V) E^2}{(\rho_L - \rho_V) g} \quad (15)$$

where the variables are those defined for Equation 1.

The value of h can be independently determined by calculating the pressure drop of two-phase flow in the Faraday gap and the adverse acceleration force. Once these are known they can be converted to equivalent fluid head and the required field strength, E , at a given acceleration calculated from Equation 15. This field strength, E , will be the theoretical minimum required to balance the forces tending to blow the liquid column out of the separator.

In calculating the pressure drop through the Faraday gap channel, the gaseous-phase pressure drop is first calculated. Then this pressure drop is corrected to give the pressure drop for isothermal two-phase flow using the method of Martinelli, as outlined in Appendix D.

4.3.3 Summary of Calculations and Results (Separators). Lacking any experimental data on the stripping efficiency of a separator device as outlined in the previous section, rough estimates were made of the required size of the separator passageways. These estimates resulted in setting the overall separator dimensions as 4-foot diameter by 4-foot height for the S-IVB hydrogen tank, and 1.5-foot diameter by 1.3-foot height for the CSM hydrogen and oxygen tanks.

In the case of the S-IVB 4 by 4 foot separator, parametric calculations were made for a fixed geometry shown in Figure 4-3. The variables were: vapor flow rate over a range of 0.06 to 0.35 lb/sec, and Faraday gap, d_f , of 0.01, 0.03, and 0.06 foot.

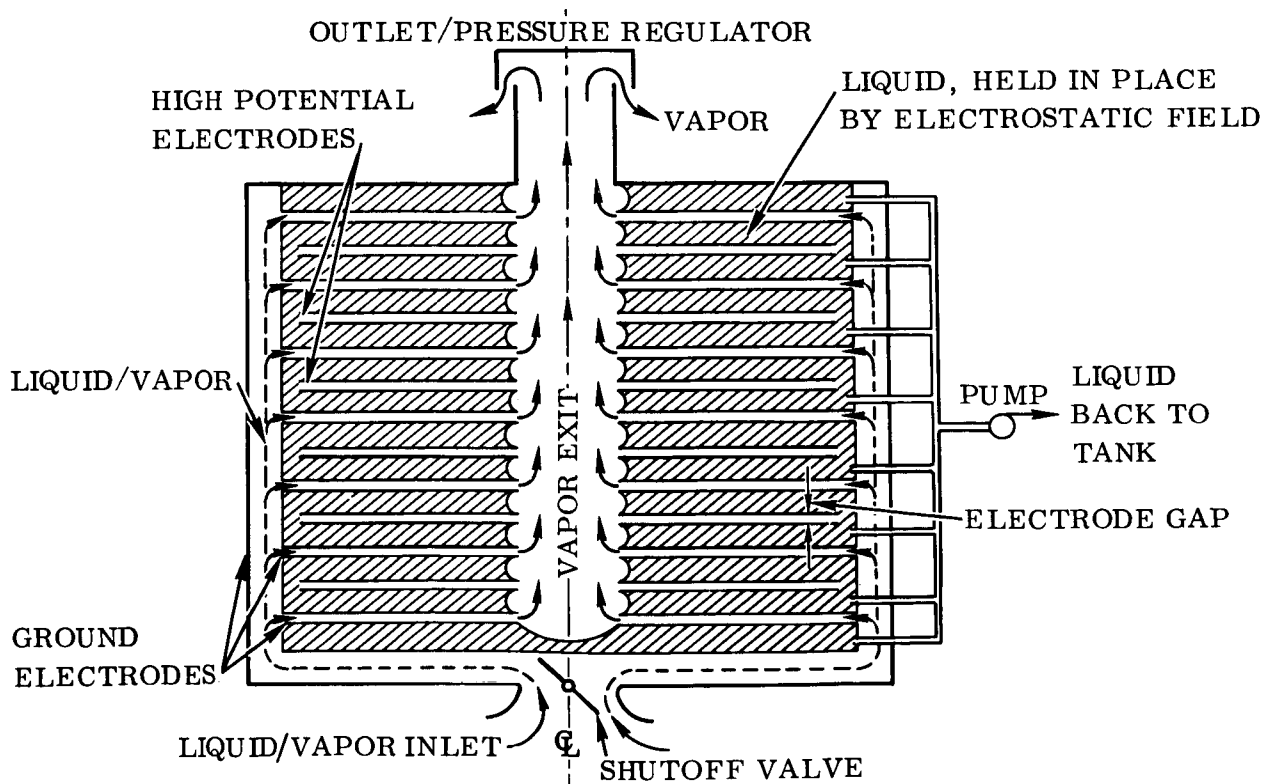


Figure 4-3. Electrostatic Field Separator, S-IVB Hydrogen Tank

Figure 4-4 depicts the gaseous channel pressure drop, Δp_g , determined as a function of vapor mass flow rate. Also tabulated in Figure 4-4 is the correction factor $(\phi_{gtt})^2$ to be applied as follows to obtain Δp_{TPF} , the two-phase flow pressure drop.

$$\Delta p_{TPF} = \Delta p_g (\phi_{gtt})^2 \quad (16)$$

Figure 4-5 depicts the required voltage between electrodes as a function of vent inlet flow rate at various qualities. This series of calculations was made for the smallest Faraday gap of 0.01 foot. Also shown in this figure is an insert graph of electrode voltage required as a function of fluid quality at a fixed vapor flow rate of 0.35 lb/sec.

The pressure drops and resultant required voltages as calculated are extremely conservative because the inlet fluid quality was assumed to remain constant during the entire residence time in the Faraday gap flow channel. The actual average fluid qualities would be higher and, consequently, the pressure drops would be lower than these.

The components of the final S-IVB separator selected for the comparison of predesigns in Section 7 are described below.

- a. Seventeen electrodes of aluminum wire screen with 0.001-foot diameter wire, 0.01-foot symmetric wire-mesh spacing, and Faraday gap of 0.01 foot, weighing 13 pounds.
- b. The outside shell, which is basically a 4-foot diameter by 4-foot high aluminum cylinder of approximately 0.050-inch thickness. The shell, stiffeners, and electrode supports would weigh approximately 130 pounds.
- c. High-voltage (550,000 volts ac across the electrodes) power supply hardware with a power output and a weight of approximately 400 watts and 60 pounds.
- d. A reversing pump with electric motor drive, weighing about 3 pounds.
- e. A modulating vent valve and shutoff valve, weighing about 6 and 4 pounds respectively.
- f. A liquid or mass sensing device to determine minimum and maximum liquid levels in the separator tank, estimated to weigh 10 pounds.
- g. Batteries and an inverter for primary power supply.

The separators for the Cryogenic Service Module hydrogen and oxygen tanks were chosen to be identical in size, resulting in a slightly greater design acceleration for the oxygen separator than the $5 \times 10^{-4} g_0$ level used for the hydrogen separator. A single Faraday gap size of 0.01 foot was used in the calculations. The components of the final separator selected for the comparison of predesigns in Section 7 are described below.

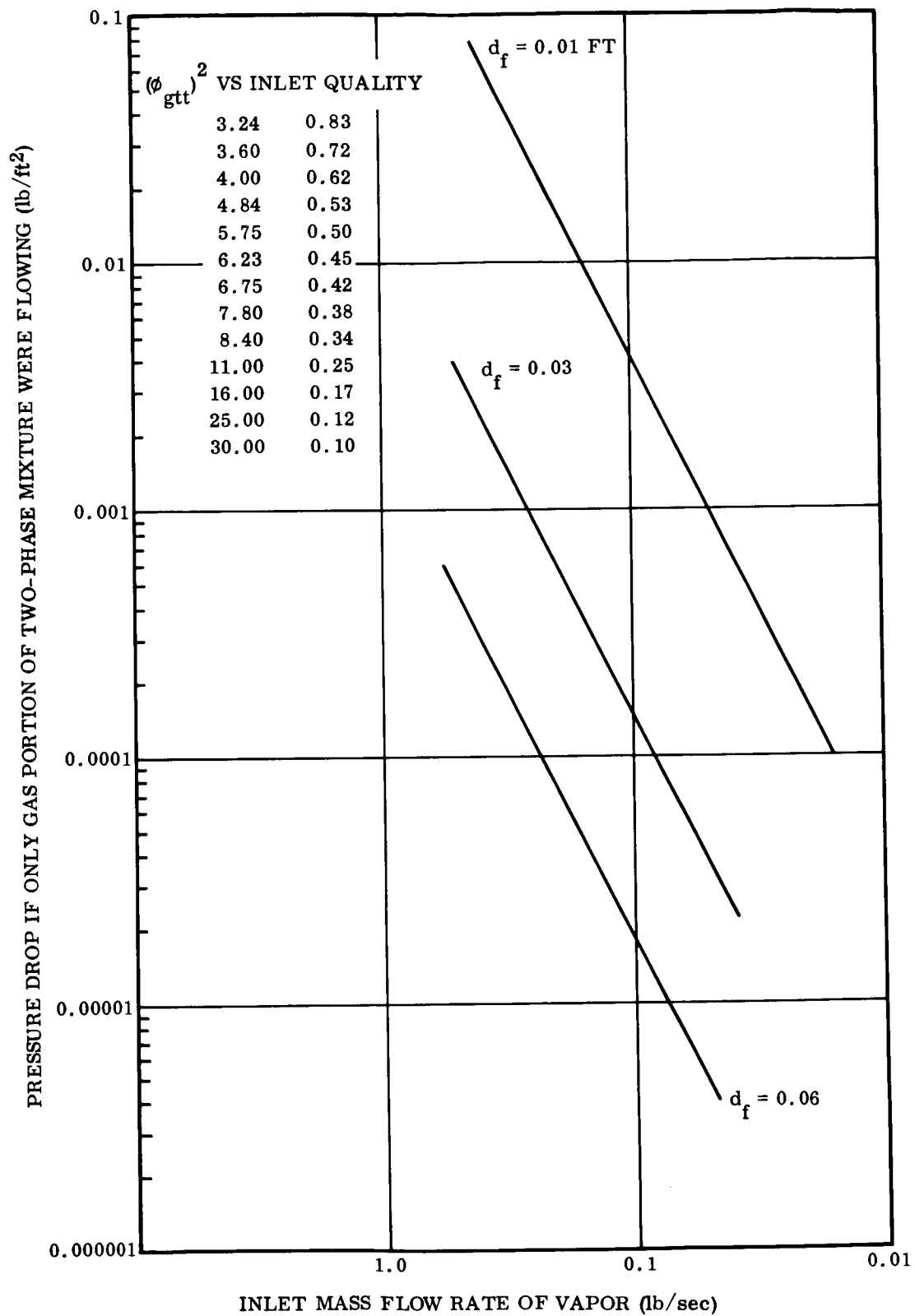


Figure 4-4. Pressure Drop in Passages Versus Mass Flow Rate (Pure Vapor Flow), S-IVB Hydrogen Tank Dielectrophoretic Separator

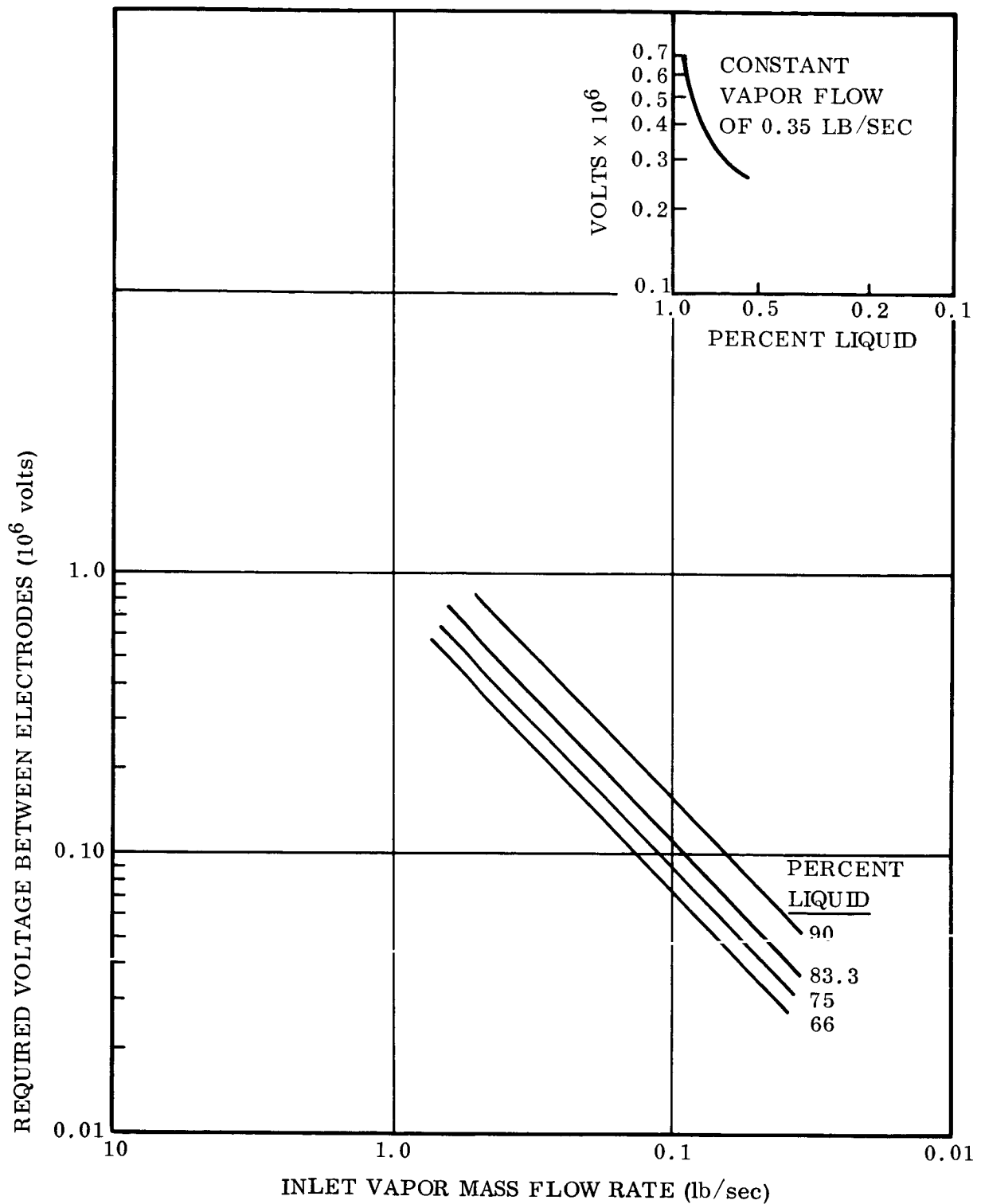


Figure 4-5. Required Voltage Between Electrodes Versus Inlet Vapor Flow Rate Into Separator for Various Inlet Qualities (Faraday Gap = 0.01 ft), S-IVB Hydrogen Tank Dielectrophoretic Separator

- a. Five electrodes, each made of a pair of aluminum wire screens of 0.001-foot wire diameter with 0.01-foot symmetrical mesh spacing, a Faraday gap of 0.01 foot, and 0.2-foot spacing between successive electrodes, weighing about 0.5 pounds.
- b. An aluminum cylindrical outer shell 1.5-foot diameter by 1.3-foot height by 0.050-inch wall thickness. The shell, stiffeners, and electrode supports would weigh approximately 12.6 pounds.
- c. High-voltage power supply hardware supplying 20 watts power at 56,000 volts ac for the hydrogen tank and 4 watts at 21,000 volts ac for the oxygen tank, weighing about 10 pounds.
- d. A reversing pump with electric motor drive, about 2 pounds.
- e. Valves weighing 3.3 pounds.
- f. A mass-sensing device, estimated to weight 5 pounds.
- g. Primary power supply, batteries or additional fuel cell weight.

Figure 4-6 shows one of the separators for the CSM.

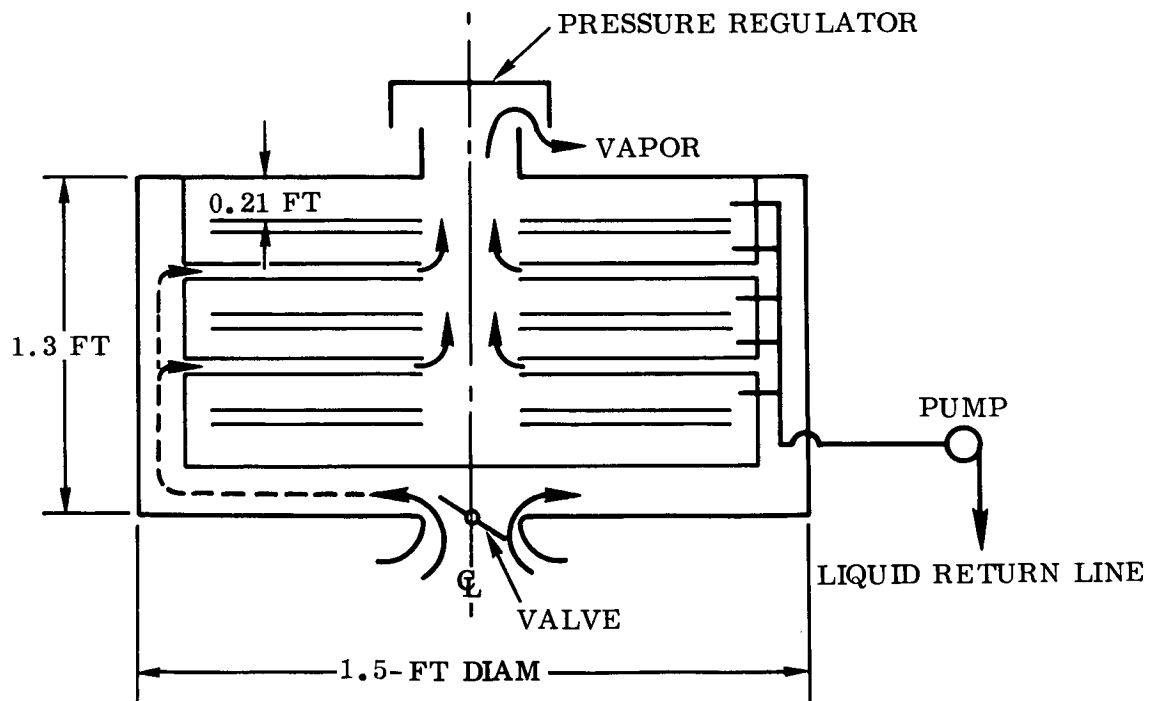


Figure 4-6. Electrostatic Field Separator, Cryogenic Service Module Hydrogen and Oxygen Tanks

4.3.4 General Discussion Applying to All Three Separators

4.3.4.1 Assumptions Underlying Function. The separation devices are almost identical in all respects to the total fluid control systems in that capacitance type electrodes are used and an electrostatic field force is applied to hold a given amount of liquid between the electrodes. However, the separation devices depend upon removing liquid and allowing only vapor to pass through the electrode Faraday gap of all the alternate (ground) electrodes. This action has been observed in experiments conducted by Dynatech on total ullage control. It is the assumption that successful "stripping" action and the attendant efficiency of separation upon which attainment of function rests are possible. There are no known experimental data on the separation efficiency for such a device. It seems not unreasonable to assume that workable stripping efficiencies can be attained if the Faraday gap is maintained small, of the order of 0.01 to 0.03 foot, and sufficient contact area is provided.

4.3.4.2 Assumptions Underlying Design. All comments previously made in Paragraph 4.3.2 apply. In addition, information and data are needed on the required contact area for liquid/vapor separation as a function of the significant variables. Also, a better basis of estimating two-phase pressure loss characteristics in porous-walled channels with mass outflow through the walls is needed. Both of these areas would require experimental tests.

4.4 FAILURES IN DIELECTROPHORETIC SYSTEMS. The following is a discussion of some typical failures that may occur in the dielectrophoretic devices. These arguments and failures apply both to total-tank-liquid control systems and to dielectrophoretic separators located within a tank.

- a. Vapor phases generally have a lower voltage breakdown level than liquid phases of cryogenic fluids. During operation, the liquid/vapor separator devices will have vapor bubbles located throughout the electrode system. Of major concern are bubbles that may lodge between a high-potential electrode and the grounded tank wall. This gap between a high potential electrode and tank-wall ground is a potential electrical-short region. The problem of shorts in this region can be avoided by proper design, allowing a gap between the ground wall and the high-potential electrode large enough that the field strength is very much less than the minimum value of voltage breakdown for the vapor. For instance, in total-fluid control systems discussed in this report, the highest voltage considered is approximately 700 kv. The minimum breakdown voltage for gaseous hydrogen is 6000 kv/foot. Therefore, if the minimum distance between a high-voltage electrode and a ground surface is kept significantly above 0.12 foot, there should be no electrical shorts without a structural failure.
- b. Structural failure of electrodes and/or electrode supports could produce shorts with attendant arcing. In the case of sparking in a hydrogen tank, combustion is precluded by the absence of oxidizer. In the event of electrode shorting in oxygen

tanks, however, there is the possibility of starting a combustion reaction between the oxygen and metal components in the tank. Proper circuit design could allow for an almost instantaneous power shutoff upon the occurrence of a short. However, the system is not functionally fail safe; i. e. , after such an abort the system would no longer separate liquid from vapor and venting would have to be accomplished with the possibility that some liquid would be vented.

- c. An adverse acceleration above the design value might completely empty some of the storage regions between the electrodes and result in liquid venting and possible termination of operation because the emptied spaces may not refill with liquid.
- d. A failure of the pump and/or motor would terminate successful separation, since it is necessary to pump liquid from the separator storage regions to keep them from filling completely.

SECTION 5

VENTING BY MEANS OF SURFACE TENSION

5.1 INTRODUCTION. The use of surface tension for control of the liquid/vapor interface of propellant in a tank under a condition of weightlessness has been proposed or considered by many writers.

In the late 1950's, when development was begun on upper stages requiring engine restarts after periods of orbital coast, practically nothing was known about the behavior or control of fluids under very low accelerations. Dr. Ta Li, at that time in the Convair research laboratories, predicted analytically that the stable zero-g configuration for a two-phase wetting fluid in a spherical tank with no external heat transfer would be a spherical annulus of liquid with the vapor ullage at the center, the configuration for which the surface free energy is a minimum. Since that time, his analysis has been extended to other fluids and more complicated configurations, and its validity has been verified by several experimental programs (Reference 5-1 through 5-7).

Reynolds, et al, (Reference 5-4) has published a good summary of basic information about liquid/vapor interfaces, particularly in low-g environments. Some of the topics included are a basic review of capillary thermodynamics and mechanics, a summary of current knowledge relating to the configuration and stability of capillary systems, and a discussion of experimental simulation of low-gravity environments. The USAF has published a number of reports dealing with expulsion, containment, and venting systems for low-gravity applications (References 5-8 through 5-10); however, this work is primarily devoted to systems using storable rather than cryogenic propellants. Otto, Masica, Petrash, and Siegert have collaborated on a number of papers describing their experimental work on liquid/vapor interface configurations, interface stability, and transient behavior under various gravitational acceleration levels (References 5-2, 5-3, 5-7, 5-11 through 5-17). Hall (Reference 5-18) presents a design concept for a controlled-ullage tank making use of porous materials. Clodfelter (Reference 5-5) and Wallner (Reference 5-19) present both experimental and analytical results relating to liquid/vapor interface configuration and control. A number of other reports are listed in the bibliography, although those listed above are considered to be of greater significance. Essentially all of the references reviewed during this study were concerned exclusively with the concept of fluid orientation by means of baffles or screens, rather than the possible use of the surface tension phenomenon to devise a smaller separator device.

The remainder of Paragraph 5.1 will be devoted to a brief review of the concept of surface tension; Paragraphs 5.2 and 5.3 will then discuss applications of the concept to the venting problem.

It has been observed that the surface of a liquid always tends to contract to the smallest possible area. Drops of liquid in a gas or bubbles of gas in a liquid become spherical, the geometry for which the surface area per unit volume is a minimum. To increase the surface area it is necessary to do work to bring molecules from the bulk of the liquid to the surface against the inward attractive force; the work required to increase the area by unit amount is called the free surface energy. The tendency for a liquid to contract may be regarded as a consequence of its possession of free energy, since approach to equilibrium is always accompanied by a decrease in free energy. As a result of this tendency to contract, a surface behaves as if it were in a state of tension, and it is possible to ascribe a definite value to this surface tension, which is the same at every point and in all directions along the surface of the liquid. It may be defined as the force acting at right angles to any line of unit length in the surface. The work done in extending the area of a surface by unit amount is equal to the surface tension multiplied by the unit distance through which the point of application of the force is moved. It follows, therefore, that the surface energy is numerically equal to the surface tension. Although the surface energy is probably to be regarded as the fundamental property of a surface, it is often convenient, for purposes of calculation, to replace it by the surface tension; the equivalence of the two quantities makes this justifiable.

A consequence of the surface free energy is that the pressure on the concave side of a liquid meniscus is greater than that on the convex side. This excess pressure is equal to $2\sigma/r$ for a spherical surface, where σ is the surface tension and r the radius of curvature of the meniscus. The familiar result that the liquid level in a small capillary tube immersed in the liquid is different from that of the main liquid is caused by this excess pressure on the concave side of the liquid meniscus.

5.2 VENTING BY MEANS OF TOTAL FLUID ORIENTATION. The first application of surface tension to the problem of vapor venting in this study was to consider total orientation of the liquid in a tank. This might be possible by installing baffles or other surfaces within the tank to allow the surface tension forces to maintain stable interfaces between the liquid and vapor regions, permitting simple venting from the vapor space.

The Bond Number Criterion has been established as a valid one for predicting regions of hydrostatic stability of surface tension dominated configurations (References 5-14 and 5-15). This criterion for a contact angle of 0 degrees (liquid hydrogen has a zero contact angle with practical structural metals, References 5-20 and 5-21) and a cylindrical container is:

$$\frac{(\rho_L - \rho_V) a r^2}{\sigma} \leq N_{BC} \quad (1)$$

(where ρ_L and ρ_V are the densities of liquid and vapor, a is the acceleration, r is the radius of the cylinder, σ is the surface tension, and N_{BC} is a critical Bond number, the value of which must be experimentally determined, for the liquid/vapor interface

to be stable. Application of this equation to liquid hydrogen in a 260-inch-diameter tank gives a critical vehicle axial acceleration, for $N_{BC} = 0.84$, of $2.3 \times 10^{-7} g_0$. Therefore, according to the Bond Number Criterion, the vapor/liquid interface will be unstable for any acceleration above this value. The analysis required to determine multiple baffle configurations and spacings in a tank to allow the surface tension forces to hold the liquid in place is more complex than the preceding application of the Bond Number Criterion to a single cylinder; however, this example serves to illustrate the general effect of acceleration and geometry upon the stability of an interface. It is obvious that numerous baffles must be used in a large tank to reduce the dimensions of an individual interface to permit even moderate adverse accelerations to be tolerated.

It was found that the multiple concentric cylinder or concentric cone configurations conceptually proposed by some writers on the subject were not feasible for tanks of the size range considered in this study because of the rapidly decreasing allowable gap between rings as the diameter increases. For example, the maximum allowable gap between successive concentric cones for which surface tension can maintain a stable liquid/vapor interface is approximated by the following equation.

$$b = \frac{4\sigma}{\pi a \rho_L r_i} \quad (2)$$

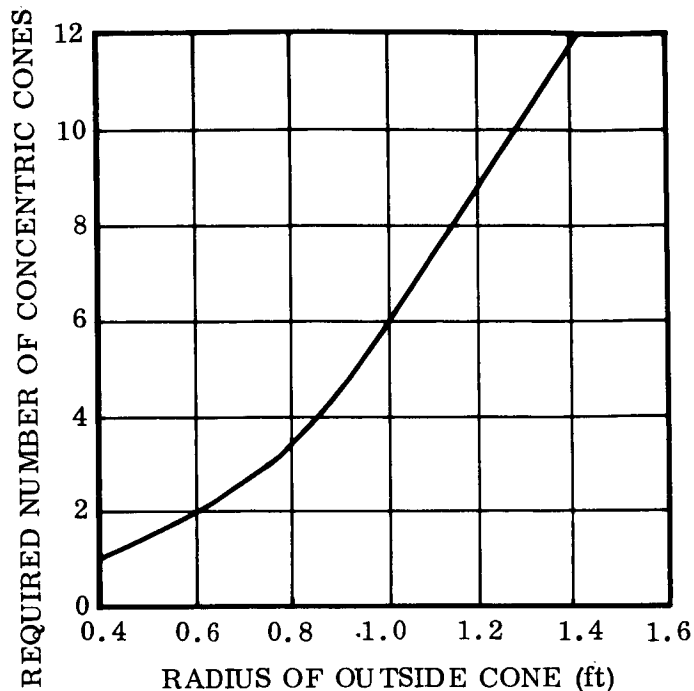
where b is the maximum allowable gap between the cone of radius r_i and the next-larger cone, and a is the disturbing acceleration perpendicular to the axis of the cones. The maximum allowable diameter of a single cone of half-angle B is approximately (Reference 5-10)

$$D = \left[\frac{8\sigma (\cos B + 0.26)}{a \rho_L} \right]^{1/2} \quad (3)$$

Applying these equations to liquid hydrogen with a disturbing acceleration of $5 \times 10^{-4} g_0$ gives the results shown in the sketch on the next page for the number of cones required to orient LH₂ versus outside cone radius at the open end.

From inspection, it can be seen that a very large number of cones would be required to orient liquid hydrogen in a large tank.

Several other geometries were considered; e.g., a tube bundle or a honeycomb structure, but the weights were also prohibitively high. Therefore, it was concluded that hydrogen venting by total fluid orientation is not promising in comparison with many of the other venting methods.



5.3 SEPARATORS

5.3.1 General Description. Attention was next given to vapor/liquid separators in a more conventional sense than the total fluid orientation concept. The most promising of several separator types considered is represented by the schematic diagram of Figure 5-1. A similar type of separator was suggested by Hall (Reference 5-18); however, he was interested in obtaining a pure liquid stream rather than pure vapor as here. In operation, the two-phase inlet stream shown in Figure 5-1 is introduced to a tube or passageway that has porous walls made of, e.g., a sintered metal or ceramic material. A wetting fluid such as liquid oxygen

or hydrogen will tend to wet and eventually fill the pores of a porous material with which it comes in contact; therefore, it should be possible to build a porous tube separator to give any desired degree of liquid/vapor separation by making the separator sufficiently large. In order to have liquid flow through the tube wall, it is necessary to maintain the pressure outside the tube wall less than that inside the tube; however, the difference must not exceed the capillary head, roughly $2\sigma/r$, where σ is the liquid surface tension and r is the effective radius of the largest capillary, or there might be vapor flow through the wall. The actual maximum permissible pressure difference across the wall would have to be determined experimentally, since a sintered metal or similar material has pores with neither constant size nor circular cross section, in general. As an approximation for the predesigns, an idealized model of the porous wall was used in which the pores were assumed to have constant area, circular cross sections.

The liquid that has passed through the porous wall, now at a lower pressure than the tank contents, must be pumped back into the tank. The pump shown does this.

A further consideration in the design for cryogenic fluids, which would be at their boiling points within the tank and, therefore, at the separator inlet, is that some cooling of the liquid passing through the porous walls would be needed to prevent partial vaporization and the possibility of a vapor breakthrough. This subcooled condition could be provided by throttling the vent stream to a lower pressure after passing through the porous tube section and then using the fluid to cool the porous wall or liquid, as was done in these predesigns generated for the comparisons. It was found necessary to have some liquid left in the stream leaving the porous tube in order to have sufficient heat capacity to cool the liquid outside the tube to its saturation temperature. This had the helpful

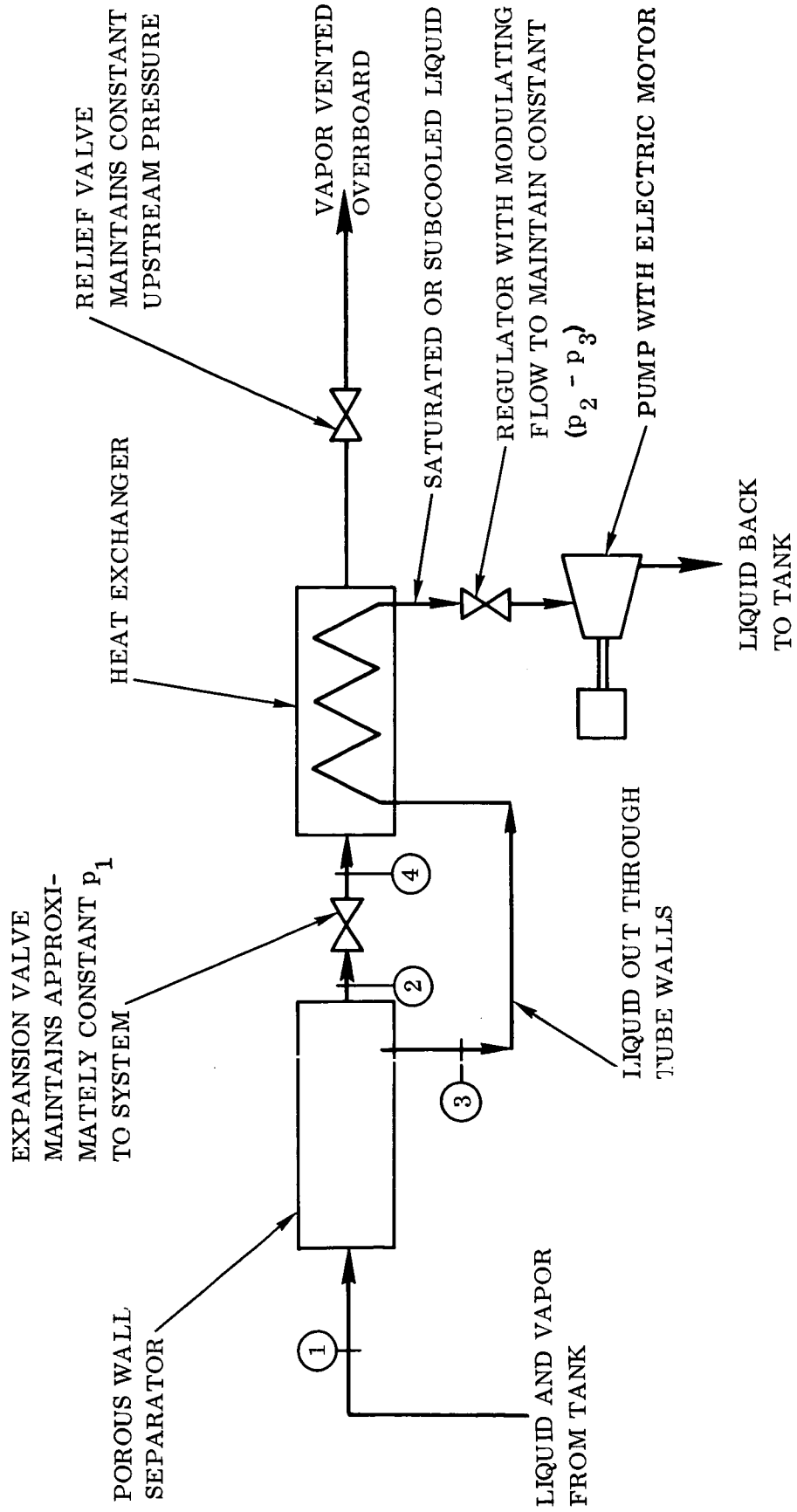


Figure 1-1. Schematic Diagram of Surface Tension Separator System

effect, however, of lowering the porous tube area required for liquid stripping. It might be found, in a development program, that the assumption that no vapor can be allowed outside the tube could be relaxed, but this would require experimental justification.

There is a trade-off in selecting the porous material for a separator. Very small pores are desirable to increase the maximum allowable pressure difference across the wall; e.g., for an idealized 5-micron hole and liquid hydrogen the capillary head, $4\sigma/D$, is 0.17 psia. On the other hand, the resistance to flow through the pores increases much faster than does the allowable pressure difference as the pore size is decreased, causing a net increase in the required wall area with a decrease in pore size. Therefore, the pressure difference across the wall should be as small as required for control purposes. The maximum pore size for a hydrogen separator should be no greater than about 5 microns to have a workable pressure difference.

Considerable study was made of the available materials from which a porous tube could be fabricated. Ceramics were judged to be much less desirable than metals because of strength, brittleness, and fabrication problems. Some of the available metal materials are listed below. Perforated Products makes fine-mesh foils with minimum hole size of $15 \pm 2 \frac{1}{2}$ microns. Huyck Corporation manufactures a sintered-type porous metal called Feltmetal in which there is a considerable range of effective pore sizes; their smallest pore sizes presently available have average pore size of 4 microns (but the 99-percentile pore-volume range extends up to 30 microns). General Electric Company manufactures "foametal" with smallest mean pore size in the 14-micron range. Buckbee Mears Company makes a perforated foil with sizes down to 5 ± 2 micron nominal size. Unique Wire Weaving Company makes a "micronic cloth with nominal rating of 3 to 5 microns." Therefore, porous metal materials with pore sizes approaching 5 microns are already available.

5.3.2 Calculations and Results. As discussed in Paragraph 5.3.1, the pressure difference across the porous wall of the separator passage should be as small as control requirements will allow to minimize the required porous tube area and total separator weight. If a pressure difference of about 0.2 psia is used as this minimum, the required porous material is slightly beyond the present state-of-the-art. However, a sintered-metal material was postulated with the following properties, based upon moderate extrapolation of existing sintered-material properties: (a) maximum effective pore diameter of 5 microns for determining the capillary head, (b) an average effective pore diameter of 2 microns for determining flow rates through the wall, and (c) a permeability with liquid hydrogen of 0.95×10^{-10} inch² (estimated from permeability data for air and water flowing through existing sintered metals). Further, the separator porous walls were assumed to be fabricated of 0.030-inch-thick, 70-percent-dense titanium sheet material.

The quality of the inlet stream from the tank to the separator, Station 1 on the schematic diagram of Figure 5-1, was assumed to be 0.1 for the S-IVB and 0.00138 for the CSM. The maximum separator exit quality, at Station 2 of Figure 5-1, was determined in each case by the required heat load to maintain the liquid stream, Station 3, at or below the saturation temperature. The pressure at Station 4 was set at 2 psia in all cases.

The maximum allowable pressure difference across the porous wall, the capillary head $4\sigma/D$, was calculated to be 0.17 psia for the 5-micron effective maximum pore size and liquid hydrogen. The theoretical required superficial tube wall area for liquid flow to remove enough liquid from the inlet stream to increase its quality from the 0.1 at inlet to the required outlet quality, was estimated from the Darcey equation:

$$A_t = \frac{\mu Q L}{K \Delta p} \quad (4)$$

where L is the porous wall thickness, K the permeability of the wall, A_t the theoretical superficial tube area, μ the liquid viscosity, Q the volumetric flow rate, and Δp the pressure difference across the wall.

The actual porous wall area required would be much higher than the theoretical area calculated above. Experimental data would be necessary to accurately estimate the stripping efficiency of a porous wall passageway. Since no such data are available, the total porous wall area required was estimated based on a model of the actual stripping process for which the ratio of superficial tube area through which liquid is flowing to the total superficial tube area in an infinitesimal length of the passage is equal to the volume fraction of liquid at that station in the tube.

$$\frac{A_t}{A} = 1 - Y \quad (5)$$

This can be developed to give

$$A = A_t \ln \left(\frac{1 - Y_1}{1 - Y_2} \right) \quad (6)$$

which permits estimation of the total required porous wall area from the theoretical area calculated from Equation 4 and the inlet and exit qualities of the vent stream.

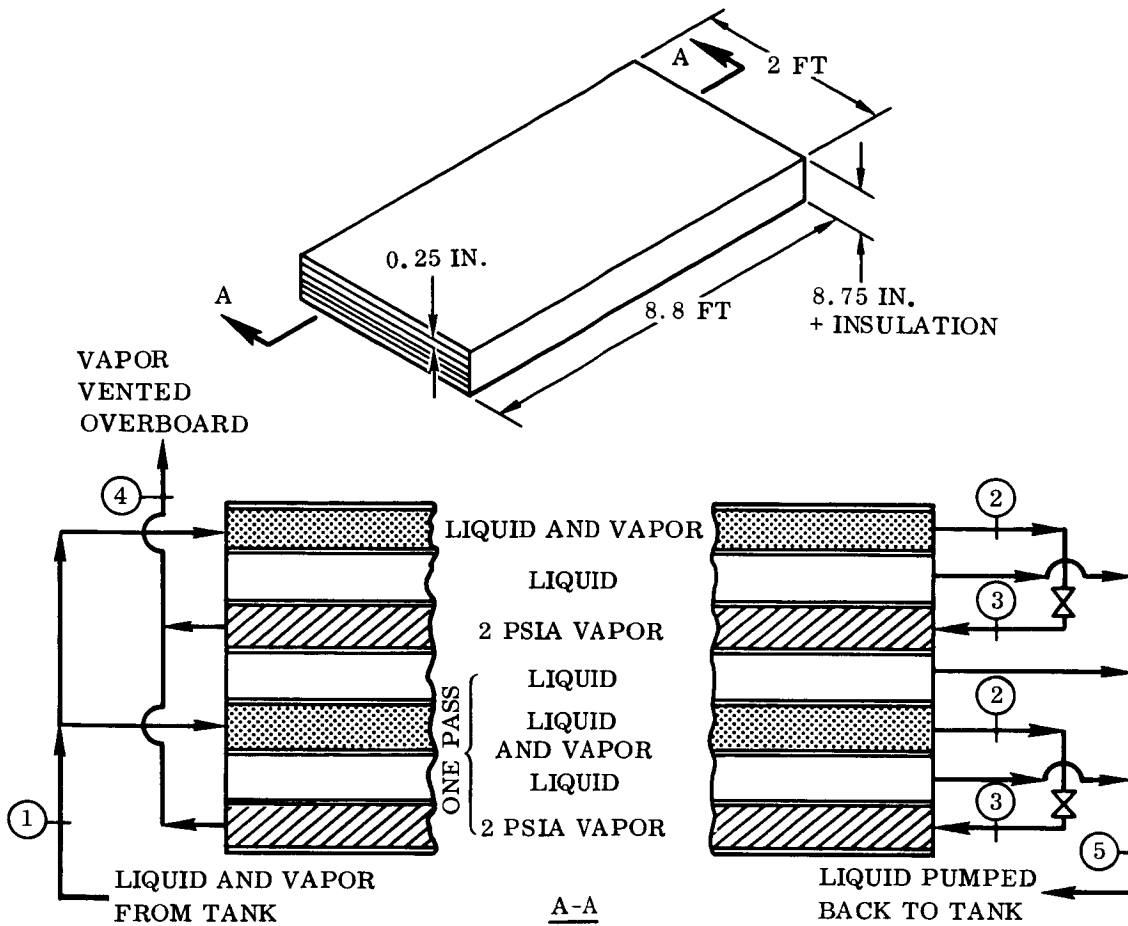
The required area for heat transfer between the liquid outside the porous tube and the vent fluid after expansion was calculated by standard means.

A number of configurations of the flow passages were considered. A rectangular, multiple-pass arrangement gave the best combination of flexibility in choosing porous wall, heat transfer, and flow cross-sectional areas, although header design would be difficult.

The final predesigns for the three vehicle-mission cases are summarized in Figures 5-2 and 5-3.

The principal uncertainties in the predesigns are:

- a. What separation efficiency can be obtained in the porous tube as a function of tube material and geometry, fluid properties, flow rate, etc.? This efficiency would have to be determined experimentally in an actual design/development study. For the present, an approximate analysis was made to estimate the ratio of tube area required for this stripping action to that required for flow of the liquid in the inlet stream across the wall under the available pressure difference.
- b. Can the assumed constraint that the outside of the tube wall must be kept free from vapor be relaxed? Again, this would have to be determined experimentally. It may well be possible to have some nominal degree of vapor flow through the wall, but this cannot be estimated analytically.
- c. Can the control problems be solved satisfactorily? This is of particular concern in controlling the pressure difference across the porous wall and would have to be answered with experimental results.
- d. What is the actual permissible pressure differential across the porous wall? It would likely be less than the capillary head calculated for a smooth cylindrical pore, but actual numbers would have to be obtained experimentally for each material of interest.



DESIGN OPERATING CONDITIONS (FOR MAXIMUM VENT RATE)

STATION NO.	\dot{m} (lb/hr)	X	T ($^{\circ}$ R)	P (psia)	COMMENTS
1	6700	0.10	38.4	20	—
2	656	0.95	38.4	~ 20	—
3	656	~ 1.0	~ 31.5	2	—
4	656	1.0	~ 36	2	SUPERHEATED VAPOR
5	6044	0.0	38.34	19.83	SAT. LIQUID

SEPARATOR HAS 8 PASSES

MAX. REQUIRED POWER INPUT TO PUMP MOTOR = 210 WATTS

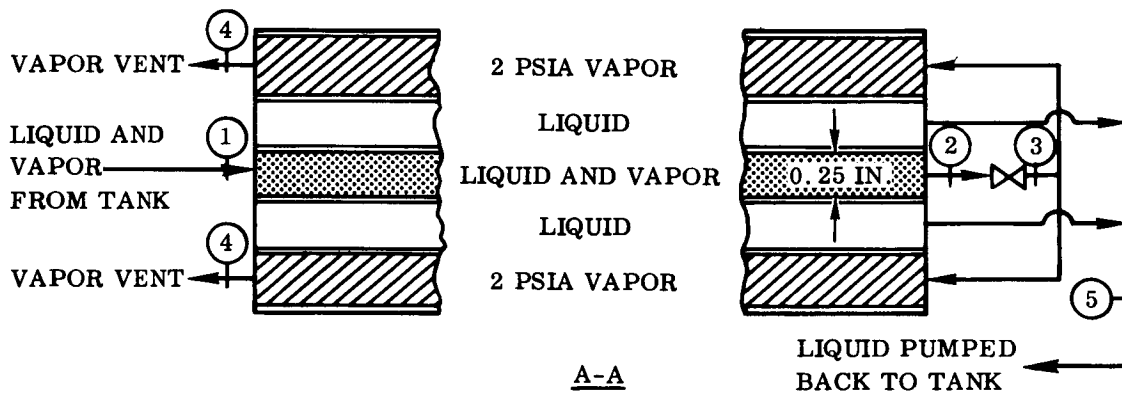
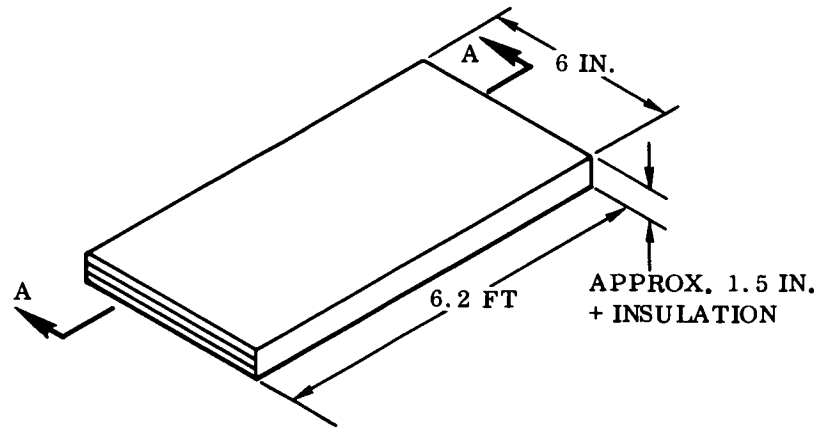
AVG. REQ'D POWER INPUT TO PUMP MOTOR = 153 WATTS

AVG. CHANGE IN BOILOFF RATE FROM BASE CASE OF 667 LB/HR OF 20 PSIA

SATURATED VAPOR = - 5.9 LB/HR

TOTAL SYSTEM WEIGHT (WITHOUT PUMP, VALVES, OR POWER SUPPLY) = 182 LB

Figure 5-2. Summary of Surface Tension Separator Predesign for Mission/Vehicle Cases I and II



DESIGN OPERATING CONDITIONS (FOR MAXIMUM VENT RATE)

STATION NO.	\dot{m} (lb/hr)	X	T ($^{\circ}$ R)	P (psia)	COMMENTS
1	725	0.00138	38.4	20	—
2	1.196	0.65	38.4	~ 20	—
3	1.196	~0.76	~ 27	2	—
4	1.196	1.0	~ 37	2	SUPERHEATED VAPOR
5	723.8	0.0	38.34	19.83	SAT. LIQUID

SEPARATOR HAS 1 PASS

MAX. REQUIRED POWER INPUT TO PUMP MOTOR = 12.9 WATTS

AVG. REQUIRED POWER INPUT TO PUMP MOTOR = 9.2 WATTS

AVG. CHANGE IN BOILOFF RATE FROM BASE CASE OF 0.5 LB/HR

OF 20 PSIA SATURATED VAPOR = + 0.145 LB/HR

TOTAL SYSTEM WEIGHT (W/O PUMP, VALVES OR POWER SUPPLY) = 16.5 LB

Figure 5-3. Summary of Surface Tension Separator for Mission/Vehicle Case III

SECTION 6

OTHER SEPARATION METHODS

A number of other separation concepts might be considered in addition to those previously discussed in Sections 2 through 5. Several of these considered during the study, but not studied in detail or included in the comparisons of Section 7, are briefly described in this section.

6.1 FLUID ROTATION. This concept considers the rotation or vortexing of part of the fluid in a storage tank, rather than rotation of the entire tank and contents, which has also been proposed as a solution to the venting problem. The latter method would be relatively undesirable because of the effects upon vehicle control, the long time intervals apparently required for start-up and shutdown, even with baffles, and the possible adverse effects on personnel.

Consider the rotation of fluid in a cylindrical chamber, as sketched in Figure 6-1, such that the fluid motion describes a helical path on the inner wall of the chamber. This motion could be established by pumping fluid tangentially into a cylindrical chamber having an annular exit for the liquid at one end of the chamber and a core vent for the gas at the other end of the chamber. An alternate configuration that would have the potential of operating even with zero inlet quality fluid would be identical to that shown in Figure 6-1 except for relocating the pump in the liquid return line. In this case, the chamber pressure would be maintained low enough to both flash part of the fluid (e.g., zero-quality, 20-psia fluid expanded to 5 psia at constant enthalpy would have a quality of about 0.05) and produce the velocity needed for separation.

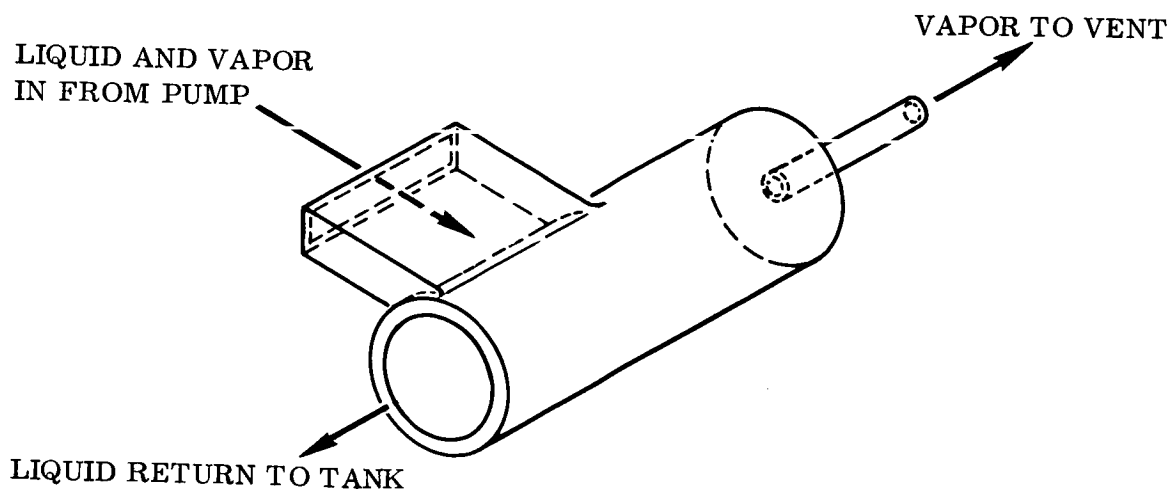


Figure 6-1. Vortex Tube Vapor/Liquid Separator Concept

A brief analysis of such a device as a vapor/liquid separator was made, based on several assumptions: (a) the elemental flow cross-sectional normal to the path of the helix is assumed to be rectangular with area ratio of two; (b) the required cross section of the core is estimated from the vent flow rate (but would need to be determined experimentally); (c) the fluid is pumped using a motor/pump combination having an efficiency of 0.6; and (d) only two 360-degree vortices are required for separation (experimental results are required to establish the actual requirements). Parametric results for the estimated required pump input power versus diameter of the vortex chamber are shown in Figure 6-2 for two inlet fluid qualities to the system, $X = 0$ and 0.1 , and two locations of the pump, at the inlet to the system and in the liquid return line. For the latter pump location, the chamber pressure is set at 5 psia to flash part of the incoming fluid and give the possibility of operation even with zero inlet quality. The configuration with the pump at the inlet could not operate with zero quality inlet unless it were modified to have a reduced chamber pressure, also.

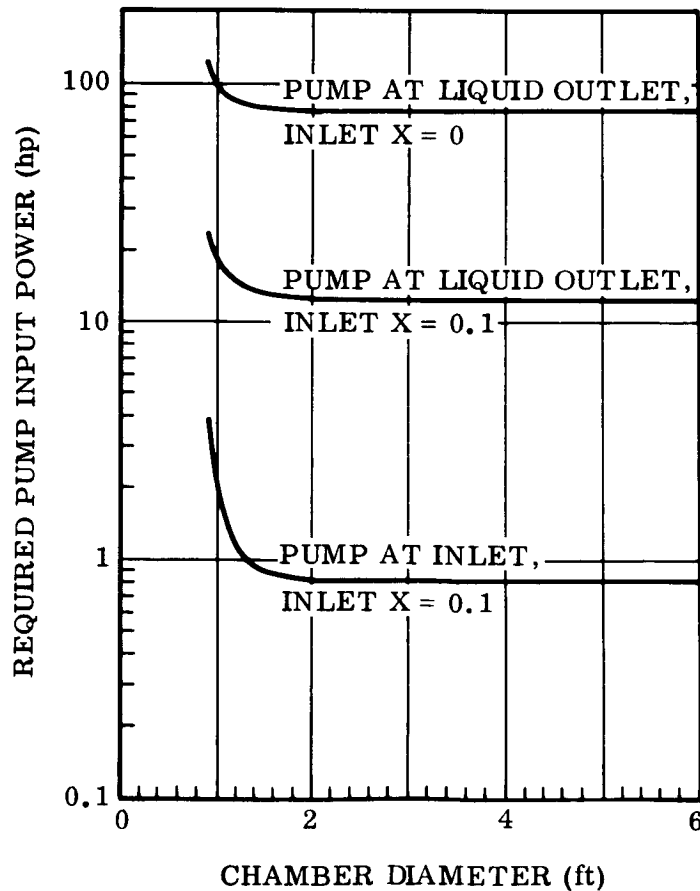


Figure 6-2. Required Pump Input Power Versus Chamber Diameter for Vortex Tube Vapor/Liquid Separator

It can be observed from Figure 6-2 that the power requirements for the two cases with the pump located at the liquid outlet are high, with the assumed chamber pressure of 5 psia. The required power could be reduced by increasing the chamber pressure, but this increase would eventually restrict the operation with zero quality inlet fluid. The required power for units with the pump at the inlet is moderate with the assumptions implicit in the bottom curve of Figure 6-2; however, since these cannot operate with zero quality inlet they cannot be directly compared with those represented by the top curve. The power requirement for the inlet pump configuration would be always higher than that for the liquid outlet pump configuration if both expanded the incoming fluid across the same pressure difference in order to permit design for zero quality inlet fluid.

This concept would be an attractive one if experimental work could satisfactorily resolve the unknowns such as: required chamber size and geometry for separation, actual power requirements for given chamber and fluid conditions, and the question of how to control the system, especially with changes in inlet quality (note, e.g., that the mass flow rate of liquid hydrogen through a fixed restriction is about seven times as high as that for gaseous hydrogen). The system would be a relatively simple one, if it could be developed to work and operate without requiring complex controls. Although this system was not considered until late in the study, it seems to warrant further work, including exploratory tests which could initially be done with wet steam. Additional study of this concept is continuing.

6.2 HYDROGEN SUBLIMATOR. One of the separation concepts considered was the "hydrogen sublimator," which would be similar to the porous plate water sublimators or boilers that are under development for cooling of electronic equipment and might properly be considered as merely a variation on the heat exchange concept already discussed in Section 2. Although it was concluded that this concept is not attractive with hydrogen as a fluid and with present knowledge, brief descriptions of the method and critique are given below.

The theorized sublimator device would consist of a porous wall exposed on one surface (internal to the tank) to tank fluid and on the other to a pressure below the triple-point pressure of hydrogen. The operation might proceed as follows, borrowing from the description of the operation of the water sublimator given in Reference 6-1, although the actual mechanism of operation of the water sublimator has not yet been determined (Reference 6-2). Hydrogen would flow partially through the porous plate until it drops below the triple-point pressure and freezes. By circulating tank fluid along the inner surface of the porous tube, which would have a reduced temperature due to the cooling within the wall, heat could be removed from the bulk fluid. This heat would then be transferred through the wall and result in propellant sublimation at the external surface. Circulation of the tank fluid could be accomplished with a simple pump.

The potential advantages claimed for the water sublimator as compared with a conventional plate and fin water boiler are primarily that the sublimator system: (a) requires fewer controls, and (b) has a lower total system weight effect, but perhaps higher

hardware weight, than a conventional boiler system (References 6-1 and 6-3). However, the controls required for a hydrogen sublimator venting system would seem to be more complex than those needed for a plate and fin exchanger. The sublimator system would have to include shutoff and flow modulating valves to shut off the device on the ground and to regulate the vent flow to maintain the desired tank pressure band. Also, there would probably have to be very precise control of the pressure difference across the porous wall during system start-up to build up the required solid hydrogen plug. If the pressure difference across the porous wall exceeded the capillary head, there could be vapor blow-through and a stable plug might never be established. This capillary head, as discussed in Section 5, is very small for hydrogen; e.g., a 5-micron hole with circular cross section could not support a head of greater than 0.17 psia. A porous material with maximum pore size of 5 microns is beyond the present state of the art. The potential advantage of lower total system weight for the sublimator system as compared with a conventional exchanger does not seem realizable for the hydrogen venting application, either. A weight comparison of water boiler systems that have been developed lists exchanger weights of 48.1 and 35.0 pounds for the porous plate and plate-and-fin (P/F) exchangers respectively (Reference 6-1). The total water boiler system weight listed for the porous plate system was smaller than for the P/F system, but only because of the greater water carryover allowance required for the latter system. There is no analogous requirement in the present hydrogen venting system; therefore, it is concluded that a porous wall exchanger would probably be heavier than a comparable plate-and-fin exchanger as described in Section 2.

In summary, there were found no advantages and several disadvantages of the hydrogen sublimator as compared with the "conventional" heat exchange system of Section 2. Therefore, the sublimator was not included in the comparisons of Section 7.

6.3 MAGNETIC POSITIONING. Magnetostatic systems utilize a magnetic field to produce a force on a liquid volume. A liquid element in a non-uniform magnetic field, whether produced by a permanent magnet or electromagnet, will tend to move to a region of increased field strength if it is a paramagnetic fluid or to a region of decreased field strength if it is a diamagnetic material. This movement of liquids in magnetic fields, sometimes called magnetophoresis, has been used in the design of several instruments for measuring magnetic susceptibility (Reference 6-4).

Reference 5-8 concludes that for the unusual case of liquid oxygen, which is a paramagnetic liquid, a static magnetic field might be considered for propellant localization, but that even for oxygen, the weight penalty prohibits its use for any but very small amounts of propellant. The specific volume magnetic susceptibilities (defined as $S_m = (\epsilon/\epsilon_0) - 1$, where ϵ and ϵ_0 are the magnetic permeabilities of the liquid and of free space respectively) of hydrogen and of oxygen are -1.89×10^{-7} and 2.86×10^{-4} respectively (Reference 5-8). The magnetostrictive pressure exerted on a liquid by a magnetic field is directly proportional to S_m .

Magnetic positioning was, therefore, not included in the venting system comparisons of Section 7.

SECTION 7

COMPARISON OF SEPARATORS

Separator systems representative of each of several separation phenomena have been predesigned for three vehicle/mission cases, as described in Sections 2 through 6. Several of the separation methods initially considered (magnetic positioning, vehicle rotation, hydrogen sublimator, and a vortex tube) were judged to be unsuitable for cryogenic propellants or unattractive relative to the four systems: heat exchange, mechanical, dielectrophoretic, and surface tension separators; therefore, the former group of separators are not included in the comparisons of this section. The ground rules describing each vehicle/mission case are given in Paragraph 7.1, followed by a discussion of the selection criteria and their evaluation in Section 7.2, and, in Section 7.3, the comparison of the predesigned separators and selection of the most promising separator for tank venting.

7.1 DESCRIPTION OF VEHICLE/MISSION CASES. There were three cases used for comparison and evaluation of the separation methods, designated as Cases I, II, and III.

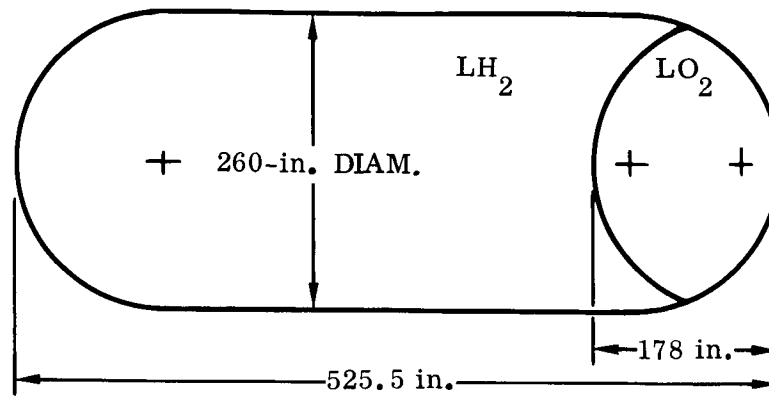
Cases I and II were similar. They both assumed the present S-IVB stage with one 4-1/2-hour coast and the configuration and background information about the stage summarized in Figure 7-1. Case I assumed the further requirements that the separator system should augment the effect of the present settling rockets, which are presently designed to provide a minimum acceleration of $2 \times 10^{-5} g_0$ during the bulk of the 4-1/2-hour coast period, and that it should be relatively simple. Case II, however, had no similar constraints.

Case III was to be a typical multi-restart, relatively small, cryogenic stage with long coast periods. A possible configuration for a Cryogenic Service Module (CSM) configuration was assumed. Its description plus other background assumptions are given in Figure 7-2.

7.2 SELECTION CRITERIA AND THEIR EVALUATION. The criteria selected for the final comparison of separator predesigns are given below.

- a. System hardware weight -- consists of weight of all hardware components such as basic separator, valves, pumps, and power conversion and storage equipment. Ratings are given as equivalent pounds of payload decrease caused by the additional hardware, using the method of calculation presented in Appendix E.
- b. Change in weight of vented propellant -- contains the effects of change in the exit enthalpy of the vented propellant as compared to the base case of saturated vapor at 20 psia, and any additional external energy dissipated in the tank, e.g., power

Sketch of S-IVB tanks



Total volume of hydrogen tank is approximately 10,450 ft³.

Total volume of oxygen tank is approximately 2830 ft³.

Tanks are 70-percent full at start of coast period.

Single 4-1/2-hour coast period.

External heat input is 567,000 Btu during 4-1/2-hour coast.

Nominal tank pressure is 20 psia.

Hydrogen vent rate range is 0.06 to 0.35 lb/sec (0.35 lb/sec used for system sizing).

Design inlet quality to separator system is 0.10.

Maximum disturbing acceleration during coast period is $5 \times 10^{-4} g_0$.

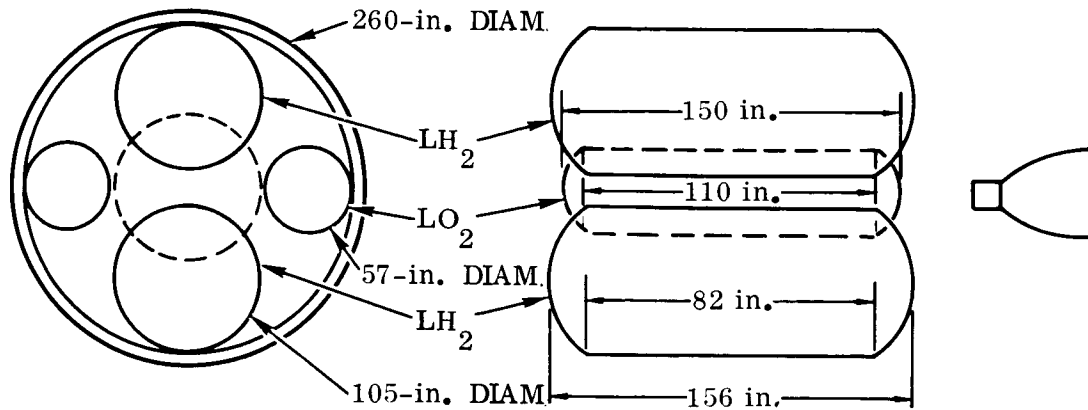
Maximum disturbing acceleration for determining propellant slosh loads is $1.6 \times 10^{-2} g_0$.

No venting of oxygen is required.

Base payload weight is 90,000 pounds.

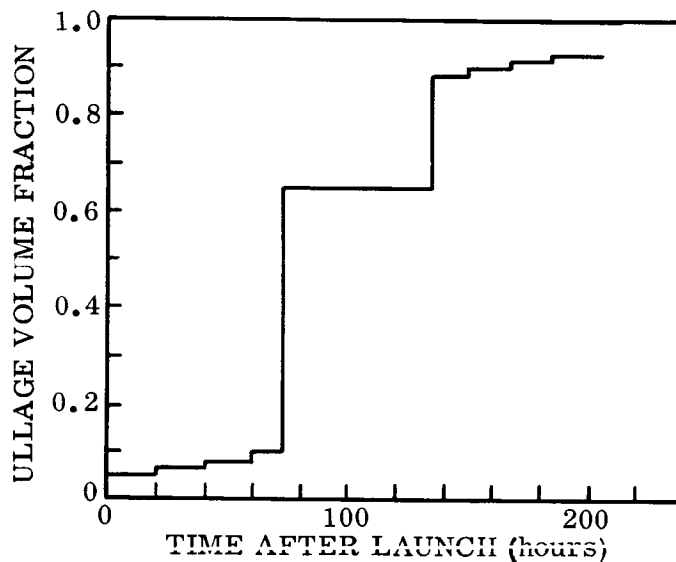
Figure 7-1. Vehicle and Mission Ground Rules Common to Both Cases I and II

Tank sketch



Note that there are two hydrogen tanks, each containing 2500 pounds of hydrogen initially, and two oxygen tanks, each initially containing 12500 pounds of oxygen.

Tanks are 95-percent full at start of 205-hour mission; ullage fraction versus time is shown below.



External heat input is 19,370 Btu to each of the two hydrogen tanks (average rate of 94.5 Btu/hr) and 9225 Btu to each of the two oxygen tanks (average rate of 45 Btu/hr).

Maximum vent rate (used for system sizing) is 1 lb/hr for each of the four tanks.

Nominal tank pressure is 20 psia.

Design inlet quality to hydrogen tank separator system is 0.00138 (corresponds to initial 5-percent ullage).

Figure 7-2. Vehicle and Mission Ground Rules for Case III, Cryogenic Service Module

from batteries to drive a pump. The payload penalty resulting from additional propellant venting varies during the mission for Case III. In all cases, the payload loss per pound of added hardware is different than the loss per additional pound of propellant vented. The method of calculation presented in Appendix E was used to put the comparisons on a common basis of payload change. Tables 7-1 and 7-2 summarize the hardware and vent weight changes for the four major separator systems.

- c. Relative failure rate of system components -- incorporates the results of a statistical failure analysis on the components of each separator system, considering the number, operating time, and generic failure rate of each component. Results for the four major separator systems are given in Tables 7-3 and 7-4. These numbers should not be considered as absolute reliability numbers, but are judged to be meaningful for comparisons between the separators.
- d. Current feasibility of successful system operation -- defined as a measure of the extent of the uncertainties of developing a successful operating system in the light of present knowledge, as distinguished from the availability of information that would be needed for design. There has been an appreciable amount of experience and testing of the principal components in a mechanical or heat exchange system. In the case of the dielectrophoretic and surface tension separators, such devices are new and almost completely untested applications of concepts that are fairly well understood; therefore, these two separators were given lower ratings (higher numerically in Tables 7-5 and 7-6 in Paragraph 7.3) than were the mechanical and heat exchange systems. The use of dielectrophoretic or surface tension forces to orient the total tank contents would be more feasible than their use in a separator, but would result in greatly increased weights. The mechanical separator was rated lower (higher numerical rating) than the heat exchange system principally because of the unknowns in moving the vapor ullage bubble to the separator -- a requirement for venting which is not necessary for the heat exchange system. Quantitative ratings were not estimated for this criterion or the following three criteria because it was felt that this would give a distorted representation of the precision of relative ranking on these criteria, which must necessarily be evaluated qualitatively.
- e. Availability of design data -- intended as a measure of how much of the data necessary to design a system in detail are available and/or how adequate the existing data are. Again, because of the experience and testing of components included in the heat exchange or mechanical separator systems there is a moderate amount of design data available. The dielectrophoretic and surface tension separators involve new and essentially untested applications of more familiar concepts; therefore, very little design data are available.
- f. Performance of system in 100-percent liquid -- the heat exchange system is the only one of the four which could continue to vent vapor from an inlet stream of 100-percent liquid and, therefore, was given the best rating on this criterion; the other three separators vary in their ability to interrupt venting during such a time to minimize the loss of liquid. An electric-motor drive with a load-sensing switch

Table 7-1. Case I and II Hydrogen Separation Systems Weight Summary

COMPONENT	SYSTEM			
	HEAT EXCHANGER (lb)	MECHANICAL SEPARATOR (lb)	DIELECTRO-PHORETIC (lb)	SURFACE TENSION (lb)
Electric Motor & Gears	15	10	1	1
Impeller, Pump, or Turbine	(Pump + Turb.)	(included with separator)	2	2
Battery		50	48	19
Inverter		32	23	17
High-Voltage Power Pack			60	
Pressure Regulator Valve	6	6	6	6
Modulating Vent Valve	12	4	4	8
Shutoff Valve	4			
Separator, Pump, Turbine	--	12.8	--	--
Heat Exchanger	80	--	--	--
Separator Core	--	--	144	182
Mass Sensor System			10	
Total System Weight	117	114.8	295	241
Equivalent Δ Payload	- 78.4	- 76.9	-197	-162
ΔH_2 Vented in 4.5 hours	- 31.5	32.4	32.5	- 26.5
Equivalent Δ Payload (negative number means decrease)	11.1	- 11.4	-11.4	9.3
Total Δ Payload	- 67	- 88	-208	-153

Table 7-2. Case III Hydrogen Separation Systems Weight Summary

COMPONENT	SYSTEM			
	HEAT EXCHANGER (lb)	MECHANICAL SEPARATOR (lb)	DIELECTRO-PHORETIC (lb)	SURFACE TENSION (lb)
Electric Motor (Including Gears if Required) Impeller, Pump, or Fan	1.0 1.5	1.0 (included with separator housing)	1.0 1.0	1.0 1.0
Added Propellant & Tank Weight for Apollo Fuel Cell High-Voltage Power Pack	0.4	0.4	9.4 14	3.0
Pressure Regulator Valve	1.5	--	--	1.5
Shutoff and Relief Valves	1.3	1.3	1.3	1.3
Orificed Check Valve	--	--	2.0	0.7
Separator Housing, Pump, Turbine	--	4.5	--	--
Heat Exchanger	3.7	--	--	--
Separator Core	--	--	12.6	16.5
Mass Sensor System	--	--	5.0	--
Total System Weight	9.4	7.2	46.3	25.0
Equivalent Δ LEM Payload	-13.4	-10.3	-66.1	-35.8
Δ H ₂ Vented in 205-hr Mission	1.9	4.0	74	29.8
Equivalent Δ LEM Payload	- 2.0	- 4.3	-79	-31.8
Total Δ LEM Payload	-15.0	-15.0	-145	-68.0

Note that all weights are given for just one of the two required hydrogen tanks shown in Figure 7-2.

Table 7-3. Case I and II Component Failure Rates and System Failures Per Mission

COMPONENT	COMPONENT FAILURE RATE (Per 10 ⁶ hours)			
	Heat Exchanger	Mechanical Separator	Dielectrophoretic	Surface Tension
Electric Motor			Reversible	20
Impeller, Pump, or Turbine		20		18
Gear Reduction	2 x 18 = 36	18	4	4
Battery		4	2	2
Inverter		2	15	15
High-Voltage Power Pack		15	5	
Pressure Regulator Valve	Inlet 15			Precision 18
Modulating Vent Valve	Outlet 15	Existing S-IVB 15		Pump Inlet 15
Shutoff Valve	(1 cycle) 2	(1 cycle) 2	Inlet (1 cycle) 2	(1 cycle) 2
Separator Housing, Heat Exchanger, etc	0.2	0.1		1
Pump Commands (Mass Sensor)			25	
Σ Failure Rates per 10 ⁶ hr	68.2	76.1	117	95
4.5-hr Mission Failure Rate	0.000307	0.000342	0.000527	0.000428
System Mission Reliability	0.999693	0.999658	0.999473	0.999572
Statistical Δ in 90,000-lb Payload (lb)	-27.7	-30.8	-47.5	-38.6

Table 7-4. Case III Component Failure Rates and System Failures Per Mission

COMPONENT	COMPONENT FAILURE RATES (Per 10 ⁶ hours)			
	Heat Exchanger	Mechanical Separator	Dielectrophoretic	Surface Tension
Electric Motor	20	20	Reversible 30	20
Impeller, Pump, or Fan	18	18	18	18
Gear Reduction		4	4	4
Connection to Existing Power	0.5	0.5	0.5	0.5
High-Voltage Power Pack			5	
Pressure Regulator Valve	(Inlet) 15			(Pump Inlet) 18
Shutoff and Relief Valve	(Outlet) 14	(Outlet) 14	(1) out (orifice) 14	(at expansion valve) 14
Orificed Check Valve			(1) in 14	(20 psia) 5
Separator Housing, Heat Exchanger Respectively	0.2	0.1	1	1
Vent Commands (Pressure Switches)	12	12	12	12
Pump Commands (Mass Sensor)			25	
Inlet Shutoff Commands (Programmer, Same as Engine Start Commands)			1	
Σ Failure Rates Per 10 ⁶ hr	79.7	68.6	124.5	92.5
205-hr Mission Failure Rate	0.016338	0.014063	0.025523	0.018963
System Mission Reliability	0.9837	0.9859	0.9745	0.9810
Statistical Δ LEM Payload (lb)	-560	-484	-877	-652

Note that all values are given for just one of the two required hydrogen tanks.

Table 7-5. Comparison of Zero-g, Vapor/Liquid Hydrogen Separation Systems for Cases I and II (S-IVB)

CRITERION	RELATIVE RATING (Lowest Rating is Best)			
	HEAT EXCHANGE SYSTEM	MECHANICAL SEPARATOR	DIELECTRO-PHORETIC SEPARATOR	SURFACE TENSION SEPARATOR
System hardware weight (as equivalent pounds payload decrease)	78	77	197	162
Change in weight of vented propellant (as equivalent pounds payload decrease)	-11	11	11	-9
Relative system components failure rate (10 ⁻⁶ failures per mission)	307	342	527	428
Current feasibility of successful system operation (on 1 to 3 scale - not relative magnitudes)	1	2	3	3
Availability of design data (on 1 to 2 scale - not relative magnitudes)	1	1	2	2
Performance of system in 100-percent liquid (on 1 to 4 scale - not relative magnitudes)	1	2	3	4
"Complexibility" - measure of complexity of device and difficulty of development to successful operational status (on 1 to 2 scale - not relative magnitudes)	1	1+	2	2

Table 7-6. Comparison of Zero-g, Vapor/Liquid Hydrogen Separation Systems for Case III (CSM)

CRITERION	RELATIVE RATING (Lowest Rating is Best)			
	HEAT EXCHANGE SYSTEM	MECHANICAL SEPARATOR	DIELECTRO-PHORETIC SEPARATOR	SURFACE TENSION SEPARATOR
System hardware weight (as equivalent pounds payload decrease)	13	10	66	36
Change in weight of vented propellant (as equivalent pounds payload decrease)	2	4	79	32
Relative system components failure rate (10^{-4} failures per mission)	164	141	255	190
Current feasibility of successful system operation (on 1 to 3 scale - not relative magnitudes)	1	2	3	3
Availability of design data (on 1 to 2 scale - not relative magnitudes)	1	1	2	2
Performance of system in 100% liquid (on 1 to 4 scale - not relative magnitudes)	1	2	3	4
"Complexibility" - measure of complexity of device and difficulty of development to successful operational status (on 1 to 2 scale - not relative magnitudes)	1	1+	2	2

and shutoff valve could conveniently be installed in a mechanical separator system to minimize liquid loss through the vent system; however, venting would have to be interrupted during liquid inundation. Similarly, a liquid position control device could probably be designed for a dielectrophoretic separator; however, this would be more complex than the control for the mechanical separator. No practical way to interrupt the vent flow during periods of 100-percent liquid inlet flow to the surface tension separator was devised; therefore, it was given the lowest (highest numeric) rating on this criterion.

- g. "Complexibility" -- a measure of the complexity of the system and the difficulty and/or cost of development to a successful operational status. It includes some of the factors considered in criteria (c) through (f) plus qualitative estimates of the difficulty and cost of technology and system development.

7.3 SELECTION OF MOST-PROMISING SEPARATOR. The comparative ratings of the predesigns for the four major types of separators on each of the preceding seven criteria are summarized in Tables 7-5 and 7-6. These ratings are based upon the pre-design work of Sections 2 through 5 and the evaluation as discussed in Paragraph 7.2.

It was recognized that the final rating technique and relative weighting of the criteria could materially affect the comparison and selection of the separator systems. Criteria (d) through (g) of Paragraph 7.2 were judged to be of considerable importance, and criteria (a) through (c) of relatively less importance, as established between Convair and the NASA Project Manager. Various rating techniques (additive, multiplicative, Thurstone-Mosteller) were considered for applicability and objectivity, but were later found to be not required for the selection, as described below.

Inspection of Tables 7-5 and 7-6 reveals that the dielectrophoretic and surface tension devices are consistently poorer than either the mechanical or heat exchange separator systems, regardless of the relative weighting of the criteria. Therefore, it was concluded that these separator systems are considerably less promising than either the mechanical or heat exchange separators for all three vehicle/mission cases.

The choice of the heat exchange system as the most promising separator system was clear-cut in Cases I and II, for which it was rated best or approximately equal to the best of the separators on every criterion. The choice for Case III was less incisive; however, placing relatively less importance upon weight and failure rate than upon the other four criteria led to the choice of the heat exchange system for Case III also. However, this is not meant to suggest that the other separation systems might never be of value in other applications and/or if other propellant control functions in addition to venting were required.

In summary, we conclude that the heat exchange venting system is the most promising one for the three vehicle/mission cases considered in this study.

SECTION 8

STUDY OF HYDROGEN HEAT TRANSFER DATA

Preliminary work on sizing the hydrogen heat exchanger disclosed an apparent lack of good data for hydrogen heat transfer, particularly in forced convection boiling and condensation. A thorough literature search was therefore made to establish the best data and calculation techniques for use in this study. Paragraph 8.1 describes the results of the literature search. Paragraph 8.2 presents the selected data and equations used in this study. The details of the heat exchanger sizing procedure and calculations are given in Paragraph 8.3.

8.1 SURVEY OF EXISTING INFORMATION

8.1.1 Flow and Heat Transfer Regimes. As a start, the possible flow and heat transfer conditions within the exchanger were described and the limiting conditions identified as far as possible. This provided direction to the literature search.

The tank fluid passing through the hot side of the heat exchanger can be all liquid, all vapor (saturated or superheated), or any combination between. The selected installation at the top of the tank and retention of the continuous axial thrust venting system will tend to provide mostly vapor to the exchanger, but the design concept requires that it operate satisfactorily even when submerged in liquid. With pure vapor at the inlet the heat transfer will be by condensation. Increasing liquid percentage will change the transfer mechanism at the wall to one of cooling the liquid, with the vapor content tending to condense into the subcooling liquid and maintain a higher overall ΔT . Preliminary calculations indicated essentially equal heat transfer coefficients for the all-liquid and all-gas situations, but with the all-liquid case tending to set the heat exchanger size because of the inlet design selected. This is because the flow direction reversal at the vent path inlet (cold side) in the common inlet header tends to give an equal or greater percentage of vapor in the cold side than in the hot side. Thus, with a high vapor percentage in the hot side, the equal or greater vapor percentage in the cold side requires relatively little heat exchange to assure all vapor to the turbine/vent. Accordingly, the greatest interest in heat transfer data for the hot (tank) side of the heat exchanger was directed toward liquid flow. Data on gas flow (condensation) were of interest primarily to permit parametric analysis of heat exchanger performance across a range of inlet conditions.

The vent fluid leaving the tank is throttled to a lower pressure of about 6 psia before entering the heat exchanger. The fluid entering the throttling valve can range from all vapor to all liquid, but the throttling process flashes-off a percentage of any liquid and assures at least part vapor at the inlet to the cold side of the exchanger. With all

saturated liquid entering the throttling valve at 20 psia, for example, the exchanger inlet receives 7-percent vapor by weight or 90-percent by volume. Subcooled liquid would reduce these percentages, but the only source of subcooled liquid is the discharge from the other side of the exchanger, and it is not sufficiently subcooled to preclude significant vapor formation. The flow into the cold side of the exchanger can thus range from all vapor, perhaps slightly superheated, to saturated two-phase flow. The heat transfer will be by forced-convection boiling when liquid is present, and this is the design-controlling situation because vapor at the inlet requires relatively little heat exchange. Heat transfer to superheated vapor is still of interest, though, because some superheat is required if the vent gas leaving the turbine is to have the same enthalpy as 20-psia saturated vapor (the baseline used for performance evaluation). Heat transfer data were accordingly sought for forced-convection saturated boiling and for superheated vapor (gas).

Since the heat exchanger will operate at low or zero gravity, data were sought on the effect of gravity on heat transfer for each of the situations discussed above.

8.1.2 Boiling Heat Transfer

Pool Boiling. Boiling heat transfer was the area of most intensive data search because of the scarcity and uncertainty of data. The subject is best approached by discussing boiling without forced convection (pool boiling), then covering the effects of forced convection, and finally considering the effects of reduced gravity.

If a heated surface (plate, rod, wire, ribbon, etc) is placed in a body of liquid and the heat flux per unit area of heater surface is gradually increased (such as by increasing the current through an electrical heating surface), the heater surface temperature will increase in a manner shown by Figure 8-1.

At low heat flux the heat transfer will be by natural convection without boiling. Even if the liquid is saturated, boiling does not occur because natural liquid convection circulates the heated liquid away from the heater before it attains a sufficient level of superheat to form bubbles. (Superheat must be great enough to overcome surface tension effects before vapor bubbles can form.) Heat balance in the case of saturated liquid occurs by evaporation at the liquid surface (normal gravity). As the heat flux is increased into Region II of Figure 8-1 boiling begins at a limited number of favored sites. (Surface cavities or irregularities serve as nucleation sites for vapor bubbles, and boiling starts first at those sites of most favorable configuration.) Some of these initial vapor bubbles may escape and rise to the liquid surface, but most will collapse as they leave the superheated region around the heater, particularly if the liquid is subcooled. As the heat flux is further increased into the nucleate boiling Region III, larger and more numerous bubbles will form and rise to the liquid surface. If the liquid is subcooled the bubbles will collapse upon leaving the heater surface, but the curve in Region

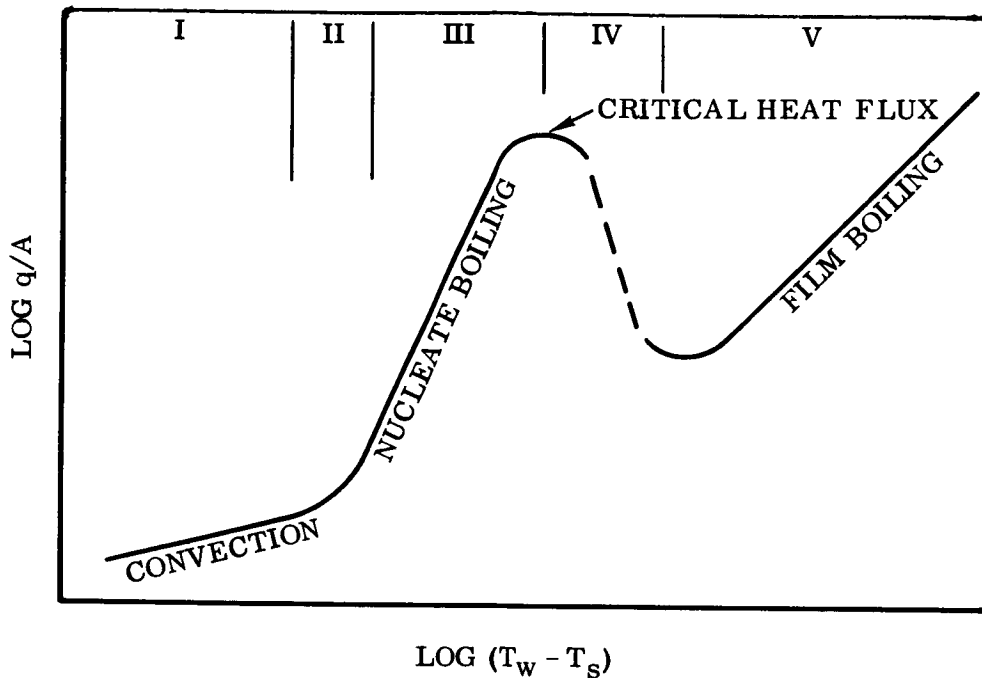


Figure 8-1. Typical Pool Boiling Curve

III will be the same provided ΔT is defined as $(T_w - T_s)$ where T_w is heater surface temperature and T_s is the saturation temperature corresponding to the existing pressure. This vigorous boiling of subcooled liquid is called surface boiling or local boiling.

As heat flux is increased in Region III, a peak is reached that is called the critical heat flux or burnout heat flux. This occurs when vapor formation has become so vigorous that it begins to blanket the surface and prevent adequate contact with liquid. An unstable Region IV marks the transition to Region V where stable film boiling occurs. In Region V the heater is surrounded by a vapor film and heat transfer is through the film. This results in reduced heat transfer unless heater temperature is raised high enough for radiation to become the predominant mode of heat transfer. It should be noted that, with a heater providing relatively constant heat flux, as the critical heat flux in nucleate boiling is exceeded the wall temperature must climb high into the film boiling region to support a higher flux. The high temperature involved frequently causes physical burnout of the heater, which accounts for the use of "burnout" as an alternate name for the critical heat flux. The term does not necessarily connote a physical burnout.

Film boiling will not be of interest for the temperature differences occurring in the heat exchanger in this zero-g separator study. Further discussion of Region III (nucleate boiling) in pool boiling is justified, however, even though the heat exchanger will employ forced convection. The reason for this will become clear when forced convection boiling is discussed later.

Nucleate pool boiling is employed in steam generation and various chemical processes, accounting for much of the experimental research in this field. Liquid hydrogen pool boiling research at standard and zero gravity has been prompted in recent years by the need to predict propellant tank heating on earth and in orbit. Data interpretations for hydrogen boiling have generally relied upon correlation methods derived earlier for water and other non-cryogenic liquids. These correlations have usually been obtained by a combination of dimensional analysis and experimentation. This has been necessary because the physical mechanisms are not sufficiently well understood to permit a complete mathematical description. Instead, theories on the physical mechanisms have provided a basis for selecting the most significant parameters and dimensionless groups, and for defining and relating these groups. Experimental data have then provided the unknown constants and exponents to complete the correlations. Most theories attribute the high heat flux in nucleate boiling to various types of stirring, agitation, pumping, or microconvection of the liquid near the surface by the vapor bubbles, rather than by the heat being transported away in latent heat of the vapor. This belief has been largely based on the work of Jakob (Reference 8-1), Gunther and Kreith (Reference 8-2), and Rohsenow and Clark (Reference 8-3). Since the heat is assumed transferred to the liquid by this convective action, most of the proposed pool boiling correlations have taken the Dittus-Boelter approach for turbulent forced convection and are of the form

$$N_{NU} = \text{constant} (\text{Re})^a (N_{PR})^b \quad (1)$$

where the physical properties are those of the liquid and lengths are characteristic bubble dimensions. The correlations differ primarily in the use of different bubble dimensions and Reynolds number definitions because of differences in the assumed physical mechanisms. Rohsenow (Reference 8-4) derived the correlation

$$\frac{h}{k_L} \left(\frac{\sigma}{g(\rho_L - \rho_V)} \right)^{1/2} = \frac{1}{C_{Sf}} \left[\frac{q/A}{\mu_L h_{fg}} \left(\frac{\sigma}{g(\rho_L - \rho_V)} \right)^{1/2} \right]^{2/3} N_{PR}^{-0.7} \quad (2)$$

where the constant, C_{Sf} , must be experimentally determined for each surface/liquid combination. Kutateladze (Reference 8-5) obtained

$$q/A = \text{constant} \left(\frac{C_L}{h_{fg} \rho_V} \right)^{1.5} \left(\frac{k_L \rho_L^{1.282} p^{1.75}}{\sigma^{0.906} \mu_L^{0.626}} \right) (\Delta T)^{2.5} \quad (3)$$

where the constant is 4.87×10^{-11} when metric units are used. (Equation 3 presents the correlation in a rearranged form which is no longer dimensionless.) Engelberg-Forster and Greif (Reference 8-6) derived, for heat flux in Btu/hr-ft²,

$$q/A = 4.3 \times 10^{-5} \frac{ac \rho_L T_S}{\sigma^{1/2} (h_{fg} \rho_V)^{3/2}} (C T_S a^{1/2})^{1/4} \left(\frac{\rho_L}{\mu}\right)^{5/8} \left(\frac{\mu C}{k}\right)^{1/3} \Delta p^2 \quad (4)$$

Labountzov (Reference 8-7) obtained

$$\frac{h}{k_L} \frac{C \rho_L}{(\rho_V h_{fg})^2} \sigma T_S = 0.125 \text{Re}^{0.65} N_{PR}^{1/3} \quad (5a)$$

for $\text{Re} > 10^{-2}$, and

$$\frac{h}{k_L} \frac{C \rho_L}{(\rho_V h_{fg})^2} \sigma T_S = 0.0625 \text{Re}^{0.5} N_{PR}^{1/3} \quad (5b)$$

for $\text{Re} < 10^{-2}$, where

$$\text{Re} = \frac{\rho_L}{\mu_L} \frac{q/A}{\rho_V h_{fg}} \frac{C \rho_L \sigma T_S}{(\rho_V h_{fg})^2} \quad (5c)$$

All of these correlations are fairly successful as will be illustrated shortly. But it should be noted that they are based on convection analogies and assume latent heat transport to be negligible. Recent work by Bankoff (Reference 8-8) and Rallis and Jawurek (Reference 8-9) indicates that latent heat transport actually might frequently account for most of the heat flux, and perhaps mass transfer models would be more appropriate for correlations.

Hydrogen pool boiling data taken from several sources and compiled by Brentari and Smith (Reference 8-10) are shown in Figure 8-2. The above correlations (Equations 2 through 5) are shown in Figure 8-3 for comparison, partly taken from Zuber and Fried (Reference 8-11). C_{sf} in the Rohsenow correlation is taken as 0.0147. It can be seen from these figures that the Kutateladze correlation represents a reasonable average of the available data, and that the other three correlations do not differ greatly from that of Kutateladze. Other correlations also exist, but differ by greater amounts from the average of the data.

The spread of data in Figure 8-2 is rather large, weakening the confidence that can be placed in predictive calculations based on it. Some of the spread is due to inevitable experimental error, aggravated by the small ΔT that must be measured. At least part of the spread, however, is presumed to result from differences in heater material and surface finish variables that have long been recognized as significant but resistant to

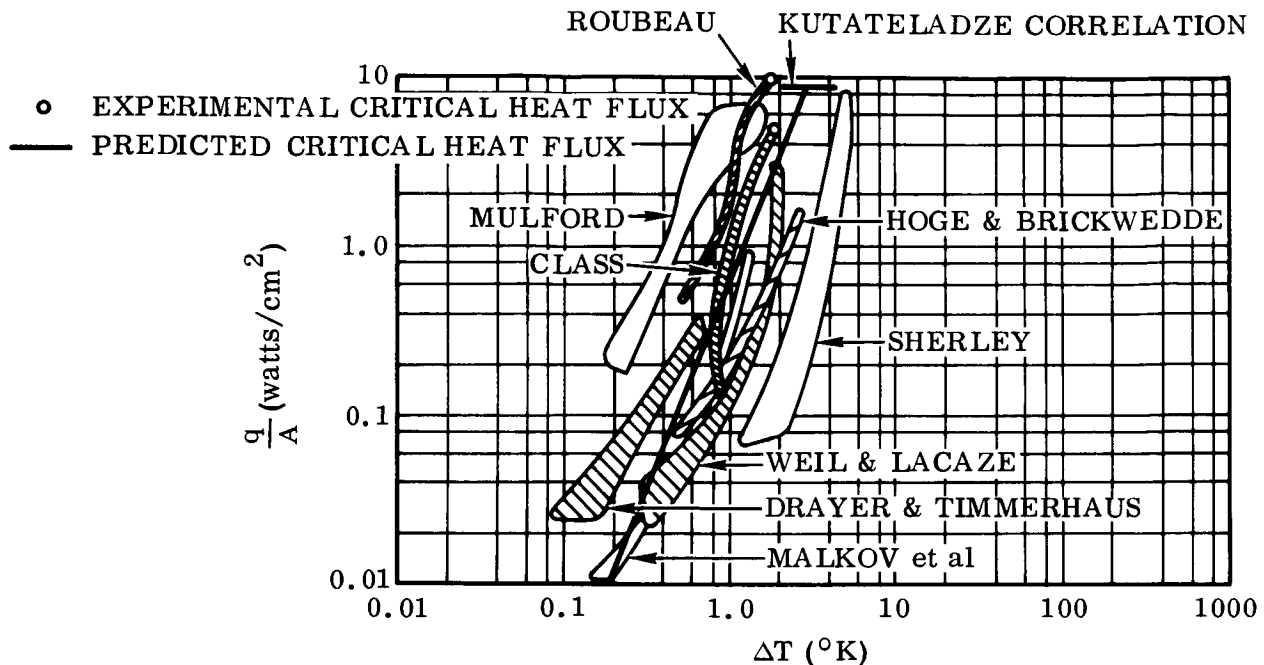


Figure 8-2. Experimental Nucleate Pool Boiling of Hydrogen at ~1 Atmosphere Compared With the Predictive Correlation of Kutateladze

analysis or control (Reference 8-12 through 8-15). None of these hydrogen tests used aluminum, which is unfortunate because it is the most likely choice for hydrogen heat exchangers.

Forced Convection Boiling. Forced convection boiling within tubes or heat exchanger passages introduces progressive vaporization and two-phase flow to the problem. To visualize the situation, consider a subcooled liquid entering a tube whose wall receives a constant heat flux (electric resistance heated). Figure 8-4 illustrates the wall and temperatures that will occur, as follows.

- a. Non-boiling forced convection of liquid.
- b. Boiling of subcooled liquid, bubbles recondense (sometimes called surface boiling).
- c. Saturated boiling with wetted wall (sometimes called bulk boiling). The fluid is 100-percent liquid at the beginning of Region C, and progressively vaporizes as it moves toward Region D. The vaporization at a constant mass flow rate requires a velocity (and momentum) increase to maintain continuity, and this comes at the expense of static pressure. Fluid saturation temperature also must drop to correspond to the lower static (saturation) pressure, which accounts for the temperature decrease across Region C. The heat exchanger in this study operates entirely in Regions C, D, and E because the inlet vent flow is already saturated and at least 7-percent vaporized at the exchanger inlet.

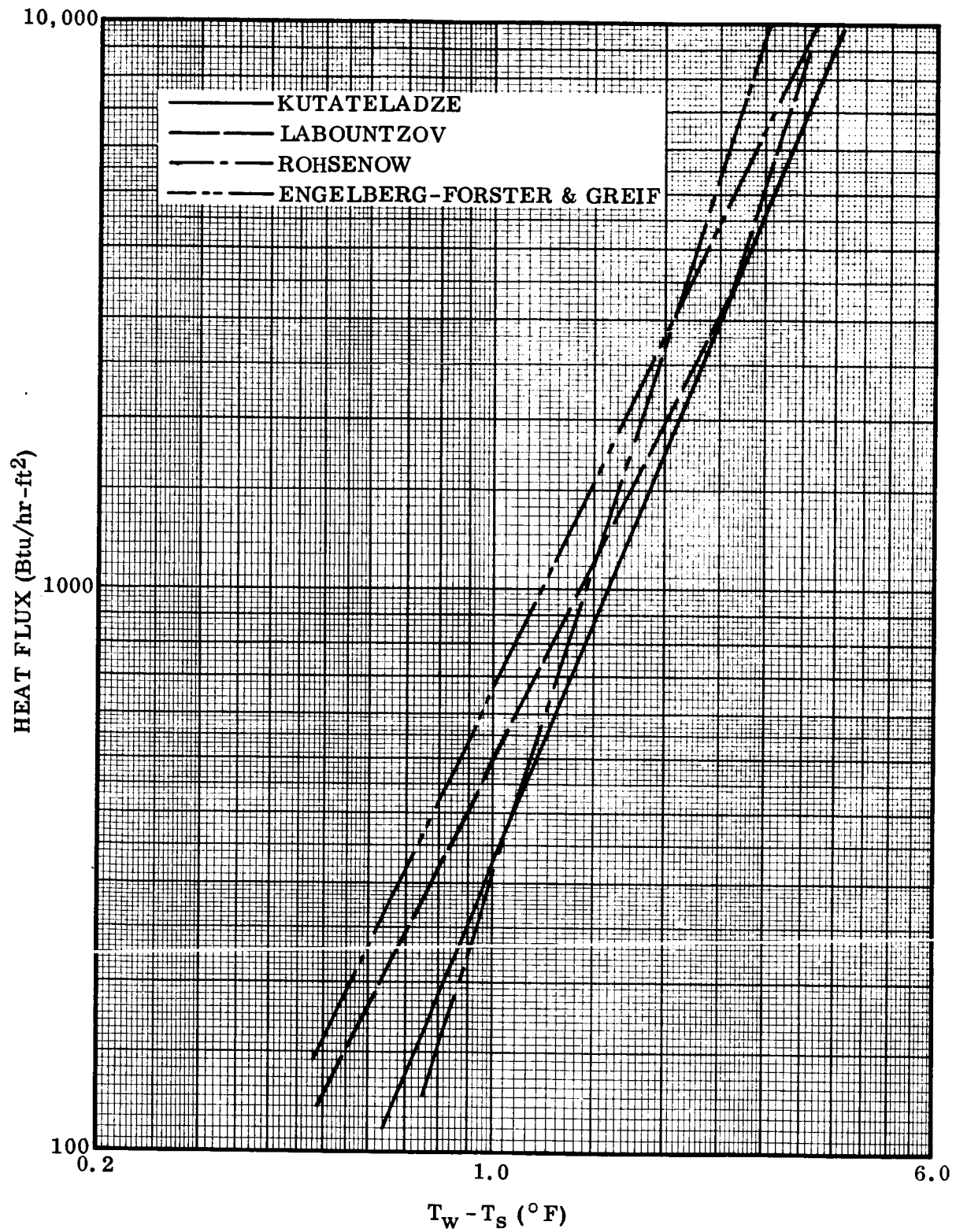


Figure 8-3. Comparison of Pool Boiling Correlations for Hydrogen at 0.8-Atmosphere Pressure

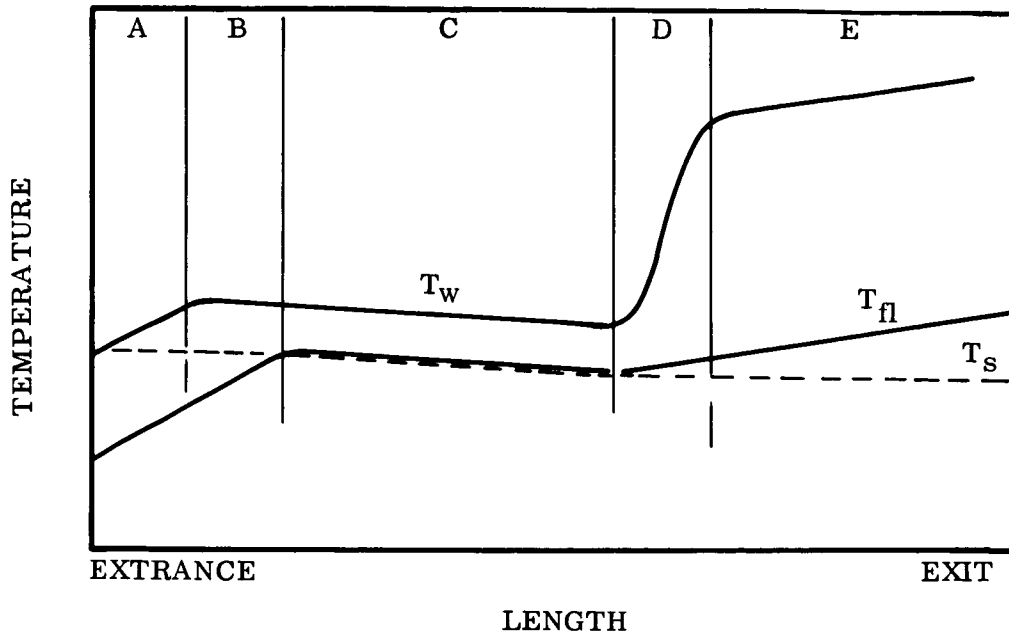


Figure 8-4. Forced Convection Boiling - Constant q/A

- d. Transition to dry wall. A point is reached where so much of the liquid is vaporized that the wall is no longer kept wet, and a transition to gas forced-convection heat transfer occurs. The heat transfer coefficient is much lower for gas forced convection than for boiling, so the ΔT between wall and fluid increases for constant heat flux. This transition is similar to the "burnout" that occurs in pool boiling at the critical heat flux, as vapor blankets the heated surface. With sufficiently high heat flux, Regions A, B, and C can be eliminated in forced convection and the entire vaporization can occur by forced-convection film boiling. This will not occur in the heat exchanger in this study, however, because the situation is more like constant wall temperature than constant heat flux, and the ΔT is low. It is expected that vaporization will be 80- to 90-percent complete before Region D occurs.
- e. Dry wall, or gas forced-convection heat transfer. It may help to view the situation from a constant wall temperature approach as shown in Figure 8-5 rather than a constant heat flux approach, since this is a little closer to what occurs in this heat exchanger. Region A of non-boiling forced convection will generally be eliminated, but it could be greatly extended. Referring back to Figure 8-4, note that boiling began when T_w rose to a sufficient margin above T_s . For the constant wall temperature case this rise in T_w is eliminated, so that T_w must either be high enough to initiate boiling immediately or else wait for pressure drop to reduce T_s sufficiently. Boiling Regions B and C are regions of very high heat flux, as will be discussed shortly. The heat flux is proportional to approximately the 2.5 power of $(T_w - T_s)$ so that it increases through Region C as pressure drop reduces T_s . A transition to dry wall, Region D, again occurs. Heat flux may diminish an order-of-magnitude or more in Region D, a fact that

Figure 8-5 does not disclose. The vapor superheats in Region E, asymptotically approaching T_w while the heat flux approaches zero.

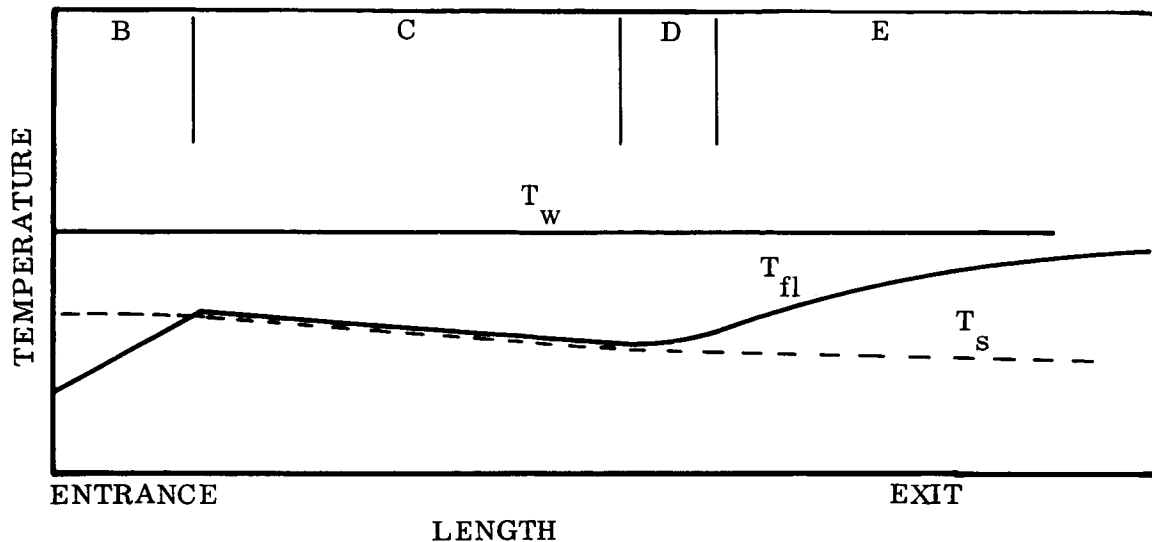


Figure 8-5. Forced Convection Boiling, Constant Tube Temperature

When the problem is approached from the standpoint of plotting heat flux versus $(T_w - T_s)$, forced convection boiling has been observed to yield curves that are similar to pool boiling curves at high heat flux and non-boiling forced convection at low flux. This has led to four similar heat transfer estimation techniques shown in Figure 8-6 as summarized by Bergles and Rohsenow (Reference 8-16). They are seen to differ mainly in definition of the transition region. (This is the transition from Region A to B of Figure 8-4.)

Bergles and Rohsenow added another technique of their own for identifying the point of incipient boiling and defining the transition. More important, they offered experimental evidence that the forced convection boiling curve is not identical to the pool boiling curve and urged that designs be based on actual forced convection boiling data. For preliminary estimates, however, they did not offer anything better than using pool boiling data.

Bergles and Rohsenow clearly limit their discussion to surface boiling, Region B. Others (Reference 8-11), including some of the originators (Reference 8-6), consider the procedures of Figure 8-6 to be applicable to much of Region C also. But the attention of most authors has been focused on Regions A and B, even if they do not clearly indicate so. This is evident from the slope of the forced convection portions of the Figure 8-6 curves. A log-log plot of forced convection for Region C has a slope of approximately 45 degrees, but Region A subcooled forced convection gives flatter slopes such as shown in the figure. This arises from the approximate direct proportionality of forced convection heat flux to ΔT (neglecting fluid property changes

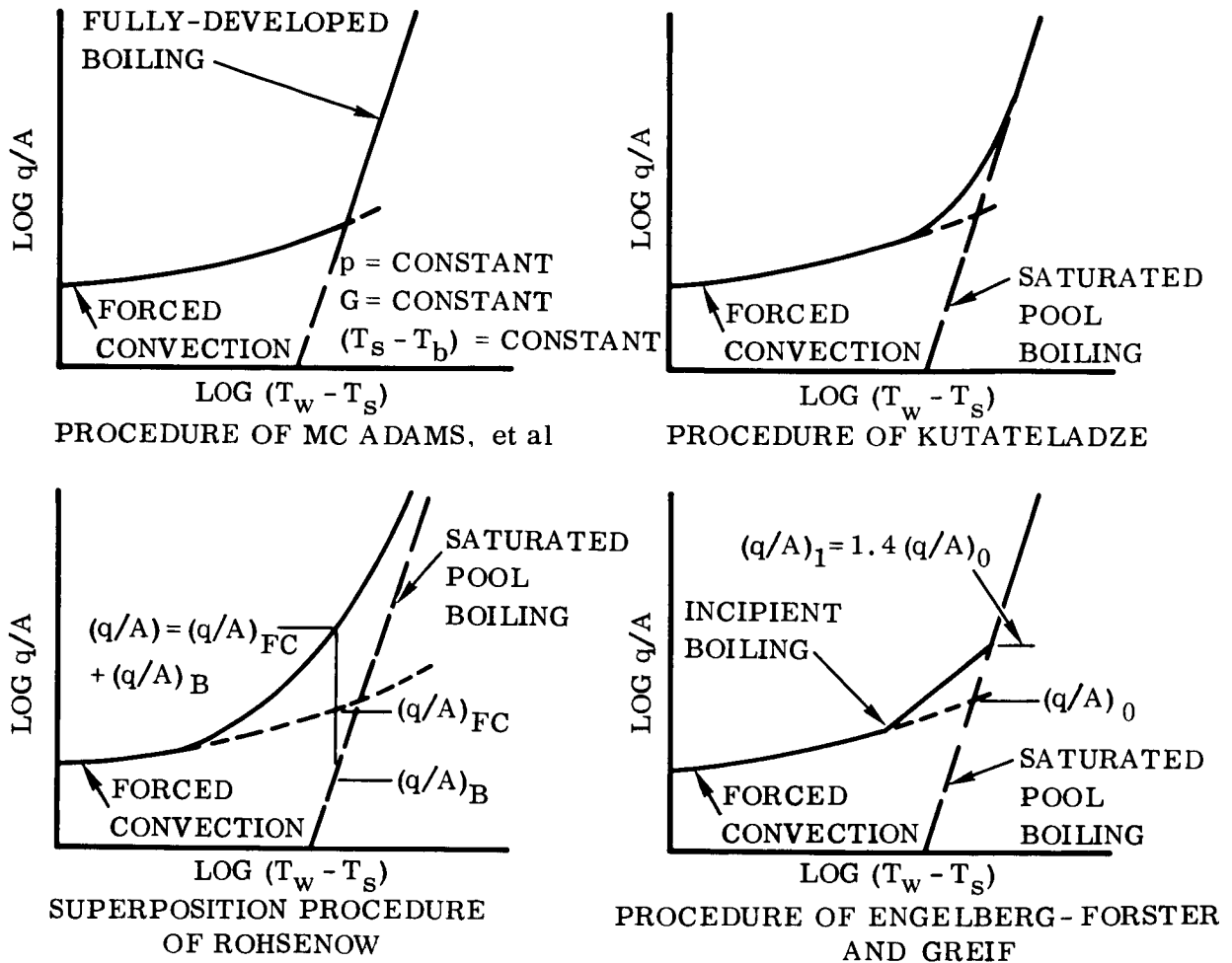


Figure 8-6. Procedures for Estimation of Heat Transfer With Forced-Convection Surface Boiling

with temperature). This ΔT is $(T_w - T_{f1})$ for Regions A and B, but $(T_w - T_s)$ for Region C. Some doubts are thus raised as to the applicability of the forced convection portions of Figure 8-6 to Region C and the heat exchanger in this study, since the procedures were developed for a different situation. Reiterating the discussion, the forced convection portion of Figure 8-6 applies to Region A of Figure 8-4 where no vapor is generated. The transition of Figure 8-6 applies to the transition from Region A to B and can result either from an increase in the heat flux, or from the rise in T_w as the fluid progresses down the tube. The steep boiling portion of Figure 8-6 then applies to Region B where bubbles form but recondense, and continues to apply well into Region C. In contrast, the heat exchanger in this study never experiences Regions A and B, since Region C exists at its entrance. The boiling curve probably is applicable if the heat flux is high enough, and the Region C data of Walters (Reference 8-17) substantiate this by showing close agreement with hydrogen pool boiling data. But what if the heat flux is low enough that Figure 8-6 indicates the forced convection curve should be used? In spite of the obscurity of the literature on

this point, it was concluded that the procedure of Figure 8-6 should still be applicable provided that vapor generation effects on convective velocity be accounted for. The physical situation is envisioned as analogous to Region I of Figure 8-1, with the liquid flowing along the wall without boiling but being superheated slightly. A central vapor core would exist and grow as superheated liquid evaporated into the core.

The forced convection heat transfer should be calculated from the Dittus - Boelter equation,

$$\frac{h_L D}{k} = 0.023 \left(\frac{DG}{\mu} \right)^{0.8} \left(\frac{C \mu}{k} \right)^{0.4} \quad (6)$$

The boiling curve should be taken from test data or one of the correlations for the appropriate pressure. The transition should be calculated by Bergles and Rohsenow's method. First a line of incipient boiling is found by an iterative graphical technique. The equation

$$T_V = (T_V - T_s R_V / h_{fg}) \ln (1 + 2\sigma / r p_L) + T_s \quad (7)$$

is plotted versus r for a given T_s to relate bubble size, r , to its vapor temperature and pressure. It is assumed the bubble will grow if

$$T_L = T_V \text{ and } \frac{dT_L}{dy} = \frac{dT_V}{dr} \text{ at } y = r \quad (8)$$

where T_L is liquid temperature at a distance y from the wall, approximately defined by

$$T_L = T_w - \left(\frac{q}{A} \right) \frac{y}{k_L} \quad (9)$$

The heat flux relations

$$q/A = -k_L \frac{dT_L}{dy} = h (T_w - T_s) \quad (10)$$

also govern, where h is given by Equation 6. This permits iterative plotting of T_L versus y and T_V versus r to find points of tangency satisfying Equation 8. A line of incipient boiling, such as shown in Figure 8-7, is thus determined. The transition from forced convection to boiling is estimated by the following interpolation formula defining q/A at any $(T_w - T_s)$.

$$q/A = (q/A)_{FC} \left[1 + \left\{ \frac{(q/A)_B}{(q/A)_{FC}} \left(1 - \frac{(q/A)_{Bi}}{(q/A)_B} \right) \right\}^2 \right]^{1/2} \quad (11)$$

where $(q/A)_{FC}$ is taken from the extrapolated forced convection curve, $(q/A)_B$ from the extrapolated boiling curve, and $(q/A)_{Bi}$ is read from the $(q/A)_B$ curve at the $(T_w - T_s)$ where the incipient boiling line intersects the forced convection curve. Figure 8-7 illustrates the interpolation.

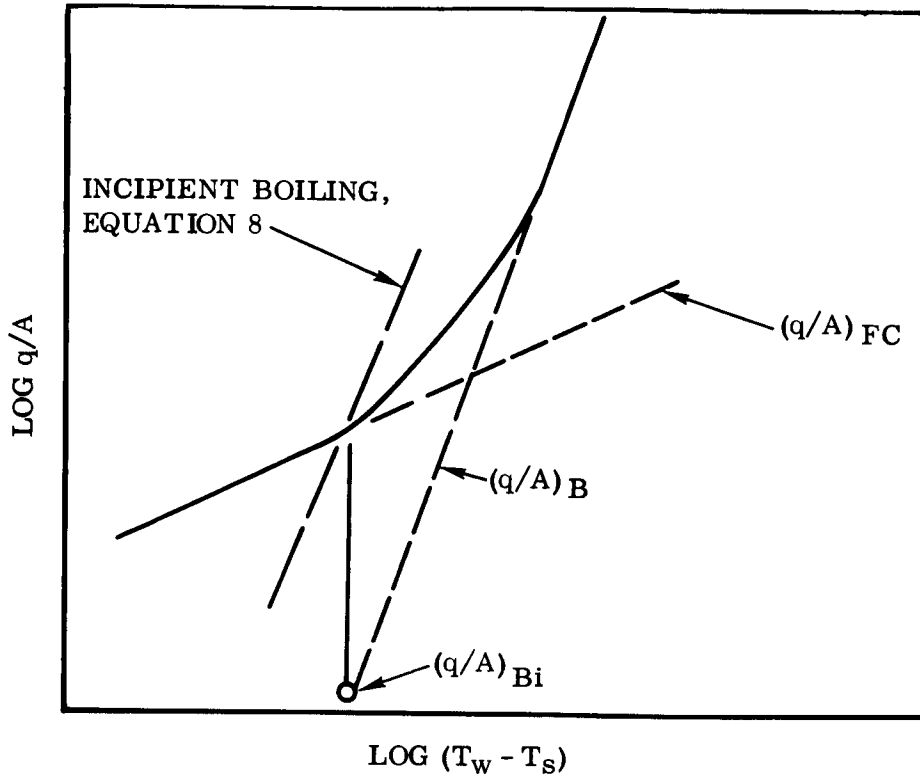


Figure 8-7. Transition From Forced Convection to Boiling

Other correlations or techniques have been proposed for forced convection boiling by other researchers. Schrock and Grossman (Reference 8-18) added two more dimensionless groups to the correlation, the Lockhart-Martinelli parameter

$$x_{tt} = \left(\frac{\mu_L}{\mu_V} \right)^{0.1} \left(\frac{u_L}{u_V} \right)^{0.5} \left(\frac{1}{X} - 1 \right)^{0.9} \quad (12)$$

and a "boiling number"

$$B_o = \frac{q/A}{G h_{fg}} \quad (13)$$

and experimentally found the following relationship (for water).

$$\frac{N_{NU}}{Re^{0.8} N_{PR}^{1/3}} = 170 B_o + 0.0255 X_{tt}^{-2/3} \quad (14)$$

These results are shown another way in Figure 8-8.

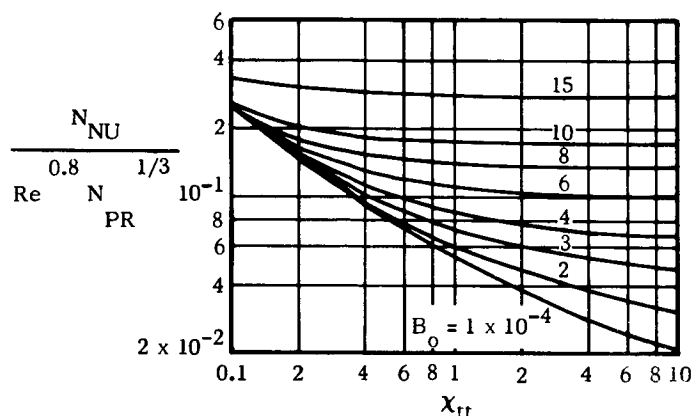


Figure 8-8. Forced Convection Boiling Heat Transfer Correlation

Equation 14 only correlated Schrock and Grossman's data within ± 35 percent, and they did not recommend it for qualities over 50 percent.

Leonhard and McMordie (Reference 8-19) derived an analytical technique for annular flow heat transfer and pressure drop that is primarily suitable for computer programming, and found it checked well with Freon experiments. Both of the latter approaches are promising but require greater substantiation before use with hydrogen.

The point at which Region D of Figure 8-4 begins, and the rate of transition to dry gas convection, are not readily predicted. The critical heat flux in pool boiling is a less complex situation, and several successful correlations have been derived from assumptions of Helmholtz and Taylor instabilities in the two-phase boiling mixture. These correlations are not applicable to forced convection because the additional mechanisms are not accounted for — the convective velocity, the progressively higher quality two-phase mixture as vaporization proceeds, the associated increase in convective velocity and momentum, and the various flow regimes that can occur (annular, mist, slug, etc). Kutateladze (Reference 8-20) has attempted to modify his pool boiling

critical heat flux correlation to include forced convection, leading to

$$(q/A)_{\max} = 0.085 \rho_V h_{fg} \left[\frac{\sigma g (\rho_L - \rho_V)}{\rho_V^2} \right]^{1/4} \left[\frac{G(-X) (\rho_L - \rho_V)^{1/4}}{\rho_L \sigma g} \right]^{1/2} \quad (15)$$

for saturated boiling. When applied to the flow conditions for the heat exchanger in this study, Equation 15 predicts burnout at 75- to 80-percent vapor quality. Although this correlation has not been verified for hydrogen, and its applicability into the liquid-deficient region is uncertain, this prediction is reasonable. McAdams (Reference 8-21) on Page 398, for example, shows forced convection boiling heat transfer coefficients staying fairly constant until 70- to 80-percent vaporization. Anderson, in the discussion following Reference 8-22, shows similar data with boiling heat transfer coefficients holding constant or rising out to 80- or 90-percent vaporization before the drop toward dry wall values begins. It therefore seems reasonable to predict that transition to dry wall will begin at about 80-percent quality in the hydrogen heat exchanger in this study, but the limited basis for the prediction should be noted. Two other correlations were investigated and found inapplicable. That by Von Glahn and Lewis (Reference 8-23) appears promising at first inspection because it includes quality as one of the parameters in the correlation. Further investigation shows that it has no predictive ability for this application. The correlation of Tippets, References 8-24 and 8-25) for water at high pressure yields unreasonably low predictions of critical heat flux for this application, suggesting that the correlation or its empirical constants are not applicable to low-pressure hydrogen.

8.1.3 Condensing Heat Transfer. Vapor, in the flow through the tank side of the heat exchanger, will tend to condense when it contacts the exchanger or subcooled liquid. The condensate, together with any liquid already present in the tank-side flow and any vapor not condensed, is forced through the exchanger by the pump. The liquid and condensate will tend to form an "annular" film in the passages with the vapor core moving at higher velocity. Most condensing heat transfer data and correlations, including the limited hydrogen data (Reference 8-26) are not applicable because they are for cases where gravity removes the condensate film and vapor velocity is negligible. Theory and data do exist for the case where vapor velocity rather than gravity predominates; but the data are limited and do not include hydrogen, and the correlations are not sufficiently established to be fully confident of their predictions for hydrogen.

The process of condensation was first mathematically described by Nusselt in 1916. His theory assumes a condensate film in laminar or viscous flow, so that heat transfer is governed by conduction through this film. The effect of vapor velocity is considered, along with gravity and condensation rate, in establishing the local film thickness. But the theory underestimates the heat transfer when vapor velocity is high because part of the film actually becomes turbulent and the mixing action transfers

heat much faster than conduction. Carpenter and Colburn assumed, as a reasonable approximation, that the entire thermal resistance was in the laminar sublayer and that the thickness of this sublayer could be determined from the velocity distribution relations for turbulent flow of liquids in pipes. They derived the following expression for the average condensing film coefficient, employing Re , N_{NU} , and N_{PR} .

$$h_c = 0.065 G_m \frac{(C_P)_L \rho_L k_L f}{2\mu_L \rho_V} \quad (16)$$

where the constant was determined from their test data, f is the Fanning friction factor for vapor flowing in the dry passages, and G_m is an average vapor mass velocity determined by

$$G_m = \frac{G_1^2 + G_1 G_2 + G_2^2}{3} \quad (17)$$

where G_1 and G_2 are the inlet and exit vapor mass velocities.

Rohsenow (Reference 8-27) extended the theory of condensation to include the thermal resistance of the turbulent portion of the condensate layer as well as the laminar sublayer. Altman, et al, (Reference 8-28) modified this analysis to cover annular flow in a horizontal tube and obtained a successful but difficult-to-utilize correlation. Altman also showed that the Carpenter-Colburn method gave a fairly good correlation of the same data. Akers, et al, (References 8-29 and 8-30) derived correlations in terms of N_{NU} , N_{PR} , $h_{fg}/c \Delta T$, and special definitions of Re that successfully correlated data over a wide range of liquid and vapor flow rates covering both laminar and turbulent condensate films.

A new method of calculating condensing film coefficients was devised and used during this study, and is described in Paragraph 8.2.2. It is similar to the method of Reference 8-29, convenient to use, and apparently slightly conservative.

8.1.4 Single-Phase Heat Transfer. Dimensional analysis has led to correlation of single-phase turbulent flow heat transfer data by a functional relationship between N_{NU} , Re , and N_{PR} as in the Dittus-Boelter equation, or between N_{ST} , Re , and N_{PR} as in the Colburn equation. These equations correlate data for many fluids flowing inside tubes. The irregular flow passages used in many compact heat exchangers result in somewhat different performance than these standard equations would predict, so that it is preferable to obtain a specific correlation for any given heat exchanger core configuration. One standard source for such specific correlations for many different core configurations is Kays and London (Reference 8-31), which presents the data as plots of $N_{ST} \times N_{PR}^{2/3}$ versus Re . Most of the test data comes from tests

using only air so that N_{PR} was not actually a test variable. Its two-thirds power was introduced on the basis of theory and experience to make the data applicable for other fluids whose N_{PR} does not differ greatly from 0.7, that of air. The N_{PR} of the GH_2 at the conditions in the heat exchanger in this study is in the region of 0.7, and for the LH_2 it is about 1.07. The Kays and London data should therefore be applicable.

A search for single-phase forced convection heat transfer test data for LH_2 and low temperature GH_2 was made, for the purpose of verifying the expected agreement with air data. No such data were found for the applicable conditions. Thus, although the Kays and London data can be used with little probability of significant error, specific confirmation is lacking. Such confirmation, or specific correlations for GH_2 and LH_2 , would be desirable to improve design confidence.

8.1.5 Zero-Gravity Effects. The survey of reduced-or zero-gravity heat transfer tests revealed that the work has primarily been concerned with pool boiling and is not applicable to this heat exchanger application where forced convection is employed. The reason for experimental neglect of reduced-gravity forced convection heat transfer is obvious. Forced convection heat transfer, by definition, is a regime where flow forces predominate and gravity forces have negligible effect. Obviously, lower gravity forces will also be negligible and forced convection correlations should remain valid down to lower flow rates than under standard-gravity conditions. The flow rates used in this study were high enough that such extrapolation was unnecessary in single-phase calculations.

In condensing correlations for high vapor velocity, a knee occurs in the curve (Reference 8-29) at a particular Re that might be attributable to gravity effects, i. e. , a change from annular flow to a situation where the condensate tends to flow along the bottom of the horizontal tube. This is supported by inspection of the Carpenter-Colburn data for vertical tubes. An extrapolation of the higher velocity data was used (see Paragraph 8.2.2), yielding more conservative condensing coefficients.

Adelberg and Jetter (Reference 8-32) present an interesting order-of-magnitude analysis for forced convection boiling to determine whether bubble drag forces (flow forces) predominate. They define a boiling Grashof number for comparing drag to bouyancy, a boiling Reynolds number for comparing drag to bubble dynamic forces, and a boiling Bond number that combines with the boiling Grashof number to compare drag to surface tension. For the flow velocities in this heat exchanger and the acceleration of the S-IVB with venting thrust, flow forces should predominate.

8.2 RECOMMENDED DATA. This paragraph presents the data and equations selected for heat exchanger sizing in this study. The justification for these selections is not fully presented, since it is implicit in the discussions in Paragraph 8.1.

8.2.1 Boiling Heat Transfer. As discussed in Paragraph 8.1.2, boiling results in high heat transfer coefficients up to the point where 80- to 90-percent of the liquid is vaporized. A smooth drop-off then occurs, with the coefficient falling to that of pure vapor (gas) at the point of 100-percent vaporization. The boiling and superheating process was divided into three phases to permit accurate but convenient calculation.

0- to 90-percent Quality. Heat flux was taken from the straight-line Kutateladze correlation shown in Figure 8-9, adjusted to other pressures by a multiplier taken from Figure 8-10. Although Figure 8-9 shows the Bergles and Rohsenow transition to boiling (see Paragraph 8.1.2) for two assumed non-boiling convective film coefficients, they were not employed in the heat exchanger sizing. Calculated non-boiling

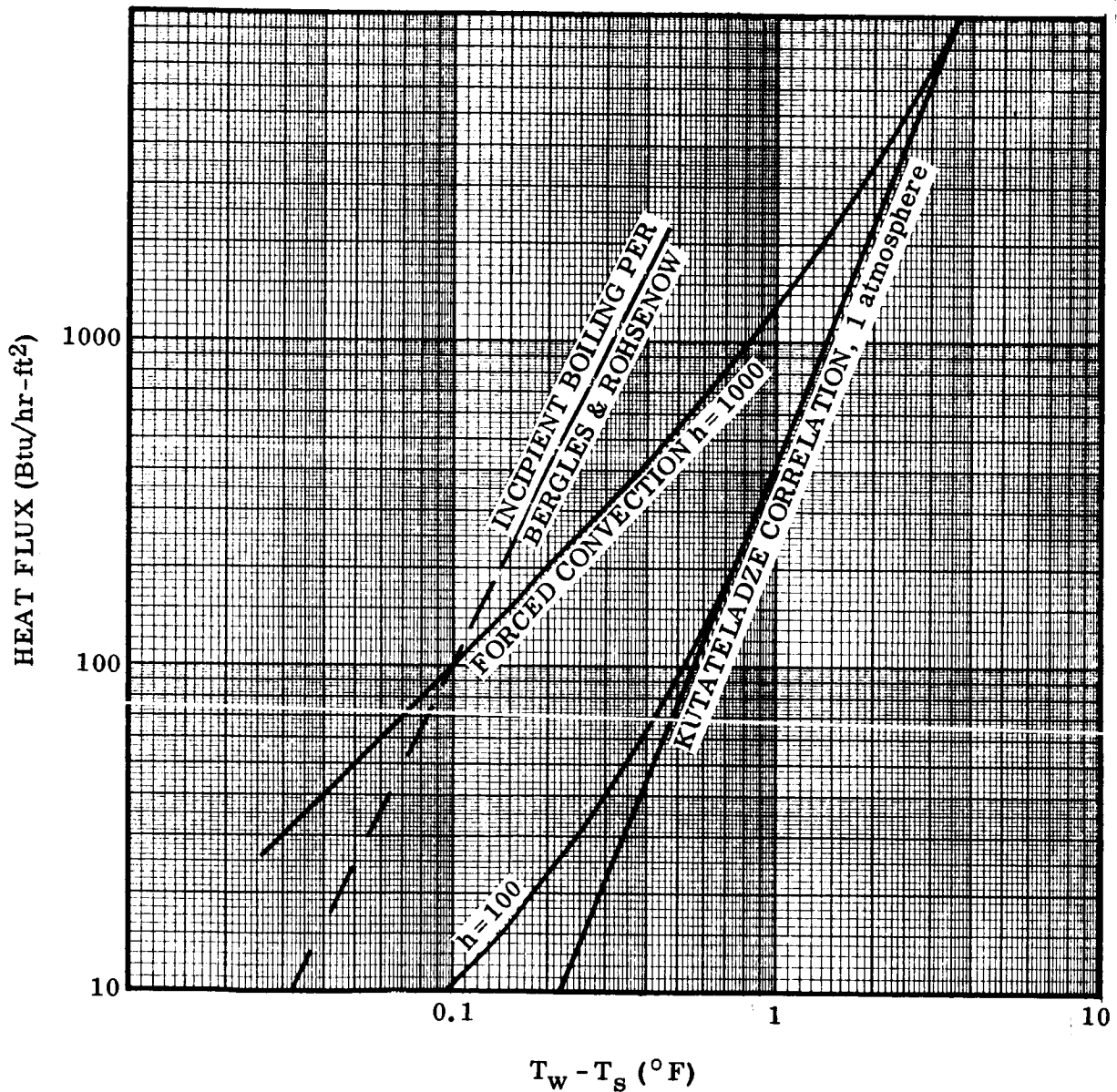


Figure 8-9. Forced Convection Boiling Heat Transfer Data Selection

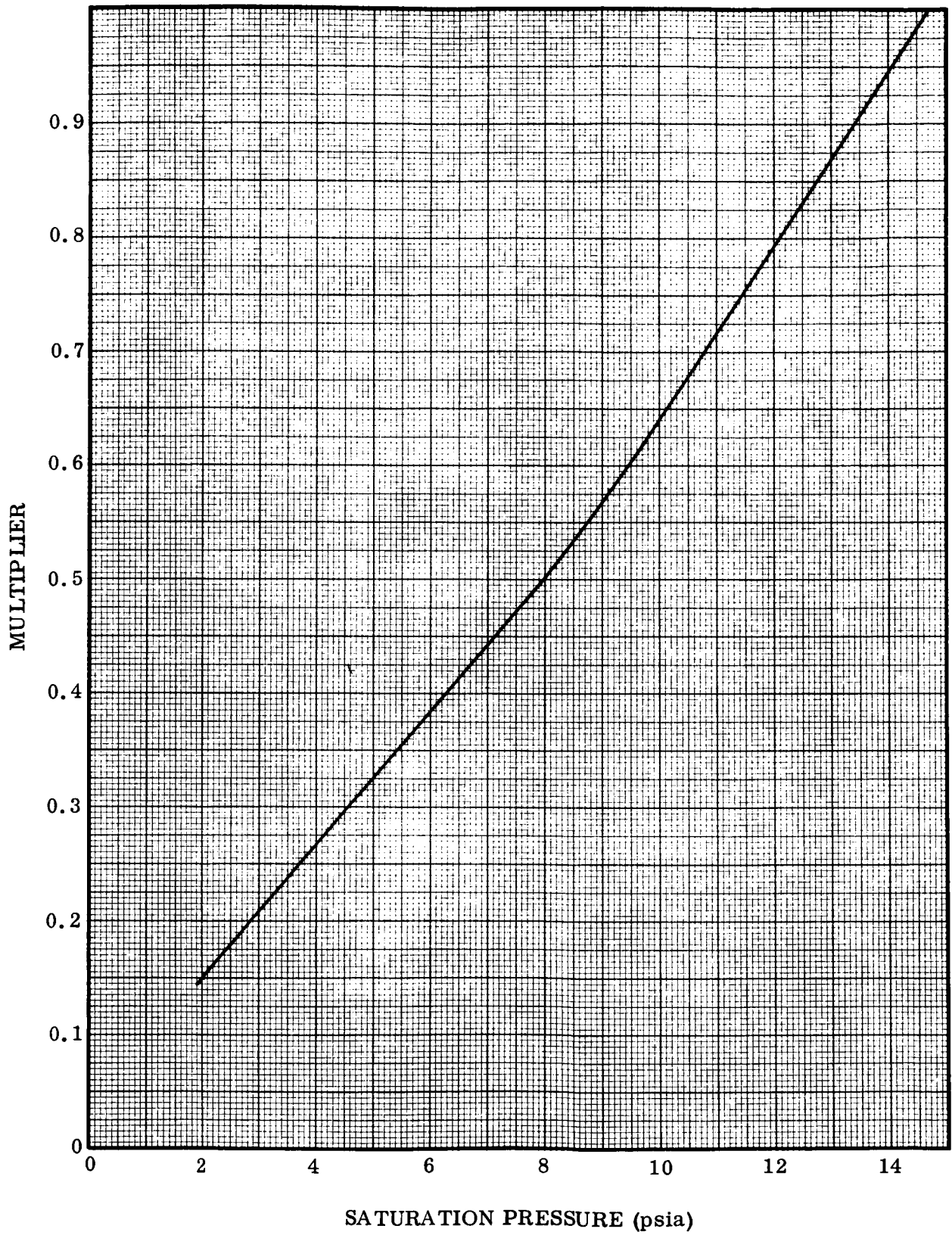


Figure 8-10. Multiplier for Adjusting 1-Atmosphere Kutateladze Correlation to Other Pressures

coefficients were low enough, and ΔT high enough, that only the Kutateladze correlation applied.

90-Percent to 100-Percent Quality. For convenience of calculation, the heat transfer coefficient was assumed to drop abruptly, at 90-percent quality, to that for dry gas (see Paragraph 8.2.3). Recognizing that the flow would still contain a fog of liquid that would tend to maintain constant temperature, the vapor temperature was assumed constant while vaporization from 90- to 100-percent quality occurred.

Superheat. This was treated as single-phase vapor per Paragraph 8.2.3, with variable temperature.

8.2.2 Condensing Heat Transfer. Akers (Reference 8-29) analyzed condensing heat transfer with high vapor velocity by assuming an annular layer of condensate and a central vapor core, and recognizing that the thermal resistance is almost entirely in the liquid near the wall and that the flow character of this liquid should determine the heat transfer. It was reasoned that the liquid flow character would remain unchanged if the vapor core were "replaced" by a liquid flow that produced the same interface shear. An equivalent mass velocity was accordingly derived as

$$G_E = \bar{G}_L + \bar{G}_V \left(\frac{\rho_L}{\rho_V} \right)^{1/2}$$

and used in calculating Re . Data correlations were then attempted along the line of the usual single-phase forced convection Dittus-Boelter correlation between N_{NU} , N_{PR} , and Re . Above $Re = 50,000$ the data almost perfectly matched the correlations obtained with single-phase fluids, but condensing heat transfer was higher than that for single phase when Re was lower than 50,000.

In this study it was recognized that the deviation obtained by Akers at lower Re might be a gravity effect as discussed in Paragraph 8.1.5, and that it might be better to use the more conservative extrapolation from high Re data. Remembering that this was essentially the standard Dittus-Boelter equation, and that the Colburn equation gives equivalent results, it was concluded that the best method for this study was to use the Colburn-type single-phase correlation from Paragraph 8.2.3. For condensing calculations, fluid temperature must be taken as constant and Re based on the equivalent mass velocity G_E defined above. This technique was checked against the Carpenter-Colburn method (see Paragraph 8.1.3) and found to be slightly more conservative.

8.2.3 Single-Phase Heat Transfer. Figure 8-11 presents the heat transfer and pressure drop data used for single-phase LH_2 or GH_2 . It is based on extrapolations of heat exchanger core data from Reference 8-31. J is equal to $N_{ST} \times N_{PR}^{2/3}$.

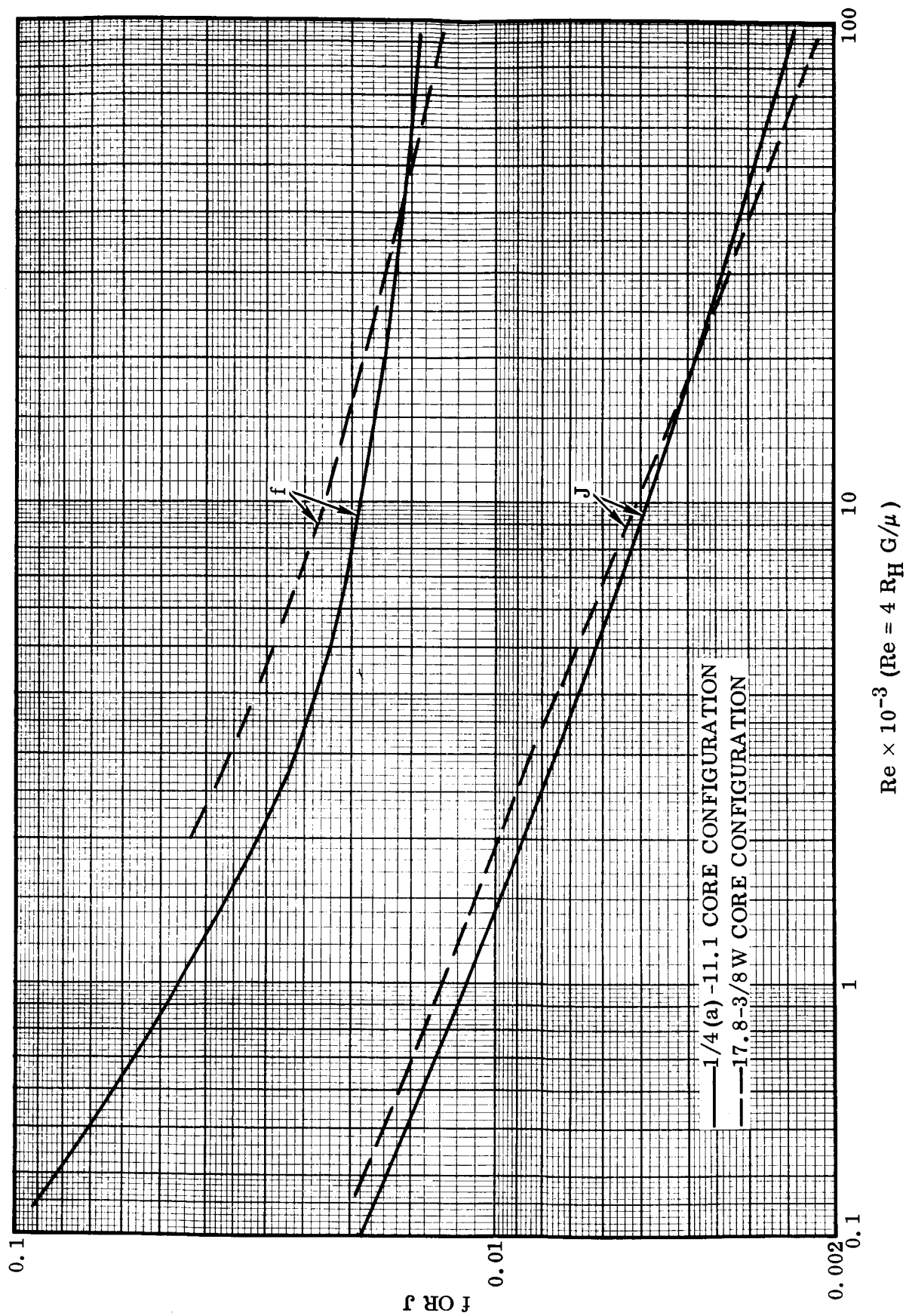


Figure 8-11. Single-Phase Heat Transfer and Friction Data

8.3 HEAT EXCHANGER SYSTEM SIZING PROCEDURES. A method of heat exchanger sizing and performance analysis was developed, based upon the heat transfer data recommended in Paragraph 8.2, for use over the full operating ranges of investigation for trade-off and parametric analyses. The method is similar to that used in the predesign calculations except for refinements in the areas involving boiling and condensing heat transfer.

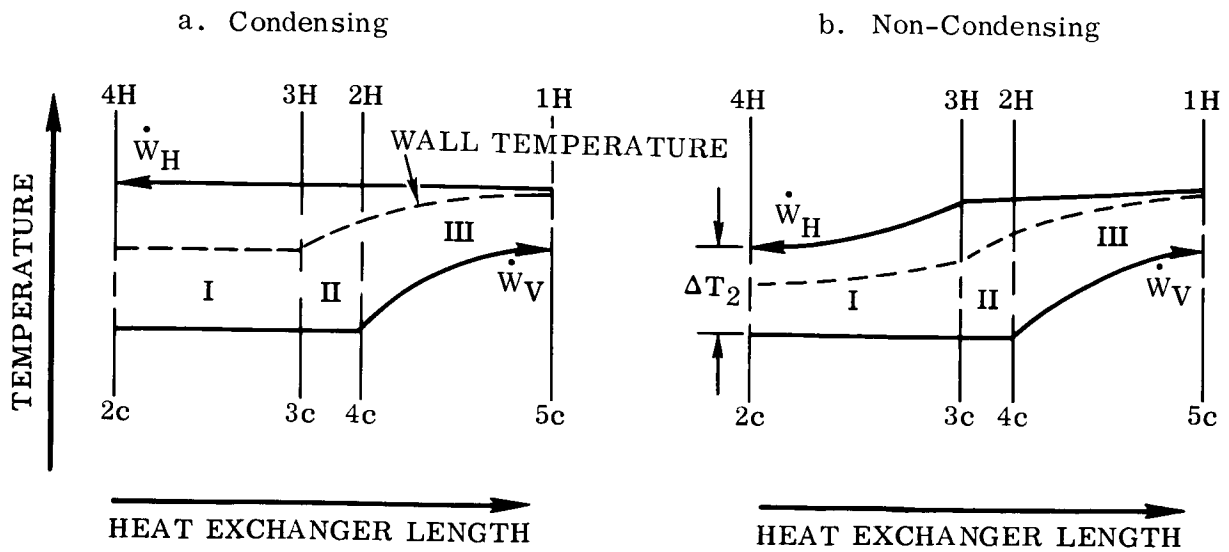
There are several problems to consider in the design of evaporative type heat exchangers. The distribution of gas and liquid throughout the heat exchanger cross section is important to have efficient operation since the presence of superheated gas in a portion of the exchanger will reduce the overall heat transfer from the hot-side fluid to the boiling fluid. Also, the velocities of the gas portion of the boiler should be kept low since carry-over (liquid droplets entrained in the gas and carried on through the exchanger) can be a problem. A counterflow plate/fin type of exchanger has been found to be effective in maintaining uniform gas/liquid distribution as well as providing efficient superheating of the exit vapor. Also, with a single pass on both hot and cold sides, as with the proposed counterflow exchanger, the circulating pump power and the vent-side velocities can be kept low. Packaging of the system appears to be relatively straightforward using the counterflow exchanger, as shown in Section 11. Therefore the counterflow type of exchanger is used as a model for the trade-off and parametric studies of Sections 9 through 12.

For these analyses the heat exchanger is considered to be divided into three sections based on the vent fluid condition.

- I Boiling up to 90-percent quality.
- II Constant temperature vapor, 90-percent to 100-percent quality.
- III Variable - temperature superheated gas.

The processes occurring through the system are illustrated in Figure 8-12 for zero-quality inlet (100-percent liquid non-condensing) and inlet qualities greater than zero (condensing). The T-S diagrams of Figure 8-12 represent the case where a common system inlet for both hot- and cold-side fluids is employed. The flow geometry is illustrated in Figure 11-1. For the hot-side condensing case, inlet qualities are assumed such that sufficient gas is present in the hot-side stream to maintain a constant condensation temperature throughout the exchanger.

8.3.1 Heat Transfer Data Used. In Region I the boiling-side (vent side) heat transfer data are taken from Figure 8-9, which is applicable for a saturation pressure of 14.7 psia. To get values at lower pressure the data from Figure 8-9 are multiplied by the correction factor from Figure 8-10. Cold-side heat transfer coefficients in Regions II and III are calculated using the curves of Figure 8-11 assuming 100-percent gas flow.



1H - HOT SIDE EXCHANGER INLET
 4H - HOT SIDE EXCHANGER OUTLET

1c - COLD SIDE THROTTLING VALVE INLET
 2c - COLD SIDE EXCHANGER INLET
 3c - COLD SIDE 90% QUALITY
 4c - COLD SIDE 100% QUALITY
 5c - COLD SIDE EXCHANGER OUTLET

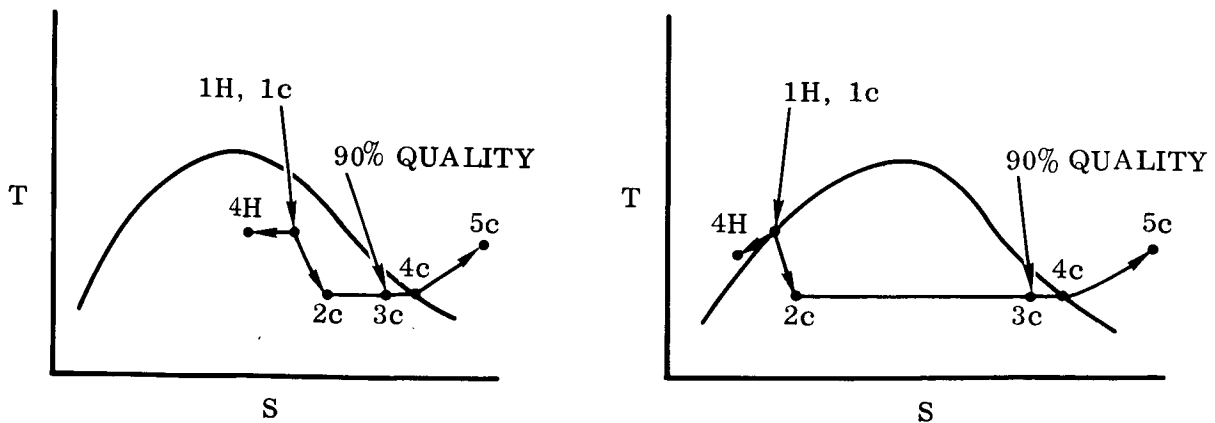


Figure 8-12. Heat Exchanger and System Flow Processes

The heat transfer coefficients on the hot-side are assumed to be constant throughout the exchanger and an average value is calculated. Where the hot-side inlet is saturated liquid (zero quality), the curves of Figure 8-11 are used. Where the hot-side fluid is a mixture of gas and liquid, it is assumed that the liquid is flowing at the heat exchange surface with a gas core in the middle condensing into the liquid surface. This model is described in Paragraph 8.2.2 and Reference 8-29. Using the method described in Reference 8-29, an equivalent mass velocity, G_E , is calculated from

$$G_E = \bar{G}_L + \bar{G}_V \left(\frac{\rho_L}{\rho_V} \right)^{1/2}$$

where \bar{G}_L is the mass velocity of the liquid flowing, taken as the average liquid flow rate divided by the total free flow area. The average liquid flow rate is an arithmetic average of the inlet and outlet liquid flow rates. \bar{G}_V is the average mass velocity of the gas calculated in the same manner as for the liquid. The amount of gas condensed in the exchanger is calculated from a hot- and cold-side heat balance

$$q = \lambda_H (\dot{W}_H)_{\text{condensed}} = \dot{W}_V (h_{5c} - h_{2c})$$

where the subscripts refer to Figure 8-12. From the calculated equivalent mass velocity an equivalent Reynolds number, $(Re)_E$, is determined from

$$(Re)_E = \frac{4 R_H G_E}{\mu_L}$$

and the data of Figure 8-11 used to determine J . The average hot-side film coefficient $(h_f)_H$ is then determined from the equivalent mass velocity, G_E , and saturated liquid properties data. From the data of Reference 8-31, heat exchanger surface effectiveness is determined as a function of heat transfer film coefficient. Values for a 1/4 (s) - 11.1 strip fin surface and the 17.8-3/8W surface used in the initial predesign of Paragraph 2.2 are plotted in Figure 8-13.

8.3.2 Exchanger Sizing Procedure. The required heat transfer areas for each region of the exchanger are calculated and summed to give the total required area. The procedures used for each section of the exchanger are discussed below.

Region I. The required heat transfer area in Region I is determined from the following heat balance.

$$q = (h_f \eta_o A_s \Delta T_f)_{fc} = (h_f \eta_o A_s \Delta T_f)_{fH} = (h_{3c} - h_{2c}) \dot{W}_v,$$

where subscripts refer to stations of Figure 8-12 and all data are for Region I. An iterative solution is required since the boiling heat transfer coefficient $(h_f)_c$ is a sensi-

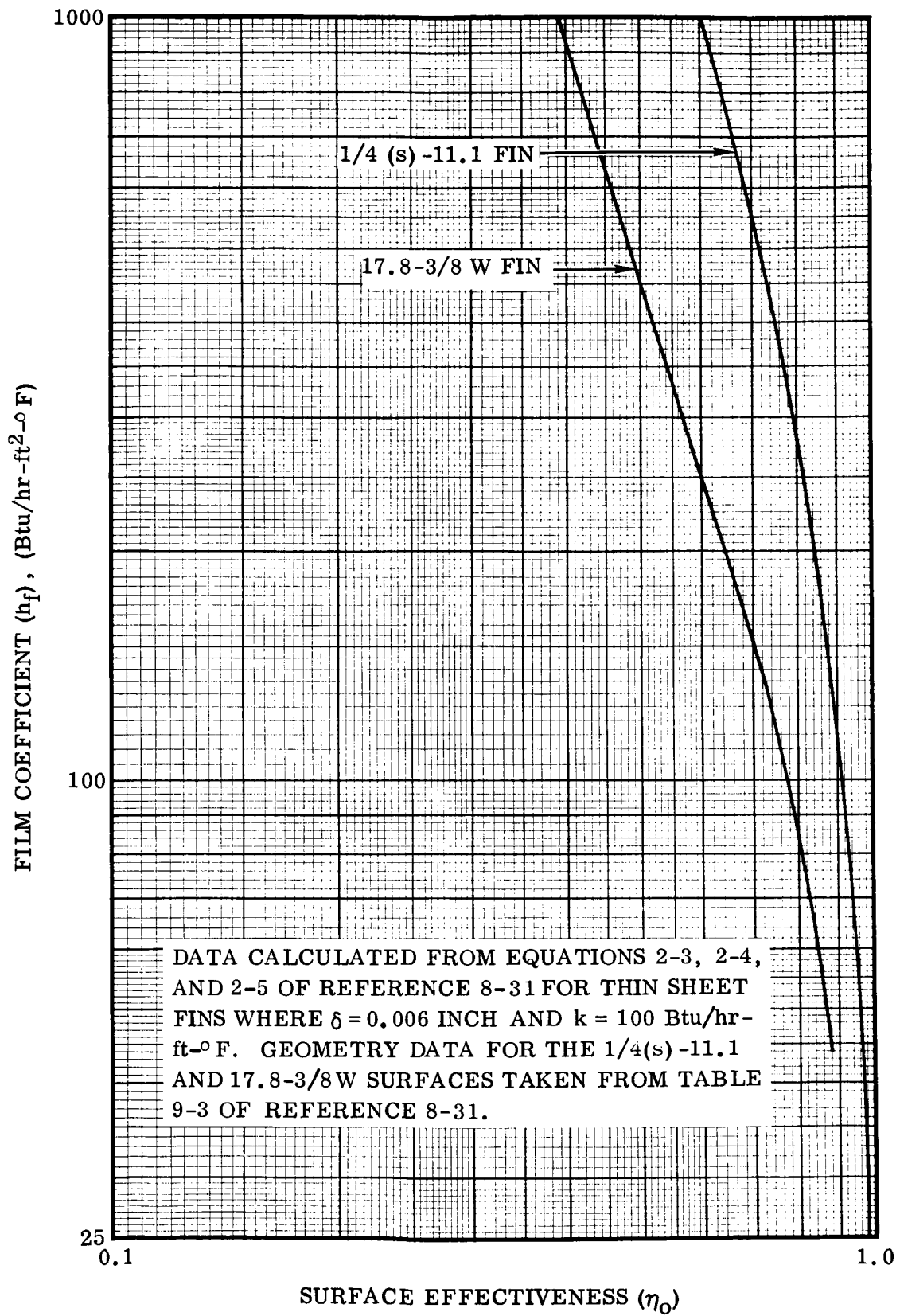


Figure 8-13. Heat Transfer Surface Effectiveness Versus Film Coefficient

tive function of the temperature difference $(\Delta T_f)_c$ between the exchanger wall and the boiling fluid saturation temperature (Figure 8-9). The iteration performed is similar to that done in Appendix B for the predesign calculations. Over the range of coefficients and wall thicknesses of the present study, the temperature gradient through the exchanger wall is determined to be negligible, and the temperature difference between the hot-side fluid and the wall $(\Delta T_f)_H$ plus that of the cold side $(\Delta T_f)_c$ equals the total temperature difference between hot- and cold-side streams.

$$(\Delta T_f)_c + (\Delta T_f)_H = \Delta T_2$$

where ΔT_2 is the temperature difference between hot- and cold-side fluids at the cold-side inlet (hot-side outlet), as illustrated in Figure 8-12. The hot-side fluid temperatures, where subcooling occurs, are calculated from $q = \dot{W}_H (C_P)_L \Delta T_H$.

Region II. From the individual hot- and cold-side film coefficients an overall heat transfer coefficient referred to hot-side surface area is determined.

$$U_H = \frac{1}{\frac{1}{(h_f)_H (\eta_o)_H} + \frac{1}{\frac{(A_s)_c}{(A_s)_H} (\eta_o)_c (h_f)_c}} \quad (18)$$

The required surface area for Region II is then calculated from the following heat balance.

$$q = U_H (A_s)_H \Delta T_m = (h_{4c} - h_{3c}) \dot{W}_v$$

where the mean temperature difference between the two streams is calculated as

$$\Delta T_m = \frac{\bar{T}_{2H} - \bar{T}_{3H}}{\ln \frac{T_{2H} - T_{4c}}{T_{3H} - T_{3c}}}$$

$$\text{and } T_{4c} = T_{3c}.$$

Where the temperatures of both streams remain constant, as where the hot-side fluid is condensing, then ΔT_m is simply $T_{1H} - T_{2c}$.

Region III. Equation 18 is used to calculate the overall coefficient U_H for Region III.

The cold-side properties are determined at the average temperature $\frac{(T_{5c} + T_{4c})}{2}$.

The heat balance is

$$q = U_H (A_S)_H \Delta T_m = (h_{5c} - h_{4c}) \dot{W}_v$$

from which the required transfer area $(A_S)_H$ can be determined. In this case

$$\Delta T_m = \frac{(T_{2H} - T_{4c}) - (T_{1H} - T_{5c})}{\ln \left(\frac{(T_{2H} - T_{4c})}{(T_{1H} - T_{5c})} \right)}$$

The normal calculation sequence is to assume a vent outlet temperature, T_{5c} , and calculate the required exchanger areas for each region and then sum the results to get a total exchanger area.

The area obtained in the above manner represents the basic straight core section and does not include inlet and outlet angle flow sections as shown in Figure 11-1. These inlet and outlet sections tend to apply a design safety factor to the system. The weights for trade-offs and parametric analyses are determined in the same manner as described in Paragraph 2.2 and Appendix B, and the 1.43 multiplication factor for total exchanger weight to basic core weight is used.

8.3.3 Pressure Drop Calculations. Heat exchanger pressure drops for single-phase fluid flow are calculated from the equations and data of Reference 8-31.

$$\Delta p_e = \frac{G^2}{2 g_o \rho} \left(\xi_c + \xi_B + \xi_e + f \frac{A_s}{A_c} \right)$$

where

ρ is the inlet fluid density

ξ_c = pressure loss coefficient due to inlet

ξ_B = pressure loss coefficient due to bends

ξ_e = pressure loss coefficient due to exit

The term $f \frac{A_s}{A_c}$ represents the loss due to flow through the core. The friction factor, f , is taken from Figure 8-11. The pressure loss in the flow ducting between the pump and the heat exchanger is determined from

$$\Delta p = \xi_T \frac{\rho u^2}{2 g_o}$$

where the total loss coefficient, ξ_T , is the sum of the individual coefficients for bends, tees, expansions, and contractions in the ducting.

Where the fluid is a two-phase mixture of gas and liquid the methods described in Reference 8-33 are used to calculate pressure drops. This method is further described in Appendix D.

The total pressure drop from pump outlet to hot-side exchanger outlet is then used to calculate the theoretical fluid horsepower required from the pump.

The cold-side free flow area is sized such that the maximum vent-side pressure drop through the exchanger is less than 0.1 psi.

SECTION 9

TRADE-OFF STUDIES FOR HEAT EXCHANGE VENT SYSTEM

9.1 INLET LOCATIONS. The heat exchange system has been found to be the most attractive of the various methods of vapor venting considered, as previously discussed in Section 7 of this report. The heat exchange system can be so designed that it will adequately vent vapor whether the system is located within the forward dome region surrounded predominantly by saturated vapor or in the lower region of the tank within a predominantly liquid hydrogen environment. Even though the heat exchanger system will perform adequately under all conditions of liquid/vapor distribution within the tank, the location of inlets still needs to be considered from the standpoint of minimization of additional boil-off; ease of system startup; facilitation of tank circulation to minimize stratification; and minimization of weight penalty for installation considering such problems as suspension, liquid surge loads, and required lengths of inlet and exit lines.

It is concluded that the heat exchanger vent system for the S-IVB hydrogen tank should be located in the forward end of the tank, suspended from the existing man-hole cover-plate if possible, and have a common inlet for both the vent- and tank-side streams. Reasons for this choice are discussed in the following subsections.

9.1.1 Common Inlet for Both Vent-Side and Tank-Side Streams. In the absence of any control over the position of the vent inlet with respect to the pump inlet, the fluid at the pump can be either gas or liquid when the most severe condition of liquid at the vent inlet exists. From the analysis described in Appendix B it can be seen that the pump speed requirement for a given turbine output power is significantly higher for pump operation in gas than in liquid, and also the start-up time would be longer with the pump in gas. The analysis of Section 10 shows that operation with start-up in liquid will not result in the loss of liquid, however, the design margin was not high. Therefore, with pump operation in gas, it is not unlikely that some liquid will be vented during start-up if the vent inlet is inundated with liquid. This most adverse combination of inlet qualities, i. e., liquid on the vent side and vapor on the tank side, can be easily avoided by designing a common inlet for both streams.

This would have the added advantage of reducing the steady-state design requirement. The design condition of 100-percent liquid at both inlets is less stringent than that of liquid on the vent side and vapor on the tank side.

Since it is a relatively simple matter to locate the pump and vent inlets together, this is recommended.

9.1.2 Effects on Tank Heat Input and Stratification. With a common inlet location for the two streams, there remain two choices of location for the inlets, and, therefore, the venting system: in the forward dome region, predominantly surrounded by gas; or near the aft end of the tank, normally immersed in liquid.

Estimates of the changes in external heat transferred into the tank between the idealized case of venting without a device, and venting with a heat exchange venting system in the two locations are given below. These estimates were based on the assumption that there is no heat transfer coupling between the liquid and vapor caused by the pump circulation within either region.

Location of system	Forward in tank (in ullage space)	Aft in tank
Estimated increase in q to tank during 4-1/2-hr coast	34,000 Btu	5500 Btu
Approximate resulting increase in boil-off	180 pounds	30 pounds

This is only part of the story, however. If the system were located in the tank bottom and there were no heat transfer between the liquid cooled by the system and the relatively hot gas, as assumed in the above estimates, part of the liquid would become sub-cooled. This would result in a faster temperature rise for vapor and the remainder of the liquid because the total external heat input would have to be stored by only part of the tank fluid. The net effect of such temperature stratification would be an increase in the weight of vented propellant above the requirement for a mixed tank. On the other hand, if this location of the device in the aft end of the tank caused liquid to be circulated over the forward dome by the pump, there would result a large increase in external heat load to the tank, of the order of 1000-pound increase in boil-off during 4-1/2 hours. Although flight results are needed to determine the behavior of the propellant in a stage with mixing, either of the above alternative possible effects would motivate installation of the venting system in the forward ullage region.

9.1.3 Installation Considerations. Locating the venting system in the forward region of the tank seems to be preferable for installation convenience. Several of the reasons for this are listed below.

- a. A low installation weight penalty would result from suspending the system from the existing man-hole coverplate located at the forward end of the tank.
- b. Suspending the system from the forward coverplate would result in convenient accessibility. The portion of the system located inside the tank would weigh approximately 95 pounds. Standard industrial practice requires any equipment over 40 pounds to be handled by two men and any equipment over 80 pounds to be handled by mechanical hoists. Installation, maintenance, and removal of the heat exchange venting system would be more difficult if it were located elsewhere in the tank.

- c. It would be desirable to connect the venting system to the existing ullage thruster and ground vent system lines. All of these are located in the forward region of the tank. Installation of the venting system in the aft portion of the tank would require long lengths of ducting to make these connections.

All of these considerations indicate an increase in the weight of the installed heat exchange system and additional installation and maintenance complexity if the system were not located in the forward end of the tank.

9.2 AVAILABLE THRUST FROM VENTED HYDROGEN GAS. For a vented propellant tank system, the vented gas can be used to provide thrust to settle the propellant in the tank during space flight. The thrust available is dependent upon the vented gas temperature and pressure.

Theoretical specific impulse data for hydrogen gas are shown in Figure 9-1 for a range of nozzle pressures and temperatures. The data were calculated, using the hydrogen property data of Appendix A and References 9-1 and 9-2. The curves show the effects of nozzle inlet temperatures corresponding to saturated vapor and for several higher temperatures. The dashed line marked "phase change" marks the boundary between nozzle inlet conditions for which condensation would theoretically occur before the pressure reaches 1 mm Hg and those conditions for which no condensation would be predicted. The comparison of these theoretical results with those expected in practice is straight-forward for the cases where no condensation is predicted analytically; however, for those sets of inlet conditions near saturated vapor for which liquid or solid hydrogen could theoretically form in the nozzle there is a question about the most accurate method of estimating nozzle performance. Theoretical results using the two most common models (equilibrium flow, which assumes the chemical composition to be in equilibrium at all points in the nozzle; and frozen flow, in which the composition is "frozen" or assumed to be constant in the nozzle) are compared in the bottom two curves of Figure 9-1. The design point for the present S-IVB nozzles is also shown on the figure. The data show that the I_{sp} calculated for equilibrium flow is approximately 20 percent greater than that calculated for frozen flow, for saturated vapor inlet to the thrusters. The two curves represent the theoretical upper and lower performance limits for the vented gas. Therefore, the actual performance would probably fall between these limits for saturated vapor conditions.

The theoretical equilibrium specific impulse for saturated vapor for nozzle pressure from 4 to 24 psia ranges from 71 to 82 seconds respectively. Although the actual nozzle performance might have a slightly greater variation at low pressures, it seems reasonable to predict that the nozzle inlet pressure can vary over a considerable range without causing a large degradation in thruster performance. Therefore, a minimum nozzle upstream pressure of 4 psia was used in the optimization studies of Paragraph 9.3.

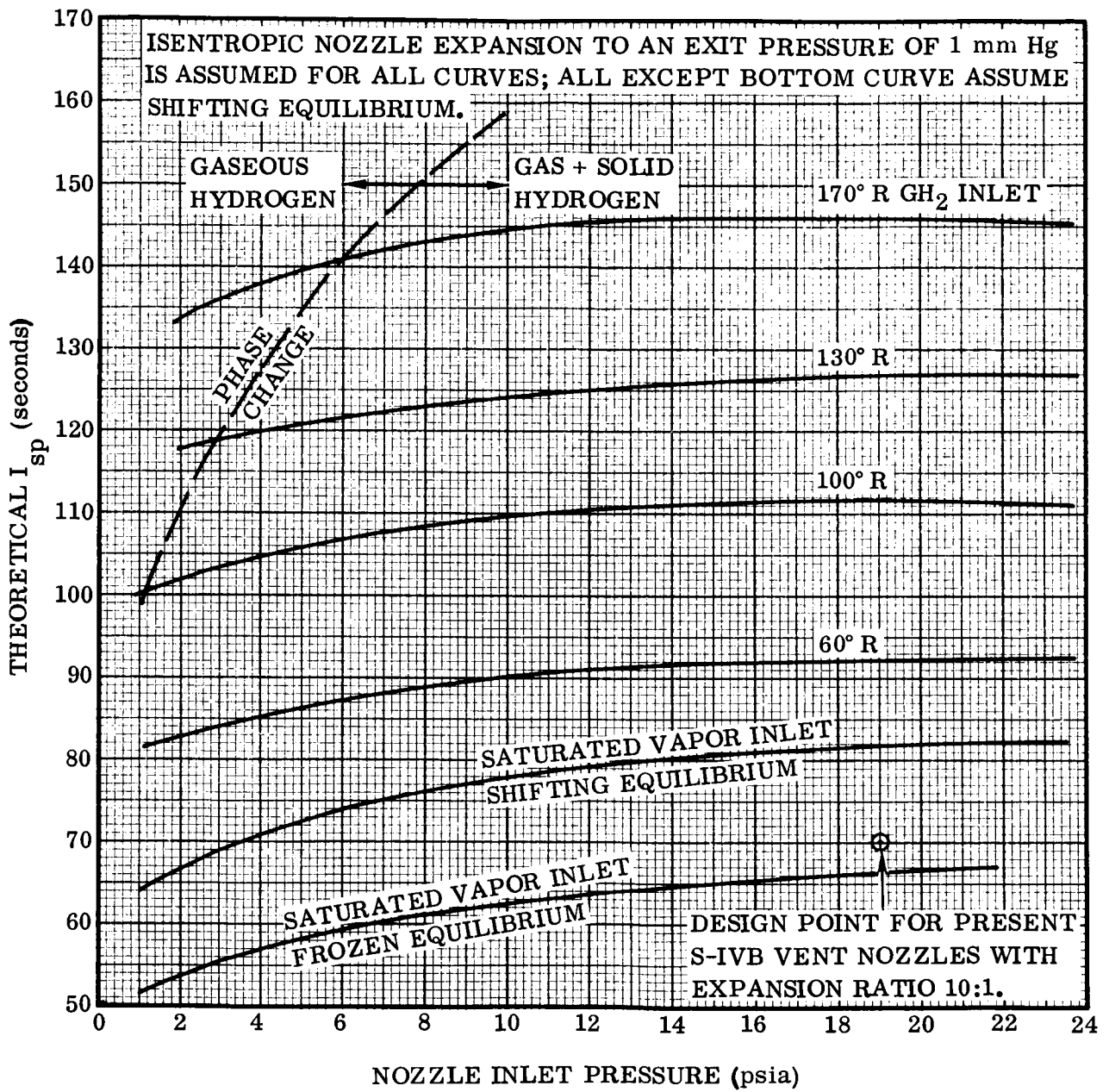
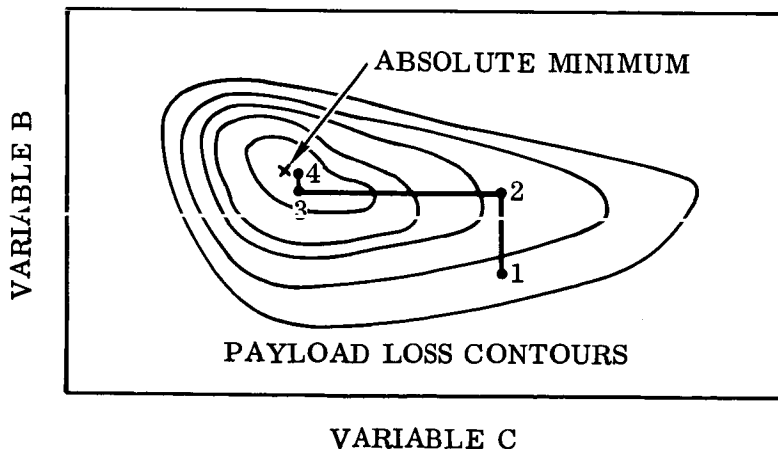


Figure 9-1. Theoretical Specific Impulse Versus Nozzle Pressure for Para-Hydrogen

9.3 OPTIMUM SYSTEM OPERATING CONDITIONS. There are many design factors that might be varied independently and have significant effects upon the size and performance of a heat exchange system. After fixing several of these variables (flow arrangement and number of passes on both vent side and tank side, inlet fluid conditions on each side, and vent flow rate), there are remaining at least the following that might be considered in trade-off studies.

- a. Exchanger cross-sectional dimensions.
- b. Number of parallel channels on each of vent (cold) and tank (hot) side exchanger passes, or plate spacing.
- c. Type and size of fins.
- d. Hot-side flow rate, within limits of available turbine power.
- e. Exchanger pressure (turbine inlet pressure is nearly the same).
- f. Temperature of vent stream at exchanger exit.

A complete optimization of a heat exchange system would require a very large number of exchanger and other system component sizings. Since this was impractical for present purposes, a simplified gradient-search procedure with only one variable changing at a time was employed to partially optimize the base system parameters and to illustrate changes possible from variations in the variables listed above. This kind of search is illustrated for two independent variables in the sketch.



The initially assumed set of variables corresponds to Point 1. Optimizing payload loss with respect to Variable B with all other variables held constant (C, in this case) would result in the improved Point 2. Then, varying C with B held constant would result in the choice of variables corresponding to Point 3. A further step in the search with B varying could be used to locate Point 4. This procedure can be extended to more than two independent variables. This was done in the trade-off studies described later in

this section, but this process is difficult to illustrate in a two-dimensional diagram. It is realized that such a search procedure will probably not quite reach the absolute minimum or might even converge toward a local minimum (if one existed), but the contour surfaces representing physical systems are seldom seriously pathological; therefore, this procedure seems adequate for the purposes of this study.

Application of this search procedure to the heat exchange system is described in the following paragraphs. The heat transfer data recommended in Paragraph 8.2, the heat exchanger sizing procedure outlined in Paragraph 8.3, and the method of turbine analysis given in Appendix F were used to develop the necessary system size and performance data. The exchanger configuration was assumed to be counter-flow with one vent-side and one tank-side pass, the inlet condition for each side taken as saturated liquid hydrogen at 20 psia, and the design (maximum) vent rate held at 0.35 lb/sec. The initial set of variable conditions included several of those used in the predesigns of Section 2 (12- by 12-inch cross section, $G_H = 106,700 \text{ lb/hr-ft}^2$, and same wavy fins with 0.413-inch plate spacing), but with a single-pass, counter-flow, 8.5-psia exchanger. The various conditions are compared on the common basis of system effect on available payload weight using the method outlined in Appendix E and previously employed in the comparisons of Section 7. The payload change is referenced to the idealized case of venting of 20-psia saturated vapor without a separator.

First, the effect of changing exchanger cross-sectional size, holding all other variables constant except the number of hot- and cold-side channels, was briefly assessed by using two sizes: the original 12- by 12-inch, and 11- by 17-inch, which is approximately the largest size that could pass through a 28-inch-diameter hole (i. e., the size of the present forward access hole in the S-IVB) with the system packaging shown in Figure 11-1. The results of these two sizes are represented by Point 1 and Curve 2 of Figure 9-2. It can be observed that the 11 by 17 size results in a considerably lower payload loss (at 8.5-psia exchanger pressure and 38°R vent temperature at exchanger exit) than does the 12 by 12 size. Therefore, the 11- by 17-inch cross section was used in all subsequent trade-offs.

Next, an alternative type of finned surface was compared with the original one. The wavy fins and 0.413-inch plate spacing used in Section 2 were compared with strip fins and 0.25-inch plate spacing, as summarized in Curves 2 and 3 respectively of Figure 9-2. The difference in payload weight loss is approximately constant, and the strip fins with 0.25-inch plate spacing show an improvement over the original core geometry for all values of vent-side exchanger outlet temperature. This may be largely due to the decreased plate spacing since it would be expected that a reduced plate spacing with resulting decrease in fin area/primary heat transfer area would be more efficient for high film coefficients such as those calculated for the boiling side. This comparison is illustrative of the changes that might result from differences in exchanger core construction.

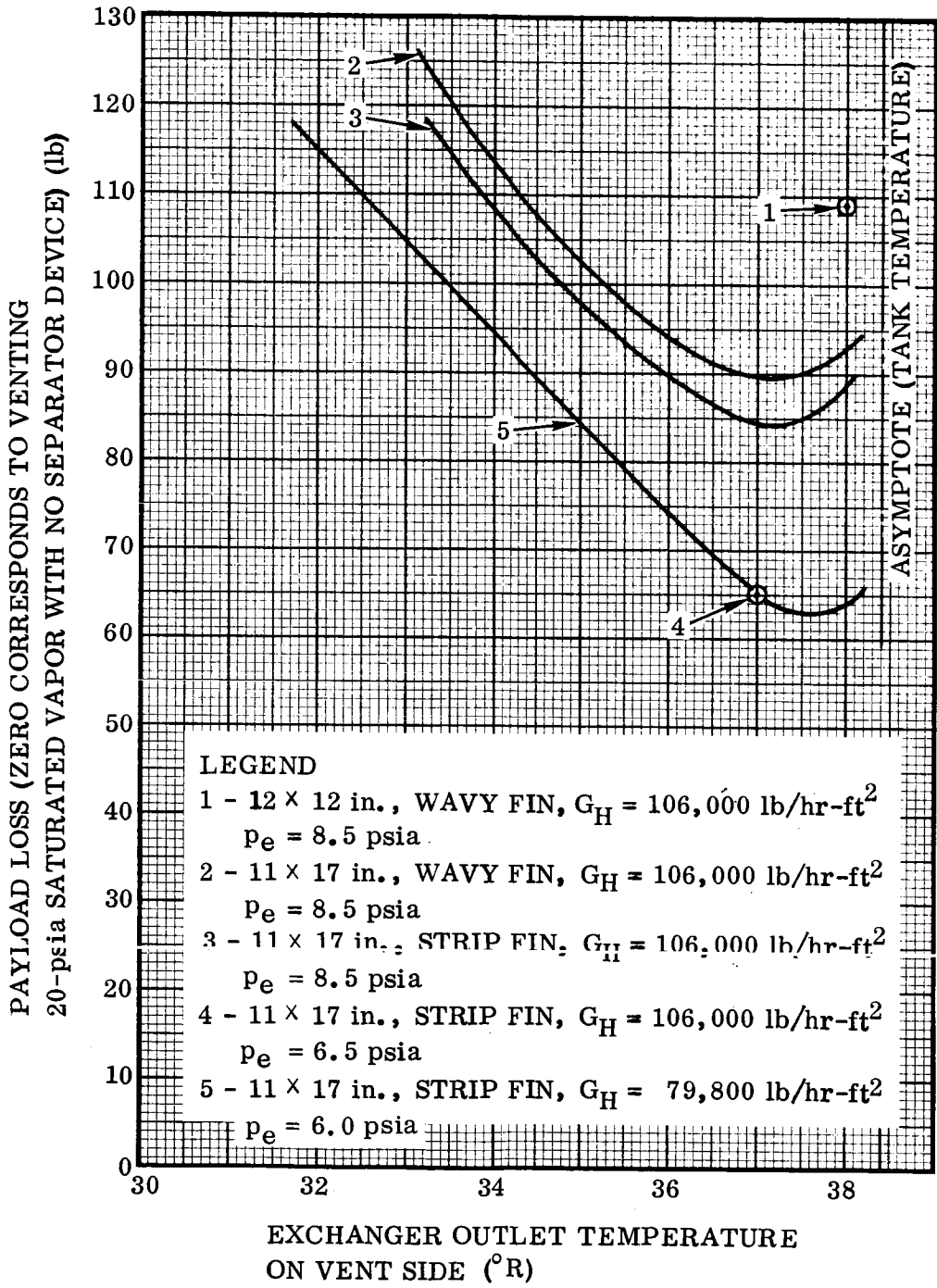


Figure 9-2. Payload Loss Versus Heat Exchanger Outlet Temperature for Various Exchanger Design Conditions

The effect of exchanger superheat (or exchanger vent stream outlet temperature) can also be seen from Curves 2 and 3 of Figure 9-2. The minimum payload loss occurred for both exchanger cores at about 37°R.

The effect of exchanger pressure for two different hot-side flow rates is shown in Figure 9-3, indicating that the exchanger pressure should be as low as possible in order to minimize total payload weight loss. The limit upon this pressure would then be imposed by the minimum allowable turbine downstream pressure, fixed by downstream requirements. The turbine downstream pressure was assumed to be 5.78 psia for the trade-offs of this study, which would allow about 4 psia at the ullage thrusters. The available turbine output power for 5.78-psia back pressure and 37.0°R inlet temperature is plotted versus turbine upstream pressure in Figure 9-4. Also shown in Figure 9-4 is the required turbine output power to pump tank fluid through the exchanger at two different flow rates. The two intersections of these curves with the available turbine power curve represent the minimum turbine upstream pressures that are possible without supplying auxiliary power. The values are about 6.0 psia and 6.5 psia for G_H of 79,800 and 106,700 lb/hr-ft² respectively. If the two G_H values are then compared at their respective minimum allowable exchanger pressures (represented by the two circles on the curves of Figure 9-3), the total loss in payload weight is approximately the same. An earlier comparison, identical to the one just described, but with the turbine downstream pressure set at 4.3 psia instead of 5.78 psia, indicated a slightly lower payload loss for the 79,800 value of G_H than for the 106,700 value. Because of this, the lower G_H value was chosen for the parametric analysis of Section 12 and the design of Section 11, although the higher G_H value would have been an almost equally good choice.

The optimum exchanger vent-side outlet temperature for a 6-psia exchanger pressure and $G_H = 79,800$ is seen to be slightly greater than 37°R from Curve 5 of Figure 9-2.

In summary, the most desirable set of system conditions found from the trade-off studies of this section, for 20-psia saturated liquid inlet to the venting system, is

Counter-flow exchanger.

One pass on each side.

11- by 17-inch exchanger cross section.

Strip fins with 0.25-inch plate spacing (more detail is given in Table 11-1).

6 psia exchanger pressure on vent side.

5.78-psia turbine back pressure.

79,800 lb/hr-ft² hot-side mass flux.

37°R cold (vent) side exchanger outlet temperature.

The changes in available payload weight caused by boil-off rate change, hardware weight, and their sum are plotted versus exchanger outlet temperature on the vent side in Figure 9-5. The total payload change curve is identical to Curve 5 of Figure 9-2.

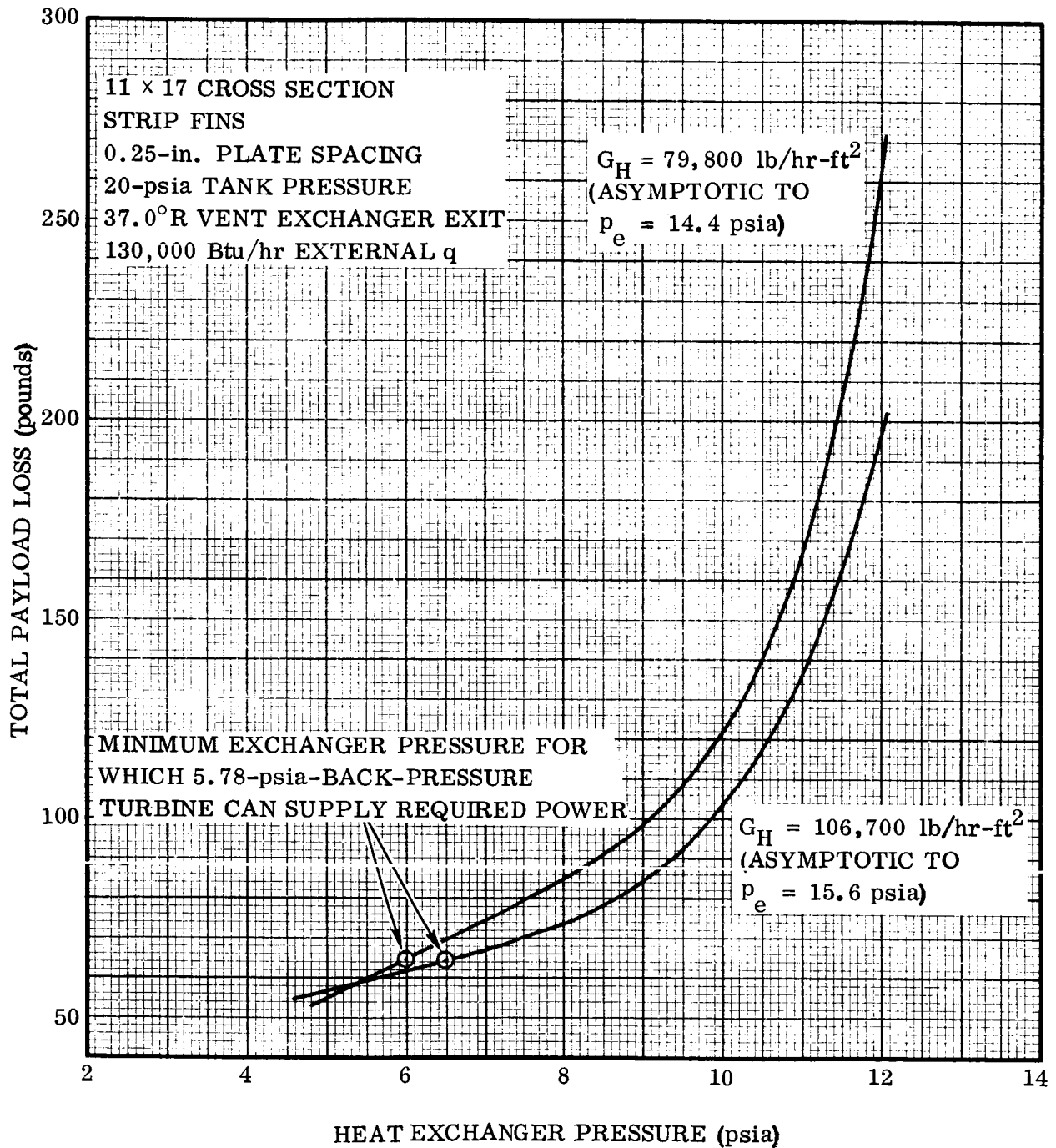


Figure 9-3. Payload Decrease Versus Heat Exchanger Pressure for Two Values of Exchanger Hot-Side Mass Flux, G_H

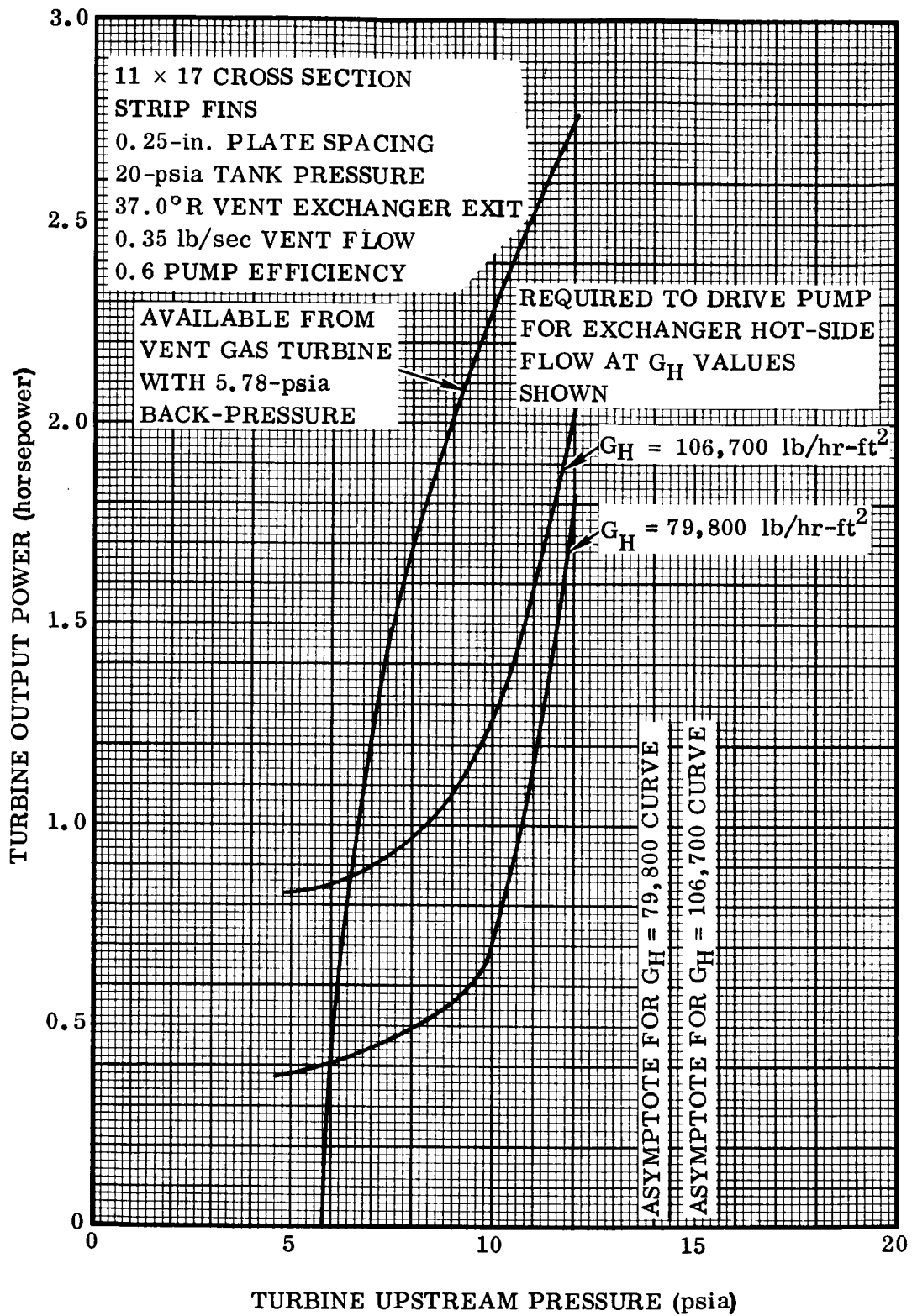


Figure 9-4. Available and Required Turbine Output Power Versus Turbine Upstream Pressure

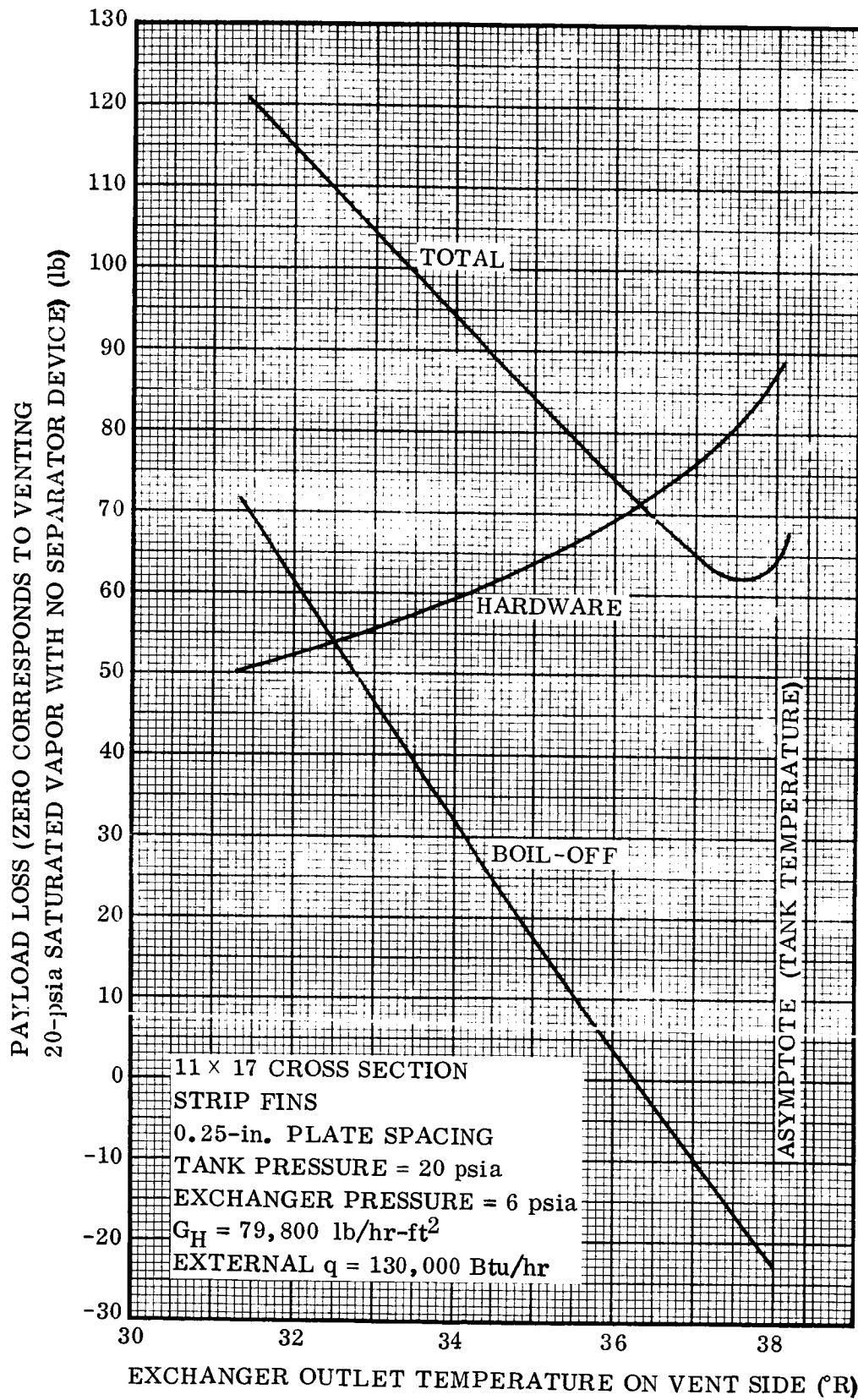


Figure 9-5. Payload Decrease Versus Vent-Side Exchanger Outlet Temperature for Set of Conditions Chosen From Trade-off Studies

SECTION 10

TRANSIENT BEHAVIOR OF HEAT EXCHANGE SYSTEM

Sudden changes in the inlet fluid quality and flow rate are the primary transients imposed on the heat exchanger type of vent system. The most severe transient condition is when the vent cycle is initiated (0 to full flow) with the vent inlet inundated with liquid. Here the time it takes for the pump to reach an operating speed sufficient to provide heat transfer to vaporize all the vent side fluid is critical. If this time exceeds the cooldown time of the heat exchanger mass, then some liquid will likely be vented. Also, with significant quantities of liquid at the turbine inlet, the turbine efficiency will be low and the unit may not reach a circulation speed sufficient to vaporize all the vent side fluid. Thus a continuous venting of some liquid would occur during periods of system inundation. The heat sink of the system components is the primary factor tending to prevent the venting of liquid during start-up.

The possibility of liquid loss during start-up in liquid hydrogen is analyzed for the S-IVB system described in Paragraph 11.1.

The turbine/pump acceleration characteristics are estimated and discussed in Paragraph 10.1. These results are then combined in Paragraph 10.2 with analysis of heat exchanger cooldown times to draw conclusions about the estimated transient behavior of the overall system. The conclusions are summarized in Paragraph 10.3.

10.1 TURBINE/PUMP ACCELERATION. The pump unit described in Paragraph 11.1 operates with a direct drive from the turbine; therefore, the pump speed equals the turbine speed. Turbine/pump acceleration is calculated from the excess of turbine output torque over pump load torque existing during start-up. The load variation as a function of speed is based on the pump laws discussed in Paragraph 2.2 and Appendix B. The turbine equations presented in Appendix F are used to calculate the available turbine torque during start-up with the condition of fixed design

where

$$\theta_0 = \text{constant}$$

$$\beta_1 = \text{constant}$$

$$\theta_1 \text{ varies from } \theta_0 \text{ at zero speed to } \beta_1 \text{ at full speed.}$$

The steady-state "design" conditions are

- a. Operation in saturated LH_2 at 20 psia.
- b. Turbine inlet pressure = 6 psia.

- c. Turbine inlet temperature = 37°R .
- d. Turbine/pump speed = 3000 rpm.
- e. Pump input/turbine output power = 0.418 horsepower.
- f. Moment-of-inertia of pump and turbine combination = $0.00583 \text{ slug-ft}^2$.

Considering the tank pressure sequences occurring in the S-IVB during ground fill and boost, it is anticipated that vapor will be trapped between the throttling regulator and the downstream shutoff valve such that upon opening of the vent valve, initial turbine operation will be with this trapped vapor. When the heat exchanger pressure drops to 6 psia, the throttling regulator will then begin controlling the exchanger and turbine pressure. The presence of vapor at start-up can also be ensured by incorporating a relief function in the heat exchanger maintaining a pressure slightly below tank pressure, such that any hydrogen trapped in the exchanger will be in a superheated condition. Another possibility is to initiate low-rate venting just prior to injection into orbit to ensure starting of the turbine with ullage gas.

The following analysis is made assuming trapped gas is available for initial turbine start-up. The turbine torque output is calculated in two phases.

- a. Bleed-down from storage pressure to normal operating pressure. During this interval the throttling regulator remains closed and u_0 and \dot{W}_V vary as a function of time, and the turbine torque varies as a function of time, \dot{W}_V , u_0 and ω . An iterative solution is performed.
- b. Steady flow at operating pressure. During this interval the throttling regulator modulates to maintain a constant turbine upstream pressure. u_0 is constant at 259 fps, \dot{W}_V is constant at 0.35 lb/sec, and the turbine torque varies solely as a function of ω .

For the bleed-down process it is assumed that the vent side of the heat exchanger initially contains 1 cubic foot of gaseous hydrogen at 19 psia and tank temperature of 38.4°R . This quantity of gas will then flow through the nozzle at a varying rate until the pressure falls to operating pressure, at which point the throttling valve opens to maintain the operating pressure constant. The approach is to assume a time interval at the initial velocity and flow rate, then from end-of-interval-density calculate the equivalent adiabatic temperature ratio and velocity ratio. From these the end-of-interval-flow-rate can be calculated and the time interval revised to correspond to an average flow rate. Without heat transfer the expansion in the chamber (vent side of heat exchanger) is considered adiabatic. Heat transfer will, however, occur at an assumed initial rate of 14.89 Btu/sec- $^{\circ}\text{F}$. The initial condition assumed for each interval is the final condition of the preceding interval. One-millisecond calculations are used.

These calculations gave a bleed-down time of 0.05 second. The torque characteristics during bleed-down were calculated from the flow and velocity determined for each interval.

The difference between turbine torque and pump torque is then the accelerating moment where torque is equal to the product of angular acceleration and moment of inertia ($\tau = I\alpha$). Then, since rotational velocity is the product of time and angular acceleration ($\omega = \alpha t$), the time to accelerate is solved as the integral $\int \frac{d\omega}{\alpha}$ where $\alpha = \frac{T}{I}$ and $\tau = f|\omega|$.

This integration is performed graphically, and the resulting acceleration time versus angular velocity is plotted in Figure 10-1 for the "trapped gas" case and for the case where there is no trapped gas (start-up with steady flow of 0.35 lb/sec).

10.2 HEAT EXCHANGER OUTLET CONDITION AT START-UP. Due to the heat capacity of the heat exchanger the initial liquid entering the system will be completely vaporized, and there will be a finite time to cool the metal to the point where all the liquid entering the system is no longer vaporized. If this "cooldown" time is long enough to allow the pump to come up to a circulation speed sufficient for external heat transfer to vaporize all further vent fluid, then it is reasonable to conclude that no liquid will be lost during start-up.

The start-up characteristics of the turbine/pump assembly were presented in Paragraph 10.1.

10.2.1 Heat Exchanger Cooldown. The method outlined in Reference 10-1 is used to determine the "cooldown" time of the exchanger. The following equation is used.

$$t_T = \frac{m_e (\bar{C}_P)_e \Delta T_e - V [\bar{\rho}_f (\bar{U}_f - h_1) - \rho_i (U_i - h_1)]}{\bar{W}_2 (\bar{h}_2 - h_1) - \bar{q}_a} \quad (1)$$

This equation represents an energy balance on the system between initial and final conditions with average values used for the system variables.

t_T is the total time for the system to go from initial to final conditions.

m_e is the mass of the exchanger.

$(\bar{C}_P)_e$ is the average specific heat of the heat exchanger material during cooldown.

ΔT_e is the temperature change of the heat exchanger between initial and final conditions.

V is the volume of the vent portion of the exchanger.

$\bar{\rho}_f$ is the final average fluid density in the exchanger.

\bar{U}_f is the final average specific interval energy of the fluid.

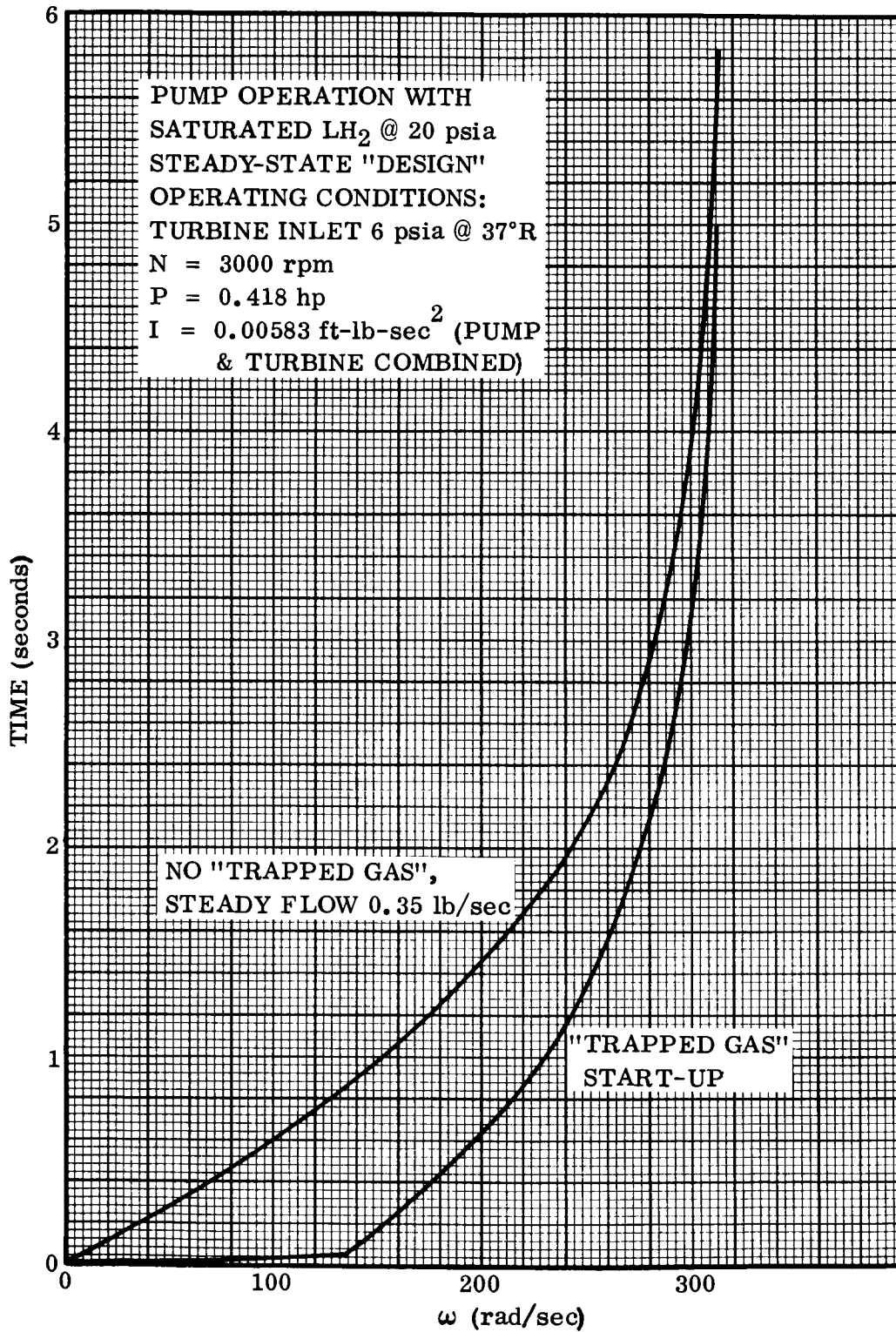


Figure 10-1. Turbine/Pump Start-up Speed Versus Time From Rest

h_1 is the specific enthalpy of the fluid entering the heat exchanger.

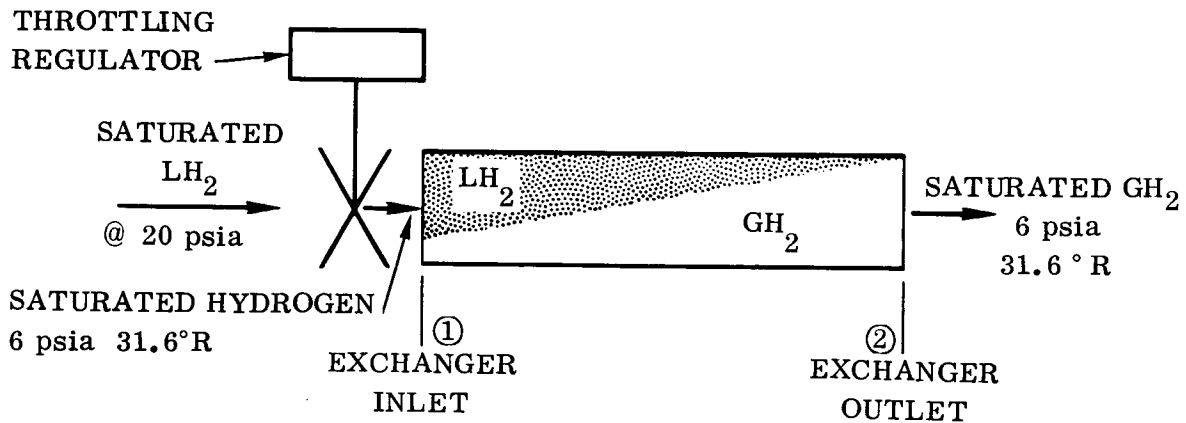
\bar{W}_2 is the average flow rate of fluid leaving the exchanger during cooldown.

\bar{h}_2 is the average specific enthalpy of the fluid leaving the exchanger.

\bar{q}_a is the average external heat transfer to the exchanger during cooldown.

The subscript i refers to the initial conditions in the exchanger at time 0, which is just prior to the first liquid entering the system.

The final condition, at time t_T , is when liquid first appears at the exchanger outlet. This condition is shown in the sketch.



$$h_1 = -104 \text{ Btu/lb}$$

$$h_2 = 74 \text{ Btu/lb}$$

$$\lambda @ 6 \text{ psia} = 193.5 \text{ Btu/lb}$$

$$\text{Saturated LH}_2 @ 6 \text{ psia}$$

$$h_L = -119.5 \text{ Btu/lb}$$

$$\rho_L = 4.6 \text{ lb/ft}^3$$

$$v_L = 0.218 \text{ ft}^3/\text{lb}$$

$$\text{Saturated GH}_2 @ 6 \text{ psia}$$

$$h_V = 74 \text{ Btu/lb}$$

$$\rho_V = 0.0375 \text{ lb/ft}^3$$

$$v_V = 26.7 \text{ ft}^3/\text{lb}$$

$$\text{Since } v_X = v_L + X(v_V - v_L) \text{ and } h_X = h_L + X\lambda$$

$$\text{Quality at Station 1, } X_1 = 0.08 \text{ and } v_1 = 2.34 \text{ ft}^3/\text{lb}$$

The various terms of Equation 1 are evaluated in the following paragraphs.

10.2.1.1 Heat Energy Extracted From the Exchanger, $m_e (\bar{C}_p)_e \Delta T_e$

$$m_e = 83.3 \text{ lb}$$

The specific heat of the exchanger is plotted as a function of temperature in Figure 10-2. The initial heat exchanger temperature will be at the tank fluid temperature of 38.4°R , and, assuming the heat transfer coefficient on the vent side is infinite with respect to the hot side during cooldown, the final exchanger temperature will be 31.6°R .

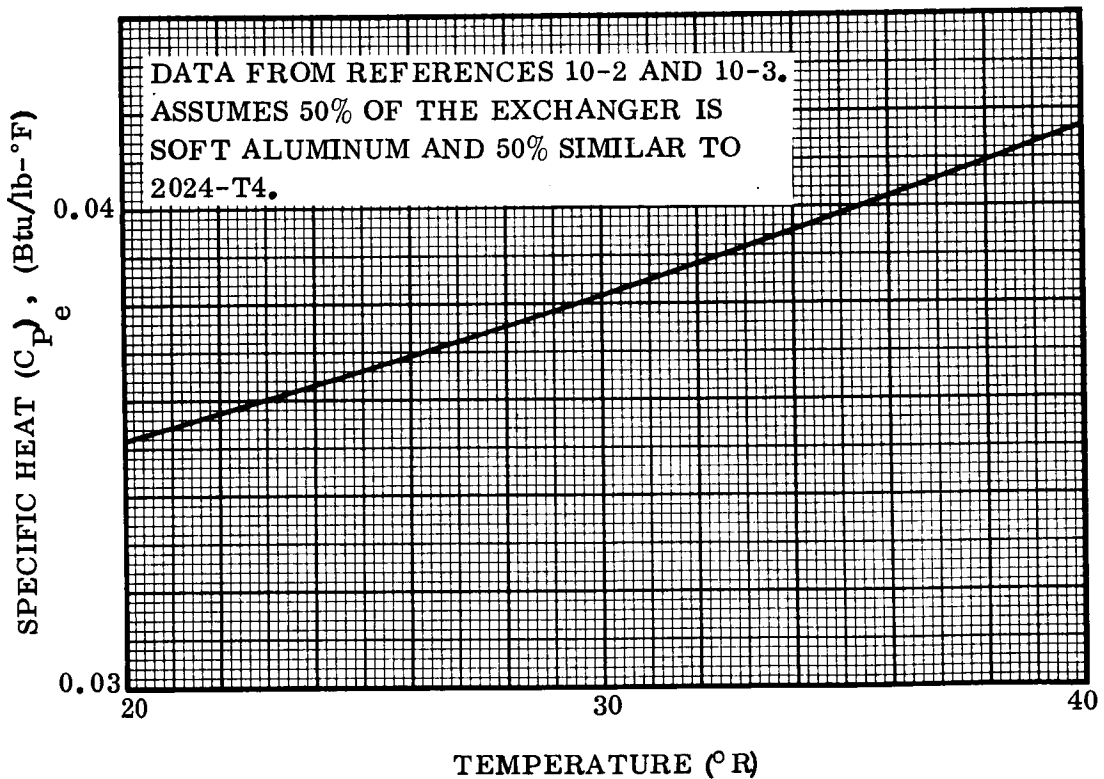


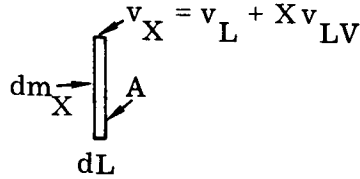
Figure 10-2. Heat Exchanger Specific Heat Versus Temperature

Then the average temperature is 35°R and, from Figure 10-2, $(\bar{C}_p)_e = 0.04 \text{ Btu/lb-}^\circ\text{F}$ and $\Delta T_e = 6.8^\circ\text{F}$.

Further,

$$m_e (\bar{C}_p)_e \Delta T_e = 83.3 (0.04) 6.8 = 22.6 \text{ Btu}$$

10.2.1.2 Final Average Fluid Properties. In determining the final average fluid density, the incremental mass elements in the exchanger are summed to get the total mass from which an average density is determined as follows.



$$m_T = \int_0^m dm_X = \int_0^{L_T} \frac{A dL}{v_L + X v_{LV}}$$

Assuming that the heat transfer from the exchanger to the vent fluid is proportional to its length, then the fluid quality distribution within the exchanger is also proportional to the length, i. e., $X \approx L$ and

$$L = L_T \frac{(X - X_1)}{(X_2 - X_1)}$$

where v_{LV} is the change in specific volume during evaporation.

$$dL = \frac{L_T}{X_2 - X_1} dX \quad \text{and} \quad m_t = \frac{A L_T}{X_2 - X_1} \int_{X_1}^{X_2} \frac{dX}{v_L + X v_{LV}}$$

$$m_t = \frac{V}{(X_2 - X_1) v_{LV}} \left[\ln \left(\frac{v_L + X_2 v_{LV}}{v_L + X_1 v_{LV}} \right) \right]$$

and

$$\bar{\rho}_f = \frac{m_t}{V} = \frac{1}{(X_2 - X_1) v_{LV}} \ln \left(\frac{v_L + X_2 v_{LV}}{v_L + X_1 v_{LV}} \right) \quad (2)$$

Substituting values into Equation 2

$$\bar{\rho}_f = \frac{1}{(1 - 0.08) 26.5} \ln \left[\frac{0.22 + 26.5}{0.22 + 0.08 (26.5)} \right] = 0.1 \text{ lb/ft}^3$$

The average final specific enthalpy of the fluid in the heat exchanger is similarly determined by an integration through the heat exchanger as follows.

$$h_T = \int \frac{h A dL}{v} = A \int \frac{(h_L + X \lambda) L_T}{(v_L + X v_{LV})(X_2 - X_1)} dX$$

$$H_T = \frac{V}{(X_2 - X_1)} \left[\int_{X_1}^{X_2} \frac{h_L dX}{v_L + X v_{LV}} + \int_{X_1}^{X_2} \frac{\lambda X dX}{v_L + X v_{LV}} \right]$$

$$H_T = \frac{V}{(X_2 - X_1)} \left[\frac{h_L}{v_{LV}} \ln \left(\frac{v_L + X_2 v_{LV}}{v_L + X_1 v_{LV}} \right) + \frac{\lambda (X_2 - X_1)}{v_{LV}} - \frac{\lambda v_L}{v_{LV}^2} \ln \left(\frac{v_L + X_2 v_{LV}}{v_L + X_1 v_{LV}} \right) \right]$$

From Equation 2

$$H_T = V \bar{\rho}_f \bar{h}_f = \frac{V \bar{h}_f}{(X_2 - X_1) v_{LV}} \ln \left(\frac{v_L + X_2 v_{LV}}{v_L + X_1 v_{LV}} \right)$$

then

$$\bar{h}_f = h_L - \frac{\lambda v_L}{v_{LV}} + \frac{\lambda (X_2 - X_1)}{\ln \left(\frac{v_L + X_2 v_{LV}}{v_L + X_1 v_{LV}} \right)} \quad (3)$$

Substituting into Equation 3

$$\bar{h}_f = -119.5 - \frac{193.5 (0.22)}{26.5} + \frac{193.5 (1-0.08)}{\ln \left[\frac{26.7}{0.22 + 0.08 (26.5)} \right]} = -48.1 \text{ Btu/lb}$$

If the energy contribution of the fluid initially in the exchanger at time 0 is neglected (a slightly conservative assumption) then $\rho_1 (U_1 - h_1) = 0$ and the heat absorbed by the fluid in the line is $V [\bar{\rho}_f (\bar{U}_f - h_1)]$.

Since

$$\bar{h}_f = \bar{U}_f + \frac{p_e}{\bar{\rho}_f},$$

then

$$V [\bar{\rho}_f (\bar{U}_f - h_1)] = V \left[\bar{\rho}_f \left(\bar{h}_f - h_1 - \frac{p_e}{\bar{\rho}_f} \right) \right] = 4.48 \text{ Btu}$$

for an exchanger volume of 1 ft³.

The average enthalpy of the exit vapor, h_2 , is 82.5 Btu/lb at 6 psia and the average exit temperature of 35°R. The exit flow rate is assumed constant at 0.35 lb/sec.

The mean rate of enthalpy efflux $\bar{W}_2 (\bar{h}_2 - h_1)$ is then evaluated as

$$\bar{W}_2 (\bar{h}_2 - h_1) = 0.35 (82.5 + 104) = 65.2 \text{ Btu/sec}$$

Substituting final values into Equation 1 gives

$$t_T = \frac{22.6 - 4.48}{65.2 - \bar{q}_a}$$

In the limiting case where $\bar{q}_a = 0$, $t_T = 0.278$ second.

10.2.2 Comparison of Cooldown With Pump Start-Up. To determine if the pump will be at a sufficient circulation speed to maintain a gas outflow from the exchanger, a heat flow balance is determined as follows. At 0.278 second (from Figure 10-1 for the "trapped gas" case) the pump speed is 165 rad/sec. The full-speed pump-flow rate is 46,000 lb/hr at a speed of 314 rad/sec, and since the flow rate is approximately proportional to the pump speed the hot-side fluid-flow rate at 0.278 second is

$$\dot{W}_H = 46,000 \left(\frac{165}{314} \right) = 24,200 \text{ lb/hr}$$

The required heat transfer rate to vaporize all incoming liquid in the present case is 222,000 Btu/hr. The heat exchanger hot-side transfer area is 535 ft². The required cold-side film ΔT is calculated from Figures 8-9 and 8-10 to be $(\Delta T_f)_c = 1.48^\circ \text{F}$ for the required q/A of 415 Btu/hr-ft². The hot-side mass velocity, $G_H = 42,000 \text{ lb/hr-ft}^2$, $(\text{Re})_H = 14,100$, $J = 0.00435$ from Figure 8-11, the hot-side film coefficient $(h_f)_H = 430 \text{ Btu/hr-ft}^2\text{-}^\circ \text{F}$, and the overall heat transfer surface effectiveness, $(\eta_o)_H = 0.735$. The required hot-side film ΔT is then

$$(\Delta T_f)_H = \frac{q}{(\eta_o)_H (h_f)_H (A_s)_H} = 1.31^\circ \text{F}$$

The temperature drop of the hot-side fluid between inlet and outlet (ΔT_H) is

$$\frac{q}{\dot{W}_H (C_P)_H} = 3.67^\circ \text{F}$$

The maximum required ΔT between hot-side inlet and the cold-side fluid for complete vaporization is then

$$\Delta T_H + (\Delta T_f)_H + (\Delta T_f)_c = 6.46^\circ \text{F}$$

The available ΔT is

$$(T_{H_i}) - T_c = 38.4^\circ R - 31.6^\circ R = 6.8^\circ F$$

which shows that the required condition for complete vaporization is met and, for the case where trapped gas is available to start the turbine, essentially no liquid will be lost during start-up and the turbine/pump should have no problem in reaching full operating speed.

10.3 CONCLUSIONS

- a. For system start-up in LH_2 where initial turbine operation is with trapped gas there will be essentially no liquid lost, and the turbine/pump combination should reach full operating speed without difficulty.
- b. Where start-up is without trapped gas there could be a loss of liquid, and the possibility exists of the turbine/pump not reaching full operating speed so long as the system is inundated with LH_2 . Further analysis of the actual hot-side heat transfer occurring during start-up is required to fully determine the characteristics of such a start-up condition.

SECTION 11

CONCEPTUAL FEASIBILITY DESIGN OF HEAT EXCHANGE SYSTEM

A feasibility design was made of a heat exchanger type zero-g, liquid/vapor vent system sized and packaged for use in the S-IVB hydrogen tank. The design and performance conditions are summarized in Figure 11-1 and Table 11-1.

As shown, the separator would be mounted directly to the hydrogen tank access cover. The cover is assumed to be capable of distributing the weight of the separator into the tank skin. A tank pressure of approximately 1 psi is adequate to support the separator in flight. Ground support with no tank pressure would have to be verified by the tank manufacturer. The vent duct would pass through the tank access cover and thus no basic tank changes would be required for incorporation. The flight tank vent regulator is separately mounted from the main heat exchanger package and is located external to the propellant tank.

Location of the heat exchanger package is not critical to its operation since vapor venting is accomplished even though the unit is completely immersed in liquid. Alternate locations are therefore left to the discretion of the prime user. Some considerations affecting location are discussed in Paragraph 9.1.

Tank venting during prelaunch operations is accomplished through the existing vent system.

11.1 DESCRIPTION OF COMPONENTS. The zero-g, liquid/vapor separator vent system consists of four major components.

- a. Heat exchanger assembly.
- b. Inlet pressure controller.
- c. Tank vent regulator.
- d. Turbine and pump assembly.

These components are discussed in the following paragraphs.

11.1.1 Heat Exchanger Assembly. The heat exchanger assembly includes the basic core, ducts, headers, distribution tubes, and mounting brackets. The basic core is of furnace-brazed construction similar to that shown in Figure 11-2. The ducts, etc are formed from sheet and tube stock and are welded to the basic core.

The turbine inlet ducts and the inlet pressure controller duct have integrally formed single convolute bellows sections to accommodate misalignments and thermal expansion.

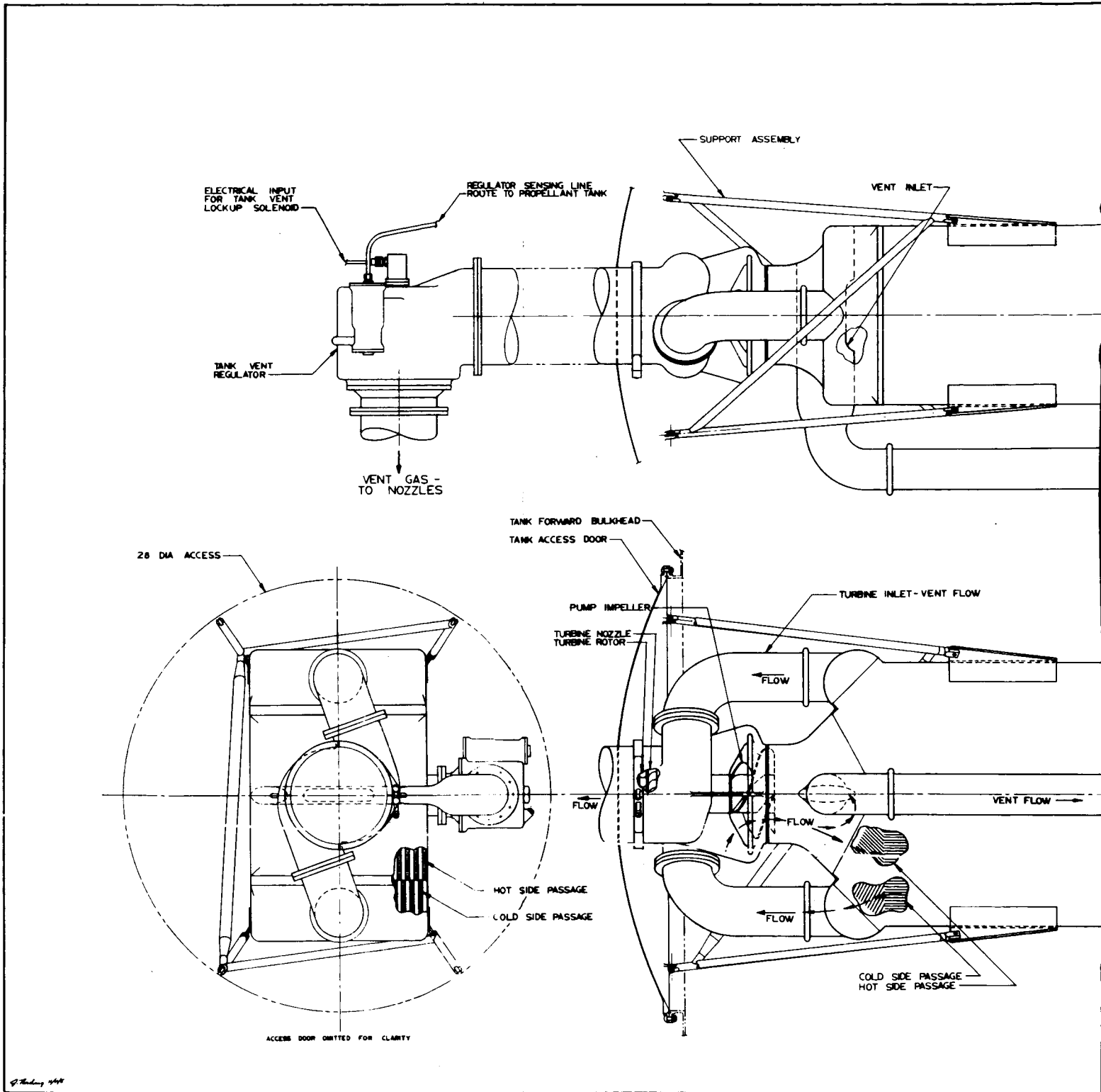


Figure 11-1. Heat Exchanger Vent System Feasibility Design

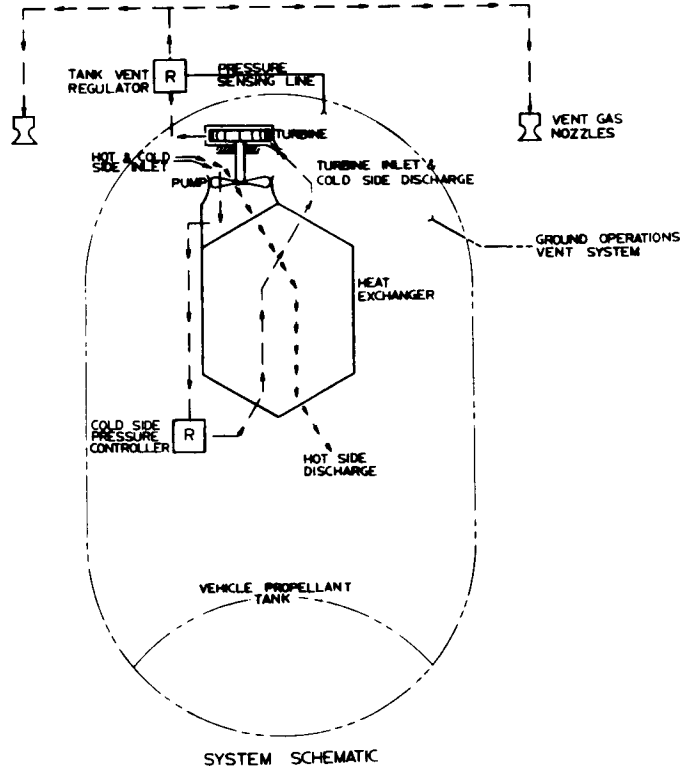
COMPACT HEAT EXCHANGER
COUNTER FLOW TYPE

6 PSIA COLD SIDE
PRESSURE CONTROLLER

HOT SIDE FLOW

HOT SIDE PASSAGE
COLD SIDE PASSAGE

HOT SIDE FLOW



SCALE
10 INCH

Table 11-1. Summary of Design Information and Conditions
for Heat Exchange Feasibility Design

DESIGN CONDITIONS

Vent-side fluid conditions at various stations in the system

LOCATION	PRESSURE (psia)	TEMPERATURE (°R)	QUALITY
Inlet from tank	20.0	38.4	0.0
Exchanger inlet	6.0	31.7	0.08
Turbine inlet	6.0	37.0	1.0
Turbine outlet	5.78	37	1.0

Vent rate = 0.06 to 0.35 lb/sec (0.35 was limiting case used for sizing)

Mass flow rate on exchanger tank side (with 0.35 lb/sec vent and 100-percent liquid inlet) = 12.8 lb/sec

Exchanger core is nominally 11 × 17 inch rectangular cross section, has 20 cold-side and 21 hot-side channels, a single pass on each side, and uses strip fins No. 1/4 (a) -11.1 of Reference 2-6 which have the heat transfer and friction flow data shown in Figure 8-11 and the following geometric data.

Plate spacing, $b = 0.25$ inch

Fin pitch = 11.1 inch^{-1}

Fin length = 0.25 inch

Fin thickness = 0.006 inch

Flow passage hydraulic diameter, $4R_H = 0.01012$ foot

Total heat transfer area/volume between plates, $\beta_E = 367 \text{ ft}^2/\text{ft}^3$

Fin area/total heat transfer area = 0.756

CALCULATED RESULTS

The total heat exchange surface area on the hot side (not including the corners, which were used to provide a design margin of safety) = 535 ft^2

Required pump output power = 0.25 hp; an efficiency of 0.6 was used to account for turbine bearing and seal plus pump losses (not including turbine thermal efficiency).

Total hardware weight of system = 113 lb (see Paragraph 11.2 for details)

Change in required boil-off rate from base case of venting 20-psia saturated vapor (using maximum power corresponding to 0.35 lb/sec, but nominal vent rate of 0.185 lb/sec to provide this) = -6.1 lb/hr (i.e., boil-off rate decreases from base case)

Equivalent changes in available (90,000-pound nominal) payload weight

due to hardware = -75.7 lb, due to boil-off change = 9.7 lb, total = -66.0 lb

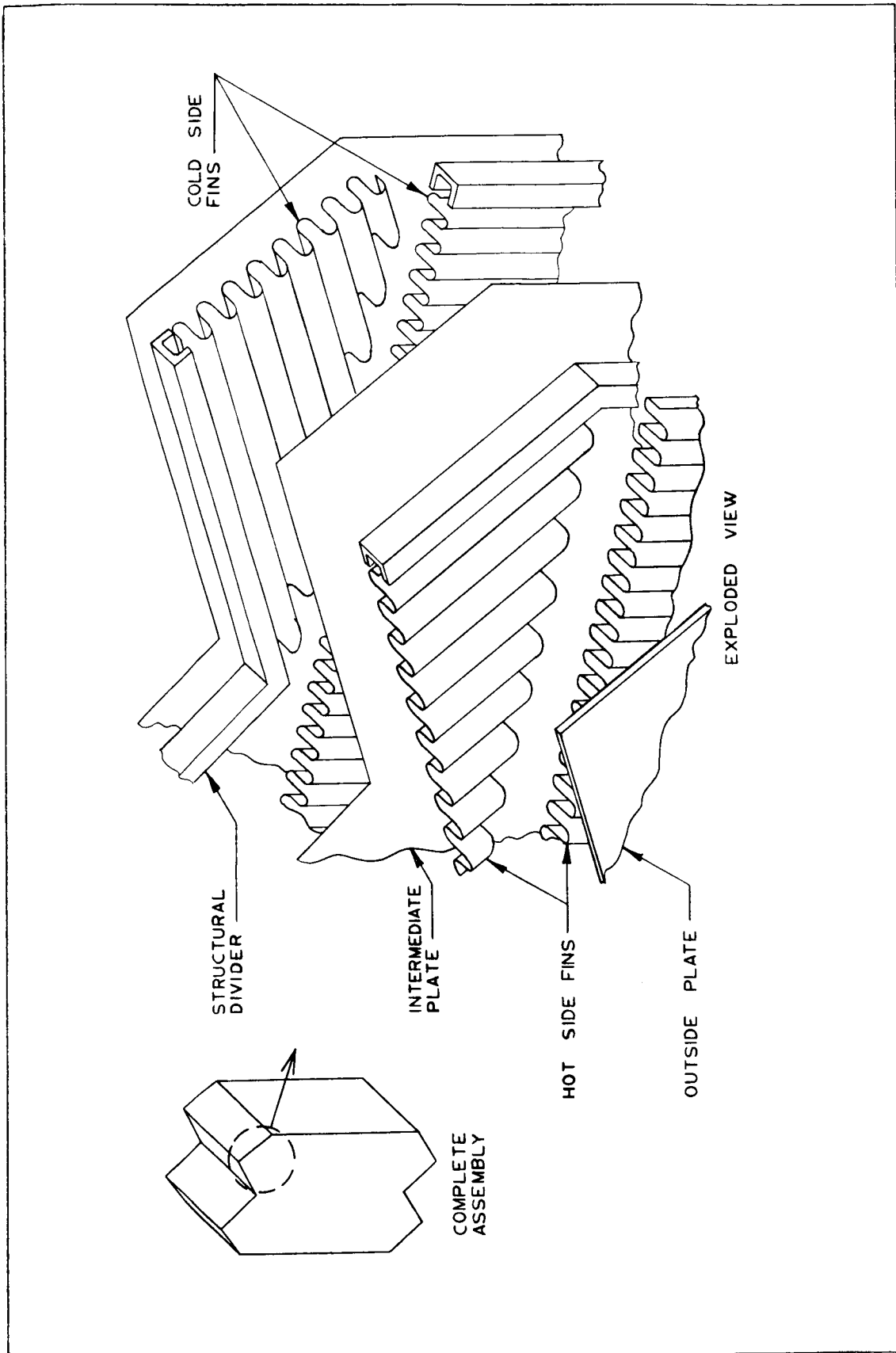


Figure 11-2. Typical Heat Exchanger Construction

The hot-side inlet header contains flow control vanes to provide even distribution of flow to the heat exchanger core and to the inlet pressure controller.

The inlet pressure controller receives its flow from the center of the hot-side inlet header. The inlet is orientated downstream so that the vent fluid must take a 180-degree turn to enter the inlet. This inlet location is chosen to ensure near-equal fluid quality to both sides of the heat exchanger with a bias toward more gas in the vent side in the case of two-phase flow. The bias is provided by the centrifugal separation encountered in making the 180-degree turn.

The core consists of alternate hot- and cold-side channels. Each channel is 0.25-inch wide with 11.1 fins per inch. The fins are 0.006-inch thick. Adjacent channels are separated by 0.012-inch-thick plates. The core has 21 hot and 20 cold channels. The two outside plates are 0.050-inch thick to provide strength and rigidity for mounting and handling.

11.1.2 Inlet Pressure Controller. The inlet pressure controller is used to maintain a constant 6-psia pressure in the cold side of the heat exchanger. The controller operates with saturated liquid, saturated vapor, or mixtures of the two. The controller uses an evacuated reference chamber to maintain the 6-psia setting independently of the local surrounding pressure; therefore, no ambient sensing lines are required. The inlet pressure controller does not require electrical lockup capability. Lockup is controlled by the tank vent regulator and is pneumatically coupled to the inlet pressure controller through the vent fluid. The inlet pressure controller is supported from the heat exchanger cold-side distribution tube. The Centaur propellant tank vent valve (Wallace O. Leonard, Inc., Part No. 200601) appears to be usable with modification, i.e., downstream sensing and new pressure setting.

11.1.3 Tank Vent Regulator. The tank vent regulator senses the propellant tank pressure and vents the tank to maintain the required 20 psia. A lockup solenoid is included to prevent venting during engine operation. When the vent regulator opens it tends to reduce pressure in the heat exchanger, which then causes the inlet pressure controller to open and thus establish a tank vent flow.

The vent regulator is mounted externally to the propellant tank and operates with nominal 5.8-psia inlet and 3.8-psia discharge pressures. A separate pressure-sensing line is routed to the propellant tank to control the regulator.

The discharge flow may be vented through nozzles to provide thrust to assist in propellant control and to minimize forward bulkhead wetting. A regulator bypass solenoid may be included to provide a fixed minimum flow for the settling nozzles.

11.1.4 Turbine and Pump Assembly. The turbine and pump assembly is used to cause forced circulation of the propellant through the heat exchanger. The pump is a three-bladed, axial-flow type with the discharge being directed into the hot-side inlet header. The pump is directly coupled through a common shaft to the turbine. The turbine is a single-stage impulse type and is powered by the vent gas from the heat exchanger cold-side outlet. A rotating seal prevents leakage from the tank into the heat exchanger. The pump and turbine assembly is mounted from the turbine discharge flange and stabilized by the heat exchanger header.

11.2 SYSTEM HARDWARE WEIGHT. The estimated vehicle hardware weight increase using a heat exchanger type of venting system is 113 pounds. The component weight estimates, summarized in Table 11-2, were based on the design of Figure 11-1 and the following factors.

The weight of the heat exchanger is based on 0.050-inch outside plates, 0.012-inch inside plates, 0.006-inch fins, 0.020-inch cold-inlet tube, and 0.050-inch ducts and headers. The fin area used for weight calculations is based on the factors of

- a. Heat exchanger surface area flow volume, $\beta_E = 367 \text{ ft}^2/\text{ft}^3$
- b. Fin surface area/total surface area = 0.756

The support assembly is $1/2 \times 0.049$ -inch aluminum alloy tubing except for the diagonal, which is $3/4 \times 0.049$ -inch aluminum.

The cold-side pressure controller weight is the same as that of the Centaur hydrogen tank vent valve (Wallace O. Leonard, Inc., Part No. 200601).

The pump and turbine assembly housing is $1/8$ -inch cast aluminum.

The duct from the access cover to regulator is 0.020×5.25 -inch aluminum alloy.

The tank vent regulator weight is an estimate based on experience with similar regulators.

Table 11-2. Summary of Component Weight Estimates
for Conceptual Feasibility Design System

COMPONENT	WEIGHT (lb)
Heat exchanger, headers, etc	81
Support assembly	1
Cold-side pressure controller	6
Pump and turbine assembly	7
Tank vent regulator	12
Duct from access cover to regulator	6
Total	113

SECTION 12

PARAMETRIC ANALYSIS AND OTHER VARIATIONS OF HEAT EXCHANGE SYSTEM

12.1 PARAMETRIC ANALYSIS. A parametric analysis of the heat exchange venting system was made to study the effects of changes in the system design conditions, or in performance of a fixed system design with changes in operating conditions. Variations in tank pressure, inlet fluid quality or condition, system pressure drop, and vent flow rate were considered in addition to the results presented in Section 9 for variations in exchanger pressure and vent stream outlet temperature. In general, each curve shown in this section represents the results of several exchanger and/or turbine plus other system component sizings. The exchanger and turbine calculations were made using the methods outlined in Paragraph 8.3 and Appendix F. The weight results are expressed as changes in available payload weight using the method of Appendix E.

The following system conditions were held constant for all of the parametric results in Paragraphs 12.1.1 through 12.1.6.

- a. The system schematic is that shown in Figure 11-1.
- b. The exchangers are counter-flow, with one pass on each of the hot (tank) and cold (vent) sides.
- c. The exchanger hot and cold sides have a common inlet and, therefore, the inlet fluid conditions and qualities can be assumed to be identical.
- d. The exchanger cores use the strip fins with 0.25-inch plate spacing described in Table 11-1.
- e. The efficiency of the pump plus turbine bearing and seal losses (i.e., overall pump-turbine efficiency divided by the turbine thermal efficiency) is 0.6.
- f. The "base case" to which changes in boil-off, hardware, and available payload weights are referenced is the idealized case of venting 0.185 lb/sec of 20-psia saturated vapor directly without a separator system.

12.1.1 Tank Pressure Variation. The effects of varying tank pressure upon the required heat exchanger area, required pump power, and the resulting vehicle weight costs (expressed as changes in available payload weight due to addition of hardware, change in boil-off resulting from change in vent gas enthalpy, and the sum of the two contributions) are shown in Figure 12-1. These results are based upon an 11 by 17-inch exchanger cross section, 6-psia exchanger pressure, G_H of 79,800 lb/hr-ft², vent-side temperature at exchanger exit 1.4°R below the tank temperature, a vent flow rate of 0.35 lb/sec used for component sizing and power calculations, and an external heat input to the tank of 130,000 Btu/hr (which corresponds to a base vent rate of 0.185 lb/sec with 20-psia saturated vapor and no vent system) upon which the payload weight change due to change in boil-off was calculated.

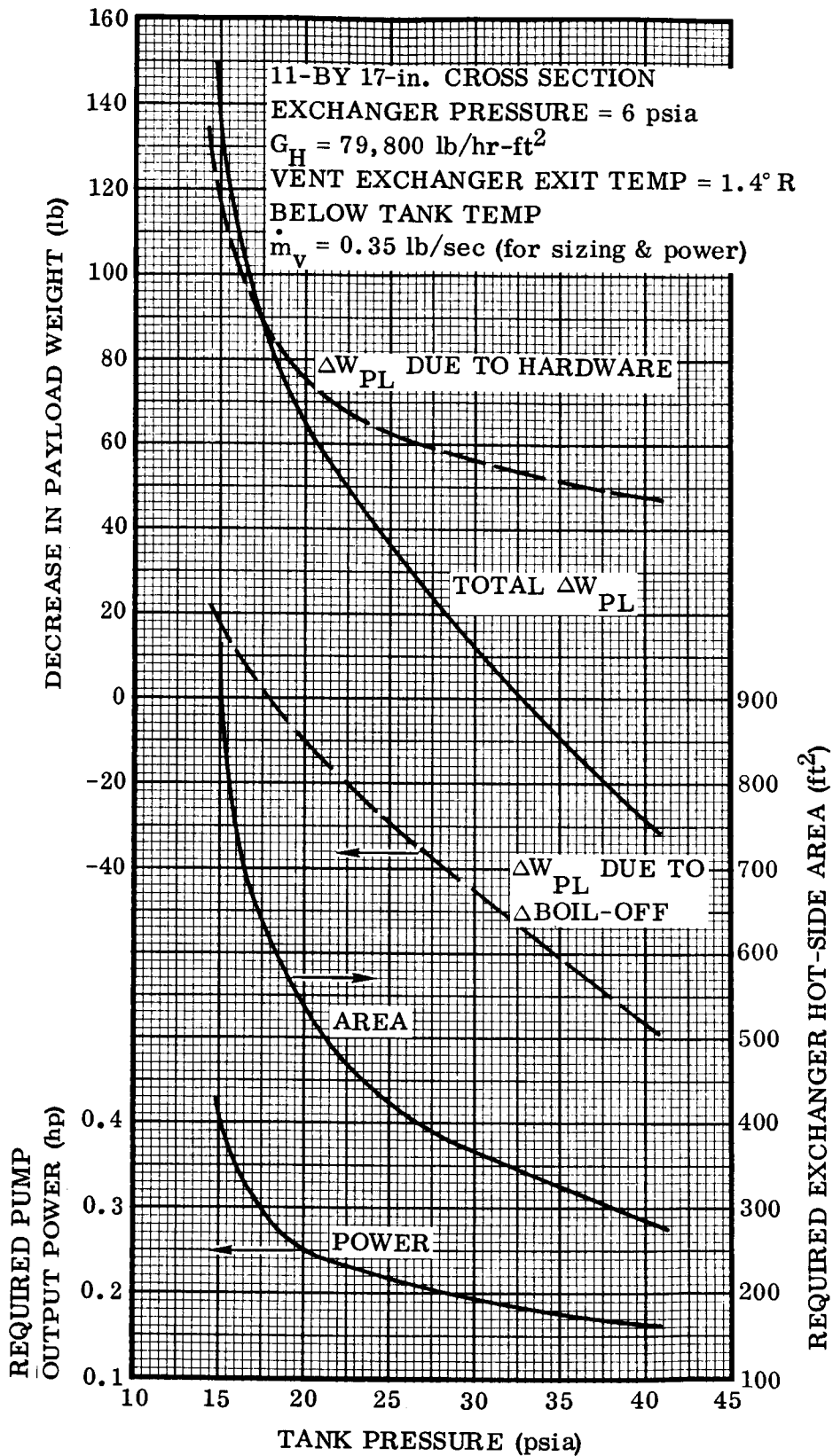


Figure 12-1. Effect of Tank Pressure Variation Upon Heat Exchanger Vent System

All five of the curves would be asymptotic to 6 psia, the exchanger pressure, and it can be seen that they all begin to rise rapidly even at a tank pressure of 15 psia. It is apparent that a considerable heat exchange vent system weight savings could be realized by increasing the tank pressure above the 15 to 20 psia level. This would not be true for a mechanical, surface tension, or dielectrophoretic separator.

12.1.2 Variation in Inlet Fluid Quality. The heat exchange type of venting system would probably be designed for a specified vent stream exit temperature with 100-percent liquid inlet and the maximum vent rate. The operation of the designed system at any higher inlet quality or lower vent rate would result in an increase in the temperature of the vent stream leaving the exchanger. This temperature could not exceed the inlet temperature of the tank fluid with which it exchanges heat, however. Thus, although the operation of a system designed for zero inlet quality would be slightly more efficient (i. e., slightly lower required vent rate) at high inlet qualities, the system operation would be relatively insensitive to inlet quality; certainly much less sensitive than any of the other separator types considered earlier in this study.

Figure 12-2 shows the variation in performance of two fixed exchanger designs with system inlet quality. The curves marked 319 ft² represent an exchanger sized to give saturated vapor at the exchanger exit with zero inlet quality to the expansion valve upstream of the exchanger, and the curves marked 535 ft² are for an exchanger with 37°R vent exit temperature when the inlet quality is zero. The decrease in total system payload loss with increasing inlet fluid quality is typical of the performance variation for a fixed design.

The effect of changing the inlet quality design condition from zero to 0.5 is illustrated by Figure 12-3, which summarizes the system parameters for designs with an inlet quality of 0.5, and Figure 9-5, which presents the parameters for designs with an inlet quality of zero. It can be seen that the optimum vent stream exit temperature design point in each case is about 37.4°R. These two sets of results can be compared on a common graph by plotting each of the two total payload decrease curves versus exchanger area, as is done in Figure 12-4. A second horizontal scale is also shown, using values of design vent exit temperature if the inlet quality were zero versus exchanger area, obtained from Figure 12-9.

One of the primary conclusions indicated by Figure 12-4 is that a change in the selected average system operating inlet quality can significantly shift the optimum exit temperature design point, if all designs are considered to be made for zero quality inlet. In the specific case shown the optimum exchanger size and design vent-stream exchanger exit temperature are about 570 ft² and 37.4°R if the average operating condition is taken to be zero quality inlet; however, if an inlet quality of 0.5 is established as the average operating condition, the optimum point corresponds to an exchanger area of about 410 ft² or a design vent outlet temperature from the exchanger with zero quality inlet of 34°R (this is the same optimum point as that corresponding to an exit temper-

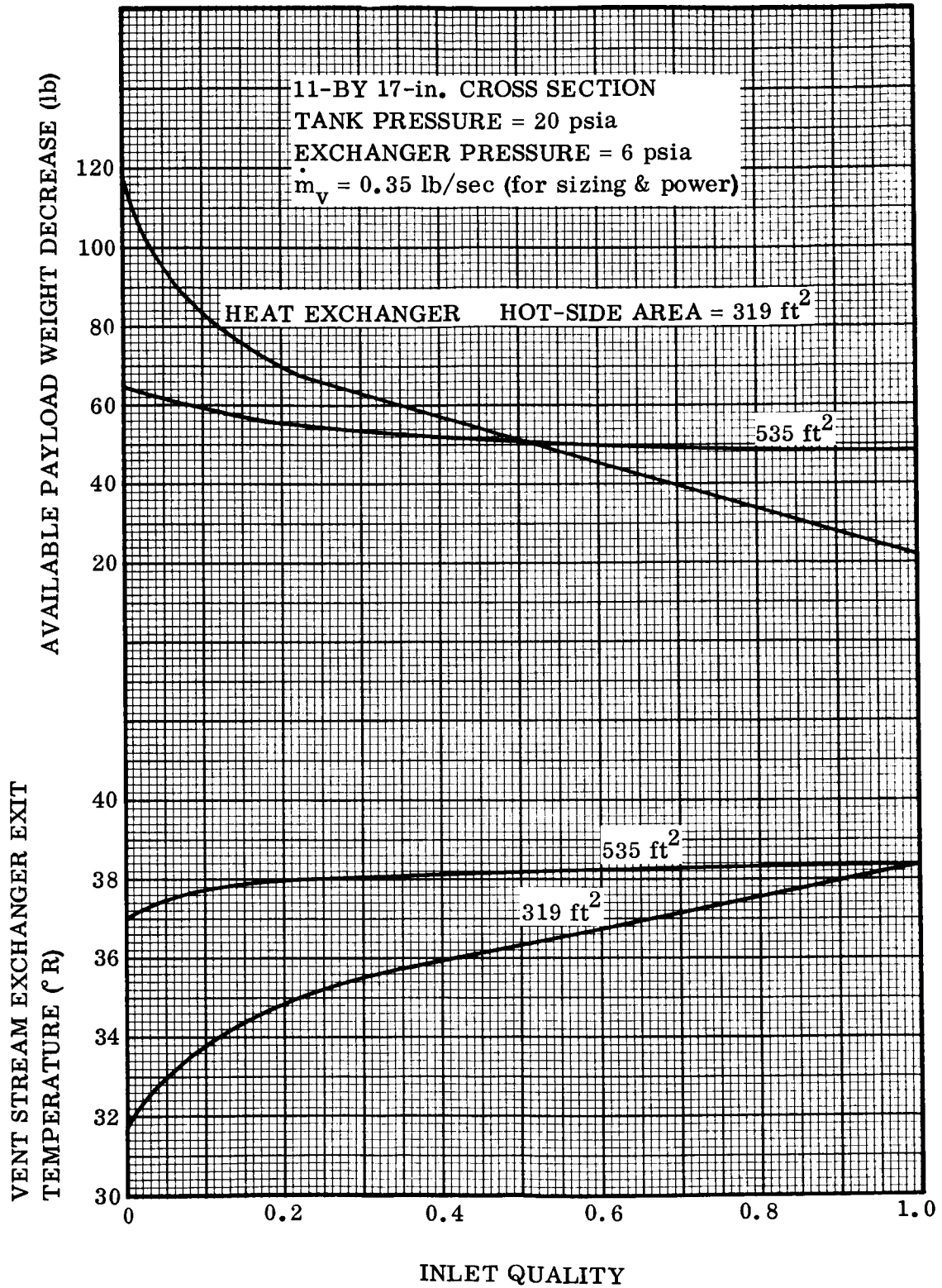


Figure 12-2. Effect of Inlet Fluid Quality Upon Performance of Fixed System Design

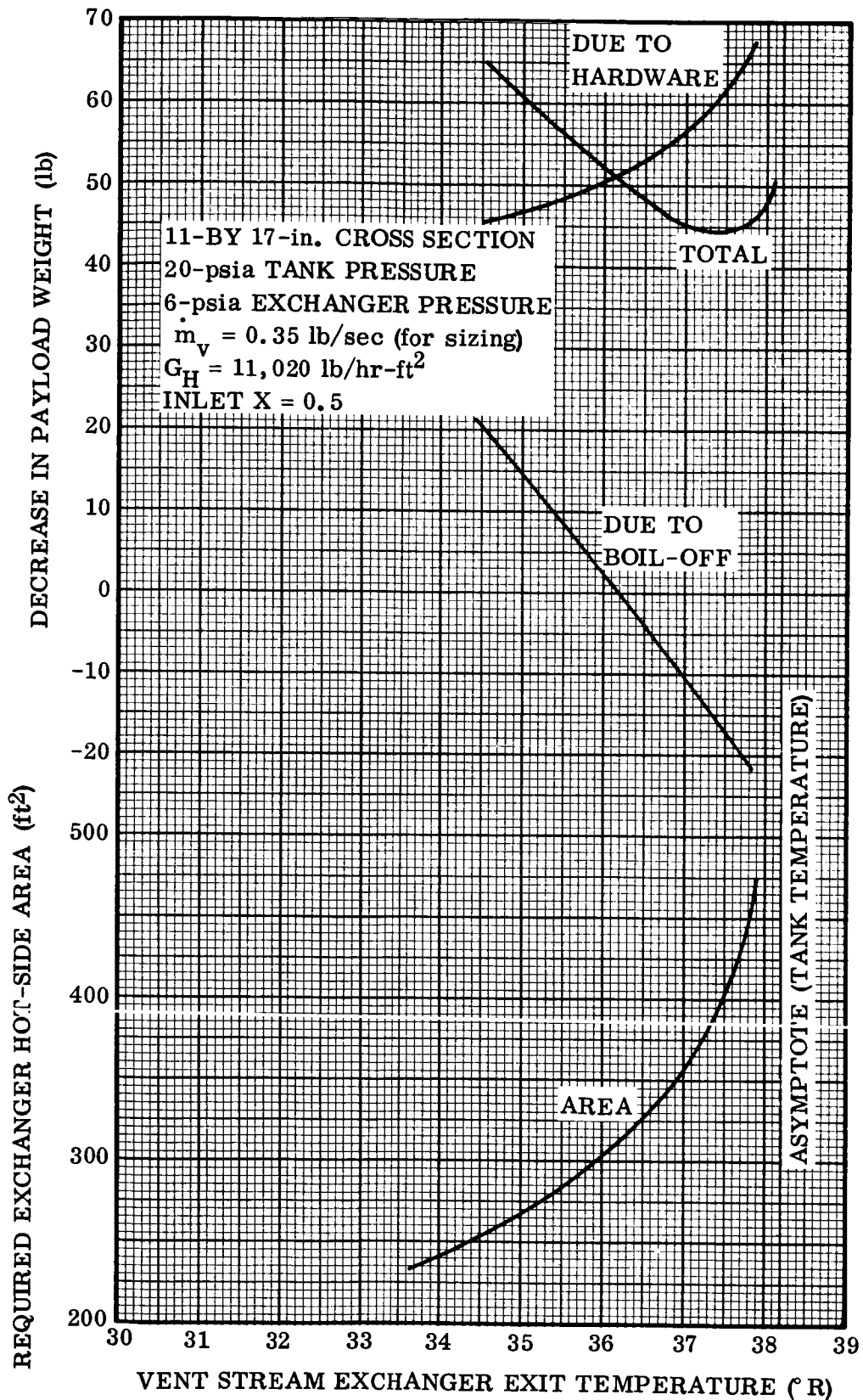


Figure 12-3. System Designs at Various Vent Exit Temperatures for 0.5 Inlet Quality to System

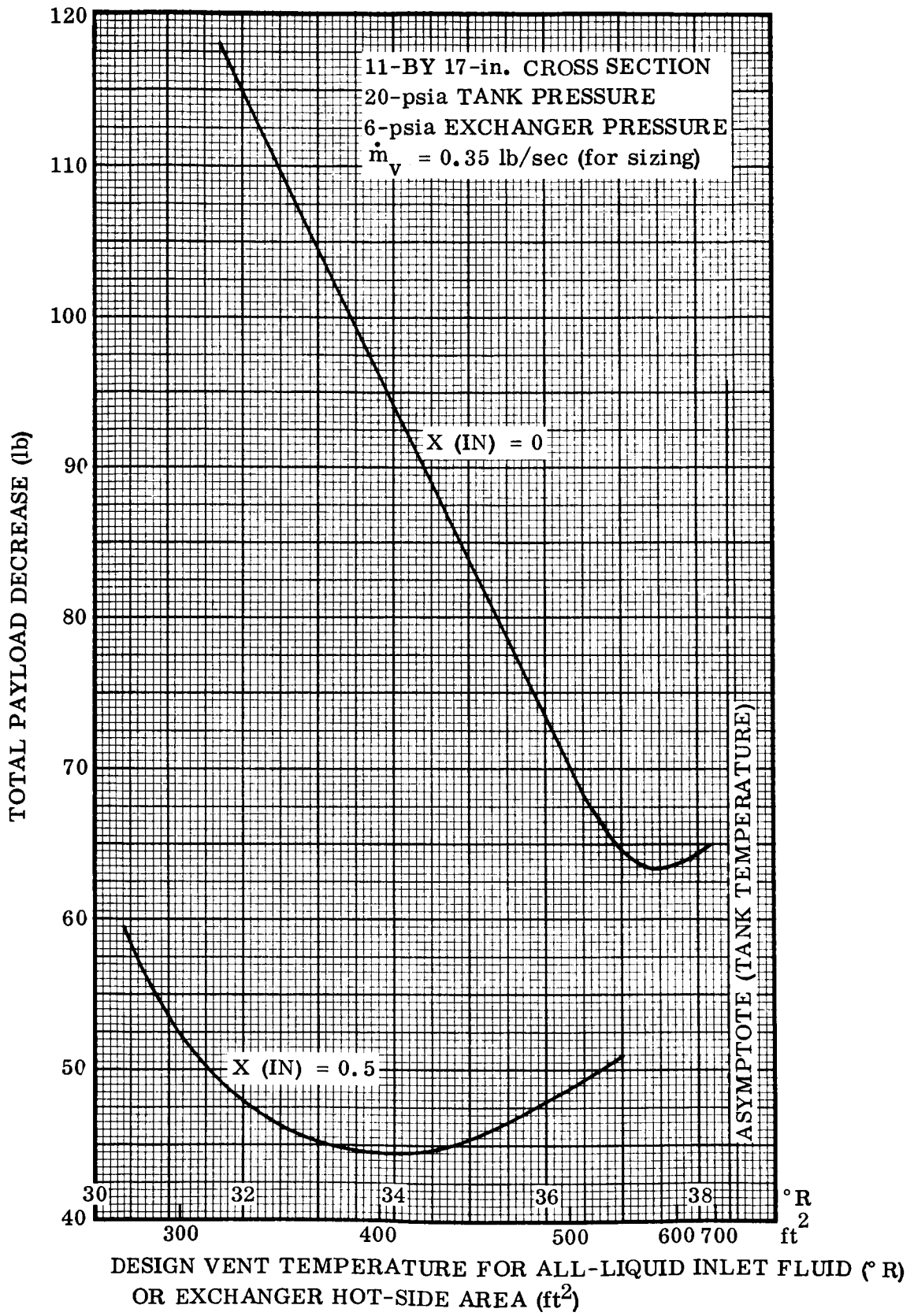


Figure 12-4. Optimum Design Vent Stream Exchanger Exit Temperature for Two Average Fluid Inlet Qualities During Operation

ature of 37.4°R on Figure 12-3). However, hydrodynamic analysis problems would make it very difficult to predict an "average" inlet quality to a vent system inlet in a propellant tank during flight, even if the inlet location in the tank and disturbing forces on the tank during the mission were known; therefore, a conservative design point should probably be selected with present knowledge. Following this philosophy, an exchanger with hot-side heat transfer area of 535 ft^2 , corresponding to a vent stream exchanger exit temperature of 37°R was selected for the design shown in Section 11.

Figure 12-5 shows the variation of system weight penalty as a function of design inlet quality. The pump output power was held approximately constant at 0.25 horsepower, the value calculated for the base design system described in Section 11, and the hot-side flow rate adjusted to fit. Also plotted on this figure are points at inlet qualities of 0.2 and 1 with different values of pump power to illustrate the effect of such power changes upon total system weight. Although an optimization was not made at each quality, it can be seen that a reduction in power from that selected for the zero quality inlet point would be desirable for high inlet qualities, but apparently unimportant for low inlet qualities. Among other conclusions, this curve further illustrates the weight savings possible if an average operating inlet quality higher than zero could be established.

12.1.3 Effect of Inlet Fluid Condition (Foam, Small Droplets, or Liquid Slugs). For a given inlet quality, the fluid inlet condition, whether small liquid slugs, foam, or small droplets, would not be important with the heat exchange type of venting system. If large liquid slugs or large and rapid changes in inlet quality were encountered, there could be undesirable control transients or a degradation in operating performance beyond that due to the average inlet quality, caused by the thermal lag between the onset of decreased inlet quality and turbine spin-up corresponding to the possibly increased vent rate caused by liquid rather than vapor passing through the expansion valve. This transient behavior was briefly examined in the work of Section 10, but more extensive work would be necessary to estimate the total effect of rapid cycling of inlet quality. Suggestions for further work are made in Section 13.

12.1.4 Variation of System Pressure Drop. Figure 12-6 summarizes the system performance expressed as a function of the pressure difference between the turbine outlet and the tank. A tank pressure of 20 psia, vent rate of 0.35 lb/sec, G_H of 79,800 lb/hr-ft², vent-stream exchanger exit temperature of 37°R , and 11- by 17-inch exchanger cross section were used for all of the points. It was found that the necessary pressure difference across the turbine to provide the required pump power is small at low exchanger pressures; e.g., at 6-psia exchanger pressure the total system pressure drop read from the bottom curve of Figure 12-6 is about 14.2 psia, therefore, the turbine Δp is about 0.2 psia. As the exchanger pressure is increased, the turbine pressure difference becomes an increasing fraction of the total system pressure drop, and eventually causes a minimum attainable system pressure difference of about 10.7 psia, with the system components and operating conditions assumed here. The existence of such a minimum is inherent in a venting system of the type analyzed in this section, although the value of the minimum pressure drop would vary with the system operating parameters held constant. If system pres-

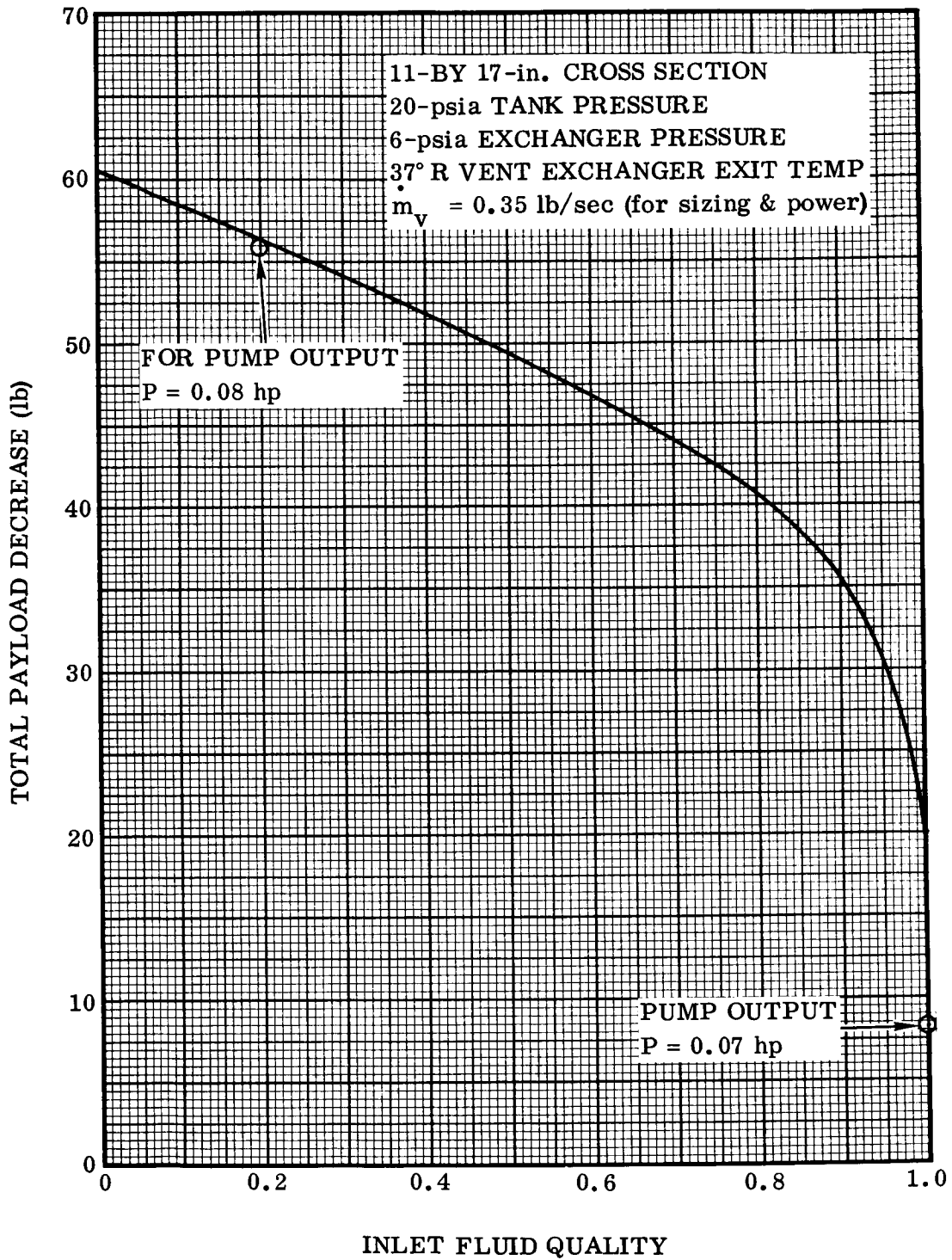


Figure 12-5. System Total Weight Penalty Versus Design Inlet Fluid Quality for Approximately Constant Pump Output Power of 0.25 Horsepower

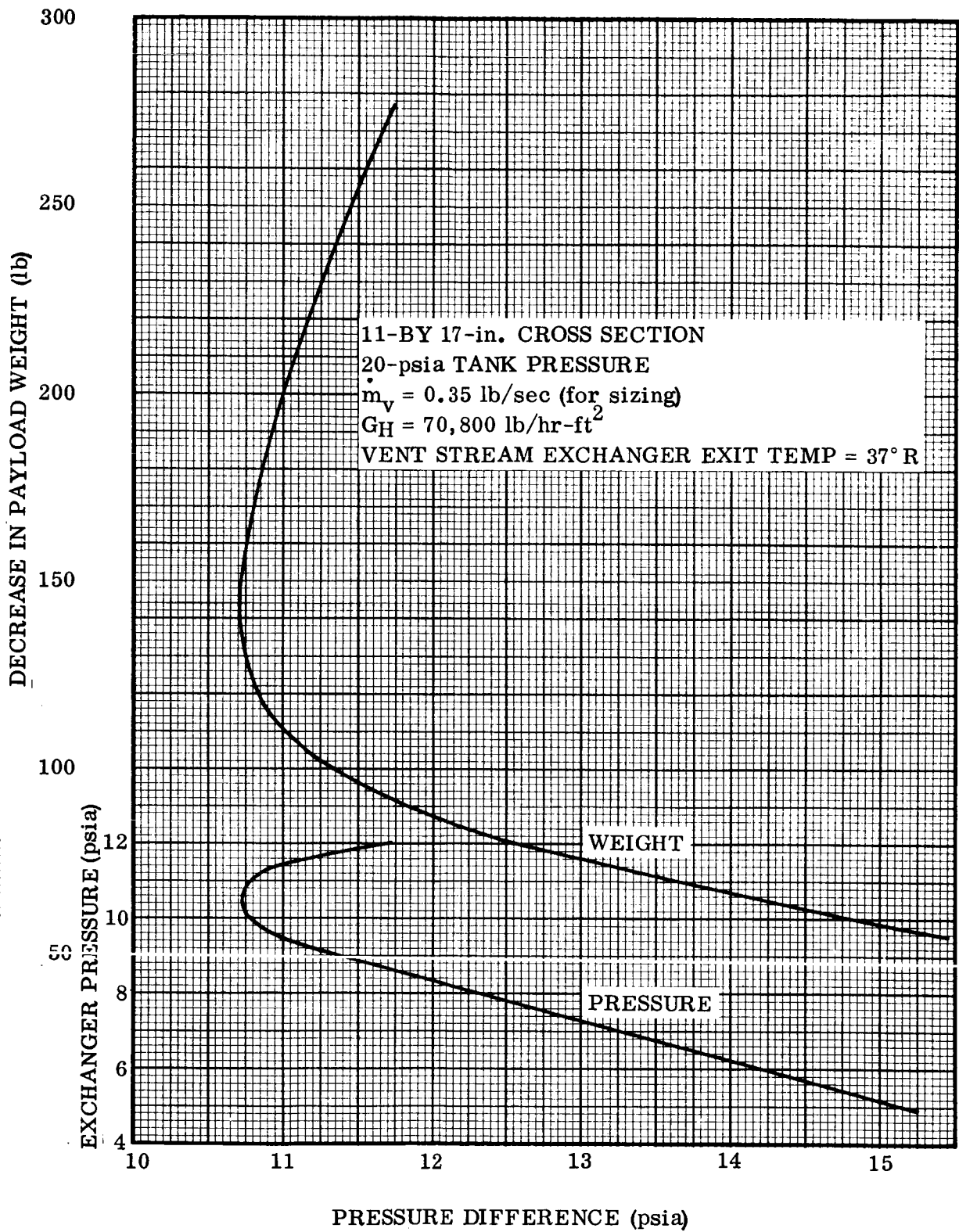


Figure 12-6. Decrease in Payload Weight and Corresponding Exchanger Pressure Versus Vent System Pressure Drop Between Tank and Outlet of Turbine

sure drops considerably below 10 psia were desired, auxiliary power would have to be supplied, causing a further increase in system weight cost.

12.1.5 Effect of Vent Rate Variation. The effects on system size and resulting payload weight are shown in Figure 12-7 for a variation in vent rate. In the designs plotted in this figure the mass flow rate per unit area, G , was held constant for both hot and cold sides at the values used for the base exchanger design of Section 11, i. e., $G_H = 79,800$ and $G_C = 2295$ lb/hr-ft². Also, the vent exit temperature from the exchanger was held at 37°R, the tank pressure at 20 psia, the exchanger pressure at 6 psia, the inlet quality at 0, and the external heat load on the tank equal to that calculated for each nominal vent rate from Equation 9 of Appendix E. Each of the curves is very nearly linear.

12.1.6 Other Parametric Results. The results of Section 9 included parametric information for variations in exchanger pressure and vent stream exchanger exit temperature. Further data that augment those presented in Section 9 are summarized in Figures 12-8 through 12-11.

12.2 EFFECT OF COMBINING THE HEAT EXCHANGER AND MECHANICAL SEPARATOR SYSTEMS. To determine the potential advantages and/or disadvantages of combining the basic heat exchanger and mechanical separator systems, for use with the S-IVB vehicle, an analysis was made and performance data presented for two system combinations. Combination 1 is the basic heat exchanger system described in Paragraph 11.1 with a mechanical vapor/liquid separator upstream. Combination 2 is the motor-driven mechanical separator described in Paragraph 3.2 with a heat exchanger added downstream.

Combination 1 is designed to operate at the maximum vent flow rate (0.35 lb/sec) with saturated gas outlet when completely inundated with liquid, while Combination 2 is designed for no liquid loss at maximum flow with 90-percent liquid inlet. Addition of the heat exchanger to the mechanical unit, Combination 2, increases the system thermal efficiency and allows operation at reduced vent flows in up to 100-percent liquid inlet with essentially no loss of liquid. For example, the heat exchanger, as sized for a nominal 37.8°R superheat temperature (Table 12-1) will operate in 100-percent liquid with a saturated gas outlet when the vent flow is approximately 0.06 lb/sec.

A comparative weight summary of the basic systems and the two combinations described above is given in Table 12-1. In all cases, the Δ vent rate is based on a system with inlet quality of 10-percent (90-percent liquid by weight).

Table 12-1 shows that the addition of a separator upstream of the heat exchanger, Combination 1, results in a fairly significant weight reduction. The combination system does add some complexity in the unit packaging, however, and the number of rotating seals is increased from one to two. The unit mounting problems with respect to bear-

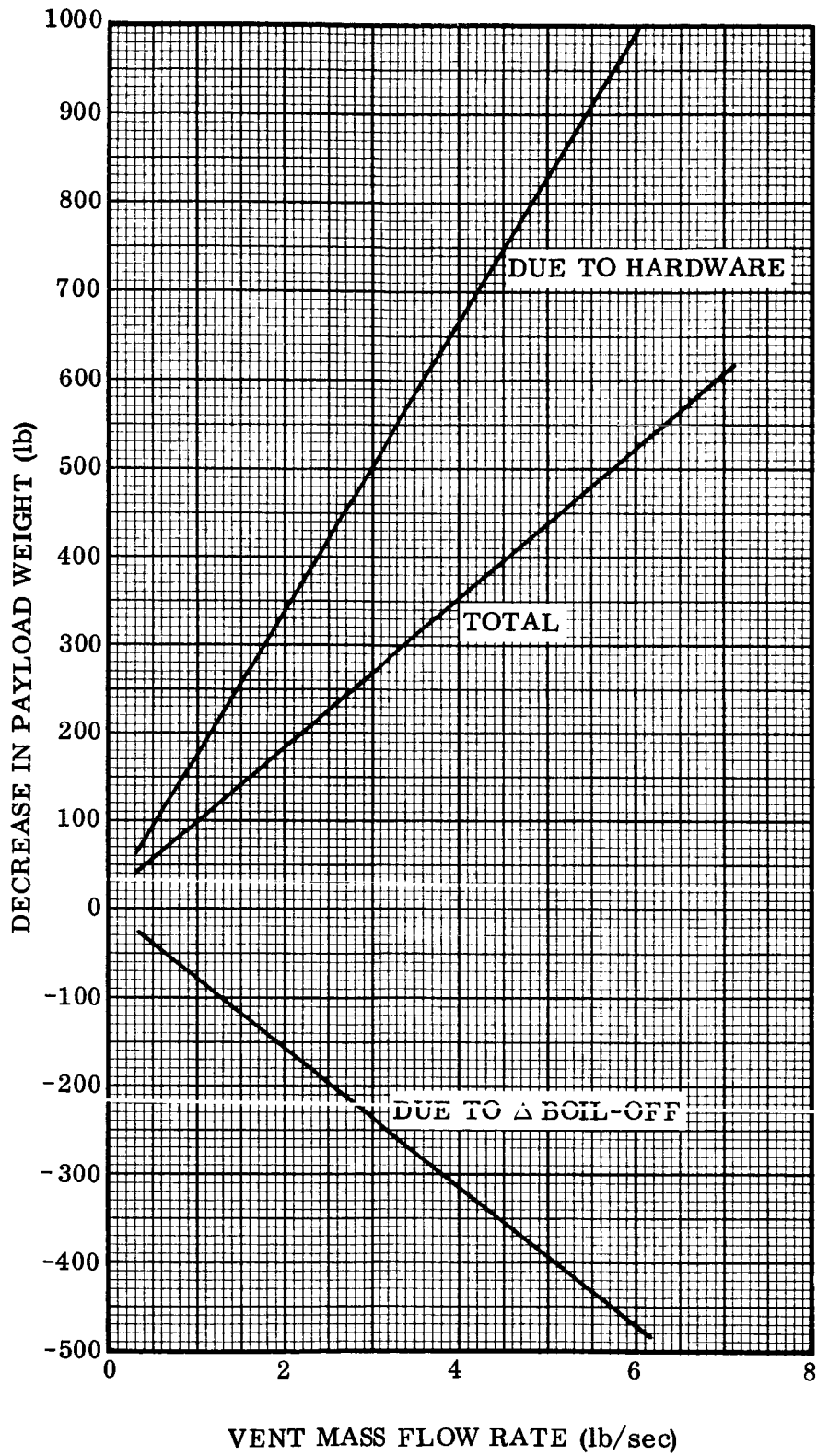


Figure 12-7. Effect of Vent Rate on Vent System Weight

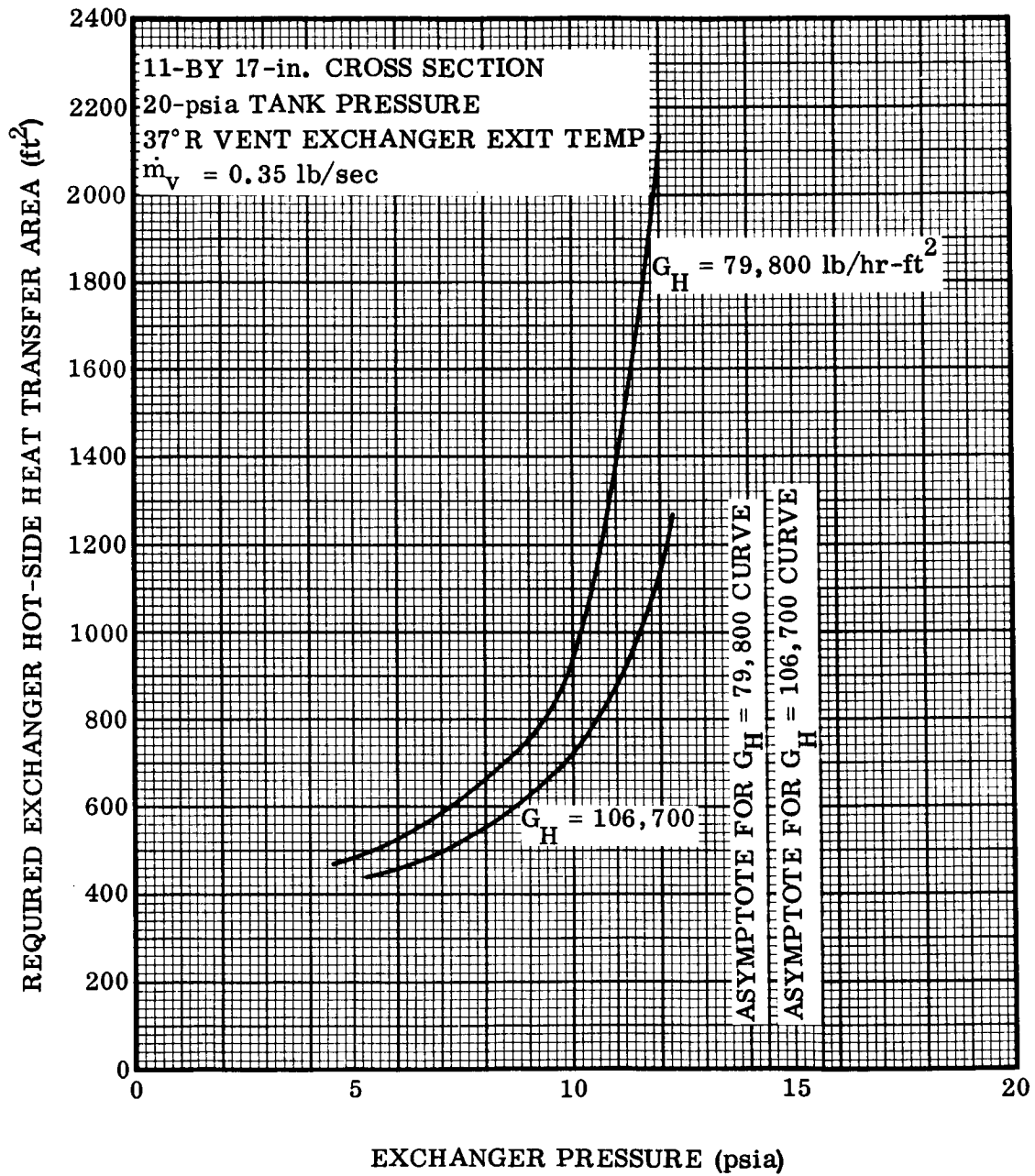


Figure 12-8. Required Exchanger Area Versus Exchanger Pressure

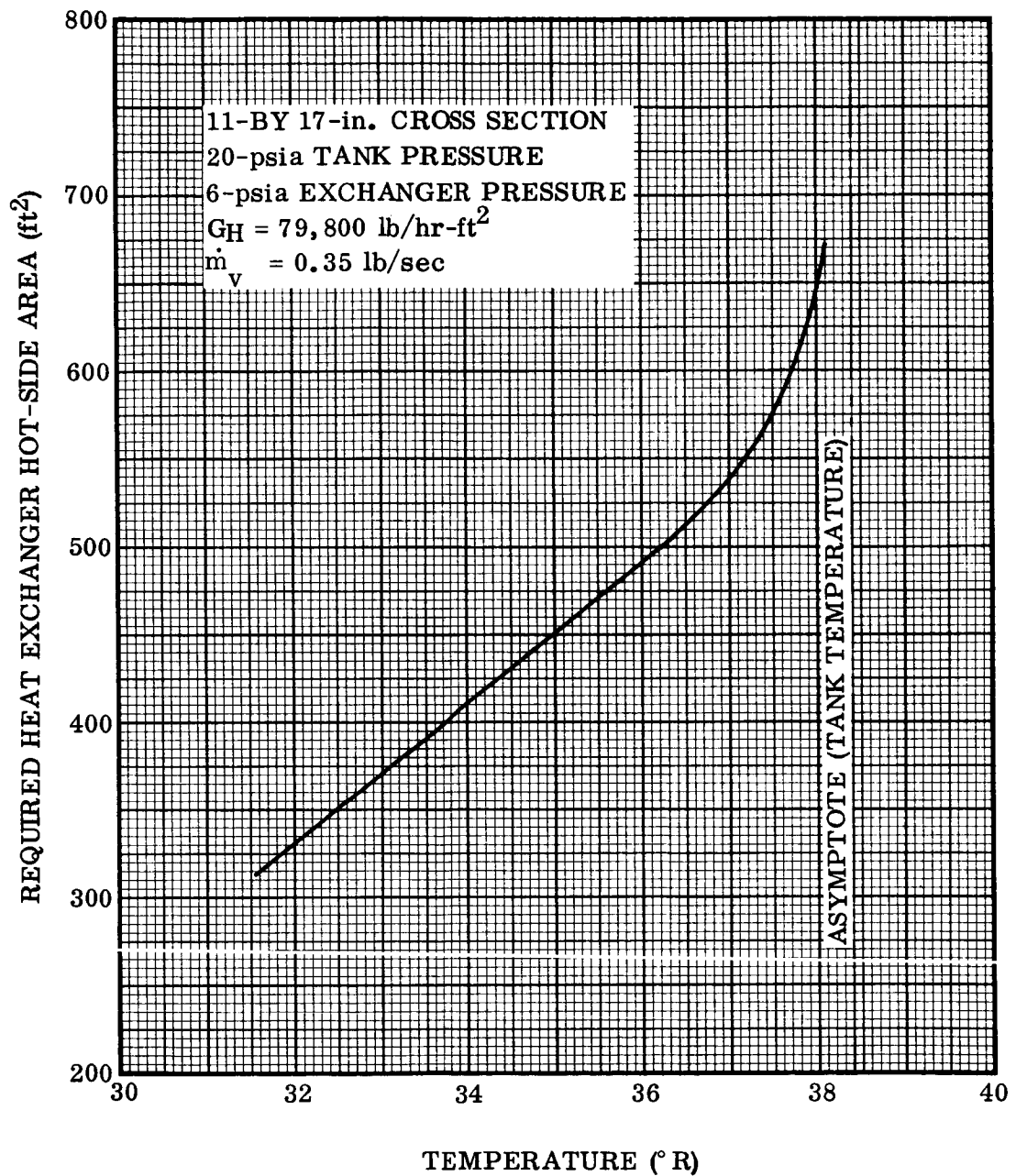


Figure 12-9. Required Exchanger Hot-Side Heat Transfer Area Versus Vent Stream Exchanger Exit Temperature for 100-Percent Liquid Inlet Fluid

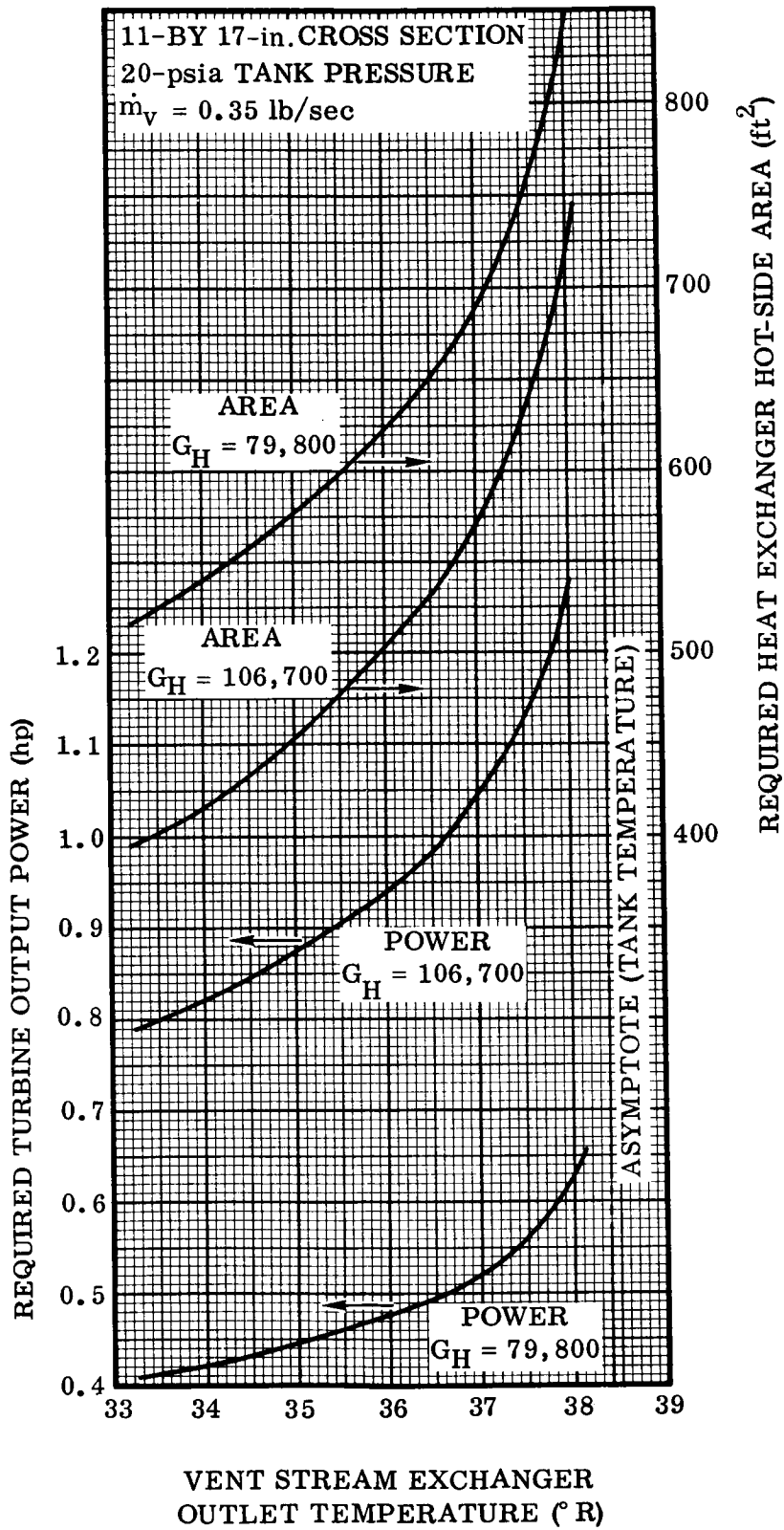


Figure 12-10. Required Exchanger Area and Turbine Power for 8.5-psia Exchanger Pressure

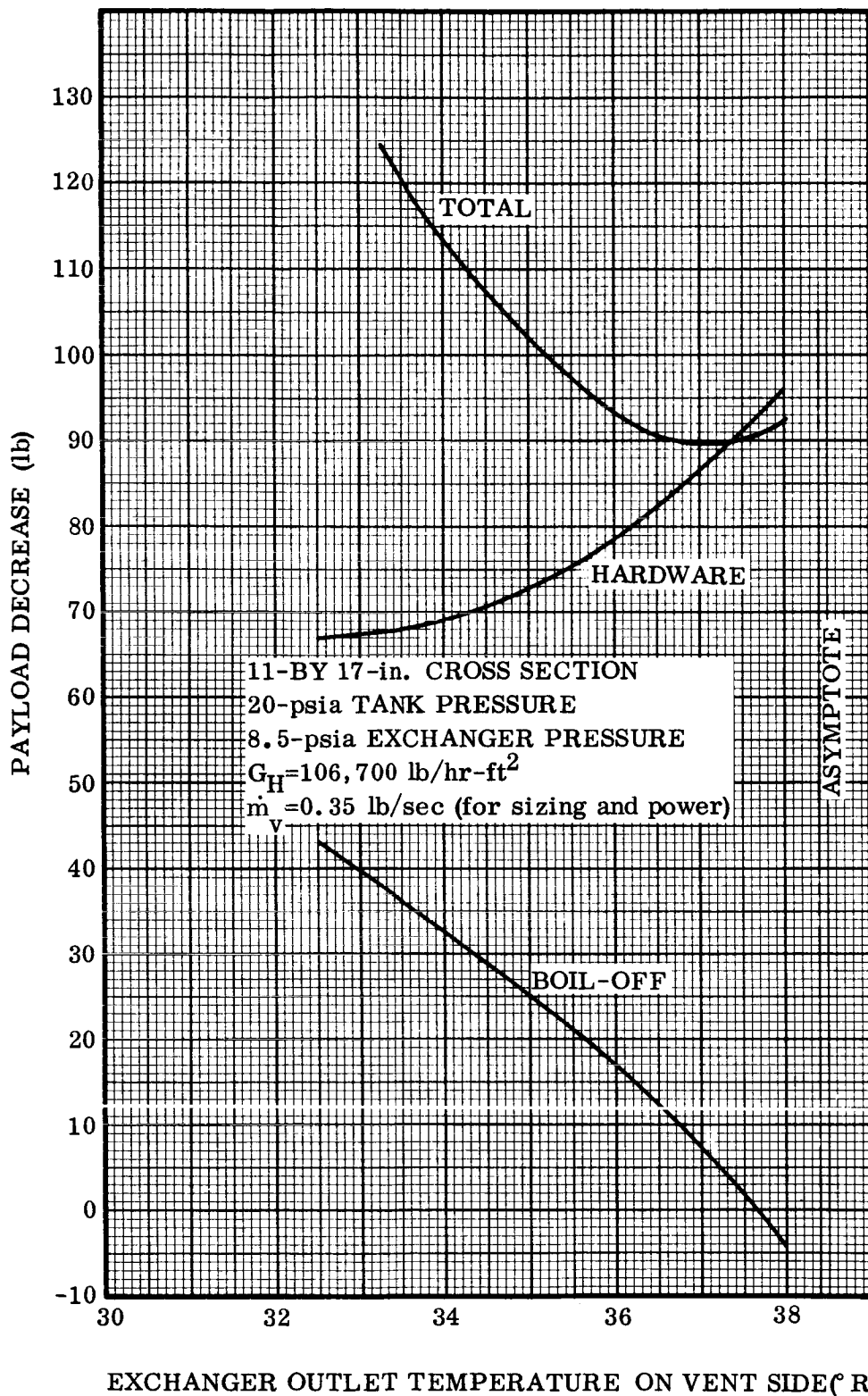


Figure 12-11. Payload Decrease Versus Vent Stream Exchanger Exit Temperature for 8.5-psia Exchanger Pressure

Table 12-1. Weight Summary -- Heat Exchanger, Mechanical Separator, and Combinations of Both

	HEAT EXCHANGER (lb)	HEAT EX. W/SEPARATOR (COMBINATION 1) (lb)	MECHANICAL SEPARATOR (lb)	SEPARATOR WITH HEAT EX. (COMBINATION 2) (lb)
Electric Motor & Gears	-	-	10	10
Separator, Pump, Turbine	7	17	12.8	15
Battery	-	-	50	50
Inverter	-	-	32	32
Pressure Regulating Valve	6	6	-	6
Modulating Vent Valve	12	12	6	12
Ducting	6	6	4	6
Heat Exchanger	82	49	-	41.3
Total System Weight	113	90	114.8	172.3
Equivalent Δ Payload (0.67 W_T)	- 75.9	-60.4	- 76.9	-115.1
Δ Vent Rate, lb/hr	- 15.5	-16.8	7.4	- 16.1
Equivalent Δ Payload (1.58 $\times \Delta \dot{W}_V$)	+ 24.4	+26.6	- 11.7	+ 25.4
Total Δ Payload	- 51.5	-33.8	- 88.6	- 89.7

	(1)	(2)	(3)	(4)	(5)
*Represents variation in heat exchanger size and outlet temperature.					
$T_{OUT} = 38.24^\circ R$	①	②	③	④	⑤
38.1°R					
37.82°R					
37.53°R					
37.14°R					
	41.3	31	20.6	15.5	10.3
	172.3	162	151.6	146.5	141.3
	-115.1	-108.5	-101.6	- 98.1	- 94.6
	- 16.1	- 14.5	- 10.2	- 8.9	- 4.55
	+ 25.4	+ 22.9	+ 16.1	+ 14	+ 7.2
	- 89.7	- 85.6	- 85.5	- 84.1	- 87.4

ing design will be somewhat greater due to the increase in length of the rotating element. The start-up problem in all-liquid will also be more critical due to the greater mass of rotating elements and the reduction in mass of the heat exchanger. These complexities are greater than those of the basic heat exchange system, but do not represent unrealistic designs. However, before a full analysis can be made of the advantages and disadvantages of adding a separator to the heat exchange system, further knowledge of the actual fluid conditions at the vent during flight is needed. For example, if the vent is covered with liquid a large part of the time, then the addition of the separator would probably show no advantage. Also if the unit were operating in all-gas for most of the time, the basic exchanger would be initially designed for no superheat during periods of liquid inundation, and the addition of a separator would not show any weight reduction.

Table 12-1 also shows that there is only a slight weight advantage for adding a heat exchanger to a predominantly mechanical separator system (Combination 2). The added complexity is basically that due to the addition of a throttling device upstream of the heat exchanger and the slight possibility of the heat exchanger itself causing leakage of liquid through a structural failure. The main advantage of such a system is that a sensing device could now be used to reduce the vent flow to approximately 0.06 lb/sec during periods of liquid inundation without loss of liquid and without complete termination of vent thrust.

12.2.1 Analysis of Heat Exchanger System with Mechanical Separator Added Upstream.

The basic exchanger described in Paragraph 11.1 is counterflow with a pressure of 6 psia. The combination system is designed to operate with a saturated gas outlet when the inlet is 100-percent liquid.

Design is based on a maximum vent flow rate of 1260 lb/hr. Mechanical separator operation is assumed to be with 10-percent quality inlet and essentially 100-percent quality outlet. The separation criterion developed in Paragraph 3.2 is used. A schematic of the proposed system is shown in Figure 12-12 and the pump-separation-turbine packaging in Figure 12-13.

Operation of the system in 100-percent liquid requires a low-head, fairly high-flow capacity pump for hot-side liquid circulation, while gas/liquid separation requires a lower flow, higher head type device. The axial-flow pump used for the basic heat exchanger system and the separation unit described in the separation predesign section can be incorporated into a single design and driven by a single vent-gas-driven turbine. The major change in design will be a higher operating speed for the separator and a resulting smaller diameter intake. The centrifugal forces imparted to the liquid by the separator must be sufficient to overcome the drag forces exerted by the gas flowing into the unit. The predesigns assumed the use of a model in which inlet flow area is a function of the diameter, and here a smaller diameter means a higher power requirement, other factors being equal. The model used was chosen for its simplicity in

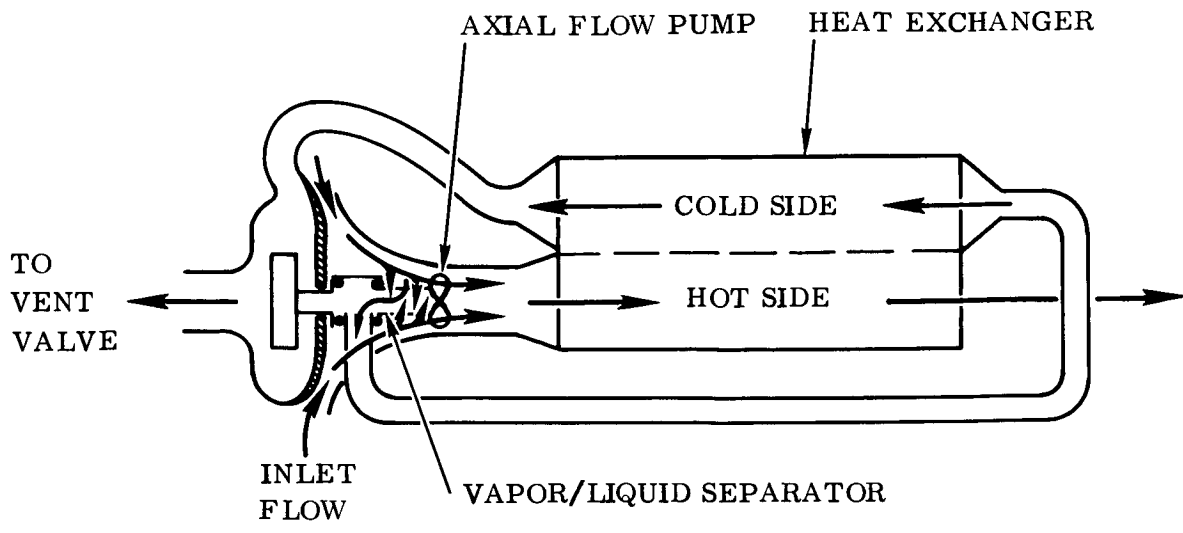


Figure 12-12. Heat Exchanger Mechanical Separator Schematic

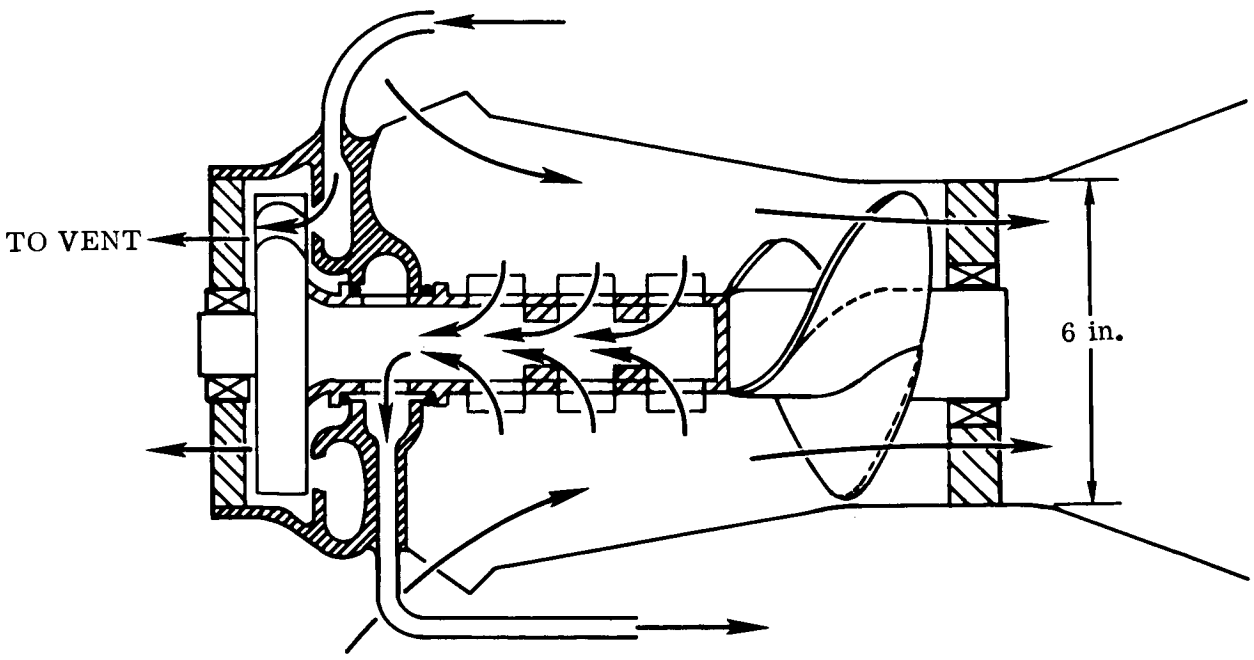


Figure 12-13. Separator-Pump-Turbine Combination

packaging. For the analysis of the combination system, it is reasonable to depart from this model and increase the inlet flow area to diameter ratio to allow for a decrease in separator diameter with no increase in the power requirement. This design approach is somewhat similar to that of the Janitrol separator described in Paragraph 3.1. The actual flow inlet area required is determined from the data of Appendix C.

Assuming the same flow rate of LH₂ (46,000 lb/hr) through the heat exchanger when operating completely submerged as for the basic heat exchanger system, the required heat exchanger hot-side area to assure saturated GH₂ at the outlet is 319 ft² (from Figure 12-9).

The basic exchanger described in Paragraph 11.1 has a total hot-side area of 535 ft² and weighs 82 pounds. Assuming the same exchanger except for reduced length, the weight is proportional to the area, and for the present analysis

$$\text{Exchanger Weight} = 49 \text{ lb}$$

Similarly the circulation power requirement is also estimated from the base case of Paragraph 11.1.

$$\text{Pump Input Power (100-percent LH}_2) = 0.327 \text{ hp}$$

Since basic design of the axial pump is for 100-percent liquid and separator design is for 10-percent quality, it is necessary to determine individual load curves over the total operating range -- from which operation of the combination unit can be determined.

To determine the power consumed by the axial flow pump when operating with 10-percent quality fluid the equations of Appendix B relating power to density and speed are used. Taking the base reference point as 0.327 horsepower at a speed of 3000 rpm and a density of 4.34 lb/ft³ (100-percent liquid), the speed versus power in 100-percent liquid is determined from

$$P_x = 0.327 \left(\frac{N_x}{3000} \right)^3 \left[0.1 \left(\frac{3000}{N_x} \right) + 0.9 \right]$$

$$\text{At } N_x = 6000 \text{ rpm}$$

$$P_x = 2.48 \text{ hp}$$

$$\text{At } N_x = 2000 \text{ rpm}$$

$$P_x = 0.102 \text{ hp}$$

The average fluid density at 20-psia tank conditions and 10-percent quality is 0.91 lb/ft³. For 10-percent quality operation

$$P_x = 0.294 \left(\frac{0.91}{4.34} \right) \left(\frac{N_x}{3000} \right)^3 + 0.033 \left(\frac{N_x}{3000} \right)^2$$

$$\begin{aligned} \text{At } N_x &= 6000 \text{ rpm} \\ P_x &= 0.627 \text{ hp} \end{aligned}$$

$$\begin{aligned} \text{At } N_x &= 3000 \text{ rpm} \\ P_x &= 0.095 \text{ hp} \end{aligned}$$

$$\begin{aligned} \text{At } N_x &= 9000 \text{ rpm} \\ P_x &= 1.967 \text{ hp} \end{aligned}$$

These data are plotted in Figure 12-14.

The separator design point is with 10-percent quality inlet. It is estimated that the separator when operating at the design point will have a speed approximately 1-3/4 times that of operation in 100-percent liquid. Therefore, for the present analysis with an operating speed of 3000 rpm in 100-percent liquid, the estimated speed with 90-percent liquid is

$$1.75 \times 3000 = 5200 \text{ rpm}$$

Load curves for the separation function are then determined from the base design point of 0.39 horsepower (from Appendix C) at 5200 rpm. Also from Appendix C, the power required for operation in 100-percent liquid at constant speed is 1.48 horsepower, and the separator power versus speed curves are reasonably taken to be of the same slope as those for the pump over the range of interest.

The total horsepower required for the combination separator-pump is the sum of that required for the separator and pump individually, i.e. theoretically, if the drag forces on the liquid from the gas entering the separator, are just equalized by the centrifugal forces imparted to the liquid, then no energy is available from the separator for heat exchanger circulation and the energy consumed by the pump for heat exchanger circulation is not directly helpful to the separator. The load curves are plotted in Figure 12-14.

The next step in the analysis is to match the turbine output power to the total load requirement. The turbine characteristic shown in Figure C-8 is assumed.

Figure 12-14 shows that at an operating speed of 3000 rpm a horsepower of 0.63 is required. Assuming a direct-drive turbine of 6-inch diameter, the bucket velocity would be

$$u_b = \omega r = \frac{(3000)}{9.56} \left(\frac{1}{4} \right) = 78.5 \text{ fps}$$

The theoretical power available from the turbine is $\Delta h_s \dot{W}_v$

where

$$\dot{W}_v = 0.35 \text{ lb/sec and } u_o = \sqrt{2g\Delta h_s}$$

The actual power available is

$$P = \eta \Delta h_s \dot{W}_v = \frac{\eta u_o^2}{2g} \dot{W}_v$$

where the efficiency, η , is determined from Figure C-8.

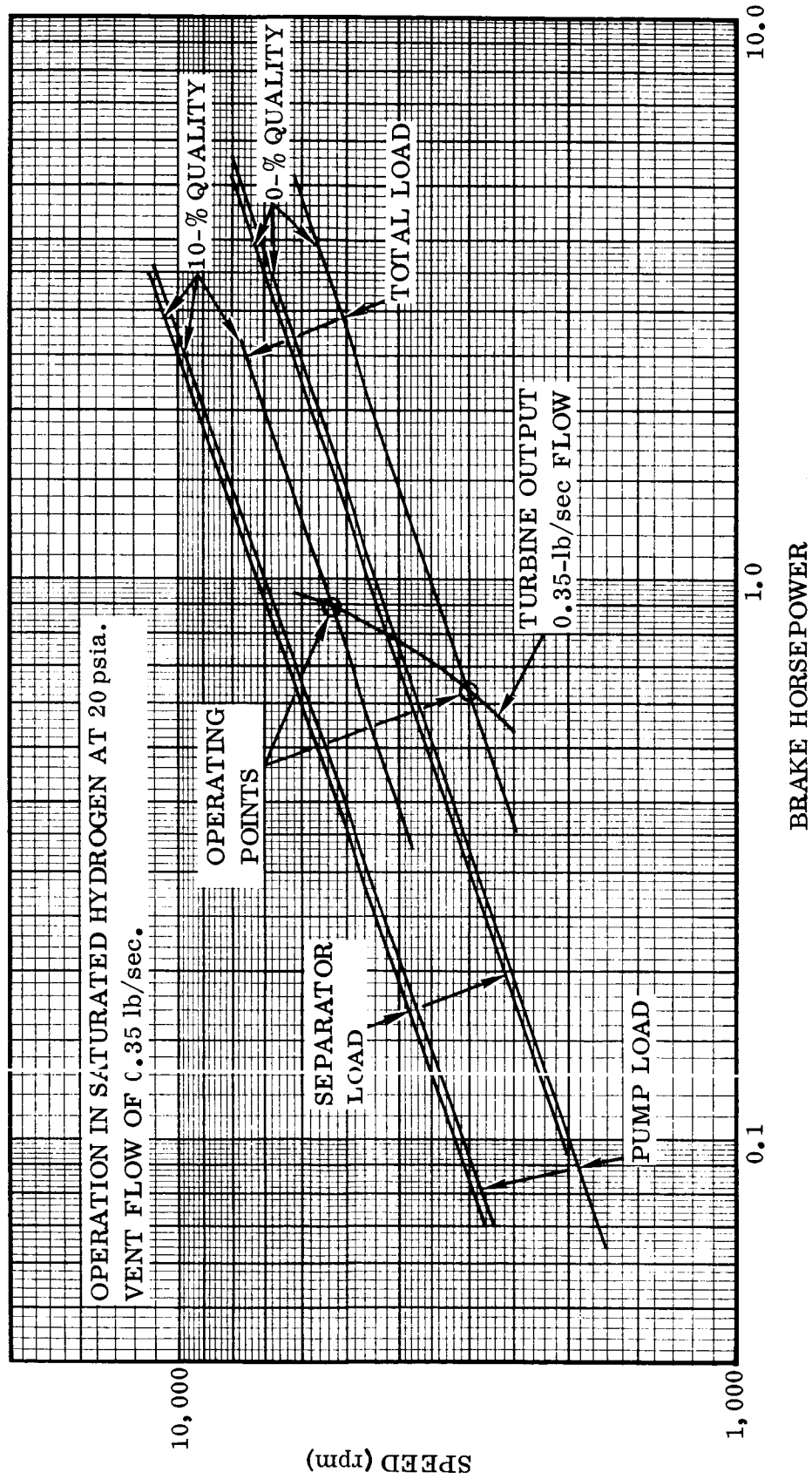


Figure 12-14. Performance of Turbine-Driven Combination Separator and Pump

Solving for the required

$$\eta u_o^2 = \frac{2 g P}{\dot{W}_v} = \frac{2 (32.2) 0.63 (550)}{0.35} = 64,000 \text{ ft}^2/\text{sec}^2 \quad (1)$$

The process of finding the required nozzle velocity, u_o , is iterative as follows.

Let $\eta = 0.4$, then from Figure C-8

$$\frac{u_b}{u_o} = 0.2775$$

and

$$\eta u_o^2 = \eta \left[\frac{u_b}{(u_b/u_o)} \right]^2 = 32,100 \text{ ft}^2/\text{sec}^2$$

which represents an inadequate power output. The nozzle velocity will need to be increased, and the efficiency will be lowered even further. An increase in turbine diameter would result in a more efficient design. For a turbine diameter of 7 inches

$$u_b = 91.5 \text{ ft/sec at 3000 rpm}$$

Letting $\eta = 0.33$, then $u_o = 440 \text{ fps}$ from Equation 1,

$$\frac{u_b}{u_o} = 0.208, \text{ and from Figure C-8, } \eta = 0.33.$$

This then sets the design of the turbine and nozzle with a wheel diameter of 7 inches and a nozzle velocity of 440 fps. The turbine power output is then determined as a function of speed. For example, at 5200 rpm

$$\frac{u_b}{u_o} = 0.36 \text{ and } \eta = 0.46 \text{ or } P = 0.878 \text{ hp}$$

The data are plotted in Figure 12-14. The actual operating condition of the combination unit with 90-percent liquid is then seen to be at 5300 rpm and 0.89 horsepower.

There are almost an infinite number of design variations which could be employed to change the actual power requirements, e.g., larger or smaller turbine wheel, and higher or lower separator and pump speeds. For predesign and comparison purposes, the above analysis is considered reasonable since the data used are common to the

separator and heat exchanger predesigns, and also, as in those cases, the operating point (with 90-percent liquid) is reasonably close to the peak turbine efficiency point.

12.2.1.1 Separator Sizing. To give an idea of the separator size requirement over and above that of the pump, reference is made to the analysis of Appendix C to determine the required separator inlet area. Taking the effective separator diameter as 2.5 inches and from

$$D_L = \frac{3}{4} \frac{\rho_v}{\rho_L} \frac{(u_v)^2}{r \omega^2} \quad (2)$$

for a liquid drop separation requirement of 0.001 inch at 5200 rpm (544 rad/sec) the maximum gas velocity into the separator

$$u_v = 11.5 \text{ ft/sec}$$

The required inlet flow area is then 39 in.^2 , or assuming total shaft surface area available for flow, the separator length would need to be

$$L = \frac{39}{\pi D} = 4.96 \text{ in.}$$

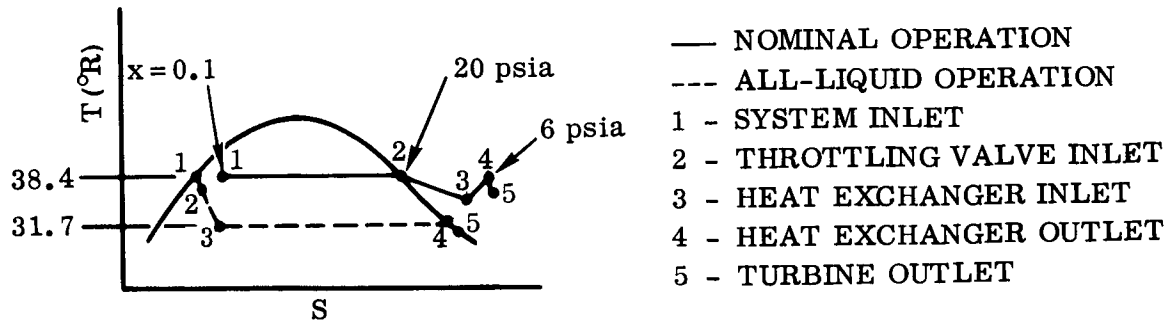
Assuming 25 percent of the surface area is required for structural rigidity then the separator length would be $4.96 (1.25) = 6.2$ inches. It would probably be desirable, and it looks reasonable, to increase the diameter of the separator portion of the unit. From Equation 2 and since the inlet area $\pi DL \approx \frac{1}{u_v}$ for constant inlet flow, it is seen

that $L \approx \frac{1}{D^{3/2}}$. Then for a separator diameter of 3 inches $L = 4.72$ in. The total

separator-pump-turbine weight is estimated to be 17 pounds.

12.2.1.2 Determination of Nominal Heat Exchanger Exit Temperature. The nominal operating condition is with 10-percent inlet quality. The fluid to the hot side of the exchanger is also essentially 10-percent quality, and the fluid at the outlet of the separator (inlet to throttling regulator) is saturated GH_2 at approximately 20 psia. Then with constant enthalpy throttling to 6 psia, the inlet to the heat exchanger is a superheated gas at 35.5°R . Furthermore, the overall heat transfer coefficient as previously determined for the superheat portion of the exchanger will apply and is approximately $30 \text{ Btu/hr-ft}^2\text{-}^\circ\text{F}$.

A T-S diagram of the system cycle is shown below.



For nominal operation the hot-side fluid will be at approximately a constant temperature of 38.4°R since the heat capacity is essentially infinite relative to the cold side.

T_4 is determined as follows.

$$q = \dot{W}_V (C_P)_V (T_4 - T_3) = U_H (A_{sH}) \Delta T_m$$

where

$$\Delta T_m = \frac{(T_H - T_3) - (T_H - T_4)}{\ln \frac{(T_H - T_3)}{(T_H - T_4)}}$$

then

$$\ln \left(\frac{T_H - T_3}{T_H - T_4} \right) = \frac{U_H (A_{sH})}{\dot{W}_V (C_P)_V}$$

and

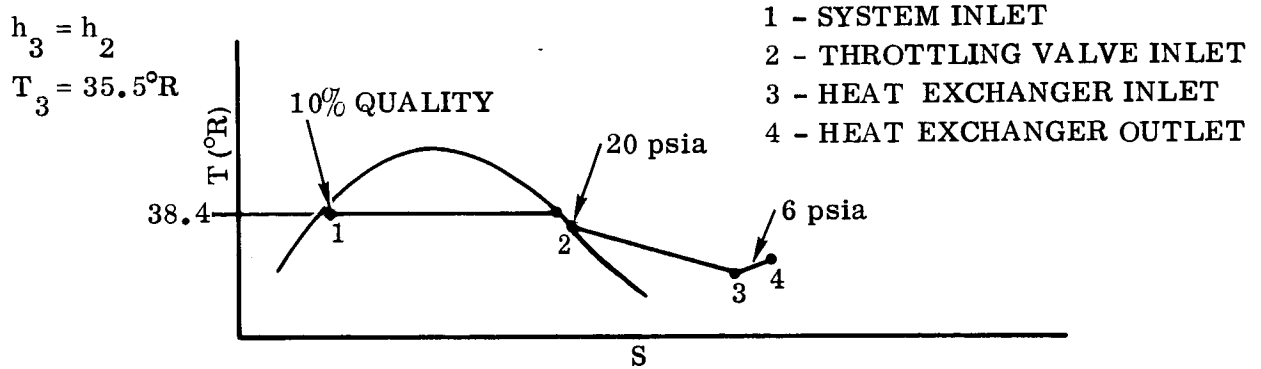
$$T_4 = T_H - (T_H - T_3) e^{-\left[\frac{U_H (A_{sH})}{\dot{W}_V (C_P)_V} \right]}$$

$$\frac{U_H (A_{sH})}{\dot{W}_V (C_P)_V} = 2.75$$

$$T_4 = 38.22^\circ \text{R}$$

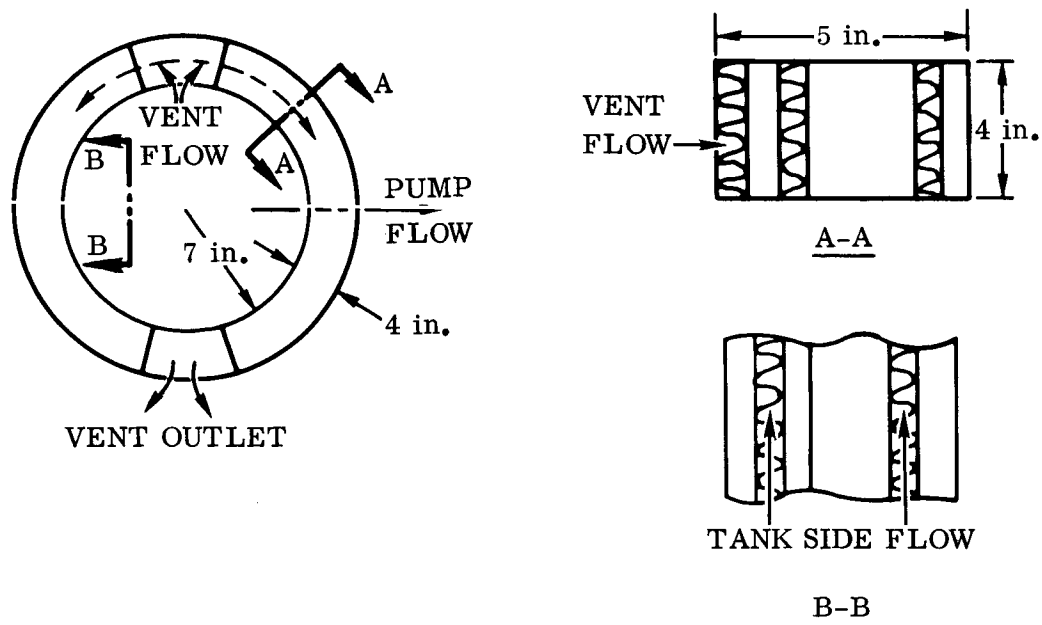
12.2.2 Analysis of Mechanical Separator System With Heat Exchanger Added Downstream. The basic system is the same as the motor-driven unit described in Paragraph 3.2. A method of packaging the separator and heat exchanger is shown in Figure 12-15. This is similar to the separator configuration developed at Convair and described in Paragraph 3.1.

The vent flow process of the proposed combination system is shown on the T-S diagram below.



The plate-fin exchanger shown in Figure 12-15 is essentially a crossflow type with a single pass on both hot and cold sides. The 1/4 (a)-11.1 fins described in Paragraph 11.1 are used.

Details of the "wrap-around" heat exchanger are given below.



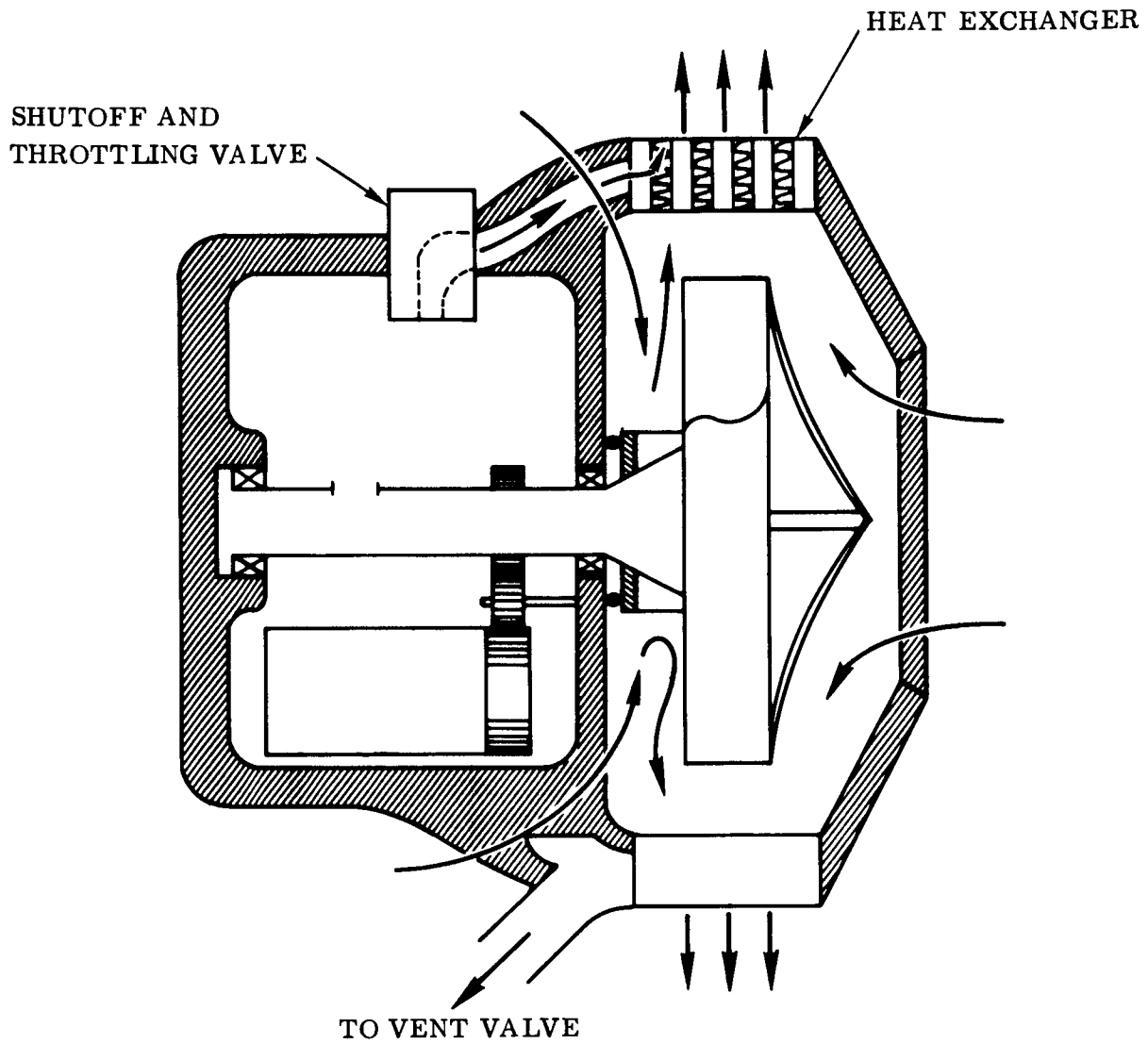


Figure 12-15. Combination Mechanical Separator and Heat Exchanger

12.2.2.1 Heat Exchanger Geometry Data. Data for 1/4 (a)-11.1 fin, from Reference 12-1, are listed below.

$\beta_E = 367 \text{ ft}^2/\text{ft}^3$ and is the ratio of the total heat transfer surface area on one side to the total volume between the plates on that side.

$$4R_H = 0.01012 \text{ ft}$$

Plate spacing, b , = 0.02083 ft = 0.25 in.

Fin area/total heat transfer surface area = 0.756

Fin thickness = 0.006-in. aluminum

Plate thickness = 0.020-in. aluminum

45 degrees or 1/8 of the circumference is taken up by the inlet and outlet headers together.

$$\text{Total number of channels, } N_T, = \frac{5 \text{ in.}}{0.25 \text{ in.} + 0.020 \text{ in.}} = 18.5$$

Nineteen channels (10 cold side and 9 hot side) will be used. In this case, cold-side channels are placed on the outside edges of the core to increase the free-flow area of this side since rough estimates indicate that the cold-side free-flow area will be small compared with that of the hot side.

The hot-side free-flow area

$$(A_c)_H = 367 (9) 0.02083 (\pi) \left(\frac{14}{12}\right) \left(\frac{0.01012}{4}\right) \frac{7}{8} = 0.56 \text{ ft}^2$$

For operation in 90-percent liquid, the rejected liquid flow rate with a vent flow of 1260 lb/hr is

$$\dot{W}_L = \dot{W}_V \left(\frac{1-X}{X}\right) = 1260 \left(\frac{1-0.1}{0.1}\right) = 11,330 \text{ lb/hr}$$

Assuming this amount of liquid nominally passes through the heat exchanger

$$G_H = \frac{11,330}{0.56} = 20,000 \text{ lb/hr-ft}^2$$

The vent-side free-flow area

$$(A_c)_c = 367 (10) 0.02083 \left(\frac{4}{12}\right) \left(\frac{0.01012}{4}\right) = 0.0645 \text{ ft}^2$$

It is assumed that the flow is split between two heat exchanger halves and

$$G_c = \frac{1260}{2(0.0645)} = 9770 \text{ lb/hr-ft}^2$$

Assuming the vent fluid is heated to 38 °F, then the average temperature of the fluid in the heat exchanger would be $\frac{38 + 35.5}{2} = 36.7^\circ\text{F}$

and from Figure A-1 $C_p = 2.89 \text{ Btu/lb-}^\circ\text{F}$

from Figure A-2 $\mu = 0.734 \times 10^{-6} \text{ lb/ft-sec} = 0.00264 \text{ lb/ft-hr}$

$$N_{PR} = 0.822; N_{PR}^{2/3} = 0.8775$$

$$Re = \frac{4 R_H G}{\mu} = 37,450$$

From Figure 8-11, $J = 0.0032$ and $f = 0.016$

To determine the vent-side pressure drop in the heat exchanger

$$\Delta p_c = \frac{G_c^2}{2g\rho_c} \left[\xi_B + \xi_e + \xi_c + f \frac{(A_{s_c})}{(A_{c_c})} \right]$$

where the loss coefficient due to two 90-degree bends and the curved heat exchanger (ξ_B) is 3.2 and $\xi_c = 0.4$ and $\xi_e = 0.3$ (ξ_c and ξ_e taken from Figure 5-5 of Reference 12-1).

$$(A_{s_c}) = \beta_E V_c = 105 \text{ ft}^2$$

V_c = volume between the plates on the cold-side. (A_{s_c}) for each half of exchanger is 52.5 ft^2 and

$$f \frac{(A_{s_c})}{(A_{c_c})} = 13.02$$

$$\Delta p_c = 75.5 \text{ lb/ft}^2 \text{ or } 0.524 \text{ psi}$$

This pressure drop is not excessive; however, it is higher than in the basic heat exchanger case. For the same exchanger pressure (6 psia), the 0.5-psi drop is reasonable since no downstream turbine is employed in the present case.

$$\text{The cold-side film coefficient, } (h)_{f_c}, = \frac{J G C_P}{N_{PR}^{2/3}} = \frac{103 \text{ Btu}}{\text{hr-ft}^2 \text{-}^\circ\text{F}}$$

and from Figure 8-13, $\eta_o = 0.9$.

$$\text{Hot-side film coefficient, } (Re)_H = \frac{0.01012 (20200)}{0.0302} = 6780$$

$$J_H = 0.0055 \text{ and } f_H = 0.0215$$

For saturated LH_2 at 20 psia $\mu_L = 0.0302 \text{ lb/ft-hr}$

$$(C_P)_L = 2.46 \text{ Btu/lb-}^\circ\text{F}$$

$$N_{PR}^{2/3} = 1.046$$

$$(h)_{f_H} = \frac{0.0055 (20200) 2.46}{1.046} = 256 \frac{\text{Btu}}{\text{hr-ft}^2 \text{-}^\circ\text{F}}$$

$$\eta_o = 0.8$$

$$(A_s)_H = (A_s)_c \left(\frac{9}{10}\right) = 94.5 \text{ ft}^2$$

$$U_H = 67.7 \frac{\text{Btu}}{\text{hr-ft}^2 \text{-}^\circ\text{F}}$$

12.2.2.2 Determining Heat Exchanger Vent-Side Outlet Temperature. We assume 100-percent liquid flow on the hot-side and take into account the subcooling of this liquid. Using the NTU approach of Reference 12-1

$$\text{NTU} = \frac{U_H (A_s)_H}{\dot{W}_V (C_P)_V} = 1.76$$

$$B_c = B_{\min} = 1260 (2.89) = 3640 \text{ Btu/hr-}^\circ\text{F}$$

$$B_H = B_{\max} = 11,330 (2.5) = 28,300 \text{ Btu/hr-}^\circ\text{F}$$

$$\frac{B_{\min}}{B_{\max}} = 0.129 \text{ and from Figure 2-14 of Reference 12-1, the ex-}$$

changer effectiveness, $E_x = 0.8$

Then the outlet temperature

$$T_4 = 0.8 (38.4 - 35.5) + 35.5 = 37.82^\circ \text{R}$$

12.2.2.3 Power Requirement for Tank-Side Circulation. We assume one 90-degree bend with a loss coefficient, ξ_B , of 1.2. The inlet loss coefficient ξ_c , from Figure 5-5 of Reference 12-1 is 0.50 and the exit loss coefficient, ξ_e , from Figure 5-5 Reference 12-1 is 0.35.

$$\Delta p_H = \frac{G_H^2}{2g_o \rho_H} \left[\xi_B + \xi_c + \xi_e + f \frac{(A)_{sH}}{(A)_{cH}} \right]$$

$$f \frac{(A)_{sH}}{(A)_{cH}} = 0.0215 \left(\frac{94.5}{0.558} \right) = 3.64$$

$$\Delta p_H = 0.64 \text{ lb/ft}^2$$

and power, $P = \frac{\dot{W}_H \Delta p_H}{\rho_L} = 0.000843 \text{ hp}$

Even with a reasonable efficiency, this power is low enough to be neglected in the present analysis.

12.2.2.4 Heat Exchanger Weight

$$(A)_{sH} = 94.5$$

$$(A)_{sC} = 105.0$$

$$(A)_{sT} = 199.5 \text{ ft}^2$$

The fin area, $(A_f)_T = 0.756 (199.5) = 151 \text{ ft}^2$

Fin weight = $\frac{0.006 (151) 144 (0.1)}{2} = 6.52 \text{ lb}$

Number of dividing plates = 20

Weight of plates = 7.92 lb

Total core weight = 14.44

Total weight including headers = $14.44 \times 1.43 = 20.65 \text{ lb}$

A 0.020-inch plate thickness is used rather than 0.012-inch due to increased fabrication problem of the curved exchanger. For perturbations about the design point, it is reasonable to assume that the weight will be proportional to the heat transfer surface area. The following data are determined for variations in heat exchanger size.

HEAT EXCHANGER HOT-SIDE AREA (ft ²)	HEAT EXCHANGER OUTLET TEMPERATURE (°R)	HEAT EXCHANGER WEIGHT (lb)
94.5	37.82	20.65
189	38.24	41.3
142	38.1	31.0
71	37.53	15.5
47.2	37.14	10.325

From the exchanger outlet temperatures and the separator power requirement (taken from Paragraph 3.2 as 420 watts), the payload change is determined using the calculation methods outlined in Appendix E.

12.2.3 Comparison of Systems. Referring to Table 12-1, the optimum exchanger corresponds to a superheat of approximately 37.5°R with a hot-side surface area of 71 ft². To estimate the maximum vent flow that can be vaporized, with the present system, assuming an all-liquid inlet a comparison is made with the basic exchanger of Paragraph 12.2.1.

The required heat transfer to vaporize a given vent flow is proportional to the vent flow rate. Also, for similar heat transfer coefficients the area required is proportional to the heat transfer, and therefore proportional to the vent flow rate. In the present case the boiling coefficients would be the same as for the exchanger of Paragraph 12.2.1. The hot-side coefficient would be somewhat lower; however, the overall

coefficient would not change very much. Then assuming the heat transfer area for complete evaporation to be proportional to the flow rate, a maximum flow that could be tolerated in the 71-ft² exchanger during liquid inundation would be

$$\dot{W}_V = 0.35 \left(\frac{71}{319} \right) = 0.078 \text{ lb/sec}$$

It is recognized that this is a rough analysis; however, it appears reasonable that the 71-ft² exchanger used in conjunction with the motor-driven separator could operate when surrounded with liquid with essentially no liquid loss at a vent flow rate of 0.06 lb/sec.

12.3 EFFECT OF ADDING PARTIAL RELIQUEFACTION CYCLE TO MECHANICAL SEPARATOR. This paragraph briefly compares the net weight effects on available payload weight of two systems: a) a mechanical vapor/liquid separator and b) a separator plus a partial reliquefaction system.

The hydrogen partial-reliquefaction system used in this example is shown schematically in Figure 12-16 (taken from Figure 1 of Reference 12-2). The system boil-off fraction (actual vent rate divided by boil-off rate in the absence of a reliquefier) is 0.546.

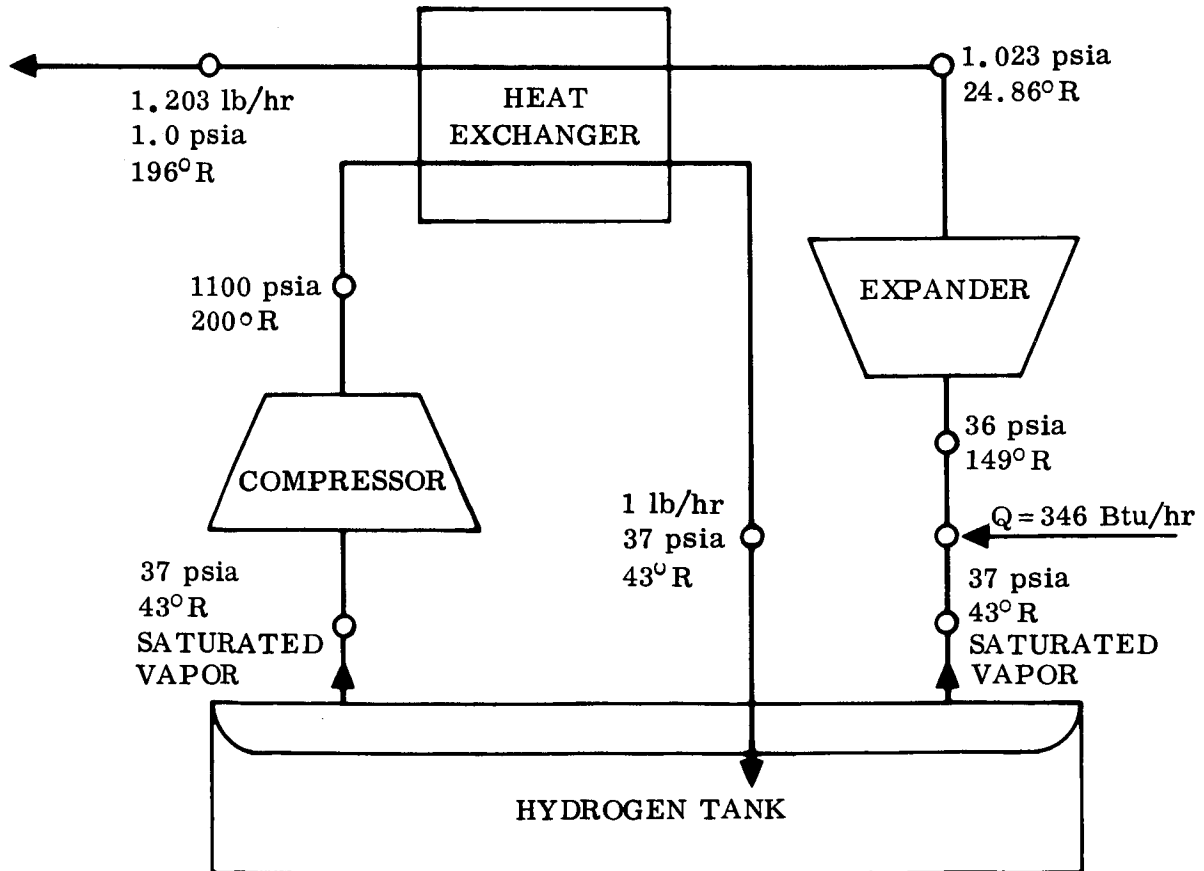


Figure 12-16. Hydrogen Partial-Reliquefaction Cycle

The system was sized for a total boil-off rate (without reliquefaction) of 2.203 lb/hr, of which, 1 lb/hr is reliquefied and 1.203 lb/hr is actually vented. Fluid inlet to the system is saturated hydrogen vapor at 37 psia. The total system weight has been roughly estimated to be 100 pounds (Reference 12-3).

The system as shown must operate with a 100-percent vapor inlet; therefore, in the comparisons it is assumed that a vapor/liquid separator is located upstream of the partial-reliquefier. The mechanical separator designed for the cryogenic service module (CSM) application and described in Paragraph 3.2.3 is used in the comparisons in order to provide 37-psia gas to the reliquefier inlet. It would be possible to use other separation methods in conjunction with the reliquefier, or to modify the reliquefaction cycle to handle a two-phase inlet fluid. However, this would require a complete re-analysis of the separator reliquefaction systems, and this was not done for this brief comparison.

The weights and power requirements for the separator are estimated values since a unit was not actually sized for the present conditions. Comparisons were made for two separator sizes and powers, which should bracket the actual requirement.

The comparisons to follow are expressed as payload loss or gain due to the addition of reliquefier and separator, referenced to a base case (zero Δ payload) of venting saturated vapor without vapor/liquid separation or reliquefaction.

The methods and data of Appendix E were used to calculate the effects of hardware weights and vent rates on payload weight. The difference in vent rate between using a partial reliquefaction system and venting saturated GH_2 at 37 psia without a system was determined directly from the boil-off fraction of the reliquefier. The 2.203-lb/hr boil-off rate was increased slightly due to the added power input to the propellant tank from the electric motor used to drive the separator.

The relative effect of hardware weight and vent gas weight on the available payload weight is dependent on the exchange ratios (Δ Payload Weight/ Δ System Weight) used. The comparative data were calculated using the exchange ratios listed in Table E-1 of Appendix E for both CSM and S-IVB cases. Data for a "hybrid" case using the CSM hardware exchange ratio and the S-IVB vent-exchange ratio were also developed to illustrate the relative effect of varying one exchange ratio while holding the other constant. The data generated are summarized in Table 12-2, and plotted in Figure 12-17 as a function of coast time.

The crossover points of the two systems (mechanical separator alone, and mechanical separator plus reliquefaction system) can be read from Figure 12-17 for four combinations of separator weight and exchange ratios. The crossover times were about 131 and 187 hours, using CSM and S-IVB exchange ratios, respectively. Cases I and II indicate that the crossover point is fairly insensitive to changes in separator weight.

Table 12-2. Comparison Data - Effect of Partial Reliquefaction of H₂ Vent Gas
 Base Vent Rate ($\Delta W_{PL} = 0$) is 2.203 lb/hr

CASE	EXCHANGE RATIOS		SYSTEM	EXTERNAL POWER (watts)	HARDWARE WEIGHT (lb)	BOIL-OFF RATE (lb/hr) (Includes effect of external power)	VENT RATE (lb/hr)	$\Delta \dot{m}_v$ (lb/hr) (Vent Rate - 2.203)	TOTAL W_{PL} LOSS (lb)
	$\frac{\Delta W_{PL}}{\Delta W_H}$	$\frac{\Delta W_{PL}}{\Delta W_V}$							
I	1.43	1.06*	R+S†	2.2	107.5	2.243	1.225	-0.978	154 - 1.04 t**
			S††	2.2	7.5	2.243	2.243	0.04	10.7 + 0.042 t
II	1.43	1.06*	R+S	4.4	115	2.283	1.247	-0.956	164.5 - 1.013 t
			S	4.4	15	2.283	2.283	0.08	21.4 + 0.084 t
III	1.43	0.352	R+S	2.2	107.5	2.243	1.225	-0.978	154 - 0.344 t
			S	2.2	7.5	2.243	2.243	0.04	10.7 + 0.014 t
IV	0.67	0.352	R+S	2.2	107.5	2.243	1.225	-0.978	72 - 0.344 t
			S	2.2	7.5	2.243	2.243	0.04	5 + 0.014 t

† Reliquefier plus separator
 †† Separator

* Represents a weighted average of values listed in Appendix E for the CSM over the total mission.

** t is the total elapsed coast time in hours.

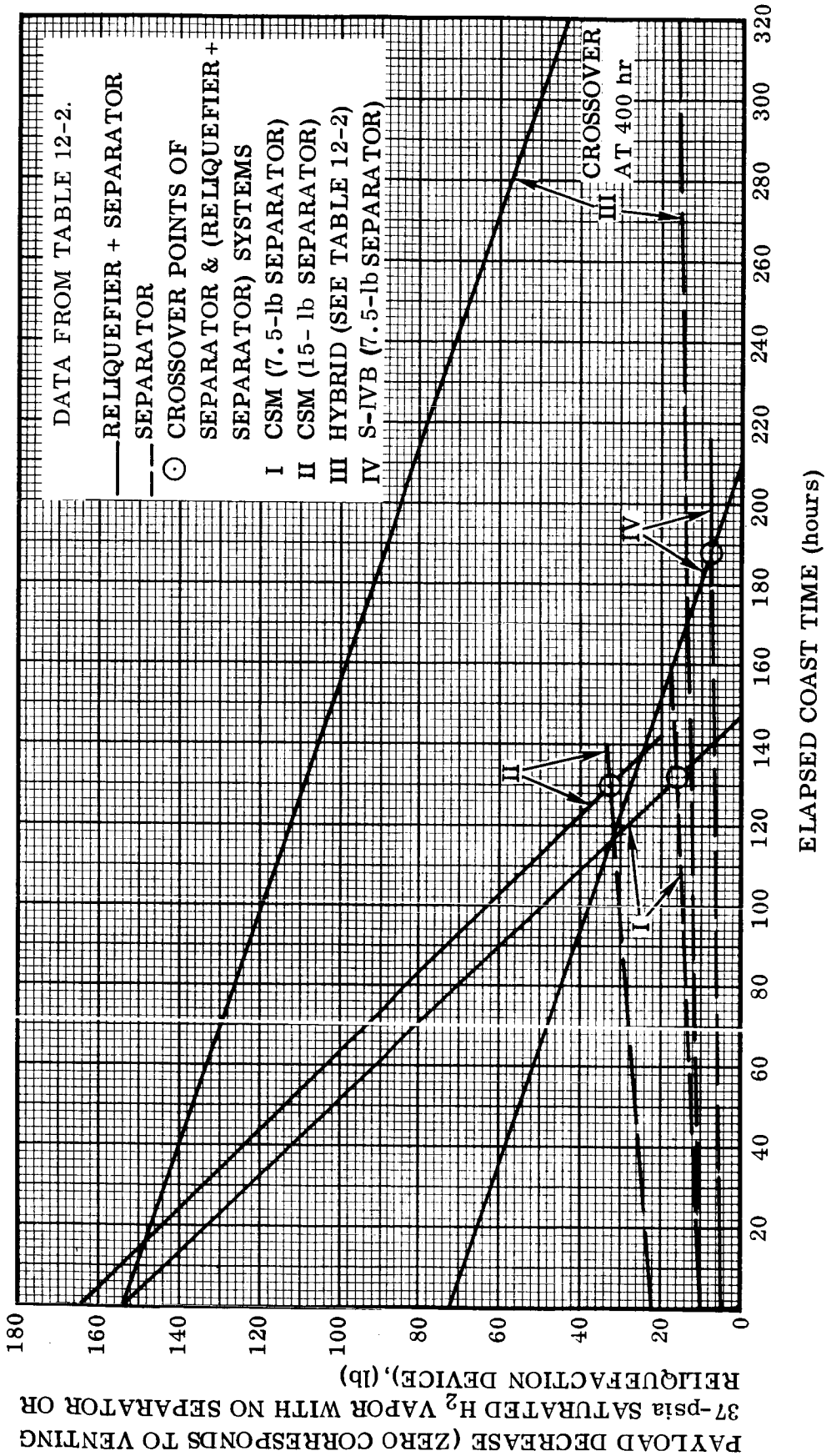


Figure 12-17. Available Payload Weight Decrease Versus Total Coast Time Comparison for Vapor/Liquid Separation and Separation Plus Partial Reliquefaction

The crossover point is seen to be sensitive to the exchange ratios used, with lower boil-off and higher hardware exchange ratios resulting in increased crossover times.

It should be noted that the example given here is representative of a vehicle similar to the cryogenic service module (CSM); however, if it can be assumed that hardware weights and power requirements for both systems are proportional to the base boil-off rate with the same reliquefier boil-off fraction, then the crossover times will not change with boil-off rate. This would not be strictly true; however, it is quite certain that the hardware weights of the reliquefaction system shown in Figure 12-16 would increase at least fast as would the separator weights with increasing vent rate. Therefore, the crossover times should not be shorter than those indicated by the present comparison.

In summary, the brief comparisons in this paragraph indicate that a partial liquefaction cycle of the type considered here would offer some weight savings over the use of a mechanical separator alone for a CSM type of vehicle/mission if the portion of the mission during which engines were restarted exceeded about 130 hours.

SECTION 13

TEST PROGRAM FOR HEAT EXCHANGE SYSTEM

13.1 TEST REQUIREMENTS. A test program will be required to prove the workability of the selected heat exchange system and provide the information needed for final optimization and production design of any such device. The S-IVB stage is a possible first and at least typical application for the heat exchange separator system; consequently, much of the design and analysis of the selected system was directed toward that application. For the same reason, the test program recommended herein is based on the following assumptions.

- a. The end goal is the development of a system for the S-IVB.
- b. The system design is as shown in Section 11, pending possible changes resulting from the test program.
- c. The schedule permits an orderly development, allowing exploratory tests and associated analyses before the S-IVB system design is finalized and fabricated for test.
- d. The test program should develop data and analyses for other potential applications besides S-IVB.

The test requirements resulting from these assumptions, and from the unknowns or uncertainties disclosed during the system study, can be logically grouped into a four-part test program.

Part I - Concept Feasibility Demonstration: Ground tests with a sub-scale breadboard system, using Freon as the working fluid, to demonstrate that the selected integrated heat exchange system can start and operate satisfactorily over a range of inlet and flow conditions.

Part II - Exploratory and Component Tests: Tests to provide data for optimization and final design of a flight system.

- a. Heat transfer tests with hydrogen and oxygen in sections of brazed aluminum heat exchanger cores.
- b. Flow distribution tests to establish the uniformity of two-phase flow distribution into the heat exchanger passages with the design shown in Section 11 and to explore means of improving the distribution.
- c. Performance, response, and two-phase flow patterns of the selected expansion device (modified S-IVB vent valve).

- d. Drop tests in connection with the three preceding test series to establish correlations between zero-g and standard-g results.
- e. Development of an analog computer simulation of the selected heat exchange system, and use of the simulation to develop further parametric data and transient response characteristics.

Part III - Tank Mixing Tests: Tests to establish natural convection or stratification, and vapor bubble size at breakaway, under low gravity. Tests to establish zero-g mixing efficiency and power requirements.

Part IV - Development and Performance Tests: Ground tests of the prototype design shown in Section 11 (perhaps modified as a result of tests outlined above) to determine its performance over a range of operating conditions. Supplementary analog computer simulations to extend the range of operating conditions investigated at minimum cost. Flight test as a final proof of performance and check on the ground test program.

These four test series are described in Paragraphs 13.2 to 13.5 respectively. Each of these paragraphs begins with a discussion of the reasons why each type of test is considered necessary. Paragraph 13.6 then discusses the flexibility of the test program, including possible changes if an S-IVB system is not required.

13.2 CONCEPT FEASIBILITY DEMONSTRATION

13.2.1 Test Justification. The recommended heat exchange system has been analytically shown to be workable and capable of stable operation if components with compatible operating characteristics are used. The prudent course when time permits, however, is to experimentally verify the analysis at an early stage in the program and at minimum cost. The recommended feasibility demonstration would accomplish this goal and also provide experimental data of possible use in the final design of the prototype flight system or in development of an analog computer simulation of the system.

Because the system design shown in Section 11 is sized and designed for flight use on the S-IVB, it will be relatively expensive to build and test. Therefore, the recommended demonstration test uses a sub-scale breadboard system and Freon as the working fluid. Three points on the importance and scope of this test should be borne in mind.

- a. If an urgent need for S-IVB flight hardware develops, this test could be deleted in favor of immediate fabrication of the Section 11 design. The added risk would be small because there really is very little doubt that the concept can be made to work. Convair has demonstrated (Reference 2-2) that LH_2 can be expanded through a fixed orifice and vaporized by passing through a heat exchanger coil immersed in LH_2 , but natural convection was employed and no work was extracted from the vent gas. In a test just completed (Reference 2-5), a further step was taken by using a pressure regulator as the inlet expansion device but a fixed orifice at the

heat exchanger outlet. The working fluid was Freon and again no work was taken from the vent gas and natural convection was used. The test demonstrated system stability and no liquid venting when the regulator inlet was alternated between liquid and gas while running. Thus, the only remaining conditions to demonstrate are regulator control of heat exchanger outlet as well as inlet, and forced convection of liquid and vapor using power from the vent gas. Analysis of the system indicates both requirements can be met, although some tailoring of component response characteristics may be necessary for stable operation under all conditions.

- b. Although the preceding paragraph indicates that the concept feasibility demonstration can be deleted at little risk, the test is still recommended if schedules permit. It is believed that optimum system performance at minimum total cost can best be achieved by first obtaining the improved data and understanding that the feasibility and exploratory tests will yield. By incorporating the design improvements or corrections indicated by these tests, the flight system will provide better performance with less development work.
- c. The concept feasibility test recommended here is a minimum one because it is assumed that it will be shortly followed by the development and performance tests on the S-IVB system. If the system for the S-IVB is not to be built and tested in the near future, it is urged that the feasibility tests be expanded to yield more performance data over a greater range of operating conditions and with LH₂ as the working fluid. Otherwise the workability and performance will not be adequately established.

13.2.2 Test Description. The recommended concept feasibility demonstration will verify that a self-powered heat exchanger vent system can start and operate under various inlet conditions and vent rates to maintain tank pressure within acceptable limits. It uses Freon-12 as the working fluid and is limited in scope under the assumption that it will be followed shortly by more extensive testing of the system shown in Section 11.

After preliminary tests, the system will be used to verify the following capabilities.

- a. Start and run with pump inlet in liquid and vent inlet in gas.
- b. Start and run with pump inlet in liquid and vent inlet in liquid.
- c. Start and run with pump inlet in gas and vent inlet in gas.
- d. Run with pump inlet in liquid and vent inlet alternating between gas and liquid.

System response to the following severe tests will also be determined, but the system is not required to pass the tests because the design of Section 11 tends to prevent these conditions.

- e. Start and run with heat exchanger in gas and vent inlet in liquid.
- f. Run with heat exchanger in gas and vent inlet alternating between gas and liquid.

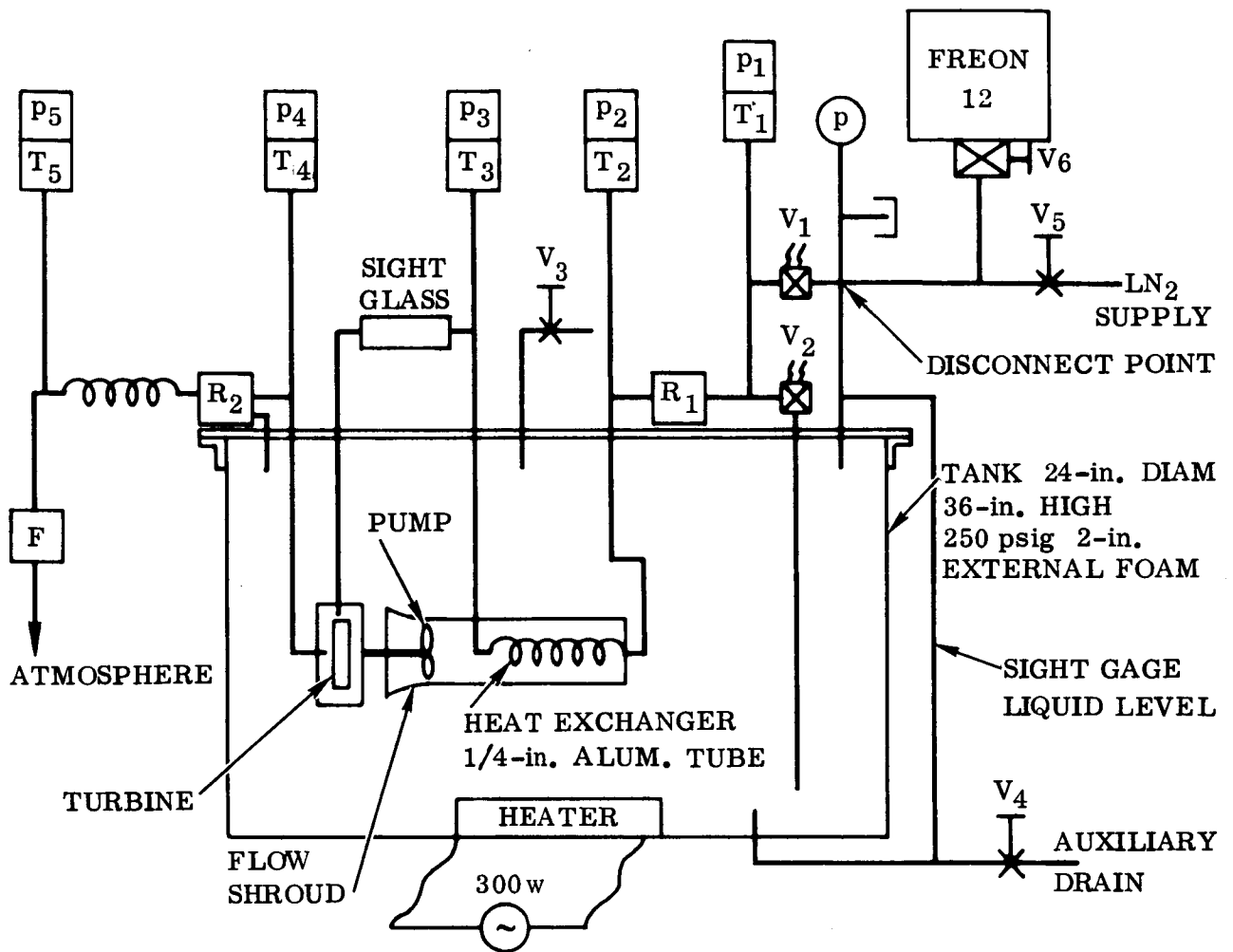
These six tests will be repeated over a range of (test tank/heat exchanger) and (heat exchanger/ambient) pressure ratios to establish the limits of successful system operation.

Figure 13-1 shows a schematic of the recommended test setup. It is very similar to the one used for the recent Convair heat exchanger vent tests (Reference 2-5) but expanded to permit forced convection, downstream pressure regulation, and a wider range of test conditions. The horizontal shroud around the heat exchanger coil directs the forced convection and tends to minimize natural convection. R_1 and R_2 are low-cost commercial pressure regulators, R_1 responding to downstream pressure and R_2 being a backpressure regulator with external sense line. The heat exchanger pump is a commercial axial flow fan. One example of the potential sources is the family of electrically driven, small axial-flow fans produced by Pesco. Such a fan could be electrically driven for preliminary tests as discussed in the next paragraph, and then modified for turbine drive. Drive turbines of appropriate size are also generally available. As a typical example of what can usually be found at a test facility, Convair has two 4.5-inch-diameter Terry turbines available as salvage (Disposition Stores Material No. 104-644800) that could be adapted for this use with minor nozzle revision.

Although it would be possible to proceed directly with integrated system testing, it is recommended that preliminary tests be run with the forced circulation pump independently powered by an electric motor or by the turbine with an independent drive gas supply. Test runs with several different circulation power inputs at each of several pressure regulator and heater settings will provide a better understanding of system behavior and improved ability to analyze the limits of system operation or stability encountered in the subsequent integrated tests.

13.3 EXPLORATORY AND COMPONENT TESTS. Experimental investigations will be conducted in the areas of heat transfer, expansion valve performance, flow distribution, and zero-g effects. Development of an analog computer simulation of the heat exchange vent system, and its use to explore system performance and transient response, will also be required in support of the final system design and optimization. The expansion valve and flow distribution tests are directed primarily toward the S-IVB system design of Section 11, although the flow distribution tests should also apply to any sub-scale system of similar configuration. The other tests will prove applicable to any size heat exchange vent system, and the heat transfer tests will be valuable basic research as well.

13.3.1 Heat Transfer Tests. Heat transfer and pressure drop data uncertainties are discussed in detail in Section 8. Boiling heat transfer coefficients are particularly uncertain, with available hydrogen data scattering over almost two orders-of-magnitude



- p PRESSURE TRANSDUCER (0-250 psi)
- T TEMPERATURE TRANSDUCER (440-610° R)
- F FLOW TRANSDUCER (0.25 lb/min NOMINAL)
- RELIEF VALVE (250 psi)
- HAND VALVE (1/4 in.)
- ⊗ REMOTE OPERATION ON/OFF VALVE (1/4 in.)
- R PRESSURE REGULATOR
- p PRESSURE GAGE (0-250 psig)

Figure 13-1. Concept Feasibility Test Schematic

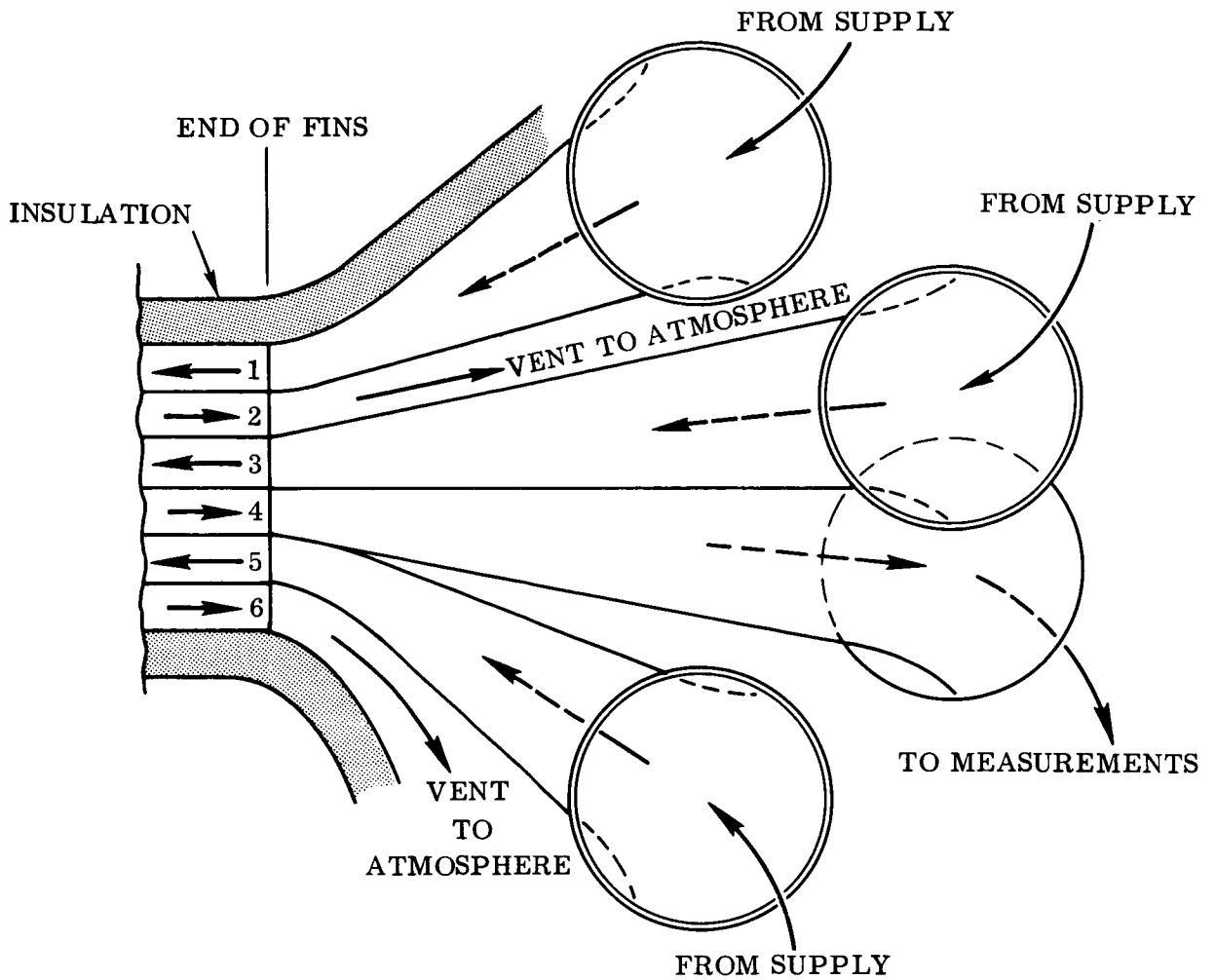
in the region of interest. Condensing coefficients may vary by a factor of 2 from calculations, and single-phase film coefficients could also be in error by 25 to 50 percent. These uncertainties make it difficult to design a minimum-size heat exchanger with confidence. Since none of the available hydrogen heat transfer data were obtained with aluminum surfaces or in heat exchanger cores, and since boiling heat transfer is significantly affected by such factors, a test program with sections of brazed aluminum heat exchanger is recommended.

A series of ground tests with liquid hydrogen will furnish the desired boiling, condensing, and single-phase heat transfer data and establish the flow velocities where gravity effects become significant in each. A limited drop test program (Paragraph 13.3.3) will then verify the points where gravity effects become significant and provide correlation between zero-g and standard-g test results at lower flow velocities. Further useful data will be obtained from the ground tests by incorporating measurement of two-phase flow pressure drop and providing for transient response tests.

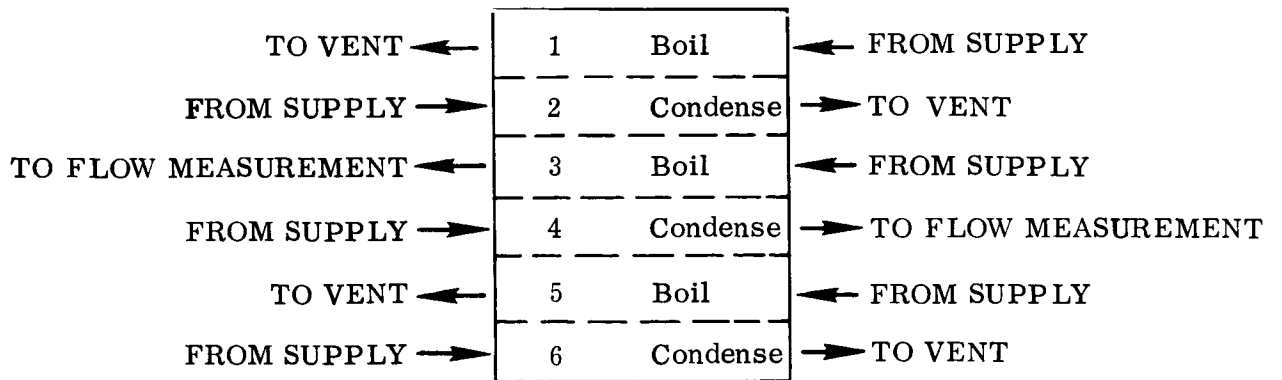
The heat exchanger test sections will use seven plates alternated with six layers of fin corrugations in a standard brazed aluminum heat exchanger core configuration. Test data are taken only for the center two of the six fin layers, with the outer layers and external insulation serving as thermal guards to assure symmetric temperature distribution in the test section. Each layer has a separate inlet and outlet header as shown in Figure 13-2. The test section is instrumented with buried germanium or thermistor elements to measure structure temperatures. Other instrumentation measures flow rates and inlet and outlet fluid conditions, including pressure, temperature and quality. Boiling will occur in Layer 3 of the test section (Figure 13-2) and condensing in Layer 4, so that each run will provide two sets of data. Runs will be made over the full range of 0- to 100-percent inlet quality in each layer to provide the desired boiling, condensing, and single-phase heat transfer data.

The test fixture will be designed so that tests can be run with the flow upward, downward, or horizontal. Test flow rates will range high enough that the orientation should have little effect on the results and low enough to find significant effects. Appropriate conditions can then be selected for reduced gravity testing per Paragraph 13.3.3.

The measurements and layout of the system are shown in Figure 13-3. The test fluid will be brought through a flowmeter to a vaporizer/mixer section. The vaporizer/mixer will employ an electric heater placed in the fluid line, thereby providing a controlled wet mixture to the exchange inlets. The quality of the mixture will be determined from the known heat input or with a quality meter such as those developed by Beach Aircraft or under development by Industrial Nucleonics. For high quality mixtures, saturated GH_2 and slightly subcooled LH_2 will be introduced into the inlet. The heater will not be used during this operation, the vaporizer/mixer section serving only to bring the gas and liquid to the same saturation temperature. For liquid/gas mixtures, the temperature measurements upstream of the heat exchanger will be used

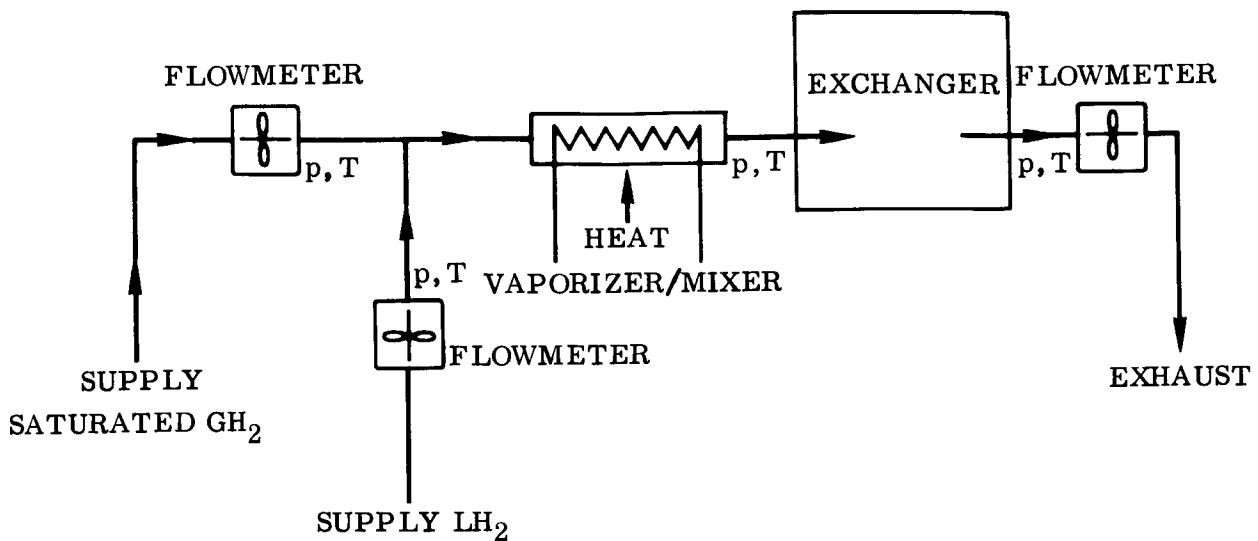


INLETS TO EXCHANGER
(ONE HALF SHOWN, OTHER HALF SIMILAR)



FLOW CHANNEL ARRANGEMENT

Figure 13-2. Heat Exchanger Test



NOTE: ONLY CHANNELS 3 & 4 HAVE FLOWMETER
DOWNSTREAM OF EXCHANGER; SEE
FIGURE 13-2 FOR CHANNEL NUMBERING

Figure 13-3. Heat Exchange Test Measurements and Layout

to verify the mixing by observing that saturation temperature has been reached. Each passageway will be fed through its own flowmeter and vaporizer mixer. A balance in mass flow will be maintained into each set of the three passages. Slight variations may occur but these will be less than the imbalance that would occur if the three passages were fed from a common header. Volume flow measurements will be made at passageway exits to determine the quality of the leaving mixtures. The flow rates will be adjusted to meet the design requirements and extend above and below these requirements. Tests will be performed with the exchanger unit mounted in various orientations. A review of the test results should allow the delineation of the flow rates (taken together with the other conditions) at which the orientation does and does not significantly affect the heat transfer.

13.3.2 Flow Distribution and Expansion Valve Tests. Achieving a uniform vapor/liquid distribution among the passages of the heat exchanger can present a problem on both the vent (cold) side and the tank (hot) side, but the tank side will have less effect on system performance and is deferred until final development tests (Paragraph 13.5.1). Uneven distribution by the vent header would seriously degrade system performance, so exploratory tests are required to prove that the selected design can achieve the acceptable uniformity by baffling and hole size adjustment. As an indication of the importance of uniform distribution, recall that in the maximum heat transfer case

when the vent-side inlet receives all liquid, expansion through the vent valve results in flashing-off 7-percent vapor by weight but 90-percent by volume. With bad distribution, 10 percent of the heat exchanger flow passages would receive all-liquid. Since most of the heat transfer is to the liquid, flow-passage length would have to be almost ten times as long as for the desired case of uniform liquid distribution. This could require an order-of-magnitude oversizing of the heat exchanger to ensure full vaporization under all conditions.

The vent header is located between the vent (expansion) valve and the vent (boiler) side of the exchanger. Schematically, it consists of a shrouded perforated tube with the fluid flowing outward. The exploratory tests will employ a valve and an experimental header setup as shown in Figure 13-4. Flow tests will start with water/air mixtures in a simple header and with visual observation of the discharge pattern. Even this crude test will almost certainly point toward header improvements, which will be made and the test repeated. As the distribution approaches a satisfactory uniformity with repeated tests and baffle improvement, the instrumentation will be refined and extended to the full set. The following measurements will be made.

- a. Water flow.
- b. Air flow.
- c. Stream temperature.
- d. Header pressure.
- e. Impact pressures.
- f. Catch basin ullage pressure.
- g. Catch basin level.

The catch basin will be used to measure flow rate and mixture ratio at selected header outlet locations as a backup to the impact probe.

The flow approaching the vent valve will be downward for bubbly water mixtures, but where the quality is high (air stream with dispersed fog or spray), it will be upward. This is intended to provide symmetrical mixture distribution into the vent valve. Both orientations will be used when there is doubt of the temporal or spatial uniformity of the mixture entering the valve. Baffle configuration will be modified as required to improve the distribution. The Baker correlation (Reference 13-1) will be used as a guide in these efforts to produce dispersed or frothy flow, since several investigators have found it valid for Freon and hydrogen.

The use of water/air mixtures for preliminary tests is believed valid if higher flow velocities are used. The actual orbital operation of a system with hydrogen will be under conditions of high Reynolds, Weber, and Froude numbers (as compared with the

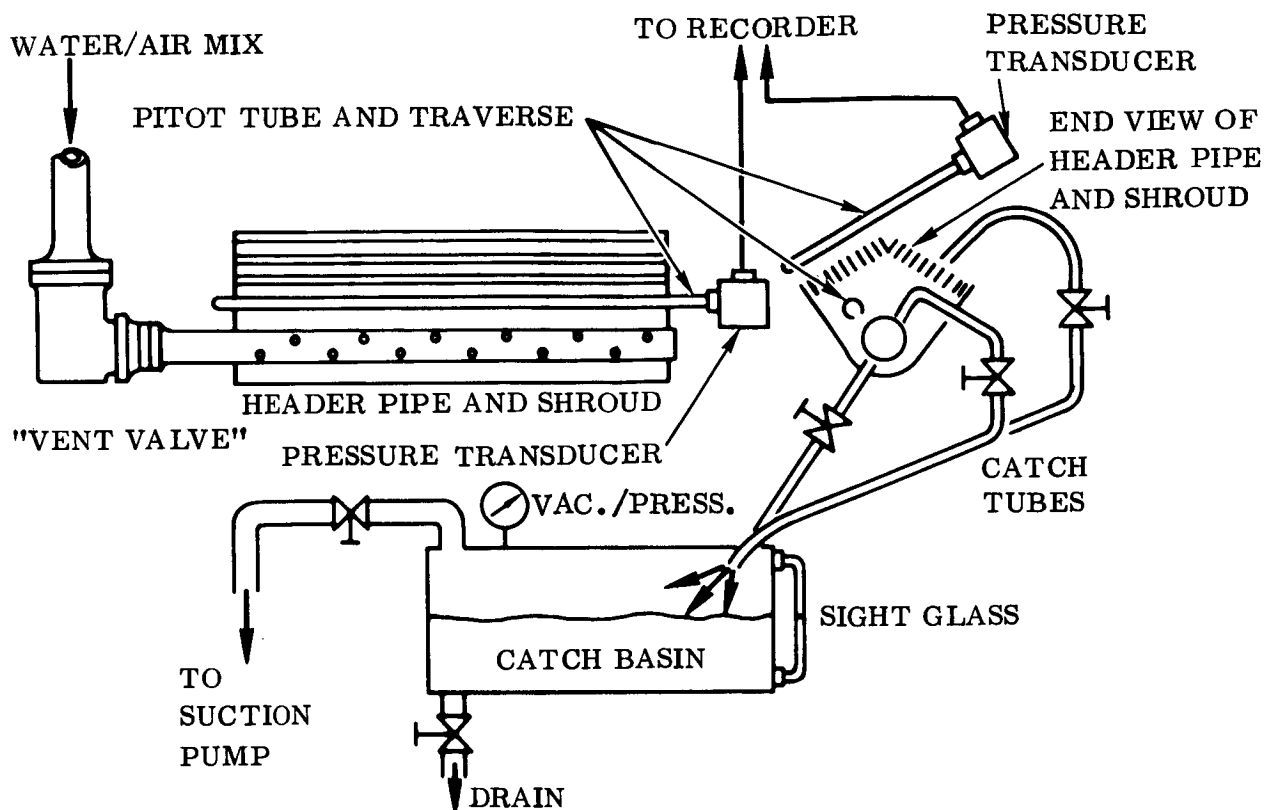


Figure 13-4. Flow Distribution Tests

critical value of each). Thus, inertial flow forces will predominate and the effects of viscosity, surface tension, and gravity on fluid flow and dispersion will be negligible. Fluid-flow model testing requires that the flow regime be duplicated by similar values of these dimensionless force ratios, although it is not necessary to use exactly the same values when model and actual values are both far above the critical value of each dimensionless ratio (Reference 13-2). Since water has higher viscosity and surface tension than hydrogen, and standard-g will exist, the test must employ flow velocities at least an order-of-magnitude higher than the actual system to obtain acceptable values of the dimensionless numbers. To verify the validity of these water/air tests, a final check with hydrogen will be obtained in conjunction with vent valve tests, which must use hydrogen for final tests. Gravity immunity will be verified by comparing runs with upward and downward flow direction.

Analysis of the internal construction and function of the Centaur/S-IVB vent valve led to the conclusion that appropriate modification to sensing ports and orifices will permit its use as a liquid/gas expansion device, even though it was designed originally only for gas venting. It remains to be proven that this is true. The proof is important because development of a new valve design would be a major cost and schedule item in development of a flight system. The same tests will provide data on the flow distribution leaving the valve, since this contributes to the header distribution problem.

Flashing-flow expansion through the vent valve pressure controller cannot be properly investigated with water/air alone. Flow distribution leaving the valve, and valve response characteristics, must be explored with two-phase saturated fluid inlet of varying quality while discharging into an ullage that simulates the vent side of the heat exchanger. Varying bleed orifices will be used on the ullage to simulate the 0.06 to 0.35 lb/sec vent rate range of the S-IVB. Preliminary tests will be run with Freon or LN₂, but LH₂ will be used for final testing.

13.3.3 Gravity-Dependence Tests. Above some critical flow velocity or Froude number, gravity effects become negligible in comparison with inertia effects, and ground tests at standard-g may be confidently used to predict zero-g heat transfer and flow distribution. Berenson (Reference 13-2) and Adelberg (Reference 8-32) agree in this matter, and suggest that ground tests with varying equipment orientation will verify gravity independence if results do not vary with orientation. Adelberg also derives a "boiling Grashof number" to predict when forced convection boiling will be gravity-independent, but its utility has not yet been established experimentally.

Although it is believed that the entire range of operation of the S-IVB system design is in the gravity-independent region, it should be verified. Also, determining the points where gravity dependence begins for each of the heat transfer regimes (boiling, condensing, single-phase) will be useful to future design work on other systems because it will define the lowest flow conditions that can be used and still rely fully on development testing under standard-g. Correlations between standard-g and zero-g heat transfer rates in the gravity-dependent region will be useful for those cases where the low flow rates must be used. Both of these goals can be achieved by an extension of the test programs previously outlined, using the same equipment.

The points of gravity-dependence will be established by running ground tests in different orientations (upflow, downflow, horizontal flow) and determining the flow velocity or Reynolds, Froude, or boiling Grashof number below which the results vary with orientation. Appropriate conditions will then be selected for reduced-g testing. A drop package will be prepared to provide such selected conditions and operated at the top of the drop facility until thermal equilibrium is established. The drop capsule will then be released, with the heat exchanger flow rates maintained, and appropriate temperatures recorded, including the temperature of the heat exchanger structure.

Any change in heat transfer rate would be reflected almost immediately as a dT/dt of the structure, and the heat rate change can be computed from the temperature rate. The sensitivity of available thermistors and germanium thermometers is very high in the LH₂ region; Radiation Research, for instance, lists a CG-3 having 325-ohm resistance at 18°K, 55-ohm at 23°K. This allows small temperature changes to be measured to 0.01 F° or better.

The results of the drop tests will then be compared with the ground test data. The expected results are qualitatively sketched in Figure 13-5. It is to be expected, but

should be verified, that drop test data would agree with ground test data at high velocities, that an averaging process would be useful at intermediate velocities, but that actual reduced-g tests are needed to assess the situation at low velocities. The delineation of these regimes is important. It should be supported by other analyses, which would draw heavily on existing heat transfer data.

Additional drop-test requirements are discussed in Paragraph 13.4.1, Item d-2.

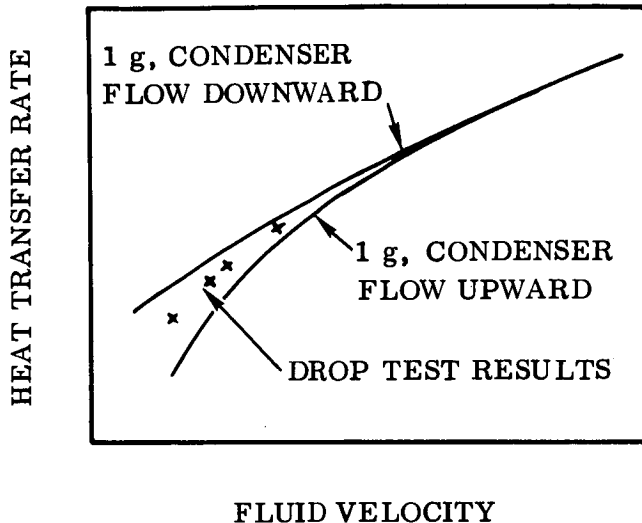


Figure 13-5. Expected Typical Gravity Dependence

13.3.4 Analog Computer Simulation of System.

An analog computer simulation of the selected heat exchange system offers a rapid, economical means of exploring a wide range of system con-

figurations and sizes, transient behavior, different working fluids and operating conditions, and system optimization for any duty cycle. It would be a valuable tool for deriving a maximum of information from a moderate amount of testing. It cannot substitute entirely for system tests, however, because the validity of the simulation must be checked and improved by comparison with test results.

The transient response of the heat exchanger system to sudden changes in flow rate and/or inlet fluid quality is an important consideration. For sudden increases in liquid flow at the heat exchanger vent-side inlet there exists the possibility of a loss of liquid, since the heat exchanger is dependent upon the turbine-driven pump for circulation on the tank side, and the turbine dependent, in turn, upon the vent-side vapor flow; i.e., there might be a troublesome "thermal time lag" between the onset of increased liquid flow at the vent inlet and the speeding up of the turbine to provide enough heat transfer to vaporize it. If liquid flow does occur at the turbine there is also the possibility that the turbine-pump would not "bootstrap" to full speed, and a significant amount of liquid could be lost.

Initial analysis of the present predesign, which has a common inlet for the vent and pump streams, indicates that the heat sink available from the heat exchanger is sufficient to allow start-up of the system without loss of liquid. The analysis, however, is quite sensitive to changes in system design variables such as heat exchanger material,

size, mass and pressure; turbine/pump performance and inertia; and the transient performance of upstream and downstream pressure regulating valves.

It is recommended that further analysis be performed on the transient behavior of the heat exchange type vent system over the full range of potential operating conditions to determine design requirements, potential problem areas, and operational limitations. Due to the complexity of the problem, a computer program should be developed. The use of analog simulation techniques has been investigated and appears suitable for the proposed analysis. Parametric data on the system response to the various operating perturbations will be generated over the same range of design combinations investigated for steady-state conditions. In particular, transient performance will be determined for sudden changes in vent fluid flow rate and quality and/or pump inlet quality. Also, the variation in propellant tank pressure during coast will be determined for the various design combinations.

As additional data on component and system performance are obtained during the test program, the computer simulation will be progressively checked and improved.

13.4 TANK MIXING TESTS. Most of the required tests in this area are already funded and scheduled. This paragraph is included in the recommended test program for the sake of completeness. It points out the data that are needed, the currently scheduled tests that will provide it, and the additional tests or analyses that should be performed. The reasons why mixing data are important can be understood by considering the operation of the system.

The selected system concept can function a) by cooling and circulating the liquid propellant sufficiently to absorb heat transfer through the tank walls before it vaporizes any propellant, b) by condensing vapor, either in the heat exchanger or by contact with subcooled liquid, at a rate equal to the rate of vapor formation at tank walls, or c) by a combination of these mechanisms. In any case, circulation of tank contents is required to take cold liquid to the tank wall or bring vapor into contact with cold liquid or into the heat exchanger. Excessive circulation is undesirable, though, because it represents an energy input to the propellant and increases venting requirements. It can also increase heat transfer from the tank wall, particularly when propulsive venting is employed to keep propellants partially settled. In that case the forward tank bulkhead is insulated by a "warm" vapor layer and heat transfer though it is reduced. Excessive circulation of tank contents could keep this bulkhead wetted, with a vent penalty possibly as high as 1000 pounds in a 4-1/2-hour-S-IVB coast. Inadequate circulation is also undesirable. It would be a serious problem if the heat exchanger were denied access to the hot vapor, and would lead to higher-than-necessary vent rates if a significant amount of liquid, subcooled from the heat exchanger, remained isolated and subcooled. Subcooled liquid serves no beneficial purpose except in absorbing heat by condensing vapor or cooling the tank wall.

13.4.1 Low-g Mixing Tests. Mixing and circulation data are required in the following areas for the low-acceleration level that exists during continuous thrust venting of the S-IVB.

- a. Mixing and temperature uniformity in the liquid resulting from natural convection and rising vapor bubbles.
- b. Mixing versus power input for forced circulation of the liquid, to determine whether forced convection would show net benefit.
- c. Mixing and temperature uniformity of the ullage gas resulting from natural convection and propellant sloshing, with particular interest in the temperature and heat flux at the forward dome.
- d. Effect of heat exchanger discharge on mixing of the ullage gas, heat flux at the forward dome, and stability of the propellant liquid/vapor interface.

The two currently planned test programs that will furnish much of the required information are the Saturn 203 experiment as described in Reference 1-1, and the mixer analysis and tests specified in NASA LeRC RFP 202193. The Saturn test will answer Items a. and c. above, and the LeRC study and test contract should provide the data to calculate the answer to Item b. Item d. will not need to be answered if the Saturn experiment shows an unstable interface or high heat flux for the present Saturn configuration, because the prime concern in Item d. is that the heat exchanger discharge might increase the heat flux through the forward dome. If Item-d. tests do prove to be required, the following two types are recommended.

- d-1 Ullage gas circulation induced by the heat exchanger discharge in the tank, and the resulting increase in heat transfer through the forward dome, could be investigated by ground tests with existing S-IVB "battleship" tanks. Besides measuring actual changes in heat transfer, flow velocity versus distance from the wall should be determined at several locations on the dome for various simulated heat exchanger discharge rates and outlet baffling. Injection of a tracer gas would also be useful in determining diffusion and mixing rates.
- d-2 The effect of heat exchanger discharge on interface stability under low-g conditions should be explored with a drop test program. Small tanks partly filled with liquid would have various simulated heat exchanger discharges directed at the interface during drop tests. Discharge configurations must be comparable with those used in a. above because it is likely that the final selection will require a compromise between interface effects and ullage circulation effects.

13.4.2 Zero-g Mixing Tests. These tests are not required for the S-IVB system, but will be needed for other possible applications such as the Cryogenic Service Module or the Kick Stage. Under conditions of true zero-g, there are no buoyant forces to bring the vapor to an ullage space where the heat exchanger is located. The heat ex-

change system does not necessarily have to "find" the vapor, of course, since it can perform its function equally well by circulating subcooled liquid to the vapor, or to the tank wall to prevent vapor formation. The main point is that circulation is required, and it must be forced because buoyant forces and natural convection do not exist. It should be possible to provide the required circulation and mixing in the tank with the same pump that is used to circulate tank contents through the heat exchanger. Mixing data are required to permit design and location of heat exchanger inlets and outlets that will provide adequate circulation with minimum energy input. Tasks III and IV of the NASA/LeRC study are expected to furnish the required data.

13.5 DEVELOPMENT AND PERFORMANCE TESTS. These tests are required as the end goal of the test program for the assumptions used, i.e., development of a flight system for the S-IVB. Working with the system design of Section 11, final development work on flow distribution is required as indicated in the discussion above regarding Part II-b. The workability of the complete system, and its performance over the full range of S-IVB operating conditions, must be established by ground tests. Flight test will then be required as final proof of performance. The details and extent of the ground test program preparing for flight test will depend on whether NASA chooses to develop the system into a qualified operational unit or only into an experimental unit that will not seriously jeopardize the primary mission.

13.5.1 Subsystem Performance Tests. These tests will be particularly addressed to the performance of the pump and the header between the pump and the condenser. They will be run with water/air mixtures for first-look testing, but the definitive results will have to be obtained with hydrogen.

The test of the pump and condenser header will be set up as shown in Figure 13-6. The pump will be run through a range of speeds and flow rates with inlet quality varied from 0 to 100 percent. Low-quality mixtures will be provided by GH_2 addition to LH_2 , and high-quality mixtures by an LH_2 shower in GH_2 . Pump torque, speed, flow rate, and pressure rise will be measured, and the header mix distribution will be inferred from the impact probe exploration.

The measurement methods require some special consideration. Pump flow will be determined from the recording of the lower chamber ullage pressure transducer output. The quick shutoff valve will be closed abruptly during the run, and the initial ullage pressure rise rate will be used as a measure of the pump flow. The LH_2 level in the upper chamber will be maintained either low or high during the run so that the recirculated flow entering the pump will be clear gas or liquid with the mixture quality established and measured by the rate of addition of LH_2 (rain) or GH_2 (bubbles).

More than one configuration of the pump header will have been created and will be tested in order to select the best. Alternate internal arrangements of baffles, liquid guide channels, etc will be available. As in the exploratory testing of the boiler header,

the fluid velocities and accelerations in the pump and condenser header will be so high that gravity should have little effect on the flow. The tests will be extended if necessary to include this high-Froude-number operation. As verification, the test of Figure 13-6 will be rearranged to provide upward flow through the pump, and the "up" and "down" results will be compared.

13.5.2 Overall Performance Test. The assembled vent separator will be mounted inside and on the end of an insulated tank venting through the separator to an air ejector that in turn compresses and delivers the vent gas to a vent stack. The vent pipe and turbine inlet will be fitted with optical liquid detectors. Temperatures, tank and vent pressures, turbine rpm, etc will be instrumented, and a pipe or pipes will be led to near the pump inlet to supply gas there when the inlet is covered with cryogenic liquid. It is expected that LN_2 will be suitable for most testing, but LH_2 can be handled by the Convair "Ramp" facility using about 1 pound per second of 600-psi air for the ejector. Over 20 pounds per second are available.

The system will be operated to demonstrate that it can control the tank pressure without liquid (high energy) loss when in the presence of liquid. The tank/separator assembly will be mounted on a swivel so that the vent flow can be up, down, horizontal, or in between. Tank feed and facility vent will be provided so that the liquid in the tank can be maintained at any desired level, and the tank will be equipped with several liquid level detectors, e. g. , heated thermistors, germanium elements, or fine wires. It should be recognized that low liquid levels and top venting favor the separator, and that bottom venting and high levels can penalize it severely. Further analysis is needed to establish the level of conservatism required to demonstrate that the separator will work in orbit. It is suggested that the final proof can be provided only by orbital testing.

13.5.3 Environmental Development Tests. It is recommended that vibration tests be conducted on prototype hardware before attempting flight tests. Critical components include particularly those with moving parts, such as the vent valve, pump, and turbine. The vent valve, however, is almost identical to the valve that has been qualified for Centaur application and can, therefore, be applied here with a generally high level of confidence. The pump and turbine will be new. The wide temperature range to which the pump/turbine unit will be exposed has a definite effect on fits and clearances of fixed and moving parts, and the response of an assembly to vibration is often appreciably affected by such dimensional changes. The pump/turbine, therefore, after the functional test will be subjected to vibration at levels up to about 20 percent over the design specification along the longitudinal and one transverse axis at ambient, LN_2 , and LH_2 temperatures.

It is not felt necessary that any other presently planned component of the vent separator system be vibrated in the development testing. The total assembly, including its mounting and bracing legs, will be vibrated in three axes throughout the design specification range with special attention to the frequencies and patterns of resonance. Very small design changes can in many cases cure serious resonance problems.

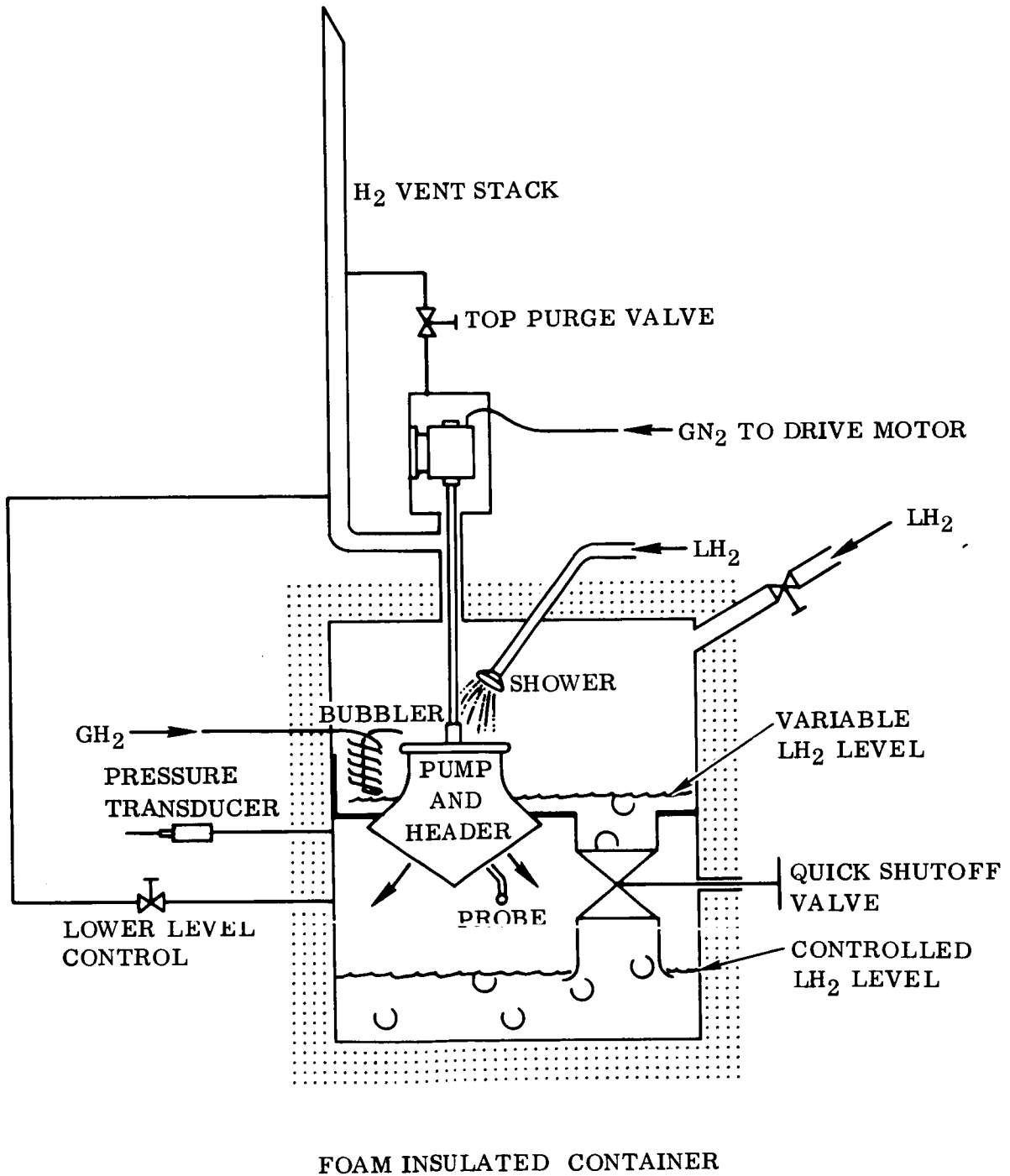


Figure 13-6. Pump and Header Test

13.6 TEST SEQUENCE AND INTEGRATION

13.6.1 Test Sequence. The various parts of the recommended test program are sufficiently independent to permit considerable flexibility in sequence. The main exception is Part IV, which should be delayed until after the completion of at least Parts I and II unless an urgent need for flight hardware arises to justify proceeding on a risk basis. Parts I, II, and III, however, can be accomplished in parallel or in almost any sequence. Although the concept feasibility demonstration of Part I would appear to be a necessary precondition to the rest of the test program, it actually will not be inefficient to conduct much of the program in parallel. The heat transfer and fluid flow studies of Part II, at standard and reduced gravity, are needed research with other possible applications and would be worthy of funding regardless of the progress of the heat exchanger separator system. Much of the required tank mixing data of Part III will be obtained from tests that are already programmed for other reasons. Initial work on developing an analog computer simulation could proceed before completion of the concept feasibility demonstration, and might even prove a useful diagnostic aid if problems were encountered with the test.

13.6.2 Test Integration. Two levels and types of test integration are required. The first is the overall planning and direction of the various parts of the test program, with appropriate revision as indicated by test results or changing vehicle requirements. At a lower level, integration of several items in the Part III tests would be efficient. Heat transfer, valve performance, and flow distribution, plus zero-g tests of each, involve such closely related components and operating conditions that they should be performed as a combined program. Development of computer simulation of the system is a logical focal point for all further analytical tasks in interpretation of test program data and the application of these data to any final system changes or optimization. The overall test program direction might also be combined with this analytical task to provide the program management with direct access to required information and insight.

13.6.3 Recommendations If S-IVB System Is Not Required. If a requirement for a heat exchange vent system for S-IVB fails to materialize, the S-IVB oriented tests of Paragraphs 13.3.2, 13.4.1, and 13.5 should be deleted. The concept feasibility demonstration of Paragraph 13.2 should then be expanded in scope to include additional development and performance tests. Beginning with the simple tests outlined using Freon and a coiled tubing heat exchanger, the program could progress through LN₂, LH₂, and more sophisticated pump and compact heat exchanger designs. The smaller size of the equipment would make this test program relatively low-cost as compared to the S-IVB system development.

After feasibility demonstration and performance evaluation in ground tests, a flight test would be desirable as a final test of performance. It would not be necessary to incorporate the heat exchange system into a vehicle propellant tank. A special small

tank containing propellant and the heat exchange system, together instrumentation and telemetry, would constitute the test package. It would be similar to the ground system shown schematically in Figure 13-1 except that the electric heater could be deleted. No propulsion system would be used, the test merely continuing until all propellant had been vented. A short test could be made at low-cost as a "piggy-back" package on an Atlas/SLV launch, but longer duration orbital testing would be preferable.

SECTION 14

CONCLUSIONS AND RECOMMENDATIONS

It was concluded that the heat exchange venting system is the most promising one for the three typical vehicle/mission cases considered in this study. The mechanical separator was a close second on most of the selection criteria except performance in 100-percent liquid. The dielectrophoretic and surface tension systems were consistently poorer than either the heat exchange or mechanical separator systems on all of the selection criteria. The vortex tube concept, investigated late in the study and, consequently, in less detail than the four systems above, offers a possibility of a relatively simple system if several unknowns, including the control problem, could be satisfactorily and simply solved by an experimental program. The relative ranking of the separator systems might change if additional requirements, such as liquid positioning for engine restart, were imposed in addition to the venting requirement.

It is recommended that the workability and performance of the selected heat exchange system concept be experimentally established at the earliest possible date. Although this study has disclosed no reasons to doubt that a successful heat exchange venting system can be developed, final proof must always be provided experimentally. Recognizing that the complete test program of Section 13 may represent a larger task than can be funded at the present time, a sub-scale "bread-board" unit feasibility demonstration is suggested as the first-priority task. Such a test is described and illustrated in Paragraph 13.2. It would provide data on steady-state and transient performance of this system concept, and verify that no serious control problems are inherent in the self-powered, dual pressure regulator configuration.

SECTION 15

REFERENCES

- 1-1 Swalley, Platt, and Hastings, Saturn V Low Gravity Fluid Mechanics Problems and Their Investigation by Full Scale Orbital Experiment, Preprint of Paper for Presentation at 1965 Low G Symposium, 24 June 1965.
- 2-1 Salvinski, R. J. , Friedlander, D.I., et al, Advanced Valve Technology for Spacecraft Engines, Report 8651-6033-SC000, Vol II, TRW Space Technology Laboratories Contract NAS 7-107, 19 July 1964.
- 2-2 Kloepfer, W. W., Liquid Hydrogen Heat Exchanger, General Dynamics Convair Report 55D-388, August 1960.
- 2-3 Roos, G. E., et al, Electrothermal Engine Propellant Storage and Feed System Study, Phase II, Beech Aircraft Corp., NASA Report CR-52, May 1964.
- 2-4 Fleming, W. T., et al, Liquid Hydrogen Storage Vessel Relief System for Zero Gravity Operation, AiResearch Manufacturing Co. Report M-754-R, 26 July 1960.
- 2-5 Stark, J. A., and Casebolt, R. W., Zero-G Vent Program, General Dynamics Convair Report GD/C-ERR-AN-811, December 1965.
- 2-6 Kays, W. M., and London, A. L., Compact Heat Exchangers, McGraw Hill, New York, 1964.
- 2-7 Rohsenow, W. M., "Heat Transfer With Evaporation," Heat Transfer Symposium Series, University of Michigan Press, pp 101-149, 1953.
- 2-8 O'Hanlon, T. W., Perkins, C. K., Wood, G. B., and Campbell, R. S., Zero-G Report, LH₂ Nucleate Boiling, General Dynamics Convair Report 55D859-1, February 1962.
- 2-9 Stepanoff, A. J., Centrifugal and Axial Flow Pumps, Wiley and Sons, 1957.
- 3-1 Vick, J. H., Evaluation of GD/A Separator, General Dynamics Convair Report 55A-881, August 1962.
- 3-2 Vick, J. H., Design Proof Test Report for the Centaur Zero-G Vent System, General Dynamics Convair GDA Report 55A1265R, 22 June 1962.

- 3-3 Vick, J. H., Individual Acceptance Test Report for the Centaur Zero-G Vent System, General Dynamics Convair GDA Report R FR-94812, 16 May 1962.
- 3-4 Walker, E., Individual Acceptance Test Report for Zero-G Separator Assembly, General Dynamics Convair Report 91509, 19 June 1962.
- 3-5 Schumann, P. O., Stratman, A. F., and Broadbent, S., Report of Design and Development of Separator Zero-G, Janitrol Part No. 93C30, May 1962.
- 3-6 Schumann, P. O., Report of Design Proof Tests on Liquid Hydrogen Separator Zero-G, Janitrol Part No. 93C30, Report 586, December 1961.
- 4-1 Pohl, H. A., "Some Effects of Nonuniform Fields on Dielectrics," Journal of Applied Physics, Vol 29, No. 8, pp 1182-1188, August 1958.
- 4-2 Pohl, H. A., Journal of Applied Physics, Vol 22, pp 869-871, 1951.
- 4-3 Blackmon, J. B., Zero Gravity Liquid Propellant Control by Dielectrophoresis, GMFSC Proceedings of the Conference on Propellant Tank Pressurization and Stratification, Vol II, 20-21 January 1965.
- 4-4 Blackmon, J., "Dielectrophoretic Propellant Orientation in Zero Gravity," Symposium on Ballistic Missile and Space Technology, N63-10381, 7 August 1962.
- 4-5 Blackmon, J. B., "Propellant Orientation in Zero Gravity With Electric Fields," S.M.F. Fund Paper FF-35, Proceedings of the Aerospace Forum II Session, New York, 21 January 1963.
- 4-6 Mitchell, R. C. & King, K. M., Comparison of Various Methods of Zero-G Propellant Control for a Centaur Type Vehicle, General Dynamics Convair Report GD/A ERR-AN-602, December 1964.
- 4-7 Reynolds, J. M., Electrohydrodynamic Propellant Management for Advanced Centaur, Dynatech Corporation PAS-250, 3 February 1965.
- 4-8 Reynolds, J. M., et al, Design Study of a Liquid Oxygen Converter for Use in Weightless Environments, 6570th Aerospace Medical Research Laboratories Report AMRL-TDR-63-42, June 1963.
- 4-9 Hurwitz, M., Fahimian, E. J., and Reynolds, J. M., Zero Gravity Control of Hydrogen and Cesium by Electrical Phenomena, APL-TDR-64-46, United States Air Force Contract AF 33(657)-10784, Aeropropulsion Laboratory, Wright-Patterson AFB, Ohio, April 1964.

- 4-10 Llewellyn-Jones, F., Ionization and Breakdown in Gases, p 99, John Wiley and Sons, Inc., New York.
- 4-11 Knowlton, A. E., Standard Handbook for Electrical Engineers, Ninth Edition, McGraw-Hill Book Co, Inc., New York 1957.
- 4-12 Lessin, I., Golden, D. E., and Fisher, L. M., "Transient Breakdown Studies of H₂ at Low Values of E/P," Physics Review, Vol 124, No. 4, p 994.
- 4-13 Mathes, K. N., "Electrical Insulation at Cryogenic Temperatures," Electro-Technology, p 77, September 1963.
- 4-14 Hurwitz, M., Dynatech Corporation, Personal Communication to V. Hudson, General Dynamics Convair, 16 July 1965.
- 5-1 Pennington, K., The Aerobee Zero-G Test Program -- A Summary of Results, General Dynamics Convair Report BTC 63-001, 22 April 1963.
- 5-2 Petrash, D. A., Effect of Surface Energy on Liquid Vapor Interface Configuration During Weightlessness, NASA TN D1582, January 1963.
- 5-3 Petrash, D. A., Nussle, R. C., and Otto, E. W., Effect of Contact Angle and Tank Geometry on the Configuration of the Liquid Vapor Interface During Weightlessness, NASA TN D-2075, October 1963.
- 5-4 Reynolds, W. C., Saad, M. A., and Satterlee, H. M., Capillary Hydrostatics and Hydrodynamics at Low g, Stanford University Technical Report LG-3, prepared under Grant NSF G-20090 for the National Science Foundation, September 1964.
- 5-5 Clodfelter, R. G., Fluid Mechanics and Tankage Design for Low Gravity Environments, AF Systems Command, WPAFB, ASD-TDR-63-506, AD-423554, June 1961 - April 1963.
- 5-6 Sherley, J. E., Merino, F., and Ballinger, J. C., The Final Report for the General Dynamics/Astronautics Zero-G Program Covering the Period from May 1960 through March 1962, Contract No. AF18(600)-1775 NASA 8-2664, General Dynamics Convair Report AY 62-0031, 15 August 1962.
- 5-7 Petrash, D. A., Nussle, R. C., and Otto, E. W., Effect of the Acceleration Disturbances Encountered in the MA-7 Spacecraft on the Liquid-Vapor Interface in a Baffled Tank During Weightlessness, NASA TN D-1577, January 1963.

- 5-8 Bell Aerosystems Co., Development of Expulsion and Orientation Systems for Advanced Liquid Rocket Propulsion Systems, EAFB SSD RRL Report SSD-TDR-62-172, Contract AF04(611)-8200, Phase I Progress Report, 1 June through 15 October 1962.
- 5-9 Bell Aerosystems Co., Development of Expulsion and Orientation Systems for Advanced Liquid Rocket Propulsion Systems, EAFB RPL Report RTD-TDR-63-1048, Contract AF04(611)-8200, Final Report, July 1963.
- 5-10 Bell Aerospace Co., Evaluation of Propellant Containment and Venting Devices for Zero Gravity Applications, EAFB RPL Report AFRPL-TR-65-118, Contract AF04(611)-9901, Final Report, June 1965.
- 5-11 Petrash, D. A., and Otto, E. W., "Controlling the Liquid-Vapor Interface Under Weightlessness," Astronautics and Aeronautics, pp 56-61, March 1964.
- 5-12 Petrash, D. A., Liquid Vapor Interface Configuration in Weightlessness, American Rocket Society Paper 2514-62, 1962.
- 5-13 Petrash, D., Experimental Study of the Effects of Weightlessness on the Configuration of Mercury and Alcohol in Spherical Tanks, NASA Report TN D1197, April 1962.
- 5-14 Masica, W. J., Petrash, D. A., and Otto, E. W., Hydrostatic Stability of the Liquid-Vapor Interface in a Gravitational Field, NASA (Lewis) TN D-2267, 1964.
- 5-15 Masica, W. J., Derdul, J. D., and Petrash, D. A., Hydrostatic Stability of the Liquid-Vapor Interface in a Low-Acceleration Field, NASA TN D-2444, August 1964.
- 5-16 Siegert, C. E., Petrash, D. A., and Otto, E. W., Time Response of Liquid-Vapor Interface After Entering Weightlessness, NASA TN D-2458, August 1964.
- 5-17 Siegert, C. E., Petrash, D. A., and Otto, E. W., Behavior of Liquid-Vapor Interface of Cryogenic Liquids During Weightlessness, NASA TN D-2658, February 1965.
- 5-18 Hall, C. N., "Subcritical Controlled-Ullage, Cryogenic Tankage Concept," Journal of Spacecraft, Vol 4, pp 370-373, July-August 1964.
- 5-19 Wallner, L. E., and Nakanishi, S., A Study of Liquid Hydrogen in Zero Gravity, NASA (Washington) TMX-723, August 1963.

- 5-20 Good, R. J., and Ferry, G. V., "The Wetting of Solids by Liquid Hydrogen," Advances in Cryogenic Engineering, Vol 8, p 307 Plenum Press, New York, 1963.
- 5-21 Li, Ta C. H., "Hydrostatics in Various Gravitational Fields," Journal of Chemistry and Physics, Vol 36, No. 9, pp 2369-75, 1 May 1962.
- 6-1 The Porous Plate Sublimator for Cooling Applications in Space, Hamilton Standard PDB 6315B, pp 1-2, 1 July 1964.
- 6-2 Sangiovanni, Joe, Hamilton-Standard, Personal Communication to R. C. Mitchell, Convair, 11 August 1965.
- 6-3 Michelson (Lt.), Saturn IB and V Instrument Unit Sublimator, George C. Marshall Space Flight Center Memorandum R-P&VE-PT-64-M-141, p 3, 10 June 1964.
- 6-4 Michaelis, L., Physical Methods of Organic Chemistry, Vol I, Part II, pp 1885-1926, (Edited by A. Weissberger), Interscience Publishers, New York, 1949.
- 8-1 Jakob, M., Heat Transfer, Vol 1, Wiley, New York 1949.
- 8-2 Gunther, F. C., and Kreith, F., "Photographic Study of Bubble Formation in Heat Transfer to Subcooled Water," Heat Transfer and Fluid Mechanics Institute, pp 113-138, ASME, 1949.
- 8-3 Rohsenow, W. M., and Clark, J. A., "A Study of the Mechanism of Boiling Heat Transfer," Transactions of the ASME, Vol 73, pp 609-620, 1951.
- 8-4 Rohsenow, W. M., "A Method of Correlating Heat Transfer Data for Surface Boiling Liquids," Transactions of the ASME, Vol 74, pp 969-976, 1952.
- 8-5 Kutateladze, S. S., Heat Transfer in Condensation and Boiling, Second Edition, State Scientific and Technical Publications of Literature on Machinery, Moscow, 1952.
- 8-6 Engelberg-Forster, K., and Greif, R., "Heat Transfer to a Boiling Liquid - Mechanism and Correlations," ASME Journal of Heat Transfer, Vol 81, pp 43-53, 1959.
- 8-7 Labountzov, D. A., "Generalized Correlation for Nucleate Boiling," Teploenergetika, Vol 7, No. 5, pp 76-80, 1960.

- 8-8 Bankoff, S. G., "A Note on Latent Heat Transport in Nucleate Boiling," A. I. Chemical E. Journal, Vol 8, pp 63-65, 1962.
- 8-9 Rallis, C. J., and Jawurek, H. H., "Latent Heat Transport in Saturated Nucleate Boiling," International Journal of Heat and Mass Transfer, Vol 7, pp 1051-1068, 1964.
- 8-10 Brentari, E. G., and Smith, R. V., "Nucleate and Film Pool Boiling Design Correlations for O_2 , N_2 , H_2 , and He ," International Advances in Cryogenic Engineering, Vol 10, pp 325-341, Plenum Press, New York, 1965.
- 8-11 Zuber, N., and Fried, E., "Two-Phase Flow and Boiling Heat Transfer to Cryogenic Liquids," ARS Journal, Vol 32, pp 1332-1341, September 1962.
- 8-12 Clark, H. B., Strenge, P. H., and Westwater, J. W., "Active Sites for Nucleate Boiling," Chemical Engineering Progress Symposium Series, Vol 55, No. 29, pp 103-110, 1959.
- 8-13 Corty, C., and Foust, A. S., "Surface Variables in Nucleate Boiling," Chemical Engineering Symposium Series, Vol 51, No. 17, pp 1-12, 1955.
- 8-14 Griffith, P., and Wallis, J. D., "The Role of Surface Conditions in Nucleate Boiling," Chemical Engineering Progress Symposium Series, Vol 56, No. 30, pp 49-63, 1960.
- 8-15 Westwater, J. W., "Things We Don't Know About Boiling Heat Transfer," Theory and Fundamental Research in Heat Transfer, pp 61-73, MacMillan, New York, 1963.
- 8-16 Bergles, A. E., and Rohsenow, W. M., "The Determination of Forced-Convection Surface-Boiling Heat Transfer," ASME Journal of Heat Transfer, Vol 86, pp 365-372, 1964.
- 8-17 Walters, H. H., "Single-Tube Heat Transfer Tests with Liquid Hydrogen," Advances in Cryogenic Engineering, Vol 6, pp 509-516, Plenum Press, New York, 1961.
- 8-18 Schrock, V. E., and Grossman, L. M., "Forced Convection Boiling in Tubes," Nuclear Science and Engineering, Vol 12, pp 474-481, 1962.
- 8-19 Leonhard, K. E., and McMordie, R. K., "The Non-Adiabatic Flow of an Evaporating Cryogenic Fluid through a Horizontal Tube," Advances in Cryogenic Engineering, Vol 6, pp 481-498, Plenum Press, New York, 1961.

- 8-20 Kutateladze, S. S., "Critical Heat Flux to Flowing, Wetting Subcooled Liquids," Energetika, No. 2, pp 229-239, 1959.
- 8-21 Mc Adams, W. H., Heat Transmission, McGraw-Hill, New York, 1954.
- 8-22 Altman, M., Norris, R. H., and Staub, F. W., "Local and Average Heat Transfer and Pressure Drop for Refrigerants Evaporating in Horizontal Tubes," ASME Journal of Heat Transfer, Vol 82, pp 189-198, 1960.
- 8-23 Von Glahn, U. H., and Lewis, J. P., "Nucleate- and Film-Boiling Studies With Liquid Hydrogen," Advances in Cryogenic Engineering, Vol 5, Plenum Press, New York, 1960.
- 8-24 Tippetts, F. E., ASME Paper 62-WA-161.
- 8-25 Leppert, G., and Pitts, C. C., "Boiling", Advances in Heat Transfer, Vol 1, pp 185-267, Academic Press, New York, 1964.
- 8-26 Drayer, D. E., and Timmerhaus, K. D., "An Experimental Investigation of the Individual Boiling and Condensing Heat Transfer Coefficients for Hydrogen," Advances in Cryogenic Engineering, Vol 7, pp 401-412, Plenum Press, 1962.
- 8-27 Rohsenow, W. M., Webber, J. H., and Ling, A. T., "Effect of Vapor Velocity on Laminar and Turbulent-Film Condensation," Transactions of the ASME, Vol 78, pp 1637-1643, 1956.
- 8-28 Altman, M., Staub, F. W., and Norris, R. H., "Local Heat Transfer and Pressure Drop for Refrigerant-22 Condensing in Horizontal Tubes," Chemical Engineering Progress Symposium Series, Vol 56, No. 30, pp 151-160, 1960.
- 8-29 Akers, W. W., Deans, H. A., and Crosser, O. K., "Condensing Heat Transfer Within Horizontal Tubes," Chemical Engineering Progress Symposium Series, Vol 55, No. 29, pp 171-176, 1959.
- 8-30 Akers, W. W., and Rosson, H. F., "Condensation Inside a Horizontal Tube," Chemical Engineering Progress Symposium Series, Vol 56, No. 30, pp 145-150, 1960.
- 8-31 Kays, W. M., and London, A. L., Compact Heat Exchangers, McGraw-Hill, New York, 1964.
- 8-32 Adelberg, M., and Jetter, R., "Effect of Gravity Upon Nucleate Boiling," Advances in the Astronautical Sciences, Vol 14, 1963.

- 8-33 Martinelli, R. C. , and Nelson, D. B. , "Prediction of Pressure Drop During Forced-Circulation Boiling of Water," Transactions of the ASME, August 1948.
- 9-1 Mullins, J. C. , Ziegler, W. T. , and Kirk, B. S. , The Thermodynamic Properties of Parahydrogen from 1° to 22° K, NBS Contract CST-7339, Technical Report 1, Project A-593, Georgia Institute of Technology, 1 November 1961.
- 9-2 Shaffer, A. , and Rousseau, J. , Thermodynamic Properties of 20.4° K-Equilibrium Hydrogen, ASD Technical Report 61-360, October 1961.
- 10-1 Pressurized Cooldown of Cryogenic Transfer Lines, A. D. Little Co. , Inc. , Special Report 106, Cambridge, Massachusetts, October 1959.
- 10-2 Stephens, P. B. , Transient Heat and Mass Transfer Phenomena in an Open-Non-Adiabatic System Consisting of a Superheated Gas and a Cryogenic Liquid, General Dynamics Convair Report GDA63-0214, 1963. Original data from Properties of Some Metals and Alloys, Development and Research Division, The International Nickel Co, Inc. , New York, 1949.
- 10-3 Watson, J. F. , Properties of Engineering Materials at Extreme Subzero Temperatures with Supplementary Information on Liquid Hydrogen, General Dynamics Convair Report EMG-44, 8 December 1958.
- 12-1 Kays, W. M. and London, A. L. , Compact Heat Exchangers, Second Edition, McGraw-Hill, 1964.
- 12-2 Marquardt Corporation, Cycle Analyses for Partial Hydrogen and Partial Oxygen Reliquefiers, Monthly Progress Report 325-24 for the period ending 16 October 1965, Contract NAS 8-5298.
- 12-3 Middleton, R. , NASA/MSFC, P&VE, Personal Communication, 14 December 1965.
- 13-1 Baker, O. , "Simultaneous Flow of Oil and Gas," Oil and Gas Journal, Vol 53, pp 185-195, 26 July 1954.
- 13-2 Berenson, P. J. , "Fundamentals of Low Gravity Phenomena Relevant to Fluid System Design," Advances in the Astronautical Sciences, Vol 14, pp 116-129, 1963.

- A-1 Liquid Hydrogen Technology, General Dynamics Convair Report AE62-0774, September 1962.
- A-2 A Compendium of the Properties of Materials at Low Temperature (Phase 1), WADD Technical Report 60-56, July 1960.
- B-1 Hansen, A. J., "Accurate Valve Sizing for Flashing Liquids," Control Engineering, February 1961.
- B-2 Ziegler, J. G., "Sizing Valves for Flashing Fluids," ISA Journal, March 1957.
- B-3 Herson, J. C., and Peck, R. E. "Flow of Two-Phase Carbon Dioxide Through Orifices," A. I. Ch. E. Journal, Vol 4, No. 2, June 1958.
- B-4 McAdams, W. H., "Heat Transmission," Third Edition, pp 260-268, McGraw-Hill, 1954.
- C-1 Binder, R. C., Fluid Mechanics, Third Edition, pp 175-189, Prentice-Hall, 1955.
- C-2 DiStefano, J. F., and Shiozawa, S., The Design and Development of a Zero G Vapor Liquid Separator for Use in Cryogenic Fluid Power Systems, Pesco Products Division, Borg-Warner Corp, Report 650322.
- C-3 Stepanoff, A. J., Centrifugal and Axial Flow Pumps, Second Edition, John Wiley and Sons, Inc., 1957.
- C-4 Harper, J. W. "The Significance of WK^2 and How to Calculate It," Product Engineering, 27 June 1960.
- C-5 Redmond, J. H., and Bott, F. W., Development of Cryogenic Electric Motors, National Aeronautic and Space Engineering and Manufacturing Meeting Paper 753D, September 1963.
- C-6 Spotts, M. F., Design of Machine Elements, Second Edition, Prentice-Hall, 1955.
- C-7 Pradham, A. V., et al, Modified Zero Gravity Vapor/Liquid Separator Summary of a Short Study, Pesco Product Division, Borg-Warner Corp. Memorandum 139, 26 March 1965.
- C-8 Mooney, D. A., Mechanical Engineering Thermodynamics, Prentice-Hall, 1953.

- D-1 Martinelli, R. C., et al, "Isothermal Pressure Drop for Two-Phase Two Component Flow in a Horizontal Pipe," Transactions of the A. S. M. E., February 1944.
- D-2 Martinelli, R. C., Nelson, D. B., "Prediction of Pressure Drop During Forced Circulation Boiling of Water," Transactions of the A. S. M. E., August 1948.
- D-3 Hatch, M. R. and Jacobs, R. B., "Prediction of Pressure Drop in Two-Phase Single Component Fluid Flow," A.I.Ch.E. Journal, Vol 8, No. 1, March 1962.
- F-1 Stodola, Dr. A., Steam and Gas Turbines, Vol 1, Peter Smith, New York, 1945.

The following reference materials were reviewed during the study and many contained useful information; however, they were not specifically referenced in the test.

- 1 Adballa, K. L., Zero-g Performance of Ullage Control Surface With Liquid Hydrogen While Subjected to Unsymmetrical Radiant Heating, NASA (Lewis) TMX-1001, August 1964.
- 2 Adelberg, M., "Effect of Gravity Upon Nucleate Boiling" Advances in the Astronautical Sciences, Vol 14, pp 195-222, 1963.
- 3 Adelberg, M., and Schwartz, S. H., Heat Transfer Domains for Fluids in a Variable Gravity Field with Some Applications to Storage of Cryogenics in Space, Douglas Paper 3516, Cryogenic Engineering Conference, Rice University, 23-25 August, 1965.
- 4 Akers, W. W., Davis, S. H., Jr., and Crawford, J. E., "Condensation of a Vapor in the Presence of a Noncondensing Gas," Chemical Engineering Progress Symposium Series, Vol 56, No. 30, pp 145-150, 1960.
- 5 Allingham, W. D., "Investigation of Positive Displacement Cryogenic Fluid Expulsion Techniques," Boeing Co. Report N64-32877, Seattle, Washington, 1964.
- 6 Asch, V., "Predicting and Using Liquid-Boiling Behavior," Chemical Engineering, Vol 70, pp 125-128, 29 April 1963.
- 7 Aydelott, J. C., Cordas, E. L., and Gruber, R. P., Comparison of Pressure Rise in a Hydrogen Dewar for Homogeneous, Normal-Gravity Quiescent, and Zero-Gravity Conditions - Flight 7, NASA TMX-1006, September 1964.

- 8 Barcatta, F. A., Daley, H. L., Firestone, A. H., and Forrester, A. T., Zero G Propellant Feed Systems for Cesium Ion Rocket Engines, AIAA 63027, Electric Propulsion Conference, Colorado Springs, Colorado, 11-13 March 1963.
- 9 Benedikt, E. T., "General Behavior of a Liquid in a Zero or Near-Zero Gravity Environment," Weightlessness - Physical Phenomena and Biological Effects, pp3-32, Pelnum Press, New York, 1961.
- 10 Benedikt, E. T. "Scale of Separation Phenomena in Liquids Under Conditions of Nearly Free Fall," ARS Journal, pp150-151, February 1959.
- 11 Benedikt, E. T., Epihydrostatics of a Liquid in a Rectangular Tank With Vertical Walls, Northrop Corp., Norair Division Report ASL-TM-60-38, November 1960.
- 12 Benedikt, E. T., and Halliburton, R. W., "Physical and Biological Phenomena in a Weightless State," Advances in the Astronautical Sciences, Vol 14, Western Periodicals Co., 1963.
- 13 Berenson, P., "Fundamentals of Low Gravity Phenomena Relevant to Fluid System Design," Advances in the Astronautical Sciences, Vol 14, pp 116-129, Western Periodicals Co., 1963.
- 14 Berman, K. and Goerke, R. F., Study of Zero-G Positive Expulsion Techniques, Bell Interim Report 8230-933007, Contract NAS 7-149, April 1963.
- 15 Berman, K., Study of Zero Gravity Positive Expulsion Techniques, Bell Aerospace Corp. Report 8230-933007, June 1963.
- 16 Bitten, J. F., Liquid Oxygen Converter, Preprint for A. I. Chemical E. 55th Symposium of Effects of Zero Gravity on Fluid Dynamics and Heat Transfer - Part II, Houston, Texas, 7-11 February 1965 (A65-15224).
- 17 Blackmon, J., "Propellant Orientation in Zero Gravity With Electric Fields," Advances in the Astronautical Sciences, Vol 14, Western Periodicals Co., 1963.
- 18 Blackmon, J. B., "Collection of Liquid Propellants in Zero Gravity With Electric Fields," AIAA Paper 64-265, June 1964, Journal of Spacecraft, Vol 2, No. 3, pp 391-398, May-June 1965.

- 19 Blackshear, W. T., and Eide, D. G., The Equilibrium Free Surface of a Contained Liquid Under Low Gravity and Centrifugal Forces, Langley Research Center, NASA TN D-2471, October 1964.
- 20 Bonneville, J. M., and Fowle, A. A., Space Transport Capabilities of Chemically Fueled Propulsion Systems Using Storable and Cryogenic Propellants, Arthur D. Little, Inc. Report C-66178, Contract NAS W-876, June 1964.
- 21 Bosworth, R. C. L., Heat Transfer Phenomena, John Wiley and Sons, New York, 1952.
- 22 Boyles, R., "Careful Design Conserves Cryogenic Stored in Near Earth Orbit Till Rendezvous," SAE Journal, p 103, June 1963.
- 23 Brazinsky, I., Photographic Study of Liquid Hydrogen Under Simulated Zero Gravity Conditions, NASA TMX 479, February 1962.
- 24 Bronson, J. C., Edeskuty, Fretwell, J. H., Hammel, E. F., Keller, W. E., Meier, K. L., Schuch, A. F. and Willis, W. L., "Problems in Cool-Down of Cryogenic Systems," Advances in Cryogenic Engineering, Vol 7, pp 198-205, Plenum Press, New York, 1962.
- 25 Carpenter, E. F., and Colburn, A. P., "The Effect of Vapor Velocity on Condensation Inside Tubes," Proceedings of the General Discussion on Heat Transfer, pp 20-26, Institution of Mechanical Engineers, London, 1951.
- 26 Chang, Y. P., and Snyder, N. W., "Heat Transfer in Saturated Boiling," Chemical Engineering Symposium Series, Vol 56, No. 30, 1960.
- 27 Chang, Y., "Some Possible Critical Conditions in Nucleate Boiling," ASME Journal of Heat Transfer, Vol 85, pp 89-100, 1963.
- 28 Chi, J. W. H., and Vetere, A. M., Two-Phase Flow During Transient Boiling of Hydrogen and Determination of Non-Equilibrium Vapor Fractions, Westinghouse Astronuclear Report WANL-SP-002, June 1963.
- 29 Chilton, T. H., and Colburn, A. P., "Mass Transfer (Absorbtion) Coefficients," Industrial and Engineering Chemistry, Vol 26, pp 1183-1187, 1934.
- 30 Clark, J., "Nucleate, Transition and Film Boiling Heat Transfer at Zero Gravity," Advances in the Astronautical Sciences, Vol 14, pp 177-195, Western Periodical Co., 1963.

- 31 Clark, J. A., A Review of Pressurization, Stratification and Interfacial Phenomena, Michigan University Report N65-11006, Ann Arbor, Presented at the Cryogenic Engineering Conference, Philadelphia, 1964.
- 32 Clodfelter, R. G., Low-Gravity Pool-Boiling Heat Transfer, Technical Report APL-TDR-64-19, Wright-Patterson AFB, AF Aero Propulsion Laboratory, March 1964.
- 33 Clodfelter, R. G. and Lewis, R. C., Fluid Studies in a Zero Gravity Environment, Aeronautical Systems Division Report TN 61-48, June 1961.
- 34 Colaprete, S. J., "Preliminary Investigation for a Zero-Gravity Water Separator," North American Aviation Inc. Report N64-19303, Los Angeles, California, 23 September 1963.
- 35 Colburn, A. P., "Problems in Design and Research on Condensers of Vapours and Vapour Mixtures," Proceedings of the General Discussion on Heat Transfer, pp 1-11, Institution of Mechanical Engineers, London, 1951.
- 36 Concus, P., "Capillary Stability in an Inverted Rectangular Tank," Advances in the Astronautical Sciences, Vol 14, pp21-37, Western Periodicals Co., 1963.
- 37 Congelli, J., "The Zero G Flow Loop: Steady Flow, Zero Gravity Simulated for Investigation of Two Phase Phenomena," Advances in the Astronautical Sciences, Vol 14, pp 223-263, Western Periodicals Co., 1963.
- 38 Costello, C. P., and Adams, J. M., "Burnout Heat Fluxes in Pool Boiling at High Accelerations," International Developments in Heat Transfer, International Heat Transfer Conference, Boulder, Colorado and London, 1961-62, published by the A. S. M. E.
- 39 Creswick, F. A., Talbert, S. G., and Bloemer, J. W., Compact Heat Exchanger Study, Battelle Memorial Institute Report AD-446233, June 1964.
- 40 Davies, J. T., and Rideal, E. K., Inter-Facial Phenomena, Academic Press, 1961.
- 41 DiMaggio, O., "Equilibrium Configuration of the Liquid Vapor Interface in a Rotating Container Under Zero G Conditions," Advances in the Astronautical Sciences, Vol 14, pp 38-48, Western Periodicals Co., 1963.

- 42 Elizaide, J. C., Orbital Tests to Investigate Thermal Behavior of Cryogens Under Weightlessness, TRW Space Technology Laboratory, November 1964.
- 43 Evans, R., "Gas Laws Help Find Propellant Mass at Zero G," Space Aeronautics, pp 115, 117, June 1963.
- 44 Fiet, O. O., et al, Advanced Valve Technology for Spacecraft Engines, TWR Space Technology Laboratories Report 8651-6032-SU000, Vol I, Contract NAS 7-107, 19 July 1964.
- 45 Fineblum, S. S., The Behavior of Liquids Under Conditions of Zero and Near-Zero Gravity, North American Aviation Inc. Report AETN 62-1, Columbus, Ohio, 6 June 1962.
- 46 Garriott, R., and Burns, G. A., "Zero G Propellant Gauging Utilizing Radio Frequency Techniques in a Spherical Resonator," IEEE Transactions on Aerospace, pp 22-29, 1965.
- 47 Gebhart, B., "Random Convection Under Conditions of Weightlessness," AIAA Journal, pp 380-383, February 1963.
- 48 Ginwala, K., Engineering Study of Vapor Cycle Cooling Equipment for Zero-Gravity Environment, WADD Technical Report 60-776, January 1961.
- 49 Gluck, D. F., and Gille, J. P., Fluid Mechanics of Zero G Propellant Transfer in Spacecraft Propulsion Systems, SAE and ASME Air Transport and Space Meeting Paper 862A, New York, April 1964.
- 50 Graham, R. W., Analytical and Experimental Study of Pool Heating of Liquid Hydrogen Over a Range of Accelerations, NASA-TN D-1883, p 51, February 1965.
- 51 Graham, R. W., Hendricks, R. C., and Ehlers, R. C., "An Experimental Study of the Pool Heating of Liquid Hydrogen in the Subcritical and Supercritical Pressure Regimes Over a Range of Accelerations," International Advances in Cryogenic Engineering, Vol 10, pp 342-352, Plenum Press, New York, 1965.
- 52 Graham, W. T., Liquid Hydrogen Stratification Test, General Dynamics Convair Report 55A2787-1, 9 October 1963.
- 53 Gunther, F. C., "Boiling Heat Transfer to Water with Forced Convection," Transactions of the ASME, Vol 73, 1951.

- 54 Halsey, G. , "Physical Adsorption on Non-Uniform Surfaces," Journal of Applied Physics, Vol 16, No. 10, pp 931-937, October 1948.
- 55 Hansen, J. , Convair Astronautics Zero-G Report, Liquid Behavior Scaling, General Dynamics Convair Report 55D859-8, 7 May 1962.
- 56 Harper, E. Y., Hurd, S. E., Levey, A. M., and Tellep, D. M. , "Analytical and Experimental Study of Stratification in Standard and Reduced Gravity Fields," Lockheed Missiles and Space Company, Published in Proceedings of the Conference on Propellant Tank Pressurization and Stratification, Vol II, G. C. Marshall Space Flight Center, 20-21 January 1965.
- 57 Hartkopf, S. E. , Zero Gravity Tests of X-15 Nitrogen Tank, AFF TC TN 60-34, USAF Flight Test Center, Edwards AFB, January 1961.
- 58 Hatch, M. R., and Jacobs, R. B. , "Prediction of Pressure Drop in Two-Phase Single-Component Fluid Flow," A. I. Chemical E. Journal, Vol 8, pp 18-25, March 1962.
- 59 Heald, D. A., and Holland, K. D. , Centaur Hydrogen Tank Venting Experience, AIAA and NASA Flight Test Conference Paper 65-216, Huntsville, Alabama, 15-17 February 1965.
- 60 Hedgepeth, L. , Zero-Gravity Boiling and Condensing, Preprint 1322-60, American Rocket Society.
- 61 Hedgepeth, L. M., and Zara, E. A. , "Zero Gravity Pool Boiling," ASD-TDR-63-706, ASD Science and Engineering Symposium, Wright-Patterson AFB, Ohio, 1963.
- 62 Hilding, W. E. , and Coogan, C. H. Jr. , Heat Transfer Studies of Vapor Condensing at High Velocities in Small Straight Tubes, University of Connecticut Report NASA-CR-124, October 1964.
- 63 Hurwitz, M. , Reynolds, J. M. , Mela, R. L. , and Welsh, W. W. , Research Program for Dielectrophoretic Oxygen Converter, Proposal PAS-164A to Office of Research Grants and Contracts, NASA, 12 May 1964.
- 64 Jahsman, W. E. , "The Equilibrium Shape of the Surface of a Fluid in a Cylindrical Tank," Developments in Mechanics, Vol 1, pp 603-612, Plenum Press, 1961.

- 65 Jetter, R. "Orientation of Fluid Surfaces in Zero Gravity Through Surface Tension Effects," Advances in the Astronautical Sciences, Vol 14, pp 60-70, Western Periodicals Co., 1963.
- 66 Keshock, E. G., and Siegel, R., Forces Acting on Bubbles in Nucleate Boiling Under Normal and Reduced Gravity Conditions, NASA (Lewis) TN D-2299, August 1964.
- 67 King, K. M., Analysis of Advanced Pressurization and Propellant Feed System Concepts, General Dynamics Convair Report ERR-AN-455, 31 December 1963.
- 68 Kirk, D. A., Means of Creating Simulated Varite Fields for the Study of Free Connective Heat Transfer, X63 14517.
- 69 Knoll, L. R., et al, Weightlessness Experiments With Liquid Hydrogen in Aerobee, NASA TM X484, June 1962.
- 70 Kremzier, E. J., and Tatro, R. E., A Status Review of Zero and Low Gravity Work Within General Dynamics/Astronautics, General Dynamics Convair Report 528-1-224, 16 June 1964.
- 71 Kutateladze, S. S., "Boiling Heat Transfer," International Journal of Heat and Mass Transfer, Vol 4, pp 31-45, 1961.
- 72 Leinhard, J. H., and Schrock, V. E., "The Effect of Pressure, Geometry, and the Equation of State Upon the Peak and Minimum Boiling Heat Flux," ASME Journal of Heat Transfer, Vol 85, pp 261-272, 1963.
- 73 Lenfestey, A. G., "Low Temperature Heat Exchangers," Progress in Cryogenics, Vol 3, Academic Press, New York, 1961.
- 74 Levy, S., "Generalized Correlation of Boiling Heat Transfer," ASME Journal of Heat Transfer, Vol 81, pp 37-24, 1959.
- 75 Li, Ta C. H., Convection in a Liquid Contained in an Axisymmetric Tank With Prescribed Heat Input and Gravity, General Dynamics Convair Report ERR-AN-149, 8 March 1962.
- 76 Li, Ta C. H., Liquid Behavior in a Zero-G Field, General Dynamics Convair AE60-0682, September 1960.
- 77 Li, Ta C. H., Cryogenic Liquids in the Absence of Gravity, General Dynamics Convair Paper Presented at the Cryogenic Engineering Conference, University of Michigan, 15 August 1961.

- 78 Li, Ta C. H., Preliminary Studies of Liquid Behavior in a Low-G Field, General Dynamics Convair Report ERR-AN-036, March 1961.
- 79 Loftus, Lt. J. P., and Hammer, Lois R., Weightlessness and Performance - A Review of the Literature, Aerospace Medical Laboratory, Aeronautical Systems Division, Wright-Patterson Air Force Base, Ohio, ASD TR 61-166, June 1961, 39 pp including 125 references.
- 80 Lustenader, E. L., Richter, R., and Neugebauer, F. J., "The Use of Thin Films for Increasing Evaporation and Condensation Rates in Process Equipment," ASME Journal of Heat Transfer, Vol 81, pp 297-307, 1959.
- 81 Lyerly, G. A., and Peper, H., Summary Report Studies of Interfacial Surface Energies, NASA CR-54175, 31 December 1964.
- 82 Martinelli, R. C., Boelter, L. M. K., Taylor, T. H. M., Thomsen, E. G., and Morrin, E. H., "Isothermal Pressure Drop for Two-Phase Two-Component Flow in a Horizontal Pipe," Transactions of the ASME, pp 139-151, February 1944.
- 83 Mason, J. L., Plate Fin 5 - A Design Program for Compact Gas-Liquid Heat Exchangers, ASD-TDR-62-559, October 1963.
- 84 McAdams, W. H., "Heat Transfer at High Rates to Water With Surface Boiling," Industrial and Engineering Chemistry, Vol 41, pp 1945-1953, 1949.
- 85 McArdle, J. G., and Nunamaker, R. R., Liquid Hydrogen Behavior With Heat Addition During Weightlessness, NASA.
- 86 McArdle, J. G., Weightlessness Experiments With Liquid Hydrogen in Aerobee Sounding Rockets; Uniform Radiant Heating, NASA TMX-718, December 1962.
- 87 McGrew, J. L., Murphy, D. W., Bailey, R. V., Boiling Heat Transfer in a Zero-Gravity Environment, SAE/ASME Paper 862C, Air Transport Meeting, New York, 1964.
- 88 Merino, F., Feasibility of Using Liquids Other Than Hydrogen for the Liquid Behavior Tests of the Zero-G Test Program, General Dynamics Convair Report AE61-0161, 15 February 1961.
- 89 Merino, F., Simulation of and Recommendation for Centaur Vehicle Pre-Start and Chillardown Flow Sequences, General Dynamics Convair Report AY62-0013, 2 August 1962.

- 90 Merino, F., Investigation of the Center Vent Tube, General Dynamics Convair Report AY 62-0012, July 1962.
- 91 Merte, H. Jr., and Clark, J. A., "Boiling Heat Transfer with Cryogenic Fluids at Standard, Fractional and Near Zero Gravity," ASME Journal of Heat Transfer, Vol 86, pp 351-359, 1964.
- 92 Merte, H., and Clark, J. A., "Boiling Heat-Transfer Data for Liquid Nitrogen at Standard and Near-Zero Gravity," Advances in Cryogenic Engineering, Vol 7, pp 546-550, K. D. Timmerhaus, Editor, Plenum Press, New York, 1962.
- 93 Merte, H. Jr., and Clark, J. A., "Pool Boiling in an Accelerating System," ASME Journal of Heat Transfer, Vol 83, pp 233-242, 1961.
- 94 Mitchell, R. C., and King, K. M., Comparison of Various Methods of Zero-g Propellant Control for a Centaur Type Vehicle, General Dynamics Convair Report ERR-AN-602, December 1964.
- 95 Moore, R. W. Jr., Conceptual Design Study of Space-Borne Liquid Hydrogen Recondensers for 10 and 100 Watts Capacity, Arthur D. Little, Inc., Report 63270-11-02, May 1962.
- 96 Neiner, J. J., The Effect of Zero-Gravity on Fluid Behavior and System Design, Wright Air Development Center (WADC) Technical Note 59-149, ASTIA AD No. AD 228810, April 1959.
- 97 Neu, J. T., and Dummer, R. S., Passive Storage of Liquid Hydrogen in Space, General Dynamics Convair Report 63-1066 ERR-AN-345, October 1963.
- 98 Neu, J. T., Behavior of a Wall-Wetting Fluid Under Zero-Gravity, General Dynamics Convair Report AE 61-0991, October 1961.
- 99 Neu, J. T., Perrisco, C. C., and Boynton, F. P., Condition of Liquid Hydrogen Under Zero-G, General Dynamics Convair Report AZJ 55-002, 6 February 1959.
- 100 Neu, J. T., and Good, R. J., "Equilibrium Behavior of Fluids in Containers at Zero-Gravity," AIAA Journal, Vol 1, No. 4, pp 814-819.
- 101 Nored, D. L., and Otto, E. W., "Fluid Physics of Liquid Propellants," NASA SP-19, Chemical Rocket Propulsion, pp 5-20, 1962. (From NASA University Conference on the Science and Technology of Space Exploration, Chicago, 1-3 November 1962.)

- 102 Nunamaker, R. R., Weightlessness Experiments With Liquid Hydrogen in Aerobee Sounding Rockets; Uniform Radiant Heat Addition - Flight 3, TM X-872, A53577, p 19, December 1963.
- 103 Nussle, R. C., Photographic Study of Propellant Outflow From a Cylindrical Tank During Weightlessness, NASA TN D-2572, p 12, January 1965.
- 104 O'Hanlon, T. W., Zero-G Report, Settling Outflow Test, General Dynamics Convair Report 55D-859-3.
- 105 Oliver, J. R., and Dempster, W. E., Orbital Storage of Liquid Hydrogen, NASA TN D-559, p 69, August 1961.
- 106 Otto, E. W., Static and Dynamic Behavior of the Liquid Vapor Interface During Weightlessness, NASA Report TMX-52-16.
- 107 Papell, S. S., An Instability Effect on Two-Phase Heat Transfer for Subcooled Water Flowing Under Zero-Gravity, ARS Paper 2548-62, September 1962.
- 108 Paynter, H. L., Zero-G Liquid Propellant Orientation by Passive Control, SAE and ASME Paper 862D, p 27, Air Transport and Space Meeting, New York, April 1964.
- 109 Paynter, H. L., "Time for a Totally Wetting Liquid to Deform a Gravity-Dominated to a Nulled-Gravity Equilibrium State," AIAA Journal, Vol 2, No. 9, pp 1627-30, September 1964.
- 110 Perkins, C. K., Zero-Gravity Effects on the Centaur Pneumatic System, General Dynamics Convair Report AE62-0833, 13 September 1962.
- 111 Ponitskii, A., "Emptying and Filling of Vessels in Conditions of Weightlessness," Planetary and Space Science, p 1343, November 1963.
- 112 Potter, J. A., Zero-Gravity Performance of a Supercritical Oxygen Storage and Supply System for Spacecraft Life Support, AiResearch Manufacturing Co., Space Systems Division Report SSD-TDR-63-241.
- 113 Rawle, M. G., Preliminary Investigation for a Zero-Gravity Water Separator, North American Aviation Report NA-63-1097, 23 September 1963.
- 114 Regetz, T. D., Weightlessness Experiments With Liquid Hydrogen in Aerobee Sounding Rockets; Nonuniform Radiant Heat Addition - Flight 4, NASA Report TMX-873, (Confidential).

- 115 Rehm, T. R., and Warner, G. E., Subcooled Boiling in a Negligible Gravity Field, Denver Research Institute, NASA CR-56013, N64-20644, 15 April 1964.
- 116 Reynolds, J. M., and Hurwitz, M., Study of Electrohydrodynamic Propellant Orientation in Centaur, Dynatech Corporation Report PAS-257, 1 February 1965.
- 117 Reynolds, J. M., "The Use of Electric Fields to Orient Dielectric Liquids in a Zero Gravity Environment," Proceedings of the First Space Vehicle Thermal and Atmospheric Control Symposium, ASD-TDR-63-260, Aeronautical Systems Division, Wright-Patterson Air Force Base, Ohio, April 1963.
- 118 Reynolds, John M., "Stability of an Electrostatically Supported Fluid Column," The Physics of Fluids, Vol 8, M.I.T., January 1965.
- 119 Reynolds, W. C., Saad, M. A., and Satterlee, H. M., Hydrodynamic Considerations for the Design of Systems for Very Low Gravity Environments, Stanford University Report LG-1, September 1961.
- 120 Reynolds, W. C., "Behavior of Liquids in Free Fall," Journal of the Aerospace Sciences, December 1959.
- 121 Rohsenow, W. M., "Heat Transfer with Boiling," Modern Developments in Heat Transfer, pp 85-158, Academic Press, New York, 1963.
- 122 Satterlee, H. M., Propellant Orientation, Venting, and Temperature Control Under Zero-Gravity Conditions, Lockheed Aircraft Corporation Report AD274482, 28 March 1962.
- 123 Satterlee, H. M., "Propellant Control at Zero-g," Space/Aeronautics, Vol 38, No. 1, July 1962.
- 124 Schwartz, S. H., and Adelberg, N., Some Thermal Aspects of a Contained Fluid in a Reduced Gravity Environment, Presented at Symposium of Fluid Mechanics and Heat Transfer Under Low Gravitational Condition, Lockheed Research Laboratories, Palo Alto, California, 24-25 June 1965.
- 125 Sherley, J. E., "Nucleate Boiling Heat Transfer Data for Liquid Hydrogen at Standard and Zero Gravity," Advances in Cryogenic Engineering, Vol 8, pp 495-500, 1963.

- 126 Sherley, J. E., and Schwartz, E. W., September-January Progress Report for the Combined Laboratory and KC-135 Aircraft Zero-g Test Program, General Dynamics Convair Report AE62-0096, 23 January 1962.
- 127 Sherley, J. E., and Ballinger, J. C., June-August Progress Report for the Combined Laboratory and KC-135 Aircraft Zero-g Test Program, General Dynamics Convair Report AE61-0871, 5 September 1961.
- 128 Sherley, J. E., et al, The Final Report for the General Dynamics/Astronautics Zero-G Program Covering the Period From May 1960 Through March 1962, General Dynamics Convair Report AY62-0031, Contracts AF18(600)-1775 and NASA-8-2664, 15 August 1962.
- 129 Shuleykin, V. V., External Shape of a Fluid Approaching Weightlessness, NASA TT-F-8373 (N63-11449) and NASA TT-F-8374, 31 January 1963.
- 130 Shuleykin, V. V., Shape of the Surface of a Liquid Losing Gravity, General Dynamics Convair Report (Translation) ACW64-023, p 9, March 1964.
- 131 Shuleykin, V. V., "Ground Experiments With Weightless Liquids," Soviet Physics - Doklady, Vol 8, No. 10, pp 985-988, April 1964.
- 132 Shuleykin, V. V., "Second Series of Ground Tests With Weightless Liquids," Doklady Akad Nauk SSSR, (N64-14996) Vol 153, No. 6, pp 1299-1302, 21 December 1963.
- 133 Siegel, R. and Keshock, E. G., "Effects of Reduced Gravity on Nucleate Boiling Bubble Dynamics in Saturated Water," A.I. Chemical E. Journal, Vol 10, No. 4, pp 509-517, July 1964.
- 134 Siegel, R., and Usiskin, C., "A Photographic Study of Boiling in the Absence of Gravity," ASME Journal of Heat Transfer, Vol 81, pp 230-236, 1959.
- 135 Siegel, R., "Transient Capillary Rise in Reduced and Zero Gravity Fields," ASME Transactions, Series E, pp165-170, p 445-446, June 1962.
- 136 Silvestri, M., "Fluid Mechanics and Heat Transfer of Two-Phase Annular-Dispersed Flow," Advances in Heat Transfer, Vol 1, pp 355-446, Academic Press, 1964.
- 137 Slager, W. L., Computer Simulation of the Operating Characteristics of a Zero "G" Vent Device for Centaur, General Dynamics Convair Report CA-E-57, 15 September 1960.

- 138 Slager, W. L., Preliminary Design Analysis of a Zero Gravity Vent Device for Centaur, General Dynamics Convair Report AE60-0779, 28 September 1960.
- 139 Slager, W. L., Hydrogen Loss From the Centaur Fuel Tank During Zero G Venting, General Dynamics Convair Report CA-E-46, 14 September 1960.
- 140 Smalley, R. A., General Dynamics/Astronautics Test Evaluation Report, Scientific Passenger Pod 18, General Dynamics Convair Report GD/A-AAX64-002, 8 April 1964.
- 141 Sparrow, E. M., and Greg, J. L., "The Effect of Vapor Drag on Rotating Condensation," ASME Journal of Heat Transfer, Vol 82, pp 71-72, 1960.
- 142 Sparrow, E. N., and Lin, S. H., "Condensation Heat Transfer in the Presence of a Noncondensable Gas," ASME Journal of Heat Transfer, Vol 86, pp 430-436, 1964.
- 143 Steinle, H. F., and Walburn, A. B., Hydrogen Propellant System Technology, General Dynamics Convair Report ERR-AN-438, 30 December 1963.
- 144 Steinle, H. F., Laboratory Drop Tests to Compare the Rate at Which Various Liquids Flow to an Equilibrium Condition Under Reduced Gravity, General Dynamics Convair Report CA-HT-188, March 1961.
- 145 Steinle, H. F., Description of the Zero-g Drop Test Apparatus Installed in the Aerophysics Laboratory, Utilizing a 3 Inch Diameter, Low Drag Drop Capsule, General Dynamics Convair Report CA-HT-193, March 1961.
- 146 Steinle, H. F., Development of an Optimum Cryogenic Tank Venting Device, General Dynamics Convair Report 528-1-51, 26 August 1963.
- 147 Steinle, H. F., Capabilities and Performance of the Zero-g Drop Test Apparatus Installed in the Aerophysics Laboratory, General Dynamics Convair Report CA-HT-190, March 1961.
- 148 Steinle, H. F., "Review of Zero Gravity Studies Performed at General Dynamics/Astronautics," Advances in the Astronautical Sciences, Vol 14, pp 95-115, 1963.
- 149 Streiff, M. L., Fluid Behavior Simulation for Zero-G Separator Tests, General Dynamics Convair S/P 7-595-1, 25 January 1961.
- 150 Streiff, M. L., Equilibrium Interface Geometry in a Low g Field, General Dynamics Convair Report, ERR-AN-040, 15 March 1961.

- 151 Streiff, M. L., Equilibrium Low-g Interface Calculations, General Dynamics Convair Report ERR-AN-053, May 1961.
- 152 Strenge, P. H., Orell, A., and Westwater, J. W., "Microscopic Study of Bubble Growth During Nucleate Boiling," A.I. Chemical E. Journal, Vol 7, No. 4, pp 578-583, December 1961.
- 153 Tatro, R. E., A Proposal for a Liquid Propellant Thermal Conditioning System, General Dynamics Convair Report GD/C PIN65-500, 15 May 1965.
- 154 Tuck, G., Perkins, C. K., Wood, G. B., and Ackley, R. A., Zero-g Report LH₂ Boiling Threshold, General Dynamics Convair Report 55D 859-3, 21 May 1962.
- 155 Unterberg, W., and Congelliere, J., "Zero Gravity Problems in Space Powerplants: A Status Survey," ARS Journal, pp 862-872, June 1962.
- 156 Usiskin, C. N., and Siegel, R., "An Experimental Study of Boiling in Reduced and Zero Gravity Fields," ASME Journal of Heat Transfer, Vol 83, pp 243-253, 1961.
- 157 Vasiliu, J., The Effect of the Liquid Volume on its Behavior Under Zero-g Conditions, General Dynamics Convair Report ERR-AN-043, 27 March 1961.
- 158 Velkoff, H. R., Electrofluidmechanics: A Study of Electrokinetic Actions in Fluids, Wright Patterson Air Force Base Report ASD-TR-61-642, February 1962.
- 159 Velkoff, H. R., and Miller, J. H., The Effect of an Electrostatic Field on the Condensation of Vapor, APL Report RTD-TDR-63-4008, February 1964.
- 160 Weiner, H., Electrostatic Separators for a Zero-Gravity Environment, AIAA Paper 64-448, for 1st AIAA Annual Meeting, Washington, D. C., 29 June - 2 July 1964.
- 161 Wood, G. B., Perkins, C. K., and Campbell, R. S., The Center Vent Shape, General Dynamics Convair Report 55D 859, 25 July 1961.
- 162 Wood, G. B., O'Hanlon, T. W., et al, Zero-g Report LH₂ Nucleate Boiling, General Dynamics Convair Report 55D 859-1, 2 February 1962.
- 163 Wood, G. B., O'Hanlon, T. W., Perkins C. K., and Campbell, R. S., "Zero-G Report LH₂ Film Boiling", General Dynamics Convair Report 55D 859-2, 2 March 1962.

- 164 Wood, G. B., O'Hanlon, T. W., Perkins, C. K., and Campbell, R. S., Zero-g Report Settling Outflow Test, General Dynamics Convair Report 55D 859-5, 25 April 1962.
- 165 Wood, G. B., McCrary, L., Perkins, C. K., and Ackley, R. A., Zero-g Report Bubble Accumulation in Simulated Boiling, General Dynamics Convair Report 55D 859-6, 1 June 1962.
- 166 Wood, G. B., Perkins, C. K., and Ackley, R. A., Liquid Response to an Orientation Maneuver, General Dynamics Convair Report 55D 859-7, 30 July 1962.
- 167 Wood, G. B., and Ackley, R. A., Zero-g Report Liquid/Liquid Models, General Dynamics Convair Report 55D 859-9, 28 May 1962.
- 168 Wood, G. B., "A Zero Gravity Liquid Behavior Problem," Advances in the Astronautical Sciences, Vol 14, pp 72-84, 1963.
- 169 Young, N. O., Goldstein, J. S., and Block, M. J., "The Motion of Bubbles in a Vertical Temperature Gradient," Journal of Fluid Mechanics, Vol 6, Part 3, pp 350-356, October 1959.
- 170 Zenkevich, V. B., "On the Behavior of a Liquid Under Conditions of Weightlessness," (UDC 532.2) Scientific-Research Institute of High Temperatures (Russian Translation) Teplofizika Vysokikh Temperatur, Vol 2, No. 2, pp 230-237, March-April 1964, (Russian Original December 1964).
- 171 Aerojet General Corp., Design Guide for Pressurization System Evaluation Liquid Propulsion Rocket Engines, Report 2334, Vol 1 - Use of Design Guide, General Design Data, 30 September 1962.
- 172 Beech Aircraft Corp., Boulder Division, Development of Positive Expulsion Systems for Cryogenic Fluids, Phase 243 Final Report, Engineering Report 13511, May 1963.
- 173 Bell Aerosystems Co., Research on Zero-Gravity Positive Expulsion Techniques, Report 7129- 33003, Final Report on NASA Contract NASr-44, September 1962.

- 174 Bell Aerosystems Co., Buffalo, N. Y., Study of Zero-Gravity Positive Expulsion Techniques, Interim Report 8230-933007, 16 March 1963 - 15 January 1964.
- 175 California Institute of Technology, JPL, Research Summary, pp 36-13, March 1962, Experimental Free Fall Capsule, pp 101-103.
- 176 General Dynamics Convair Huntsville Engineering, A Proposal for the Cryogenic Liquid Experiments in Orbit, General Dynamics Convair Report GD/A-DDF64-007, Vol 1, 16 June 1964.
- 177 General Dynamics Convair, Research and Development Capabilities Relevant to Zero Gravity Problems, General Dynamics Convair Report 528-1-060, 63-0941, 18 September 1963.
- 178 General Dynamics Convair, Individual Acceptance Test Report for the Centaur Zero G Vent System, General Dynamics Convair Report FR-94812, 16 May 1962.
- 179 NASA, Saturn IB Liquid Hydrogen Experiment Preliminary Launch Vehicle Design Definition, TM X-53139, 2 November 1964.
- 180 Rocketdyne Division, North American Aviation, Inc., Motion Picture and Presentation to Convair on Direct Pressurization Expulsion Techniques (Screen Tension), July 1965.

APPENDIX A
HYDROGEN PROPERTIES

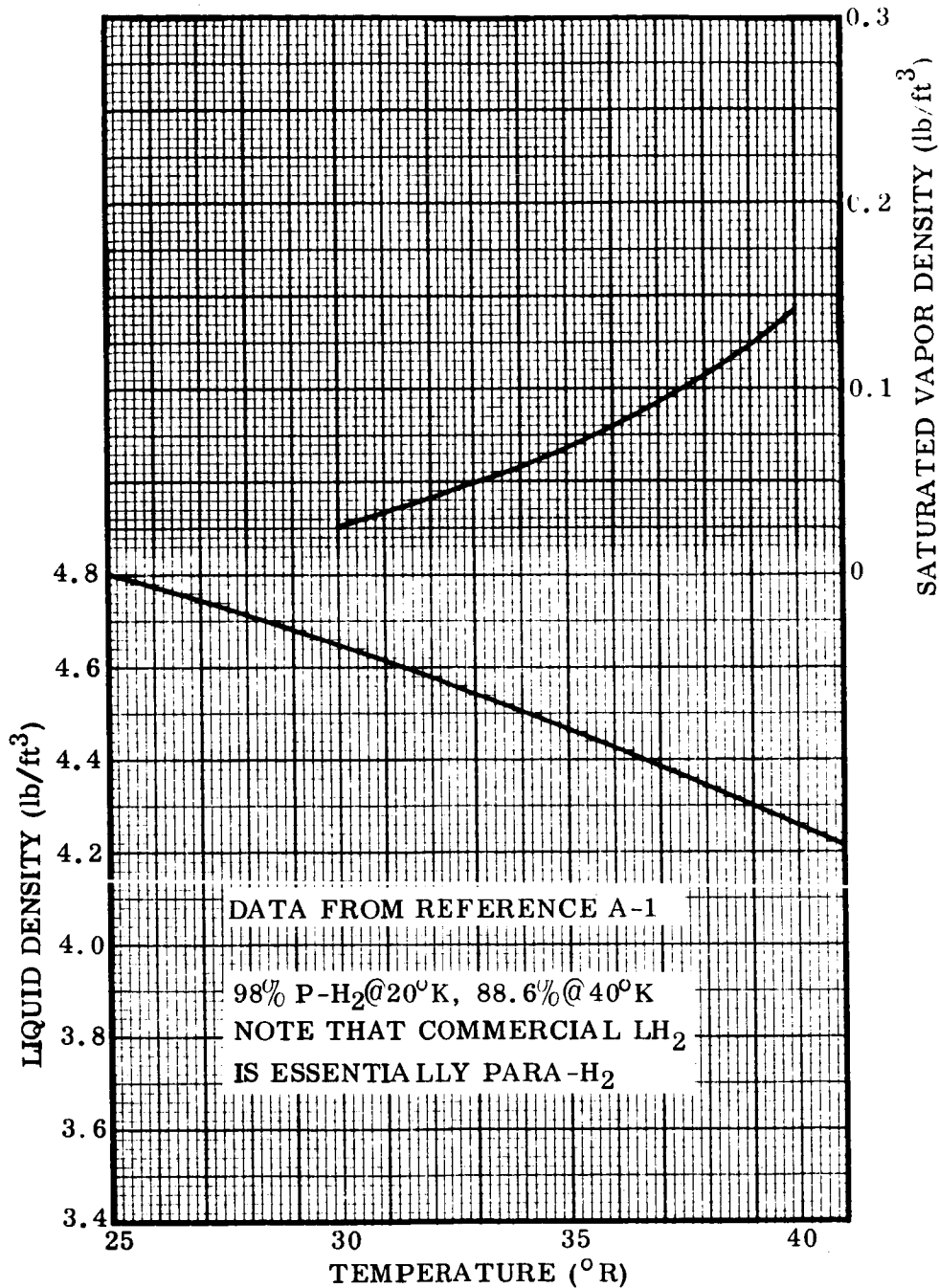


Figure A-1. Density Versus Temperature of Liquid Para-Hydrogen and Saturated Equilibrium Hydrogen Vapor

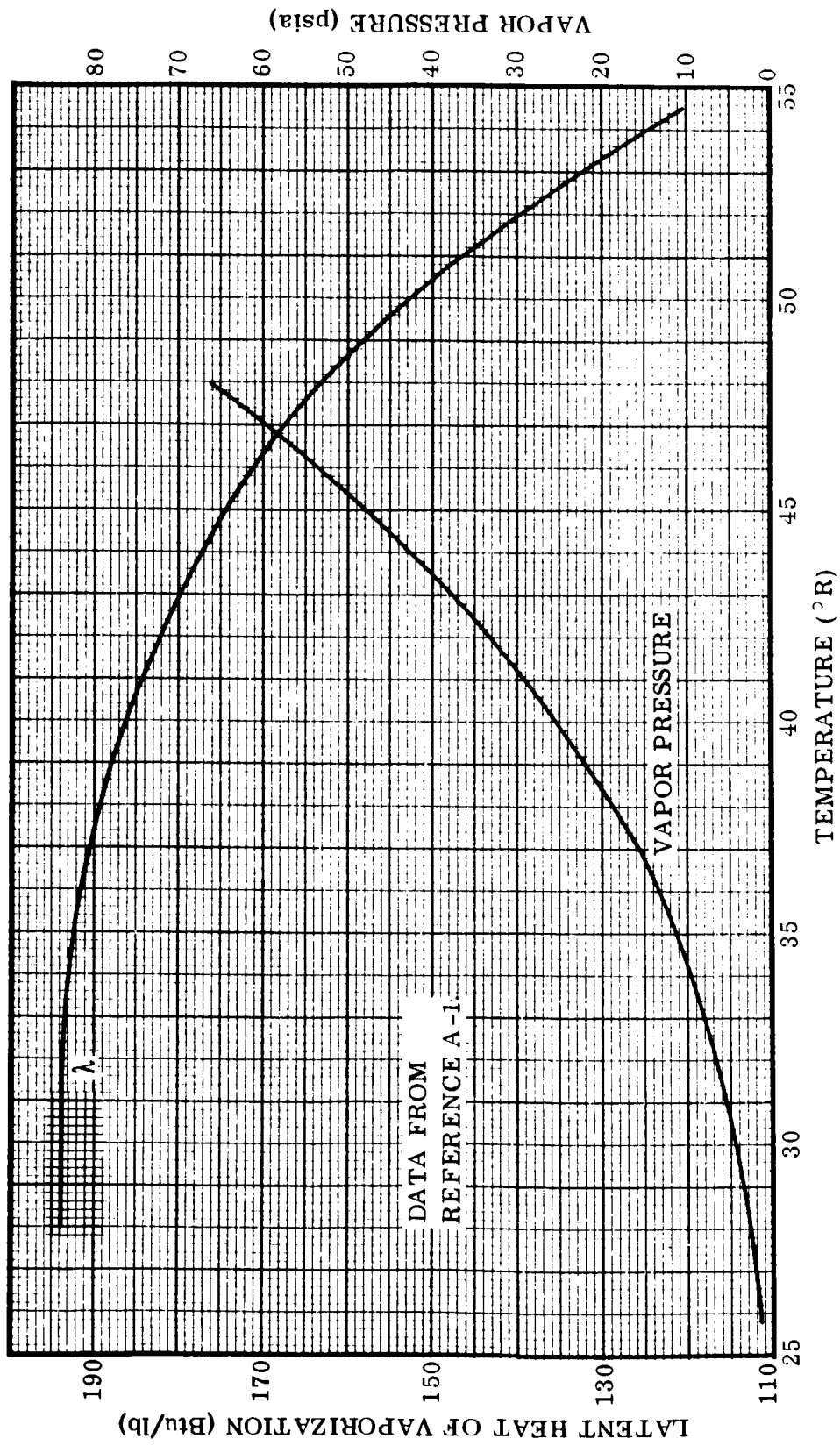


Figure A-2. Vapor Pressure and Latent Heat of Vaporization Versus Temperature for Para-Hydrogen

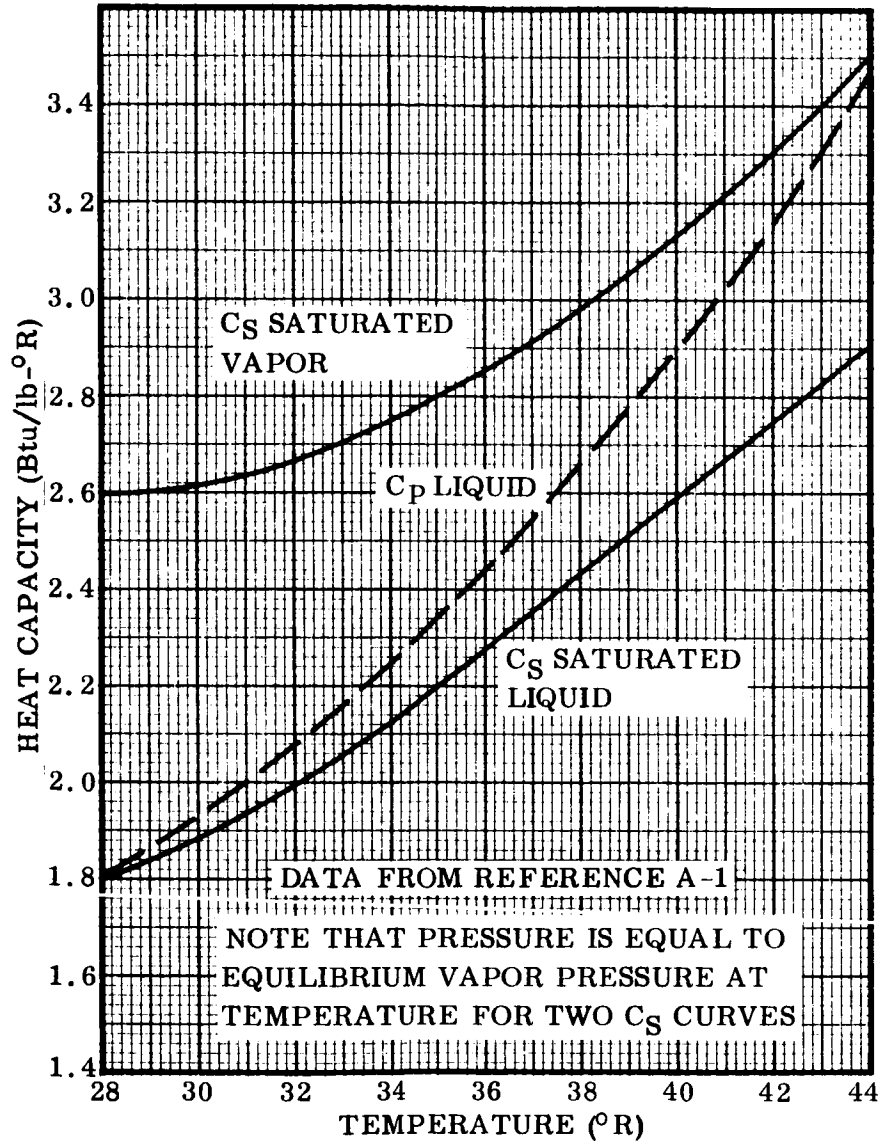


Figure A-3. Heat Capacity of Hydrogen Liquid and Vapor Versus Temperature

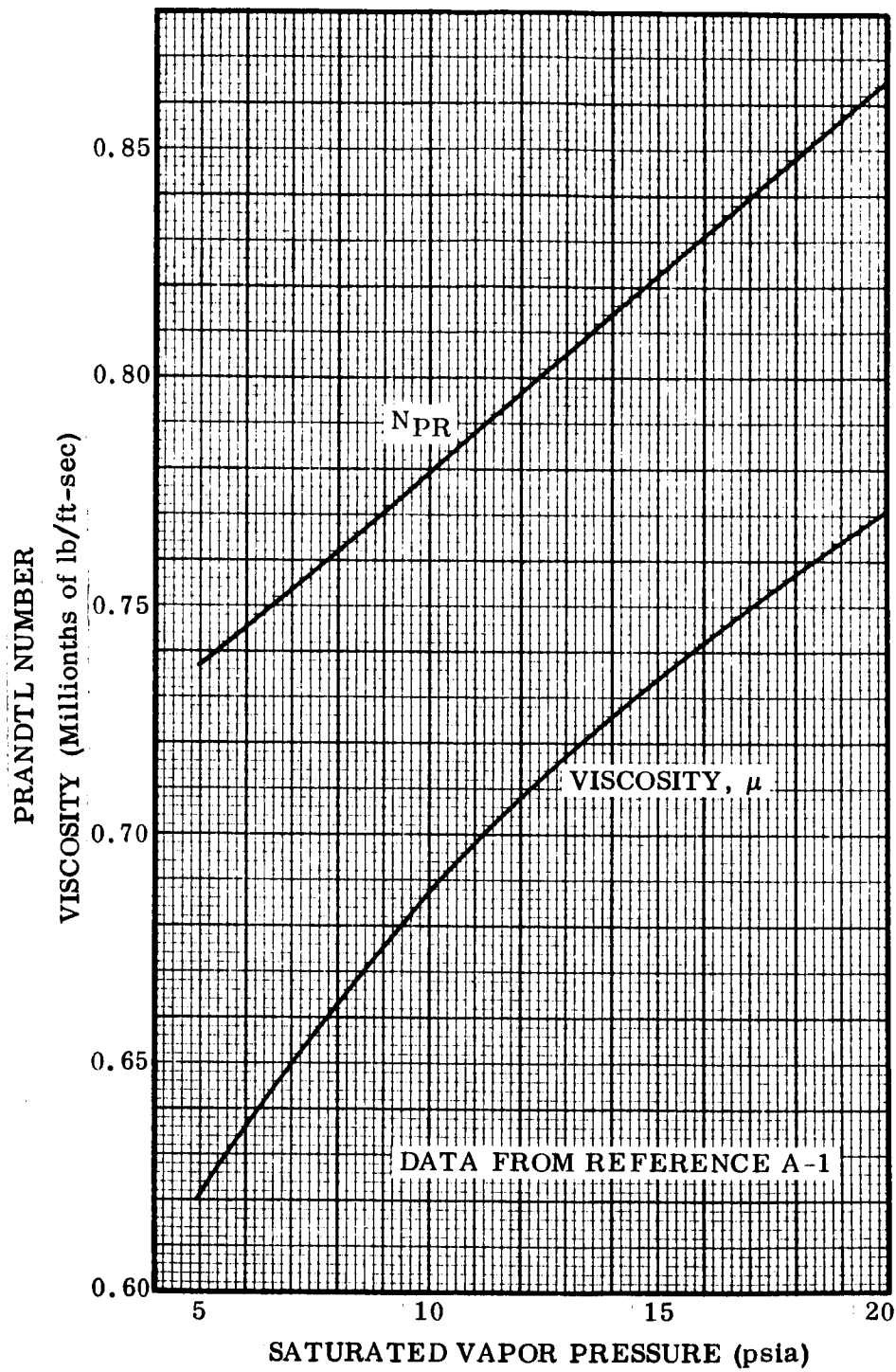


Figure A-4. Prandtl Number and Viscosity of Saturated Gaseous Hydrogen

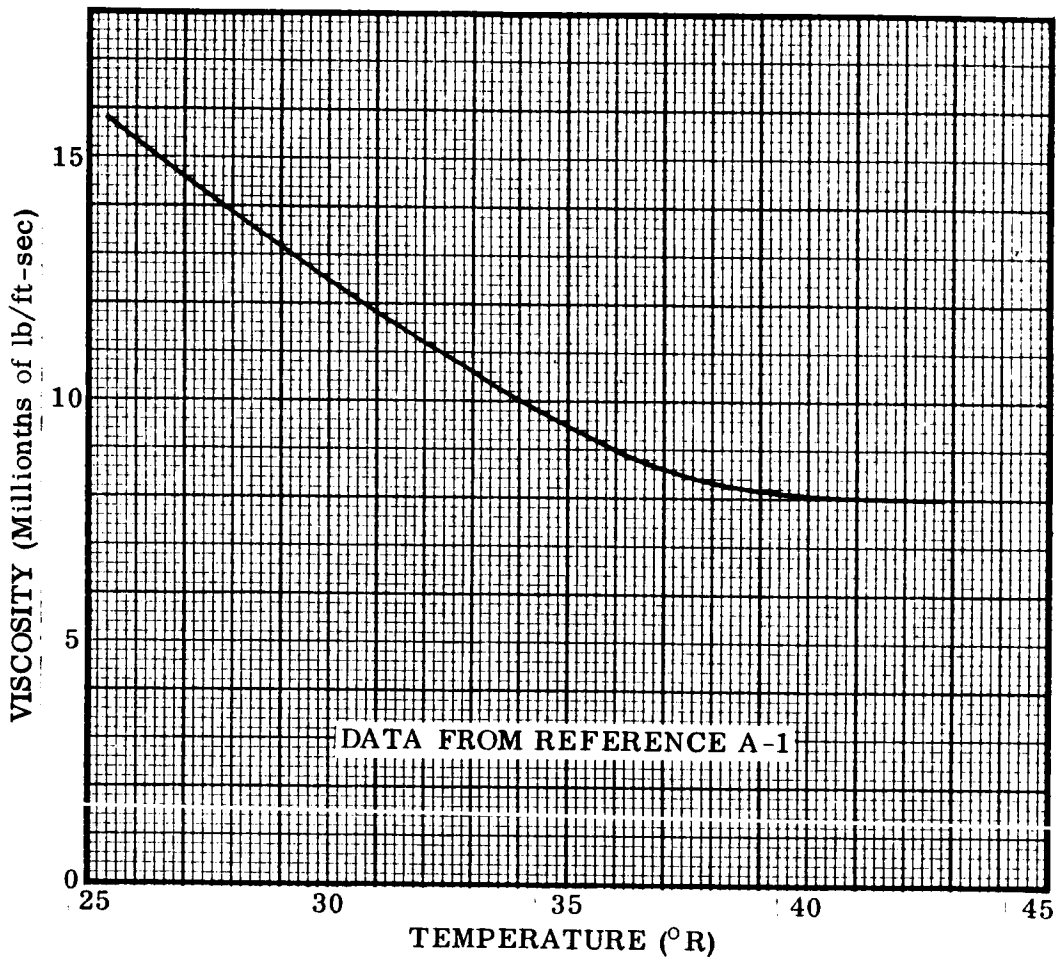


Figure A-5. Viscosity of Liquid Hydrogen Versus Temperature

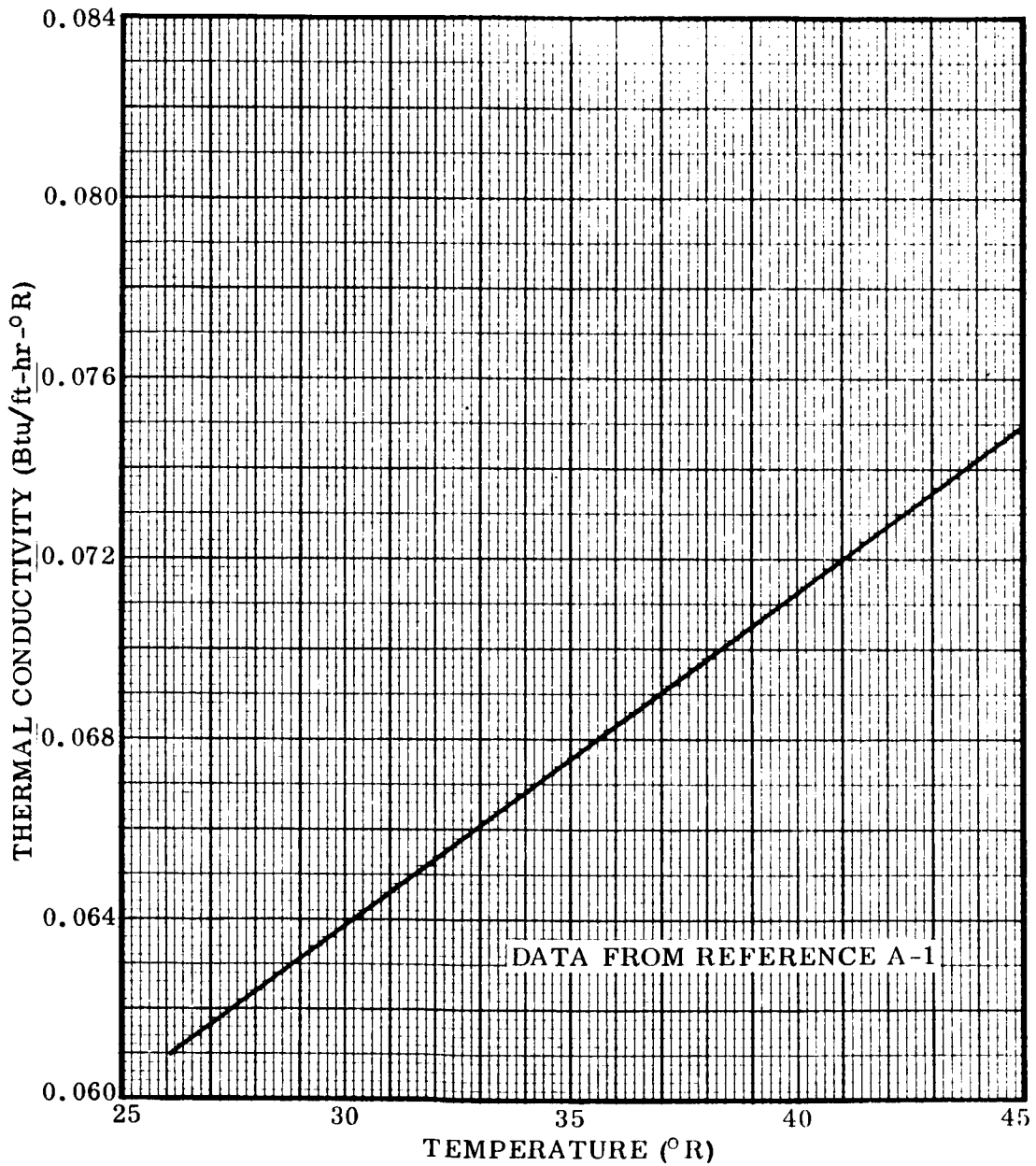


Figure A-6. Thermal Conductivity of Liquid Para-Hydrogen or Normal Hydrogen Versus Temperature

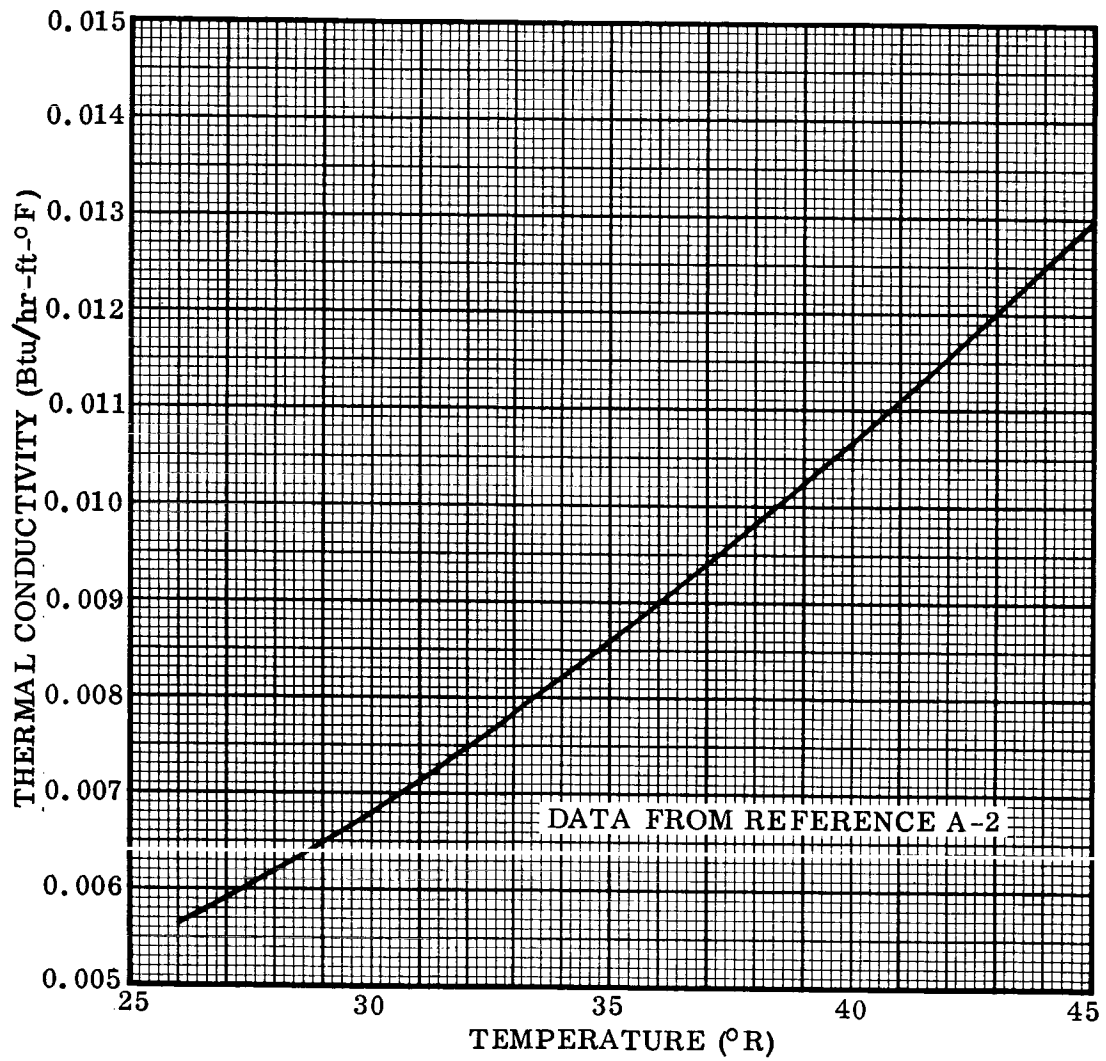


Figure A-7. Thermal Conductivity of Gaseous Para-Hydrogen Versus Temperature

APPENDIX B

HEAT EXCHANGER PREDESIGN CALCULATIONS

B.1 GENERAL PROCEDURE. For ease in following through the detailed calculations, a general outline of the procedure used for sizing and performance calculations applying to the S-IVB design case is presented.

B.1.1 Initial Sizing Cut. Sizing of a heat exchanger system to meet the requirements outlined in Paragraph 2.2.1 is an iterative process. To obtain a starting point an initial size is determined by estimating an overall average heat transfer coefficient, U , calculating the required heat transfer rate, $q = \dot{W}_V (h_o - h_i)$, and determining the required heat exchanger surface area from

$$A_s = \frac{q}{\eta_o U \Delta T_m}$$

From the geometry data of Table 9-3 of Reference 2-6, a heat exchanger configuration meeting the estimated area requirement is then determined.

B.1.2 Performance Calculations at Design Conditions. The heat exchanger outlet temperatures and pressures, and pump and turbine requirements are determined for the worst case (liquid on vent side, vapor on tank side). A further iteration of the heat exchanger size determined in the previous section will probably be required since the actual heat transfer coefficients are likely to deviate from the initially assumed values. The independent variables are the exchanger size and the hot-side flow rate. For a given heat exchanger size the heat transfer can be increased by raising the hot-side flow rate, causing an increase in film coefficient. This increase is limited by the fact that at values of the coefficient significantly in excess of that existing on the cold side, any increase in hot-side coefficient causes very little change in the heat transfer rate; also, the required circulating pump power is approximately proportional to the cube of the flow rate. The power required by the pump results in an increase in propellant heating and required vent rate. A minimum hot-side flow of twice that required for complete condensation is assumed in order to prevent condensation buildup on the heat transfer surface (i. e., $\dot{W}_{H, \min} = 2q/\lambda$).

For calculation purposes the heat exchanger is assumed to be divided into a vaporization portion and a superheat portion. The heat transfer calculations must treat each portion independently due to the different characteristics of the respective heat transfer coefficients. Boiling heat transfer coefficients vary as a function of wall-to-fluid temperature gradient whereas heat transfer coefficients in the superheat region are essentially independent of temperature gradient. The forced convection boiling heat transfer coefficient is taken as the sum of that calculated for forced convection (assum-

ing all fluid is liquid) and that determined from pool boiling tests, as suggested in the method presented in Reference 2-7. The NTU method outlined in Reference 2-6 is used for calculations in the superheat region.

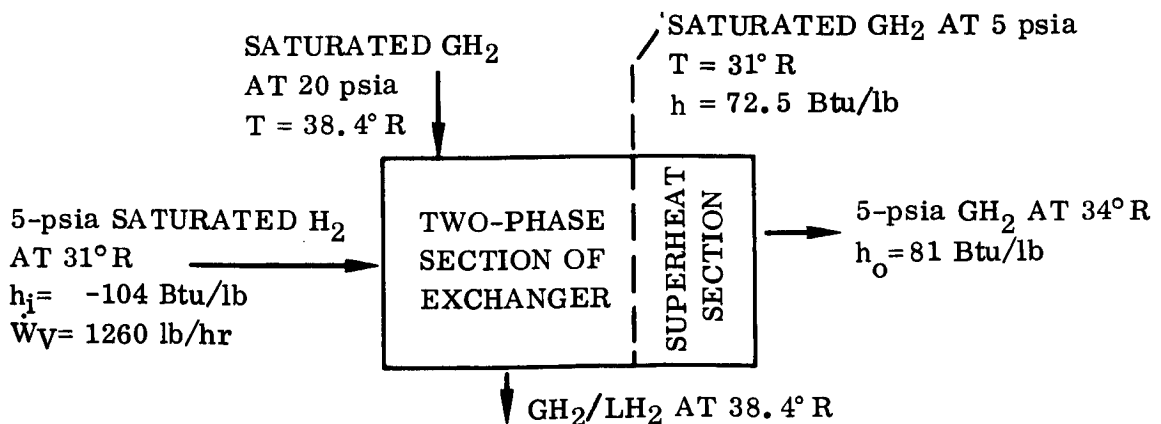
B.1.3 Overall Performance Calculations. Having determined a heat exchanger meeting the design requirements, the detailed performance of the exchanger, pump, and turbine when operating at off-design conditions are determined. The hot-side fluid can be gas, liquid, or a two-phase mixture. The fluid at the vent-side inlet can also be gas, liquid, or a mixture, and the vent flow rate can vary between 0.35 lb/sec and 0.06 lb/sec.

Having determined the pump power requirement at the design point, an approximate pump configuration and speed are estimated in conjunction with a consideration of turbine flow characteristics. Fixing a pump operating point (speed, horsepower, and fluid density) allows a determination of the variation in pump speed and capacity at off-design conditions based on standard pump laws (Reference 2-9). A turbine diameter and nozzle area are also fixed and curves of turbine speed versus horsepower determined at off-design conditions for vent flow rates of 0.35 and 0.06 lb/sec. System operating points are found from the intersection of the pump load curves with the turbine output curves. The turbine-pump performance curves generated for the S-IVB case are shown in Figure B-1.

Final vent fluid conditions are then calculated at the system operating points, and the effect on required vent flow due to a difference in actual vent enthalpy from that of saturated gas at 20 psia is determined. In the cases where at least one side of the exchanger does not have two-phase heat transfer, the NTU approach of Reference 2-6 is used in determining heat exchanger outlet conditions.

B.2 S-IVB PREDESIGN CALCULATIONS

B.2.1 Initial Sizing. The basic flow data are illustrated in the sketch.



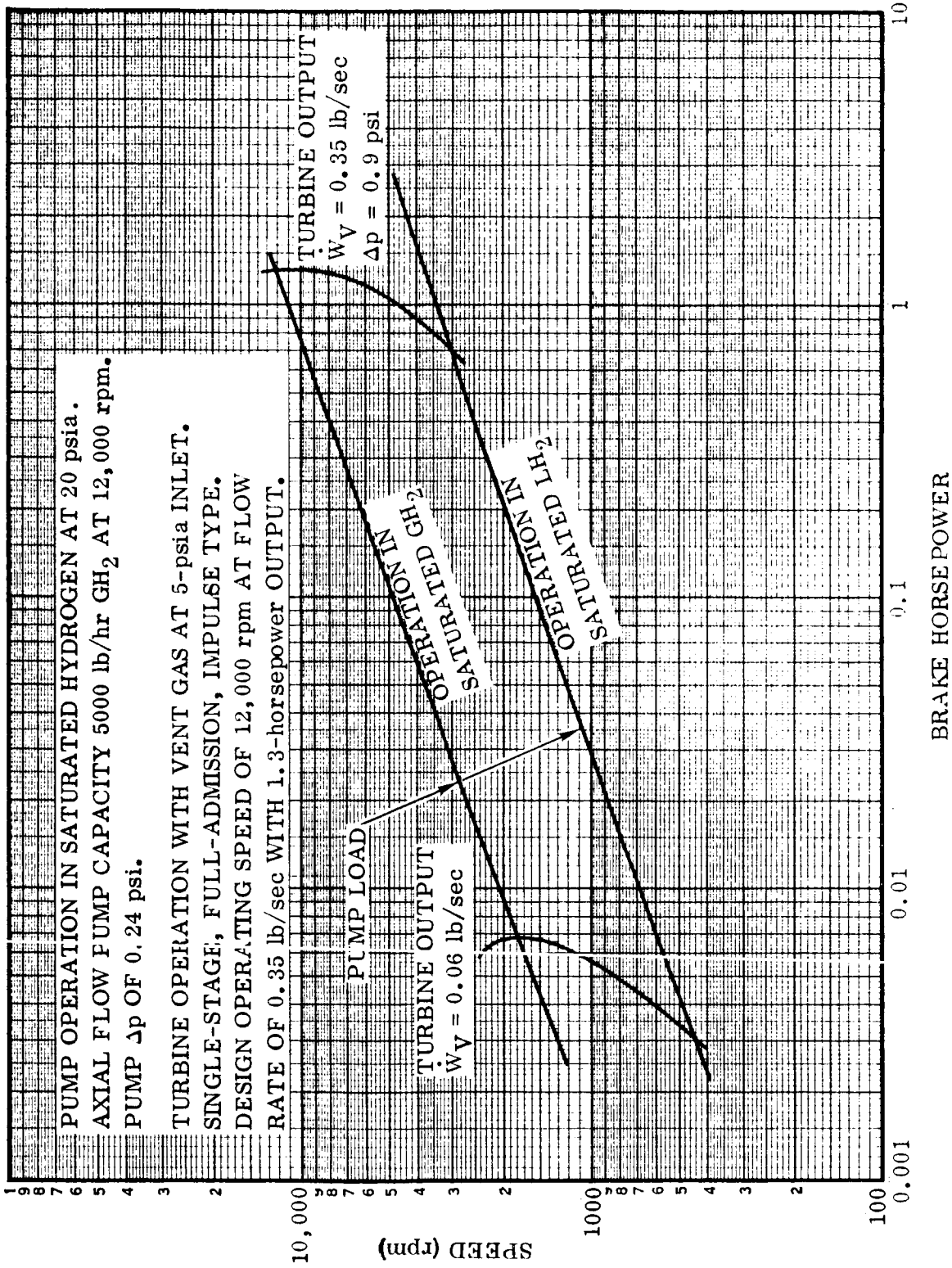


Figure B-1. Turbine-Pump Performance for S-IVB Heat Exchanger System Pre-design

The required heat load and hot-side flow rate are

$$q = 0.35 (81 + 104) 3600 = 232,600 \text{ Btu/hr}$$

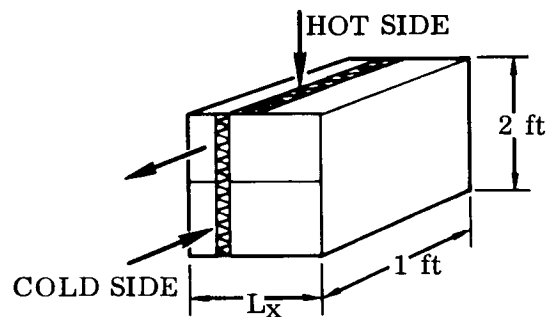
$$\dot{W}_H = \frac{2 (232,600)}{189} = 2500 \text{ lb/hr}$$

Estimating the average overall $U = 77.5 \text{ Btu/hr-ft}^2\text{-}^\circ\text{F}$ gives a value of $\eta_o = 0.8$, from Figure 8-13, and a required heat exchanger area

$$A_s = \frac{q}{\eta_o U \Delta T_m} = \frac{232,600}{77.5 (0.8) (7.5)} = 500 \text{ ft}^2$$

$$\text{The volume between plates on each side} = \frac{A_s}{\beta_E} = \frac{500}{514} = 0.974 \text{ ft}^3$$

The heat exchanger geometry shown in the sketch is assumed for a first cut.



where

$$\text{Hydraulic diameter, } 4R_H = 0.00696 \text{ ft}$$

$$\text{Fin thickness, } \delta = 0.006 \text{ in.}$$

$$\text{Fin wavelength} = 0.375 \text{ in.}$$

$$\text{(Heat transfer area)/(volume between plates), } \beta_E = 514 \text{ ft}^2/\text{ft}^3$$

$$\text{(Fin area)/(total area)} = 0.892$$

$$\text{Plate thickness, } l = 0.001 \text{ ft}$$

$$\text{Plate spacing, } b = 0.0345 \text{ ft}$$

Determination of L_x . Assume an equal number, n , of channels on hot and cold sides. Cold-side volume between plates, $V_c = 0.974 = (1)(2)(b)(n)$

$$L_x = 2nb + 2na = \frac{2(b+a)V_c}{2b} = 1 \text{ ft}$$

$$\text{Free flow area cold side, } (A_c)_c = \frac{A_s R_H}{L} = 0.435 \text{ ft}^2 = (A_c)_H$$

where L = total length of the flow path.

$$G_c = \frac{\dot{W}_c}{(A_c)_c} = 2900 \text{ lb/hr-ft}^2; G_H = 5750 \text{ lb/hr-ft}^2$$

Pressure Drop for Gas Flow on the Cold Side. Consider interconnecting header as equivalent to two 90-degree angle square bends with $\xi = 1.2$ for each and let $\rho_1 = \rho_2 = \rho_m$; then the pressure drop can be expressed as

$$\Delta p = \frac{G^2}{2g_o \rho_1} \left(\xi_c + \xi_b + \xi_e + f \frac{A_s}{A_c} \right) \quad (1)$$

For $p = 5$ psia and $T = 36^\circ\text{R}$, $\rho_1 = 0.0261 \text{ lb/ft}^3$, and from Figure 5-5 of Reference 2-6, $\xi_c = 0.45$ (2); $\xi_e = 0.25$ (2).

$Re = \frac{4R_H G}{\mu} = 8000$; therefore, from Figure 8-11 for the 17.8-3/8W surface, $f = 0.0245$;

$$\frac{f A_s}{A_c} = 0.0245(1150) = 28.2, \text{ and}$$

$$\Delta p = \frac{(0.805)^2 (0.9 + 2.4 + 0.5 + 28.2)}{2(32.2) (0.0261) (144)} = 0.086 \text{ psi}$$

Hot-Side Pressure Drop. Assuming all-gas flow and letting $\rho_1 = \rho_2 = \rho_m = 0.112 \text{ lb/ft}^3$, Equation 1 applies.

$G_H = 5750 \text{ lb/hr-ft}^2$, $Re_H = 14,830$, $f = 0.0205$, $\xi_c = 0.45$, and $\xi_e = 0.25$; therefore

$$\Delta p_H = 0.0596 \text{ psi}$$

$$\text{Required fluid power} = \frac{\dot{W}_H \Delta p_H}{\rho_V} = \frac{2500 (0.0596) 144}{0.112 (3600) 550} = 0.0966 \text{ hp}$$

With a 60-percent pump efficiency, required pump power = 0.161 hp

Heat Exchanger Weight. Cold-side fin area = $0.892 (500) = 446 \text{ ft}^2 = \text{hot-side fin area.}$
Assuming aluminum alloy with $\rho = 0.1 \text{ lb/in.}^3$,

$$\text{Total fin weight} = \frac{\delta (A_F)_T \rho}{2} = \frac{0.006 (2) 446 (0.1) 144}{2} = 38.6 \text{ lb}$$

Weight of plates = $L_1 L_2 l \rho n_T = 9.68 \text{ lb.}$ Core weight = (fin weight) + (plate weight) = 48.28 lb.

Allowing for headers and mounting, total heat exchanger weight = $48.28 (1.43) = 69 \text{ lb}$

Cold-Side Forced Convection Coefficient in the Boiling Region With 100-Percent Liquid Flow

$$\text{Re} = \frac{0.00696 (1260)}{0.435 (0.414)} = 487$$

From Figure 8-11, $\frac{h}{GC_p} (N_{PR})^{2/3} = 0.0175$ where $N_{PR}^{2/3} = 1.184$

and

$$h_{fc} = \frac{0.0175 (1260) 2}{1.184 (0.435)} = 85.5 \text{ Btu/hr-ft}^2 \text{-}^\circ\text{F}$$

Hot-Side Film Coefficient With 100-Percent Gas Flow

$$\text{Re}_H = 14,830$$

From Figure 8-11, $\frac{h_f}{GC_p} (N_{PR})^{2/3} = 0.0045$

$$(h_f)_H = \frac{0.0045 (2500) 3}{0.435 (0.83)} = 92.5 \text{ Btu/hr-ft}^2 \text{-}^\circ\text{F}$$

$$\eta_o = 0.773$$

Determination of Heat Exchanger Area Required for Complete Evaporation With No Superheat. The heat transfer required to bring the vent fluid to saturated vapor at 5 psia is 222,000 Btu/hr, and the total ΔT across the exchanger is 7.5°F .

Determine minimum hot side film $(\Delta T_f)_H$ from

$$q_H = (h_f)_H (A_s)_H (\Delta T_f)_H (\eta_o)_H$$

We can calculate $(\Delta T_f)_H = \frac{222,000}{92.5 (500) 0.773} = 6.21^\circ\text{F}$, which results in $(\Delta T_f)_c = 7.5 - 6.21 = 1.29^\circ\text{F}$

Then from Figure 9 of Reference 2-8, $(q/A_s)_{\text{boiling}} = 145 \text{ Btu/hr-ft}^2$ and the total cold-side film coefficient

$$(h_{fc}) = 85.5 + \frac{145}{1.29} = 197.7 \text{ Btu/hr ft}^2\text{-}^\circ\text{F}, (\eta_o)_c = 0.635$$

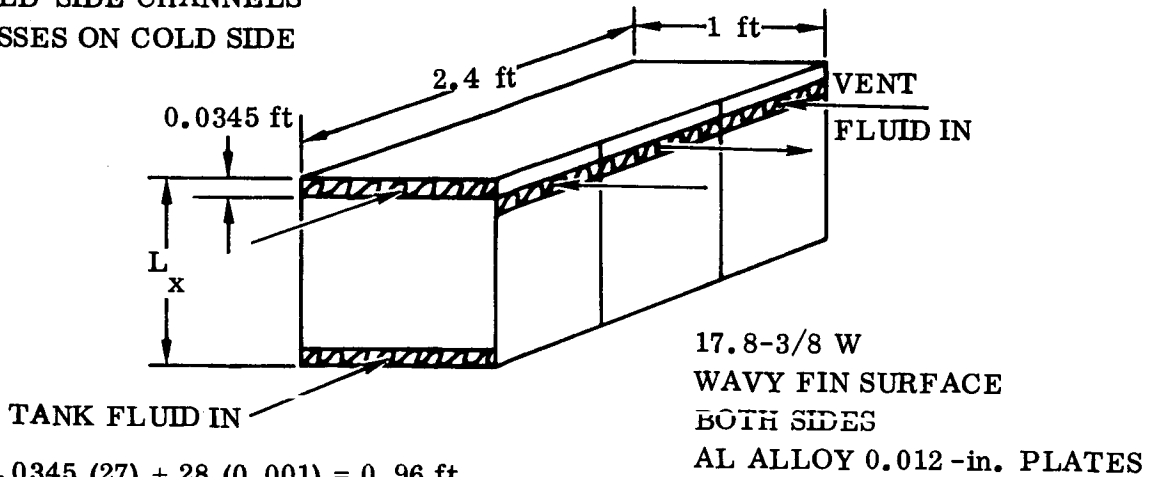
and

$$q_c = 197.7 (500) 1.29 (0.635) = 81,000 \text{ Btu/hr}$$

This shows the assumed heat exchanger to be too small for the present flow conditions. The heat transfer could be increased by increasing the hot-side flow rate; however, the flow rates required to produce any amount of superheat in the present heat exchanger are estimated to be quite high and the pump power required would be excessive since it is approximately proportional to the cube of the flow. Therefore, it is decided to try a larger heat exchanger.

B.2.2 Detailed Heat Exchanger Performance. The heat exchanger configuration shown below is assumed, and the detail performance characteristics determined.

- 14 HOT-SIDE CHANNELS
- 13 COLD-SIDE CHANNELS
- 3 PASSES ON COLD SIDE



$$L_x = 0.0345 (27) + 28 (0.001) = 0.96 \text{ ft}$$

The heat exchanger is designed for maximum vent flow condition of 0.35 lb/sec with gas flow on the hot side.

$$\text{Hot side } A_s = 514 \times 1 \times 2.4 \times 0.0345 \times 14 = 595 \text{ ft}^2$$

$$\text{Cold side } A_s = 514 \times 1 \times 2.4 \times 0.0345 \times 13 = 552 \text{ ft}^2$$

$$\text{Fin area hot side} = 0.892 \times 595 = 530 \text{ ft}^2$$

$$\text{Fin area cold side} = 0.892 \times 552 = 493 \text{ ft}^2$$

Heat Exchanger Weight

$$\text{Fin weight} = 44.2 \text{ lb}$$

$$\text{Weight of the plates} = 11.6 \text{ lb}$$

$$\text{Total core weight} = 55.8 \text{ lb}$$

$$\text{Total weight, allowing for headers and mounting} = 55.8 (1.43) = 79.6 \text{ lb}$$

$$\text{Hot-side free flow area } (A_c)_H = \frac{(A_s)_H R_H}{L} = 0.431 \text{ ft}^2$$

$$\text{Cold side } (A_c)_c = 0.321 \text{ ft}^2 \quad G_c = 1.09 \text{ lb/sec-ft}^2$$

Cold-Side Forced Convection Coefficient for 100-Percent Liquid, Boiling Section

$$\text{Re} = 661 \quad \text{From Figure 8-11, } \frac{h_f}{GC_P} (N_{PR})^{2/3} = 0.0153$$

$$h_{fc} = 101.4 \text{ Btu/hr-ft}^2\text{-}^\circ\text{F}$$

Hot-Side Film Coefficient. Assume saturated GH_2 with flow rate of 2500 lb/hr

$$G_H = \frac{2500}{0.431} = 5790 \text{ lb/hr-ft}^2$$

$$\text{Re} = 14,920 \quad \text{From Figure 8-11, } \frac{h_f}{GC_P} (N_{PR})^{2/3} = 0.0044$$

$$f = 0.0205 \quad (h_f)_H = 92 \text{ Btu/hr-ft}^2\text{-}^\circ\text{F} \quad \eta_o = 0.774$$

Letting ΔT_f on cold side = 3°F then from h_{fc} above and Figure 9 of Reference 2-8

$$(h_f)_c = \frac{345}{3} + 101.4 = 216.4 \text{ Btu/hr-ft}^2\text{-}^\circ\text{F} \quad \eta_o = 0.62$$

$$q_c = (A_s)_c (h_f)_c (\eta_o)_c (\Delta T_f)_c = 222,000 \text{ Btu/hr}$$

The available hot-side film $\Delta T_f = 4.5^\circ\text{F}$ and $q_H = 191,000 \text{ Btu/hr}$, which shows that the minimum required heat transfer of $222,000 \text{ Btu/hr}$ will not be met.

Increasing the Flow Rate of Hot-Side Fluid to 5000 lb/hr

Then

$$G_H = 11,580 \text{ lb/hr-ft}^2 \quad \text{Re} = 29,840$$

$$(h_f)_H = 140 \text{ Btu/hr-ft}^2\text{-}^\circ\text{F} \quad \eta_o = 0.7 \quad f = 0.017$$

Letting

$$(\Delta T)_{fH} = 4.2^\circ\text{F} \quad q_H = 244,000 \text{ Btu/hr}$$

The temperature difference between the heat exchanger wall and the cold-side fluid $(\Delta T)_{fc}$ is then 3.3°F .

$$(h_f)_c = \frac{400}{3.3} + 101.4 = 222.6 \quad \eta_o = 0.614 \quad q_c = 248,000 \text{ Btu/hr}$$

The actual operating condition is when $q_H = q_c$. Iterating further let $(\Delta T)_{fH} = 4.23^\circ\text{F}$ then $q_H = 246,000 \text{ Btu/hr}$ and $(\Delta T)_{fc} = 3.27^\circ\text{F}$ $(h_f)_c = 222$ $q_c = 246,000 \text{ Btu/hr}$

The required heat transfer in the evaporator section is 222,000 Btu/hr and since total transfer areas were used in the above analysis the areas required for evaporation are $\left(\frac{222,000}{246,000}\right) (A_s)_T$ and for the superheat section $\left(1 - \frac{222,000}{246,000}\right) (A_s)_T$ or in the present case 498.5 ft^2 on the cold side and 537.4 ft^2 on the hot side for evaporation and 53.5 ft^2 on the cold side and 57.6 ft^2 on the hot side for superheating.

Superheat Section

The hot-side heat transfer coefficient is constant at $140 \text{ Btu/hr-ft}^2\text{-}^\circ\text{F}$. The cold-side coefficient is recomputed as follows. Assuming superheat to 35.5°R , the cold-side average temperature is 33.25°R and

$$\mu_{\text{avg}} = 0.07 \times 10^{-5} \text{ lb/ft-sec} \quad (C_P)_{\text{avg}} = 2.78 \text{ Btu/lb-}^\circ\text{R}$$

$$N_{\text{PR}} = 0.80 \quad N_{\text{PR}}^{2/3} = 0.862$$

$\text{Re}_c = 10,870$ and from Figure 8-11, $(h_f)_c = 63.4 \text{ Btu/hr-ft}^2\text{-}^\circ\text{F}$ and $(\eta_o)_c = 0.827$ then for the superheat region

$$U_H = \frac{1}{\frac{1}{(\eta_o)_H (h_f)_H} + \frac{1}{\frac{(A)_{sc}}{(A)_H} (\eta_o)_c (h_f)_c}} = 32.5 \text{ Btu/hr-ft}^2\text{-}^\circ\text{F}$$

To determine the actual temperature of the vent gas out of the exchanger

$$B_{\min} = B_c = \dot{W}_V (C_P)_V = 3500 \text{ Btu/hr-}^\circ\text{F}$$

$$B_{\max} = B_H = \infty$$

$$(\text{NTU})_H \equiv \frac{(A)_s U_H}{C_{\min}} = 0.535$$

$$\text{Heat exchanger effectiveness, } E_x = 1 - \frac{1}{e^{\text{NTU}}} = 0.415$$

$$\text{and } (T_c)_{\text{out}} = E_x [(T_H)_{\text{in}} - (T_c)_{\text{in}}] + (T_c)_{\text{in}} = 0.415 (38.5 - 31) + 31 = 34.12^\circ\text{R or } 3.12$$

degrees of superheat, which meets the original requirement of $4 \pm 1^\circ\text{F}$ (Paragraph 2.2).

Pump Power Requirement

$$A_{\text{fr}} = 1 (0.96) = 0.96 \text{ ft}^2 \quad \xi_c = 0.45 \quad \xi_e = 0.25 \quad f = 0.017$$

From Equation 1

$$\Delta p_H = \frac{(11,580)^2}{2 (32.2) 0.112 (3600)^2} \left(0.45 + 0.25 + 0.017 \frac{595}{0.431} \right)$$

$$\Delta p_H = 34.6 \text{ lb/ft}^2$$

$$\text{Theoretical fluid power} = \frac{5000 (34.6)}{0.112 (550) 3600} = 0.78 \text{ hp}$$

$$\text{Required brake horsepower, bhp} = \frac{0.78}{0.6} = 1.3 \text{ hp}$$

Minimum Velocity of the Gas on Hot Side. For the total gas flow of 5000 lb/hr and $A_c = 0.435 \text{ ft}^2$, then with 1250 lb/hr condensed, a minimum gas flow of 3750 lb/hr exists at the exit, and from $\dot{W}_v = \rho_v A_c u_v$

$$(u_v)_{\min} = 21.4 \text{ fps}$$

This velocity should be capable of breaking liquid from the heat transfer surfaces and thus preventing a large insulating liquid layer from forming.

B.2.3 Overall System Performance at Design Conditions. (Liquid vent inlet, gas tank side, 0.35 lb/sec vent)

Pump Analysis. Assume a pump speed of 12,000 rpm

and

$$H = \frac{\Delta p_H}{\rho_V} = \frac{34.6}{0.112} = 309 \text{ ft} \quad Q = 5,550 \text{ gpm}$$

then specific speed, $n_S = \frac{N, \text{ rpm} \sqrt{Q, \text{ gpm}}}{(H, \text{ ft})^{3/4}} = 12,100$ which is typical of an axial flow

pump. From Reference 2-9 a reasonable tip velocity is calculated to be

$$u = 2.13 \sqrt{2gH} = 2.13 \sqrt{2(32.2)309} = 300 \text{ fps}$$

and since $u = r\omega$ then $r = 2.86 \text{ in.}$ or a 5.75-in.-diameter pump

Pump Load Curves. At 12,000 rpm, the total required power is 1.3 horsepower when operating in saturated gaseous hydrogen at 20 psia. Assume

$$\text{Mechanical losses} = (0.10)(1.3) = 0.13 \text{ hp} \quad \rho_V = 0.112 \text{ lb/ft}^3$$

$$\text{Remainder} = (0.9)(1.3) = 1.17 \text{ hp} \quad \rho_L = 4.34 \text{ lb/ft}^3$$

For a fixed pump operating at off-design conditions, the power consumed by mechanical losses (HP_M) is approximately proportional to the square of the speed and independent of the fluid density. The remainder, or fluid power (HP_F) is proportional to the cube of the speed at constant density and approximately proportional to density at constant speed.

That is

$$HP_M \approx N^2$$

and

$$HP_F \approx N^3 \text{ at constant density}$$

$$HP_F \approx \rho \text{ at constant speed}$$

$$\text{Total power, } P = HP_F + HP_M = 1.3 \text{ hp}$$

Thus, the total power, P_x , at an arbitrary speed, N_x , at constant density is related to the design power, P , and design speed, N , by the following equation.

$$P_x = P \left(\frac{N_x}{N} \right)^3 \left[0.1 \frac{N}{N_x} + 0.9 \right] \quad (2)$$

At a density ρ_x different from the design condition ρ , the following relation holds.

$$P_x = HP_F \left(\frac{\rho_x}{\rho} \right) \left(\frac{N_x}{N} \right)^3 + HP_M \left(\frac{N_x}{N} \right)^2 \quad (3)$$

Then for saturated gas, $P = 1.3 \text{ hp @ } 12,000 \text{ rpm}$, and from Equation 2

@ 2400 rpm	$P_x = 0.01456 \text{ hp}$
@ 4800 rpm	$P_x = 0.0957 \text{ hp}$
@ 7500 rpm	$P_x = 0.337 \text{ hp}$
@ 1200 rpm	$P_x = 0.00247 \text{ hp}$

For saturated LH_2 , from Equation 3

@ 2400 rpm	$P_x = 0.3545 \text{ hp}$
@ 4800 rpm	$P_x = 2.76 \text{ hp}$

The above data are plotted in Figure B-1.

Turbine Performance. To allow for full-flow-admission at the design vent rate, the use of a 6-inch-diameter turbine appears reasonable. Assuming an operating speed of 12,000 rpm, the turbine bucket velocity $u_b = r\omega = 314 \text{ fps}$ for the 6-inch-diameter turbine. The inlet to the turbine at the design operating point is a superheated gas at 5 psia and 34°R with an enthalpy of 80.5 Btu/lb and flow rate of 0.35 lb/sec. The required output is 1.3 horsepower.

The characteristic nozzle velocity

$$u_o = \sqrt{2g_o \Delta h_s} = 223.7 \sqrt{\Delta h_s, \text{ Btu/lb}} \quad (4)$$

For 0.35 lb/sec turbine flow

and

$$\Delta h_s = 6 \text{ Btu/lb}$$

$$\text{Theoretical power} = \dot{W}_v \Delta h_s = 2.97 \text{ hp}$$

$$u_c = 223.7 \sqrt{6} = 548 \text{ fps}$$

$$u_b/u_o = \frac{314}{548} = 0.573$$

and from Figure C-8

$$\eta_t = 0.486$$

$$\text{Brake horsepower, bhp} = 0.486 (2.97) = 1.445 \text{ hp}$$

This is greater than required.

Let

$$\begin{aligned} \Delta h_s &= 5.5 \text{ Btu/lb} & u_c &= 525 \text{ fps} & P_{\text{theo}} &= 2.725 \text{ hp} \\ u_b/u_o &= 0.598 & \eta_t &= 0.48 & \text{bhp} &= 1.31 \text{ hp} \end{aligned}$$

Turbine design is then for $\Delta h_s = 5.5$ Btu/lb, which corresponds to a turbine nozzle pressure drop of 0.8 psi.

Then at 3000 rpm

$$u_b = 78.5 \text{ fps} \quad \eta_t = 0.255 \quad \text{bhp} = 0.695 \text{ hp}$$

and at 6000 rpm

$$u_b/u_o = 0.2996 \quad \eta_t = 0.419 \quad \text{bhp} = 1.14 \text{ hp}$$

The above data are plotted in Figure B-1.

B.2.4 System Performance with LH₂ Vent Inlet. The performance data of Figure B-1 show an operation point with the pump in LH₂ at approximately 3000 rpm and 0.69 hp. Assuming that $Q \approx N$ for fixed downstream pump restriction then the weight flow of the liquid,

$$\dot{W}_L = 5000 \left(\frac{3000}{12,000} \right) \left(\frac{4.34}{0.112} \right) = 48,400 \text{ lb/hr}$$

and

$$G_H = \frac{48,400}{0.431} = 112,000 \text{ lb/hr-ft}^2 \quad \text{Re} = 25,400 \quad f = 0.0177$$

From Equation 1

$$\Delta p_H = 86.7 \text{ lb/ft}^2$$

$$\text{Theoretical fluid power} = \frac{\dot{W}_L \Delta p_H}{\rho_L} = 0.489 \text{ hp}$$

This corresponds to 70-percent pump efficiency.

Adjusting the actual flow rate (\dot{W}_H) to 46,000 lb/hr gives $P_{\text{theo}} = 0.42$ hp (61-percent pump efficiency).

Heat Exchanger Operation

$$G_H = 106,700 \text{ lb/hr-ft}^2 \quad \text{Re} = 24,200$$

From Figure 8-11, $(h_p)_{FH} = 913 \text{ Btu/hr-ft}^2\text{-}^\circ\text{F}$ $\eta_o = 0.403$

$$q = (C_P)_L \dot{W}_L [(T_H)_{in} - (T_H)_{out}]$$

for evaporator portion

$$\Delta T_H = \frac{222,000}{2.5(46,000)} = 1.93^\circ\text{F} \quad T_{Havg} = 37.53^\circ\text{R}$$

The average temperature difference between hot and cold fluids in the boiling region is then 6.53°F .

Iterating between hot side and cold side as in Paragraph B.2.2 to determine the areas required for evaporation and available for superheat

$$q_c = q_H = 405,000 \text{ Btu/hr}$$

and

$$\left(1 - \frac{222,000}{405,000}\right) 595 = 269 \text{ ft}^2 \text{ available for hot-side superheat}$$

$$A_s = 552(0.452) = 250 \text{ ft}^2 \text{ available for cold-side superheat}$$

In the superheat region the cold-side film coefficient is $63.4 \text{ Btu/hr-ft}^2\text{-}^\circ\text{F}$ from Paragraph B.2.2, and the hot side $913 \text{ Btu/hr-ft}^2\text{-}^\circ\text{F}$.

Then

$$U_H = 43 \text{ Btu/hr-ft}^2\text{-}^\circ\text{F}$$

$$B_{\min} = 3500 \text{ Btu/hr-}^\circ\text{F} = B_c \quad \frac{B_{\min}}{B_{\max}} = 0.03045$$

$$B_{\max} = 115,000 = B_H$$

$$\text{NTU} = 3.3$$

$$E_x = 0.95$$

and heat exchanger vent gas exit temperature $(T_c)_{out} = 36.3^\circ\text{R}$

B.2.5 System Performance at Vent Flow of 0.06 lb/sec. (LH₂ vent inlet, gas on hot side.) For flow through the turbine

$$\dot{W}_v = C_{vV} A_v \sqrt{2g_o \rho \Delta p}$$

$$\dot{W}_v = \rho A_v u_o$$

$$\Delta h_s = \frac{u_o^2}{2g_o} \qquad P_{\text{theo}} = \dot{W}_v \Delta h_s$$

Relating turbine conditions at 0.06 lb/sec to those at 0.35 lb/sec for C_v , A_v , and ρ constant gives

$$(P)_{0.06} = \left(\frac{\dot{W}_{0.06}}{\dot{W}_{0.35}} \right)^3 \quad (P)_{0.35} = 0.0137 \text{ hp}_{\text{theo}}$$

$$(u_o)_{0.06} = \left(\frac{\dot{W}_{0.06}}{\dot{W}_{0.35}} \right)^3 \quad (u_o)_{0.35} = 90 \text{ fps}$$

Referring to Figure C-8 and calculating turbine output as a function of speed

$$\text{@ 1200 rpm} \quad u_b = 31.4 \text{ fps} \quad u_b/u_o = \frac{31.4}{90} = 0.349$$

$$\eta_t = 0.453 \text{ and } P = 0.453 (0.0137) = 0.0062 \text{ hp}$$

$$\text{@ 2400 rpm} \quad u_b/u_c = 0.698 \quad \eta_t = 0.421 \quad P = 0.00576 \text{ hp}$$

$$\text{@ 1800 rpm} \quad u_b/u_c = 0.524 \quad \eta_t = 0.496 \quad P = 0.0068 \text{ hp}$$

$$\text{@ 600 rpm} \quad u_b/u_c = 0.1745 \quad \eta_t = 0.289 \quad P = 0.00396 \text{ hp}$$

These data are plotted in Figure B-1.

Pump operating point in GH_2 for the 0.06 lb/sec vent case, from Figure B-1 is 1800 rpm at 0.0068-horsepower input. The pump flow rate is calculated to be

$$\dot{W}_H = 725 \text{ lb/hr}$$

then

$$(\text{Re})_H = 4330$$

$$G_H = 1680 \text{ lb/hr-ft}^2$$

$$(h_f)_H = 43.7 \text{ Btu/hr-ft}^2 \text{-}^\circ\text{F}$$

$$\eta_o = 0.87$$

For liquid on the vent side and saturated gas on the hot side, the required heat transfer to completely vaporize the vent fluid is

$$q = 222,000 \left(\frac{0.06}{0.35} \right) = 38,000 \text{ Btu/hr}$$

$$G_c = 673 \text{ lb/hr-ft}^2 \quad (\text{Re})_c = 113.4$$

$$(h_f)_c = 34.1 \text{ Btu/hr-ft}^2\text{-}^\circ\text{F}$$

Iterating as in Paragraph B.2.2, a match point is found at

$$q_c = q_H = 120,000 \text{ Btu/hr}$$

$$(\Delta T)_{fh} = 5.3^\circ\text{F} \quad (\Delta T)_{fc} = 2.2^\circ\text{F}$$

$$\text{Cold-side superheat area} = \left(1 - \frac{38,000}{120,000}\right) 552 = 377 \text{ ft}^2$$

$$\text{Hot-side superheat area} = 406 \text{ ft}^2$$

Cold-side heat transfer coefficient in the superheat region

$$\text{Re} = 1,860 \quad (h_f)_c = 22 \text{ Btu/hr-ft}^2\text{-}^\circ\text{F}$$

$$U_H = 12.68 \text{ Btu/hr-ft}^2\text{-}^\circ\text{F}$$

$$B_c = 600 \text{ Btu/hr-}^\circ\text{F} \quad B_H = \infty$$

$$\text{NTU} = 8.6 \quad E_x \cong 1 \quad (T_c)_{\text{out}} \cong 38.5^\circ\text{R}$$

B.2.6 Calculation of Δ Vent Rates. Venting of saturated gas at 20 psia is considered as the base for comparison of the various vent systems. The difference between the actual vent enthalpy and that of saturated gas at 20 psia is taken account of by an increase or decrease in the required vent flow. The enthalpy of the fluid as it leaves the tank boundary is taken as the vent enthalpy. The $\Delta \dot{W}_v$ is calculated below for the various heat exchanger operating conditions.

0.35 lb/sec LH₂ Vent Inlet, GH₂ Tank Side. Vent fluid at turbine exit is at 4 psia and 32°R or $h_v = 79.4 \text{ Btu/lb}$

$$h_{sg} = 85 \text{ Btu/lb at 20 psia}$$

Based on the heat of vaporization available at the 20-psia tank condition of 189 Btu/lb then

$$\Delta \dot{W}_v = \left(\frac{85 - 79.4}{189}\right) 0.35 (3600) = 37.3 \text{ lb/hr}$$

0.35 lb/sec LH₂ Vent, LH₂ Tank Side

$$h_v = 86.08 \text{ Btu/lb}$$

$$\Delta \dot{W}_v = \left(\frac{-1.08}{189} \right) 1260 = -7.2 \text{ lb/hr}$$

0.06 lb/sec LH₂ Vent, GH₂ Tank Side

$$h_v = 92.5 \text{ Btu/lb}$$

$$\Delta \dot{W}_v = \left(\frac{-7.5}{189} \right) 0.06 (3600) = -8.55 \text{ lb/hr}$$

B.2.7 Sizing of System Components and Ducting. For saturated liquid at inlet to a valve, the equation

$$\dot{W} = C_v A_v \sqrt{2 g_o \Delta p \rho} \quad (5)$$

is used, where $(\Delta p \rho)$ is taken as the integrated $(\Delta p \rho)$ through the valve. This method has shown reasonable correlation with test results (References B-1 and B-2). The method assumes that the enthalpy through the valve remains constant. A curve of density versus pressure for constant enthalpy flow is shown in Figure B-2. A curve of the integrated $\Delta p \rho$ is given as a function of Δp in Figure B-3 for saturated liquid hydrogen at various initial saturation pressures. The data are taken from areas under the curves of Figure B-2. For gas at inlet to a restriction

$$\dot{W} = C_v A_v \sqrt{p_u \rho_u 2 g_o} \sqrt{\frac{\gamma}{\gamma-1} \left(\frac{p_d}{p_u} \right)^{2/\gamma} - \left(\frac{p_d}{p_u} \right)^{1+\gamma/\gamma}} \quad (6)$$

For a saturated gas inlet it is assumed that the gas is in a supersaturated condition behaving as a superheated vapor for flow through a short restrictor (Reference B-3).

Where flow is critical, i.e., where

$$p_d \leq p_u \left(\frac{2}{\gamma+1} \right)^{\gamma/\gamma-1}$$

Equation 6 reduces to

$$\dot{W} = C_v A_v \left(\frac{2}{\gamma+1} \right)^{1/\gamma-1} \sqrt{p_u \rho_u 2 g_o \frac{\gamma}{(\gamma+1)}} \quad (7)$$

The subscripts used below refer to valves and stations of Figure 2-2.

Minimum Area of R₁ Regulator

Assume

0.06 lb/sec flow, saturated LH₂ at inlet

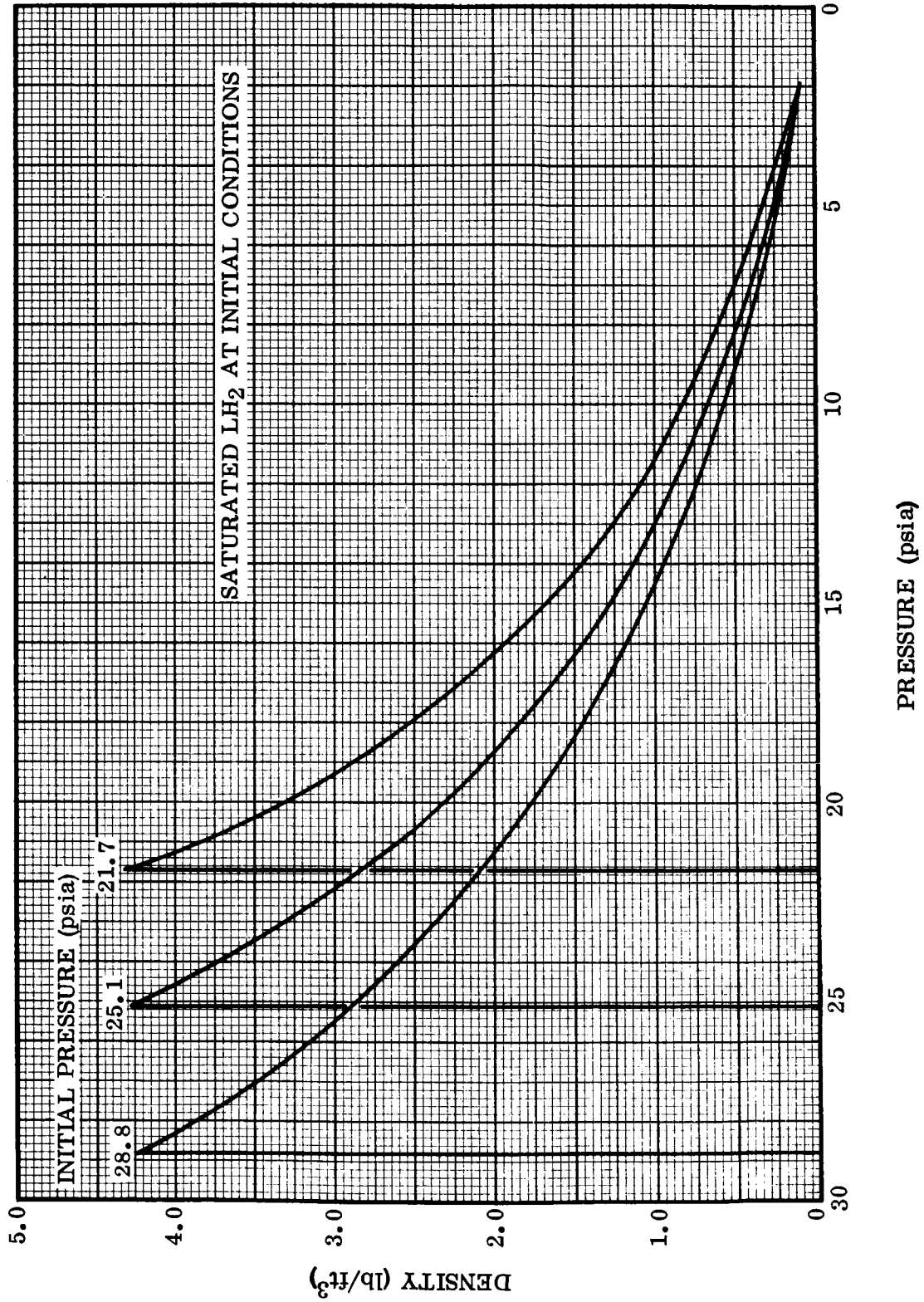


Figure B-2. Density Versus Pressure for Constant Enthalpy Flashing Flow Across a Restriction

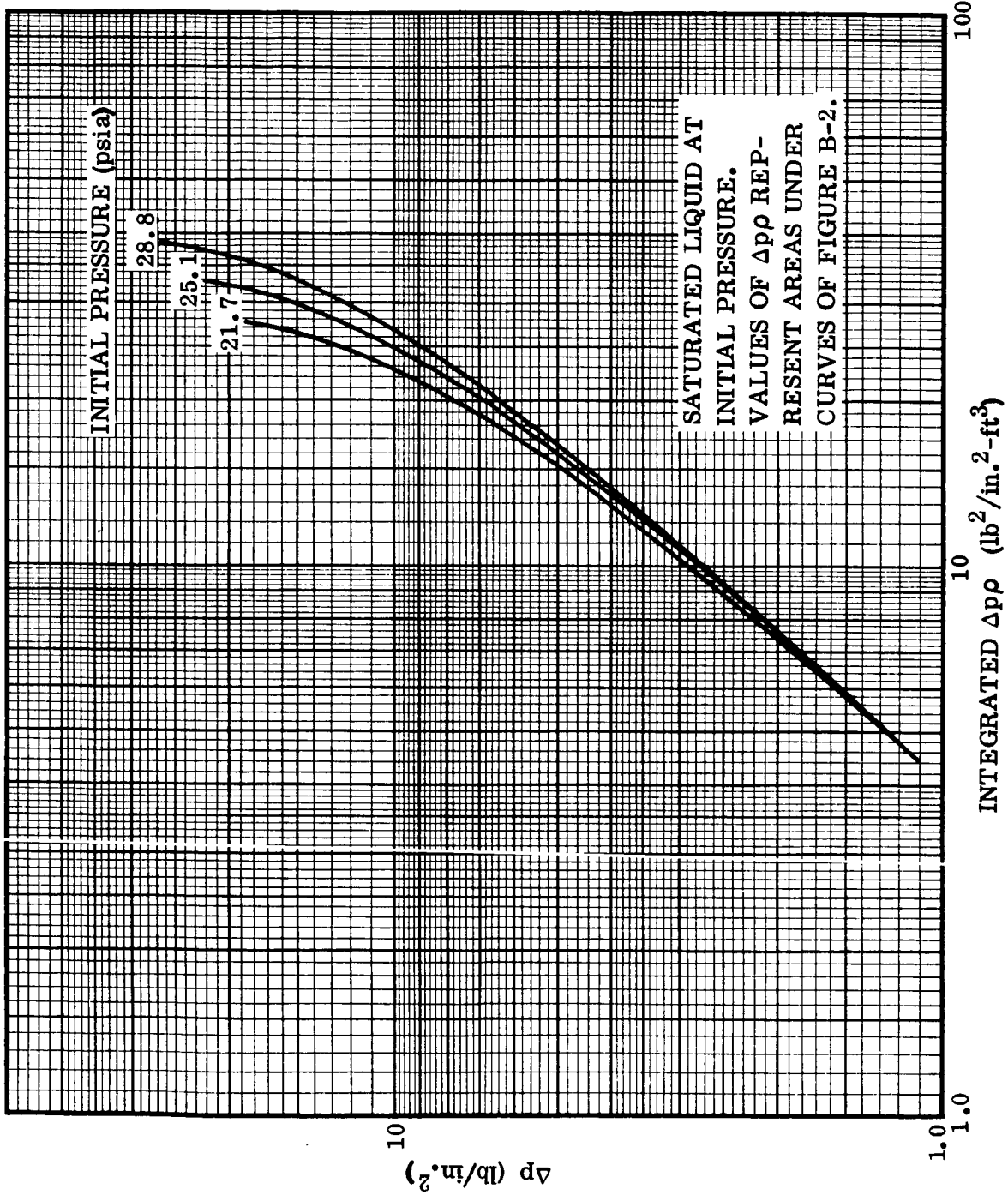


Figure B-3. Integrated $\Delta p\rho$ for Constant Enthalpy Flashing Flow Across a Restriction

$$p_u = 20 \text{ psia}$$

$$p_d = 5 \text{ psia}$$

$$C_v = 0.8$$

Then from Figure B-3 the integrated $\Delta p \rho = 25 \text{ lb}^2/\text{in.}^2\text{-ft}^3$ and from Equation 5

$$\text{Minimum operating area} = 0.02245 \text{ in.}^2 \text{ or equivalent diameter} = 0.169 \text{ in.}$$

Maximum Area of R₁ Regulator

Saturated H₂ gas at 20-psia inlet and 5-psia downstream, with 0.35 lb/sec flow.

$$C_v = 0.8$$

$$\rho_u = 0.112 \text{ lb/ft}^3$$

Using Equation 7 for critical flow, with $\gamma = 1.35$

$$\text{Required, full-open valve area} = 0.916 \text{ in.}^2 \text{ or equivalent diameter} = 1.08 \text{ in.}$$

Sizing of the Turbine Nozzle Flow Area. (For 0.35 lb/sec and $\Delta p = 0.8$ psi)

Hydrogen at inlet to nozzle is, at design conditions,

$$p_u = 4.9 \text{ psia}, T_u = 34.1^\circ\text{R}; \text{ and } p_d = 4.1 \text{ psia} \quad \rho_u = 0.027 \text{ lb/ft}^3$$

Then from Equation 6 for $p_d/p_u = \frac{4.1}{4.9} = 0.836$ and $C_v = 1$

$$\text{Total nozzle area} = 3.92 \text{ in.}^2$$

Sizing of Downstream By-Pass (R₃). (For a minimum flow rate of 0.06 lb/sec with gas at inlet to the system.)

Since the pressure drop through the turbine nozzle is very low for the 0.06 lb/sec flow rate, the Δp across the nozzle can be found with sufficient accuracy using Equation 5 for gas flow. For the 0.06 lb/sec flow condition

$$p_3 = 5 \text{ psia}$$

$$T_3 = 38.5^\circ\text{R}$$

$$\rho_3 = 0.0244 \text{ lb/ft}^3$$

$$\text{Nozzle area} = 3.92 \text{ in.}^2$$

$$C_v = 1$$

and

$$\text{Turbine } \Delta p = 0.0215 \text{ psi}$$

Then for critical flow through R₃ with $p_4 = 4.98$ psia;

$$\rho_4 = 0.0244 \text{ lb/ft}^3$$

$$C_v = 0.8$$

$$\gamma = 1.35$$

Then from Equation 7

$$\text{By-pass area} = 0.673 \text{ in.}^2 \quad \text{or} \quad \text{diameter} = 0.925 \text{ in.}$$

Sizing of Downstream Valve (R_2), for a Total Flow Rate Through Both (R_2) and (R_3) of 0.35 lb/sec With a Gas Inlet to the System.

For

$$p_4 = 4 \text{ psia} \quad T_4 = 37^\circ\text{R} \quad \rho_4 = 0.0203 \text{ lb/ft}^3$$

from Equation 7 for critical flow where $C_v = 0.8$

$$A_{R2} + A_{R3} = 4.8 \text{ in.}^2$$

and

$$R_2 \text{ valve area} = 4.8 - 0.673 = 4.127 \text{ in.}^2 \text{ or equivalent diameter} = 2.3 \text{ in.}^2$$

The actual area would probably be somewhat larger depending on the minimum pressure allowed upstream of the vent thrust nozzles. Assuming a 0.5-psi drop across the valve, calculations show a required valve area of approximately 8 in.² or equivalent diameter of 3.2 inches for a valve loss coefficient of 3 (typical of a popet type valve).

Estimation of Line Sizes. The lines are sized for a Mach number of 0.1 to minimize pressure drop and velocity effects. The critical case for line sizing is when all-gas enters the system.

Upstream of R_1

$$p_1 = 20 \text{ psia} \quad T_1 = 38.5^\circ\text{R} \quad \gamma = 1.4 \quad R = 767 \text{ ft-lb/lb-}^\circ\text{R}$$

Then

$$c_s = \sqrt{\gamma g_o RT} = 1153 \text{ fps} \quad u_1 = 115.3 \text{ fps}$$

and from $\dot{W} = \rho_1 A_1 u_1$

$$A_1 = 3.9 \text{ in.}^2 \quad D_1 = 2.225 \text{ in.}$$

At Station 2

$$p_2 = 5 \text{ psia}; \quad T_2 = 35.5^\circ\text{R}; \quad \rho_2 = 0.0264 \text{ lb/ft}^3$$

Assuming the velocity of sound does not change significantly from 1153 fps

$$A_2 = 16.55 \text{ in.}^2 \quad D_2 = 4.6 \text{ in.}$$

At Station 3

$$\text{Maximum } T_3 = 38.5^\circ\text{R}$$

$$p_3 = 4.9 \text{ psia}$$

$$\rho_3 = 0.02385 \text{ lb/ft}^3$$

and

$$A_3 = 18.3 \text{ in.}^2$$

$$D_3 = 4.82 \text{ inches}$$

At Station 4

$$p_4 = 4 \text{ psia}$$

$$T_4 = 37^\circ\text{R}$$

$$\rho_4 = 0.0203 \text{ lb/ft}^3$$

$$A_4 = 21.5 \text{ in.}^2$$

$$D_4 = 5.24 \text{ inches}$$

B.3 HEAT EXCHANGER SIZING, CRYOGENIC SERVICE MODULE. For the low vent flows required (approximately 1 to 2 lb/hr), the heat exchanger itself can be made very light. The power required to operate the circulating pump is an important factor in the overall weight considerations. For the system to operate properly the tank content must be mixed to prevent the formation of hot spots, since no settling thrust is assumed with accompanying buoyancy forces. For comparison purposes the same mixing requirement is assumed for the cryogenic service module heat exchanger system as for the mechanical separator system. Based on mixing requirements for the LH₂ tank an average fluid velocity of 0.1 fps (Paragraph C.4) is available for forced convection heat transfer. A plain tube type heat exchanger is assumed. The calculations follow.

Assuming liquid flowing at right angles to the outside of a cylindrical tube, the basic equation for the film coefficient is, from Reference B-4

$$\frac{h_m D_o}{k_f} = 0.35 + 0.56 \left(\frac{D_o G}{\mu_f} \right)^{0.52}$$

h_m = mean film transfer coefficient Btu/hr-ft²-°F, i.e., mean transfer coefficient around entire tube

Assuming a 1/2-inch-diameter tube

$$D_o = 0.0416 \text{ ft}$$

$$k_f = \text{thermal conductivity of fluid at film temperature, Btu/hr-ft-}^\circ\text{F} = 0.069$$

$$\mu_f = \text{absolute viscosity of fluid at film temperature} = 8.5 \times 10^{-6} \text{ lb/ft-sec}$$

G = mass velocity of fluid, lb/hr-ft²

$G = u \rho_L$ and $u = 0.1$ ft/sec

then

$$G = 4.34 (0.1) 3600 = 1560 \text{ lb/ft}^2\text{-hr}$$

$$h_m (0.0416) = 0.35 (0.069) + 0.0386 (5420)^{0.52}$$

$$h_m = 81.4 \text{ Btu/hr-ft}^2\text{-}^\circ\text{F}$$

To vaporize 1 lb/hr vent

$$q = 189 \text{ Btu/hr} = U_m A_s \Delta T$$

at $\Delta T = 7.5^\circ\text{F}$ and letting $U_m = h_m$. The required surface area $A_s = 0.31 \text{ ft}^2$.

For Gaseous Flow Over the Tube

$$\frac{h_m D_o}{k_f} = B \left(\frac{D_o G}{\mu_f} \right)^n \text{ from Reference B-4 where } B \text{ and } n \text{ are functions of } Re$$

$$Re = \frac{D_o G}{\mu_f}$$

$$D_o = 0.0416 \text{ ft}$$

$$G = \rho_v u = 0.115 (0.1) 3600 = 41.4 \text{ lb/hr-ft}^2$$

$$\mu_f = 2.52 \times 10^{-3} \text{ lb/ft-hr}$$

$$Re = 684 \quad k_f = 0.009 \text{ Btu/hr-ft-}^\circ\text{R}$$

From Table 10-3 of Reference B-4

$$n = 0.466$$

$$B = 0.615$$

$$h_m \frac{(0.0416)}{0.009} = 0.615 (684)^{0.466} = 2.8 \text{ Btu/hr-ft}^2\text{-}^\circ\text{F}$$

Letting $h_m = U_m$

$$q = h_m A_s \Delta T$$

$$A_s = \frac{189}{2.8 (7.5)} = 9 \text{ ft}^2$$

$$\text{Required length of tubing } L = \frac{A_s}{\pi D_o} = 825 \text{ in.}$$

Assuming the use of 0.02-inch wall aluminum alloy tubing

$$\text{Tubing weight} = \pi 0.5 (0.02) 825 (0.1) = 2.59 \text{ lb}$$

Allowing for fittings and mounting

$$\text{Total weight} = 2.59 (1.43) = 3.7 \text{ lb}$$

For Gaseous Flow Using a 1/4-in. Tube

$$\frac{h_m D_o}{k_f} = B \left(\frac{D_o G^n}{\mu_f} \right)$$

$$k_f = 0.009 \text{ Btu/ft-hr-}^\circ\text{F} \quad D_o = 0.0208 \text{ ft} \quad G = 41.4 \text{ lb/hr-ft}^2$$

$$\mu_f = 2.52 \times 10^{-3} \text{ lb/ft-hr}$$

$$\text{Re} = 328$$

then

$$n = 0.466$$

$$B = 0.615$$

$$h_m = 4.6 \text{ Btu/hr-ft}^2\text{-}^\circ\text{F}$$

$$A_s = 5.5 \text{ ft}^2$$

$$L = 1050 \text{ in.}$$

Vent-side pressure drops are determined for a single length of tubing with a gaseous hydrogen flow of 1 lb/hr.

Heat exchanger pressure is 5 psia, and average gas density 0.0261 lb/ft³.

For the 1/2-in. -diameter tube by 825-in. long

$$\text{Flow area } A_c = 0.196 \text{ in.}^2$$

$$G = 735 \text{ lb/hr-ft}^2$$

for

$$\xi_c = 0.45, \quad \xi_e = 0.25 \text{ and } f = 0.03 \quad f \frac{L}{D} = 49.5$$

and from Equation 1

$$\Delta p = 0.0087 \text{ psi}$$

It is seen from the above analysis that the pressure drop is approximately inversely proportional to tube diameter to the fifth power and directly proportional to length.

Then for the 1/4-in. -diameter tube by 1050-in. long, the estimated pressure drop

$$\Delta p = 0.0087 (32) \left(\frac{1050}{825} \right) = 0.354 \text{ psi}$$

To maintain a minimum pressure drop, it is decided to use the 1/2-inch-diameter tube for the predesign with the worst case of GH_2 on the outside of the tube.

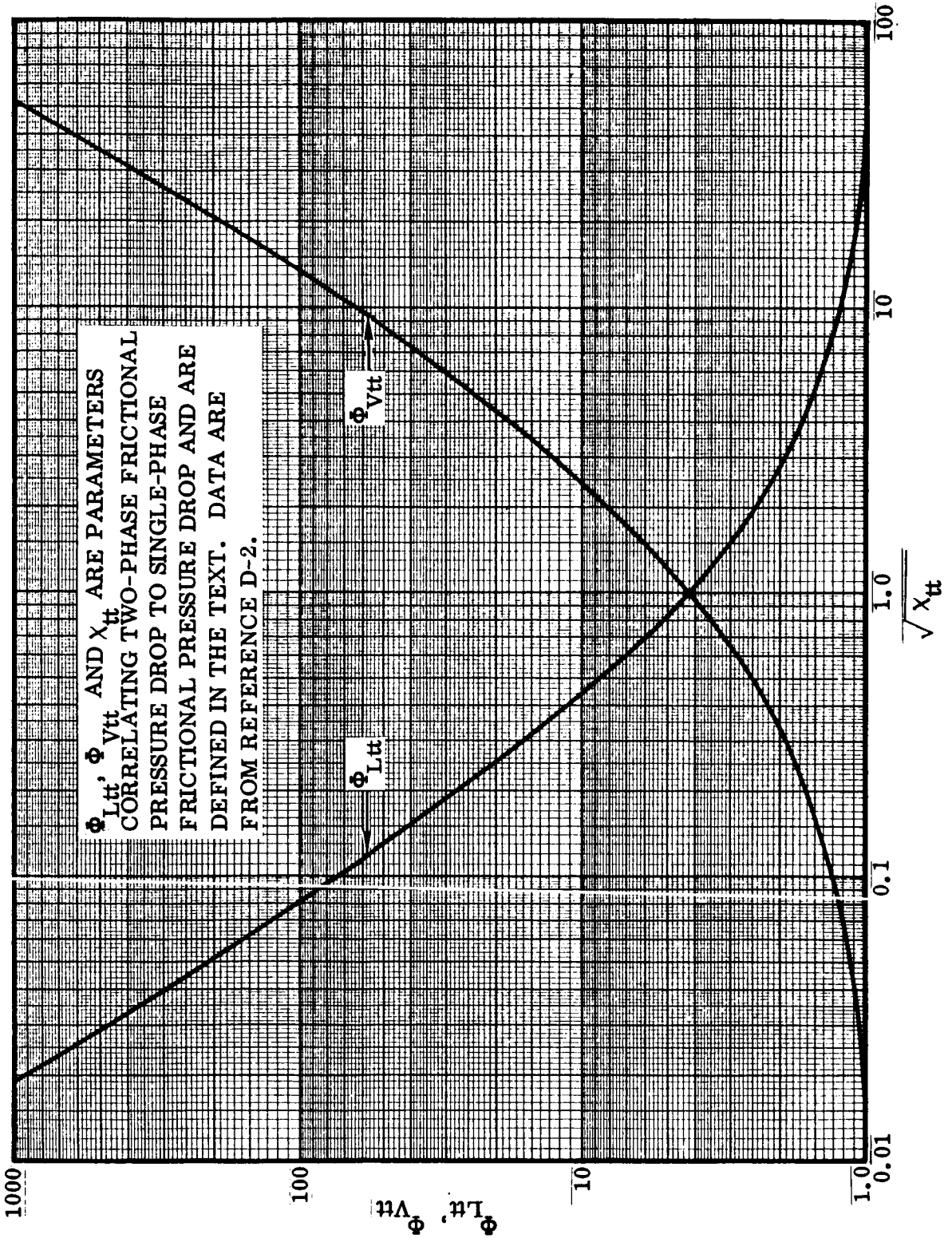


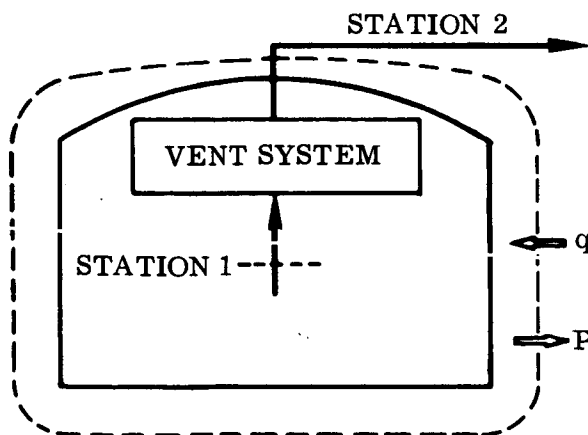
Figure D-1. Φ_{Ltt} and Φ_{Vtt} Versus $\sqrt{\chi_{tt}}$

APPENDIX E

CALCULATION OF SEPARATION SYSTEM EFFECT ON PAYLOAD WEIGHT

If a vehicle with a vent separator system is compared with one without such a system and that idealistically vents only saturated vapor (no liquid), there are three factors that can cause a difference in vehicle performance or available payload weight: separator hardware weight, exit enthalpy of the vent stream, and external energy dissipated in the tank. Therefore, the following method of estimating system effects upon payload was developed for a common basis for comparing the weight and performance of different separation systems. First, in Paragraph E.1, an expression is derived for the change in vent rate required to maintain constant pressure in a tank which is subjected to changes in external heat and power input and in vent stream enthalpy. This result is used in Paragraph E.2 as part of the outline of calculation of total change in payload weight.

E.1. VENT RATE REQUIRED TO MAINTAIN TANK AT CONSTANT PRESSURE. Consider a propellant tank with total volume V_T ; constant heat input rate, q , and power output, P ; and tank pressure, p , and temperature, T , which are constant both with position in the tank and with time. The inlet stream to the vent system, Station 1 in the sketch, will then have the same T and p as the tank bulk fluid. There is assumed to be no thermal stratification in the tank.



The following mass and volume balance equations can be written for the tank, with subscripts L, V, and T referring to the liquid in the tank, vapor in the tank, and total tank contents respectively.

$$m_L + m_V = m_T$$

$$\frac{m_L}{\rho_L} + \frac{m_V}{\rho_V} = V_T \quad (2)$$

These can be manipulated into the following form, where e is defined as the vapor density to liquid density ratio in the tank.

$$m_L = \frac{m_T - V_T \rho_V}{1 - e} \quad (3)$$

In a differential time interval, dt , this becomes

$$dm_L = \frac{dm_T}{1 - e} \quad (4)$$

and, by noting that $dm_2 = -dm_T$ and $dm_V = -e(dm_L)$, Equation 4 yields the following two equations.

$$dm_L = -\frac{dm_2}{1 - e} \quad (5)$$

$$dm_V = \frac{e dm_2}{1 - e} \quad (6)$$

Application of the First Law of Thermodynamics to the total tank system for unit time gives

$$\frac{dE_T}{dt} = q - P - \dot{m}_2 h_2 \quad (7)$$

where dE_T/dt is the time rate of change in internal energy of the tank contents, which can also be expressed as

$$\frac{dE_T}{dt} = \left[(h - p/\rho)_L \dot{m}_L + (h - p/\rho)_V \dot{m}_V \right]_T$$

$$= \left[\frac{eh_L - h_V}{1 - e} \right] \dot{m}_2 \quad (8)$$

Combining Equations 7 and 8 gives the following expressions for the required vent rate to maintain constant pressure in the tank.

$$\dot{m}_2 = \frac{q - P}{h_2 + (h_V - eh_L)/(e - 1)}$$

$$\dot{m}_2 = \frac{q - P}{e\lambda/(1 - e) - h_2 - h_L} \quad (9)$$

Here λ is the heat of vaporization at tank conditions and e , as previously defined, is equal to ρ_V/ρ_L .

We now consider two tank systems with different heat input and energy output rates, but with identical tank temperatures and pressures. With the original case and new case designated by subscripts o and n , respectively, and letting $P_o = 0$, Equation 9 can be applied to give

$$\Delta \dot{m}_2 = \dot{m}_{2n} - \dot{m}_{2o}$$

$$\Delta \dot{m}_2 = \frac{(h_{2o} - h_{2n}) \dot{m}_{2o} - P_n}{e\lambda/(1 - e) + h_{2n} - h_L} \quad (10)$$

E.2. METHOD OF CALCULATING PAYLOAD WEIGHT CHANGE. The separation system hardware weight, external power requirement, and exit vent fluid enthalpy are determined by conventional engineering techniques; Sections 2 through 6 are illustrative. The original or base case tank conditions are then assumed in order to evaluate the corresponding terms in Equation 10. For most comparisons in this report the tank base conditions were taken to be 20-psia saturated hydrogen. The base case vent rate, \dot{m}_{2o} , was taken to be 667 lb/hr for the S-IVB (except for a few of the parametric results in Section 12) and 1/2 lb/hr for each tank of the two-tank CSM. The change in vent rate is then calculated from Equation 10. In this study, the total changes in vented propellant weight were based on operational times of 4.5 hours for the S-IVB and 205 hours for the CSM. The total change in payload weight, which is the sum of the hardware and change in vent weight contributions, is calculated from the hardware weight, change in vented propellant weight, and the proper exchange ratios (i. e., change in payload weight per unit change in hardware, or vented weight) for each contribution taken from Table E-1. For the two overall vehicle configurations indicated, Table E-1 gives the loss in LEM gross weight (pounds) per 1-pound increase in the hardware weights and propellant boiloff weights shown.

Table E-1. Exchange Ratios

	CURRENT SATURN- APOLLO-LEM	CURRENT SATURN AND O ₂ /H ₂ APOLLO SERVICE MODULE
S-IVB Hardware	0.67	0.75
S-IVB Boiloff in Parking Orbit	0.352	0.394
Service Module Hardware	---	1.43
Service Module Boiloff During Earth Orbit and 72-hr Transfer to Lunar Orbit	---	0.75
Service Module Boiloff During Stay in Lunar Orbit (62 hr)	---	1.0
Service Module Boiloff After Departure From Lunar Orbit (71 hr)	---	1.43

APPENDIX F

TURBINE ANALYSIS

The method used for turbine analysis in the work described in Sections 9 through 12 is outlined in this section.

The turbine is assumed to be a single-stage impulse, axial flow, full admission type. Nominal operation is with a gas inlet. The buckets are symmetrical (equal inlet and outlet angles) for ease of manufacture. A velocity diagram is shown in Figure F-1. Turbine performance is determined from using the methods and the data given in Reference F-1.

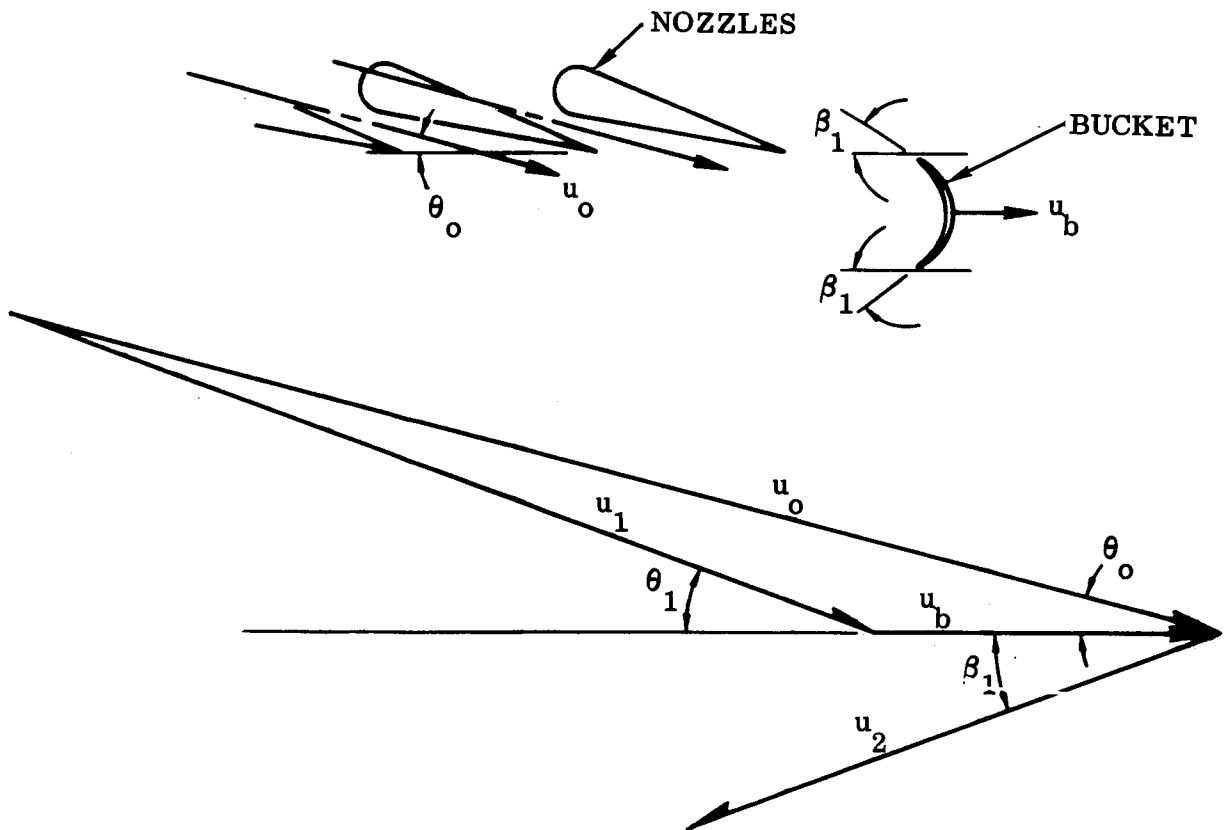


Figure F-1. Impulse Stage Velocity Diagram

The following equation is used to determine the tangential driving force, F_b , exerted on the turbine buckets by the vent gas.

$$F_b = \frac{\dot{W}_V}{g_o} (u_1 \cos \theta_1 + u_2 \cos \beta_1) \quad (1)$$

The terms are as defined in Figure F-1. Optimum turbine performance is obtained when the relative fluid inlet angle θ_1 is equal to the bucket inlet angle β_1 . Taking this as the design condition at the nominal operating point and introducing a velocity loss coefficient, ψ , ($u_2 = \psi u_1$), to account for the various turbine inefficiencies permits Equation 1 to be written as

$$F_b = u_1 \frac{\dot{W}_V}{g_o} (1 + \psi) \cos \beta_1 \quad (2)$$

where $\psi = \psi_1 - 0.000432 \nu^{4/3}$ and the bucket turning angle $\nu = 180^\circ - (\theta_1 + \beta_1)$.

The coefficient ψ_1 is a function of the relative entrance velocity, u_1 , and is plotted in Figure F-2.

The torque is calculated from an extension of Equation 2.

$$\tau = F_b r_t = r_t \frac{\dot{W}_V}{g_o} u_1 (1 + \psi) \cos \beta_1 \quad (3)$$

and the power from

$$P = \tau \omega_t = \omega_t r_t \frac{\dot{W}_V}{g_o} u_1 (1 + \psi) \cos \beta_1 \quad (4)$$

The minimum practical fluid entrance angle, θ_1 , is estimated to be 20 degrees (Reference F-1).

The equations are also used to calculate turbine performance of a fixed design at off-design conditions where, in this case, the bucket angles, nozzle angle (θ_o), and flow area are kept constant.

Where $\theta_1 \neq \beta_1$ at off-design conditions equations for torque and power are written as

$$\tau = r_t \frac{\dot{W}_V}{g_o} u_1 (\cos \theta_1 + \psi \cos \beta_1) \quad (5)$$

$$P = \omega_t r_t \frac{\dot{W}_V}{g_o} u_1 (\cos \theta_1 + \psi \cos \beta_1) \quad (6)$$

It is noted that the maximum turbine efficiencies calculated using the above equations are about 60 percent, which is a slightly higher value than the maximum used for the predesigns discussed in Paragraph 2.2 and Appendix B.

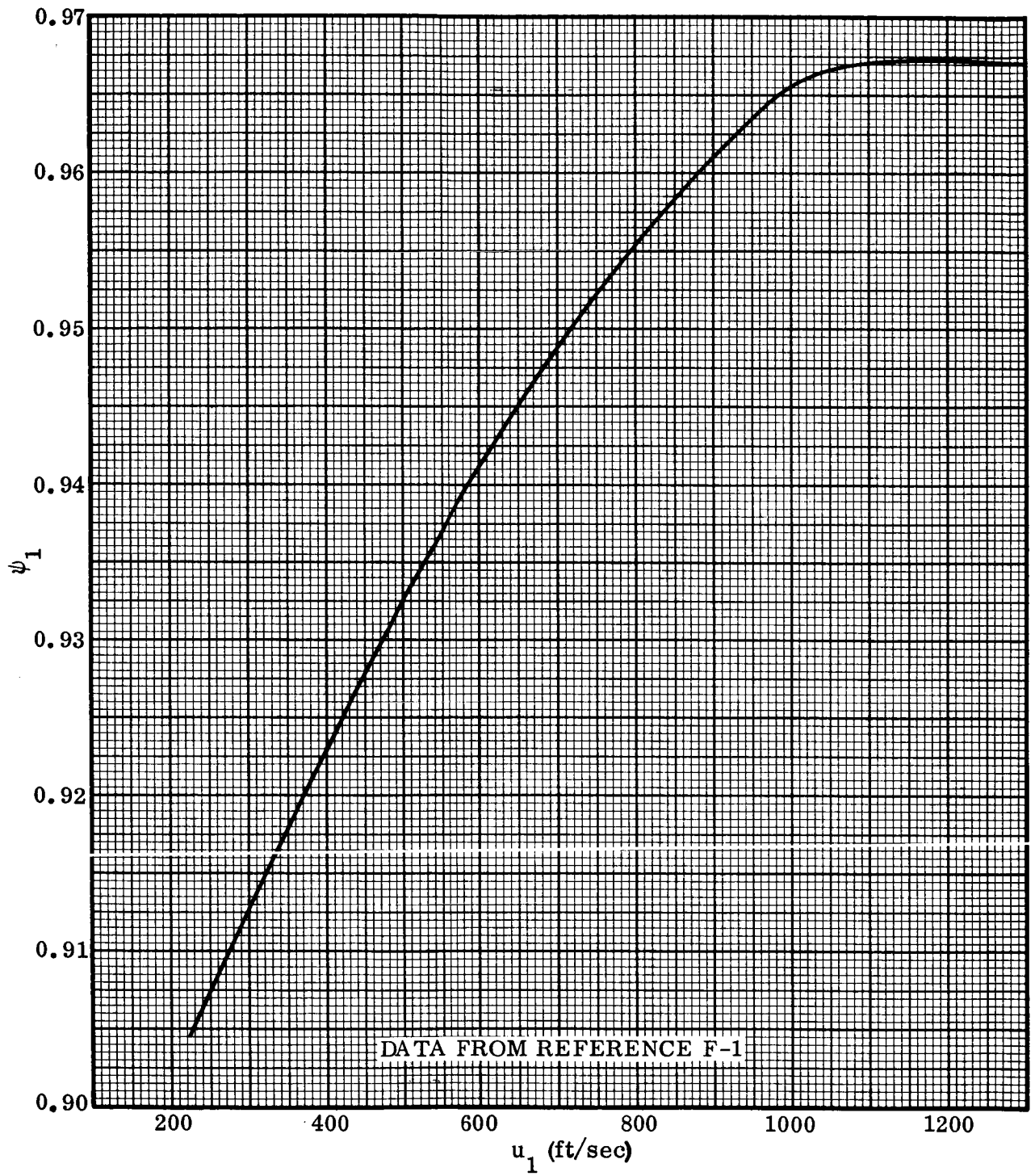


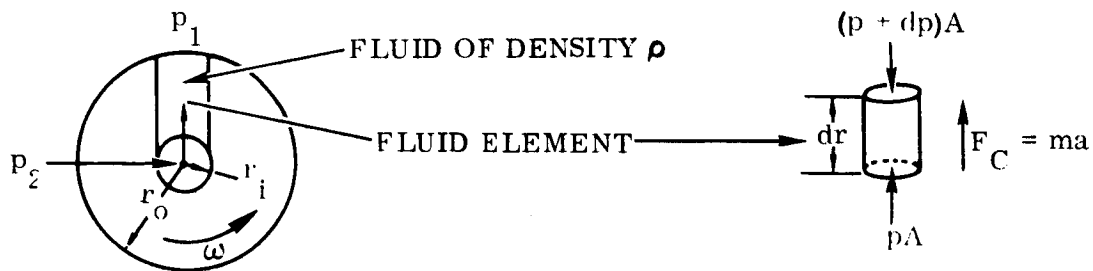
Figure F-2. Turbine Bucket Velocity Loss Parameter

APPENDIX C

MECHANICAL SEPARATOR PREDESIGN CALCULATIONS

C.1 SEPARATION CRITERIA. In the case of the mechanical-type separator, vapor/liquid separation is accomplished by centrifugal forces imparted to the liquid by the separator wheel. Applicable separation equations are derived in terms of the major forces involved. The following analysis is made for a separator passage completely filled with liquid.

The sketch shows a force balance on fluid entrapped in the separator



where F_C = centrifugal force on the fluid element.

For zero flow of the fluid

$$pA + (\rho A dr) r \omega^2 = (p + dp)A \quad (1)$$

and

$$\int dp = \int \rho \omega^2 r dr \quad (2)$$

For constant ρ and ω and integrating between the limits p_2 , p_1 and r_i , r_o

$$(p_1 - p_2) = \frac{\rho \omega^2 (r_o^2 - r_i^2)}{2g_o} \quad (3)$$

and for the limiting case where $r_i = 0$

$$(p_1 - p_2) = \frac{\rho \omega^2 r_o^2}{2g_o} \quad (4)$$

Then for a given Δp across the separator and a value of ωr_o greater than that calculated from Equation 4 the liquid will be thrown out of the separator.

Looking now at the case where the liquid exists as fine droplets, it is seen that the drag force on the liquid of the gas flowing into the separator is the primary force causing liquid to enter the separator. Centrifugal force imparted to the liquid by the separator is the dominant force in keeping liquid out of the unit. The analysis assumes inlet design such that the worst separation case is when liquid droplets are rotating with the wheel, i. e., small droplets that are not rotating with the wheel will impinge on the wheel, coalesce, and be thrown out. This is accomplished by the use of curved inlet vanes.

The drag force on a drop is

$$F_D = \frac{C_D \rho_V (u_V)^2 A_D}{2g_o} \quad (\text{Reference C-1}) \quad (5)$$

Assuming a spherical drop

$$V_L = \pi D_L^3 / 6$$

$$A_L = \pi D_L^2 / 4$$

and

$$F_D = \frac{C_D \pi \rho_V D_L^2 (u_V)^2}{8g_o} \quad (6)$$

The centrifugal or outward force on the drop is

$$F_C = ma = \rho_L \frac{\pi D_L^3 r \omega^2}{6} \quad (7)$$

Equating the drag force (6) to the centrifugal force (7) to determine conditions at which liquid will not enter the separator gives an equation for the theoretical droplet size that will just be "separated". Where the flow past the drop is turbulent such that the drag coefficient (C_D) can be assumed to be 1, then

$$D_L = \frac{3}{4} \frac{\rho_V (u_V)^2}{\rho_L r \omega^2} \quad (8)$$

It is seen from Reference C-1 that $C_D = 1$ is a reasonable and slightly conservative assumption for $\left(Re = \frac{\rho_V u_V D_L}{\mu_V}\right)$ values above 100. Reynolds number versus gas velocity

as a function of droplet diameter, D_L , is presented in Figure C-1, showing the range of applicability of Equation 8. Based on Equation 8, plots of gas velocity versus the theoretically-separated-drop diameter are shown in Figure C-2 as a function of $r\omega^2$.

From flow and speed data obtained from testing with GH_2/LH_2 , a satisfactory (separation was accomplished) operating point of the Convair separator is shown in Figure C-2. The estimated operating point of the Pesco separator is also indicated on Figure C-2.

To compare the separation requirement when the liquid exists as small drops (Equation 8) with that for liquid in large slugs (Equation 4), an inlet gas velocity of 42 ft/sec and a separator diameter of 9 inches is assumed. This condition is somewhat similar to the operating conditions existing with the Convair separator. For the case where the liquid exists as droplets of 0.001-inch diameter, it is seen from Figure C-2 that a separator speed of approximately 10,000 rpm is required to separate. For this inlet gas velocity the pressure drop across the separator is calculated from

$$\Delta p = \xi \frac{\rho_V u_V^2}{2g}$$

where the loss coefficient $\xi = 3$ corresponds to an equivalent orifice coefficient of 0.575.

Then

$$\Delta p = \frac{3 (0.112) (42)^2}{2 (32.2)} = 9.2 \text{ lb/ft}^2$$

and from Equation 4 the required separation speed for a liquid-filled passage is

$$\omega = \sqrt{\frac{(9.2) 2 (32.2) 144}{(4.34) (4.5)^2}} = 31.2 \text{ rad/sec}$$

or only 298 rpm.

The pressure drop of the gas flow into the separator due to centrifugal force on the gas should also be considered and is calculated from Equation 4 at 300 rpm as 0.245 lb/ft^2 , resulting in an insignificant change in the answer above. This analysis agrees with unpublished test data obtained at Convair showing the critical separation case to be when small liquid droplets occur at the separator.

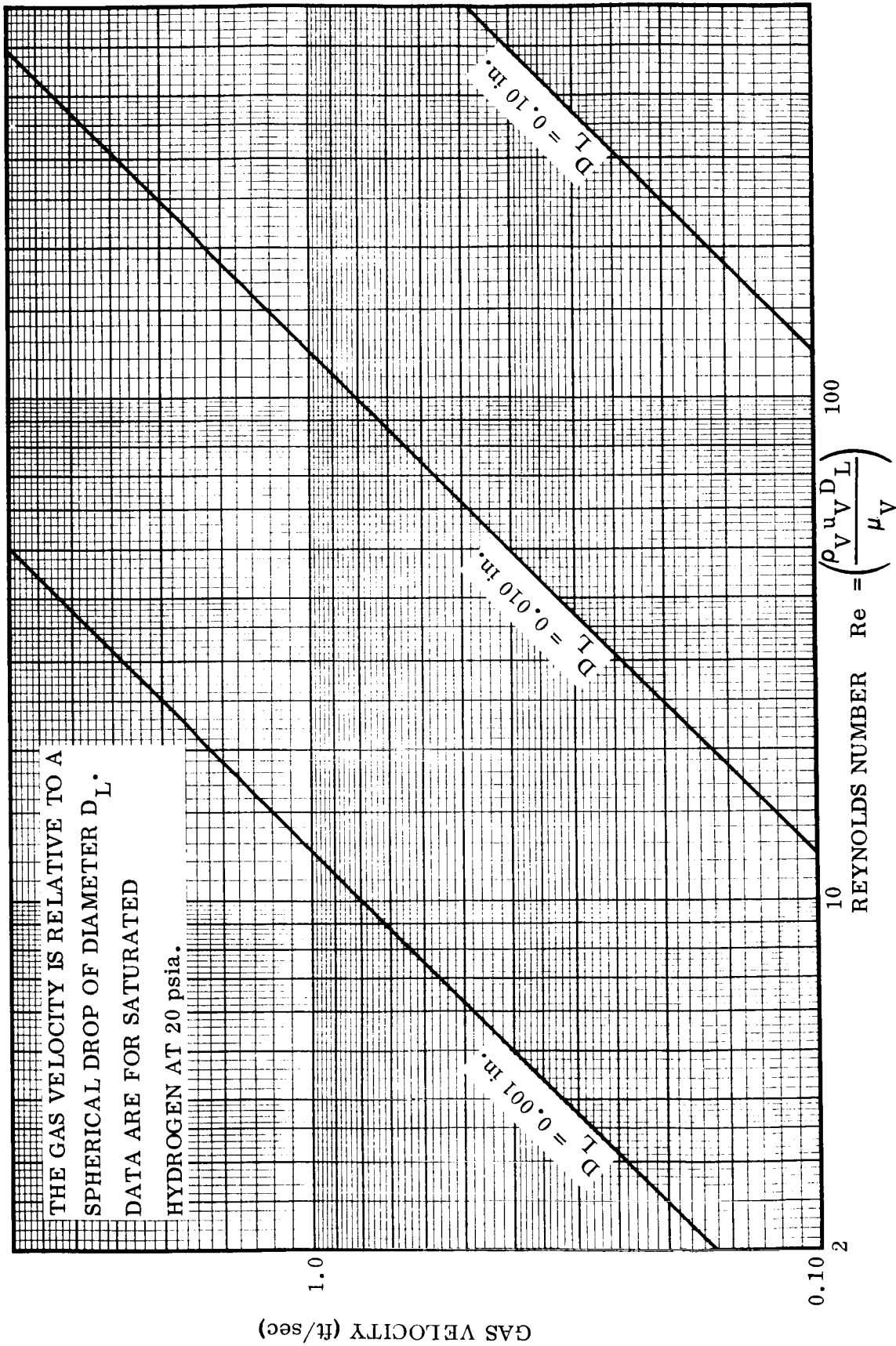


Figure C-1. Reynolds Number Versus Gas Velocity for Various Liquid Drop Diameters

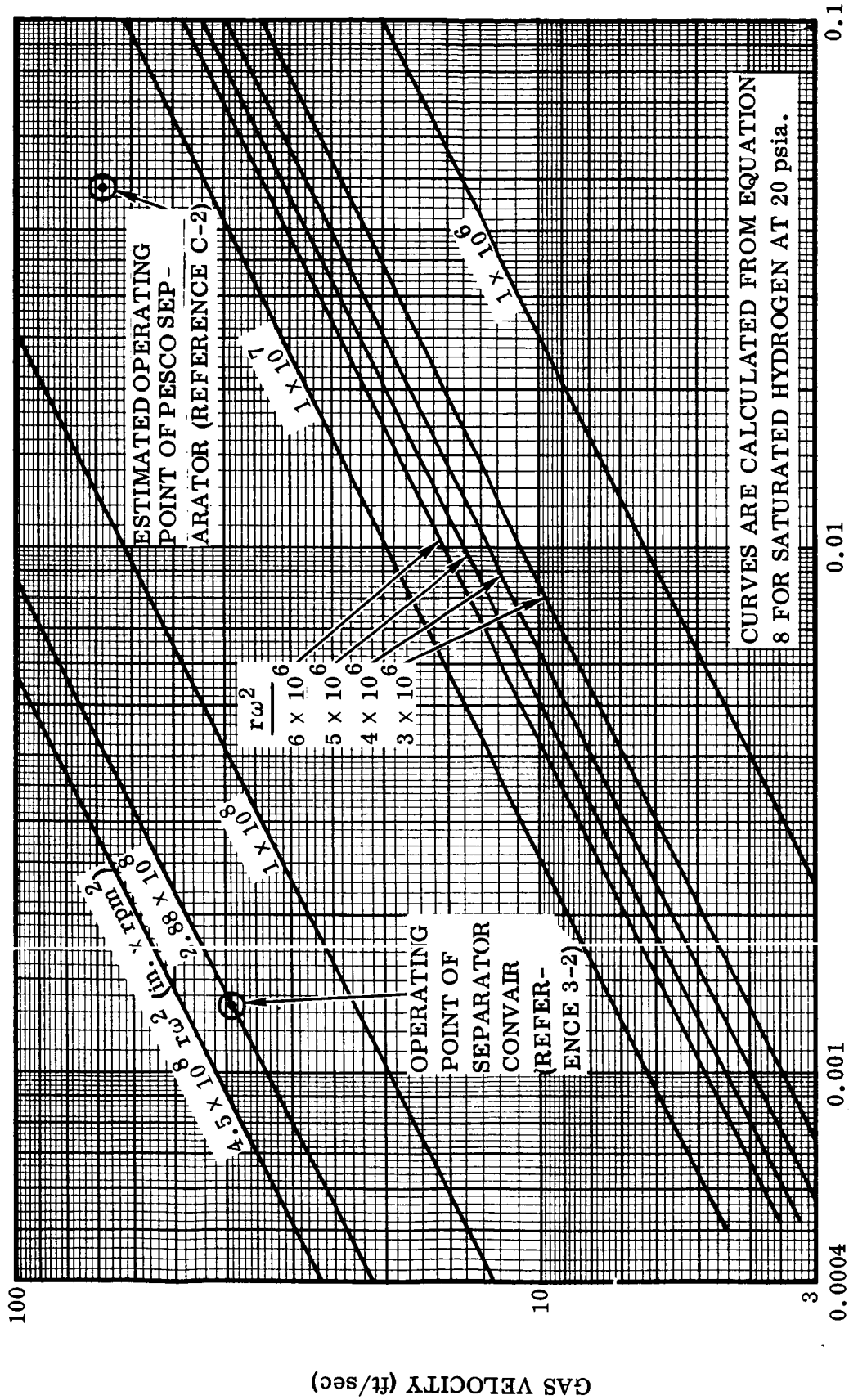


Figure C-2. Inlet Gas Velocity Versus Separated-Drop Diameter as a Function of Separator Speed and Radius

Based on the foregoing analysis, it is assumed for the separator predesign calculations that the separation of all liquid drops greater than 0.001 inch is required. The test data indicate this to be a reasonably conservative assumption and should result in essentially 100-percent separation efficiency at inlet qualities above 10 percent (90-percent liquid by weight).

It is interesting to note that measurements of stable water fog droplets in the air show a size range of from 15 to 40 microns or on the average approximately 0.001 inch.

C.2 POWER REQUIRED TO SEPARATE. The dynamic head or kinetic energy that needs to be imparted to the fluid to prevent its entering the separator is represented by $\frac{r^2 \omega^2}{2g_o}$; i. e., the energy required to accelerate the liquid particle to its rotational velocity required for "separation".

Taking the total separator pumping power as

$$P = (\text{Head}) (Q) \rho \quad (9)$$

we have the theoretical power required for separation of \dot{W}_L lb/sec of liquid as

$$P = \frac{r^2 \omega^2}{2g_o} \dot{W}_L$$

In the present analysis \dot{W}_L is assumed to be equal to the maximum amount of liquid coming into the vicinity of the separator during venting. For a gas vent rate, \dot{W}_V , and an average fluid quality, X , the amount of liquid requiring separation will be

$$\dot{W}_L = \dot{W}_V \left(\frac{1-X}{X} \right) \quad (10)$$

and the required power is

$$P = \frac{r^2 \omega^2}{2g_o} \dot{W}_V \left(\frac{1-X}{X} \right) \quad (11)$$

It should be noted that Equation 11 represents only the theoretical design point of the separator. At qualities lower than design or at flow rates higher than design, the unit separation efficiency will drop off sharply. For a particular separator operating at off-design conditions, the power consumed will be approximately proportional to the average density of the operating medium at a constant speed and for operation at constant density the power will vary approximately as the cube of the speed (Reference C-3).

C.3 DEVELOPMENT OF PREDESIGN DATA FOR THE S-IVB CONTINUOUS VENT CASE. Weight and performance data are generated for the model shown in Figure 3-3. To define representative dimensions of the unit over a range of operating conditions it is assumed that the width of the separator inlet is one-fourth its diameter, i. e., the

maximum inlet flow area is $\frac{\pi D^2}{4}$ where D is the diameter of the separator disk. This length-to-diameter ratio is chosen because it allows reasonably optimum packaging of the unit throughout a range of sizes. Then from the continuity equation ($\dot{W}_V = \rho_V A u_V$) and Equation 8 the minimum size drop that will be separated is

$$D_L = \frac{3}{4} \frac{\dot{W}_V^2}{\rho_L \rho_V \pi^2 r^5 \omega^2} \quad (12)$$

For the maximum flow rate of $\dot{W}_V = 0.35$ lb/sec and 20-psia saturated hydrogen, Equation 12 is solved for droplet diameter versus required separator speed and the results plotted in Figure C-3 for various separator wheel radii. Inlet gas velocities versus separator diameter and total flow area are also plotted for general information in Figure C-4 for vent gas flow rates of 0.35 and 0.06 lb/sec. The theoretical power requirement is calculated from Equation 11 and plotted as a function of separator speed in Figure C-5 for various wheel radii for a vent gas flow rate of 0.35 lb/sec and a quality of 0.10 (90-percent liquid by weight). From Figures C-3 and C-5 it is seen that, for the model chosen, the larger the wheel diameter the lower the power requirement for a given separation requirement. For the requirement to "separate" all liquid droplets greater than 0.001 inch in diameter a reasonable compromise for the present case between power, size, and speed appears to be a separator diameter of 10 inches. This design results in a separator speed of 1300 rpm and a theoretical power requirement of 0.29 horsepower. The actual horsepower required to drive the separator must include inefficiencies in the pumping action and bearing and seal losses. Disk friction losses are not included since the analysis assumes such action of the disks contributes to the total pumping required for separation. In the present case it is assumed that bearing and separation losses result in an overall separator efficiency of 75 percent, giving a total power requirement of 0.39 horsepower and a torque of 1.574 ft-lbf.

An equation for average fluid density as a function of quality is derived from the relation $v_X = v_L + X v_{fg}$ as

$$\rho_X = \frac{1}{\frac{(1-X)}{\rho_L} + \frac{X}{\rho_V}} \quad (13)$$

For $X = 0.1$ and saturated hydrogen at 20 psia $\rho_X = 0.91$ lb/ft³. The horsepower required for unit operation in 100-percent LH₂ and 100-percent GH₂ at 1300 rpm is calculated as follows.

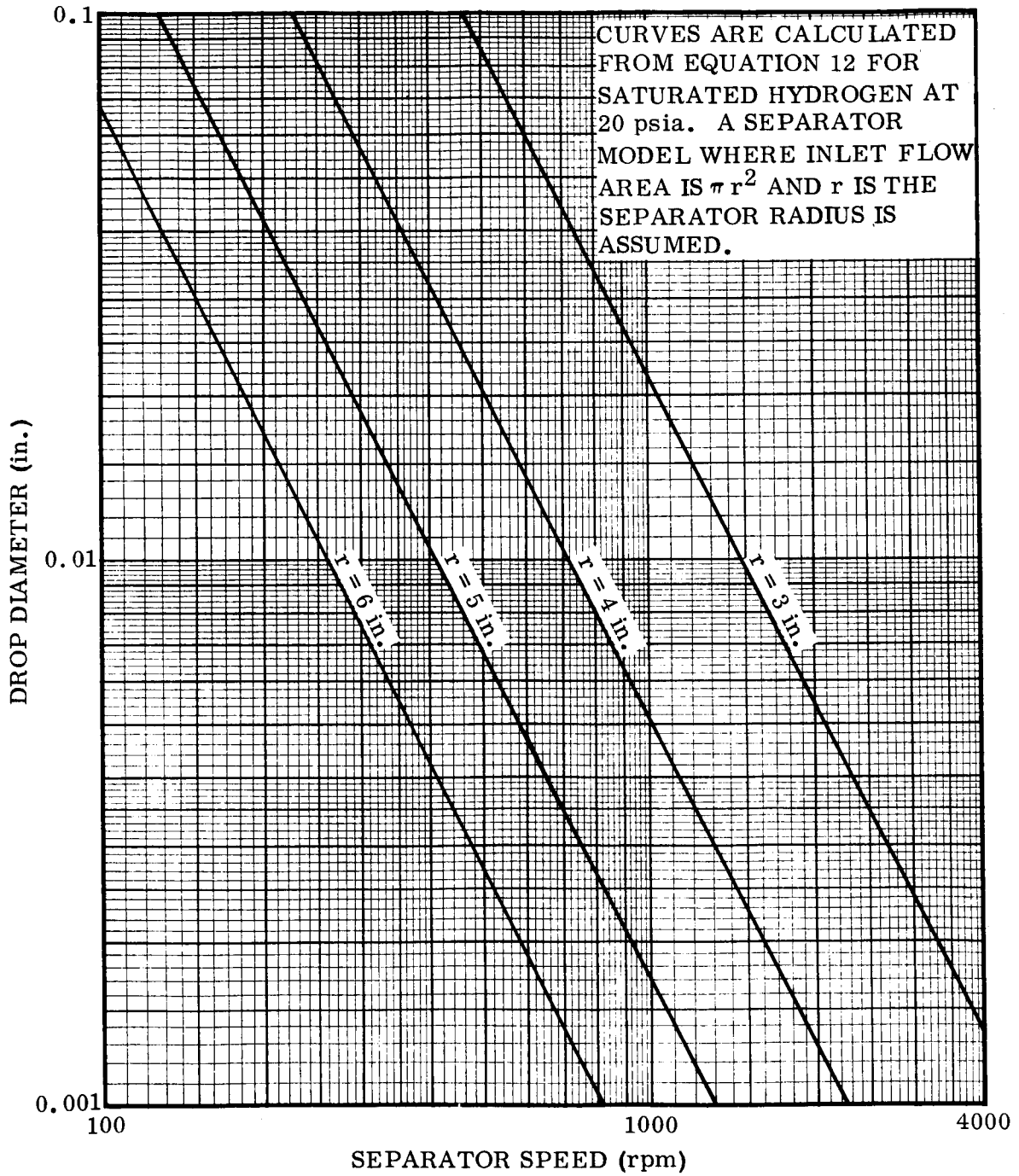


Figure C-3. Required Separator Speed Versus Separated-Drop Diameter for Various Wheel Radii

INLET AREA = $\pi D^2/4$
 VELOCITY = $\dot{W}/\rho_V A$
 DATA FOR SATURATED
 HYDROGEN AT 20 psia.

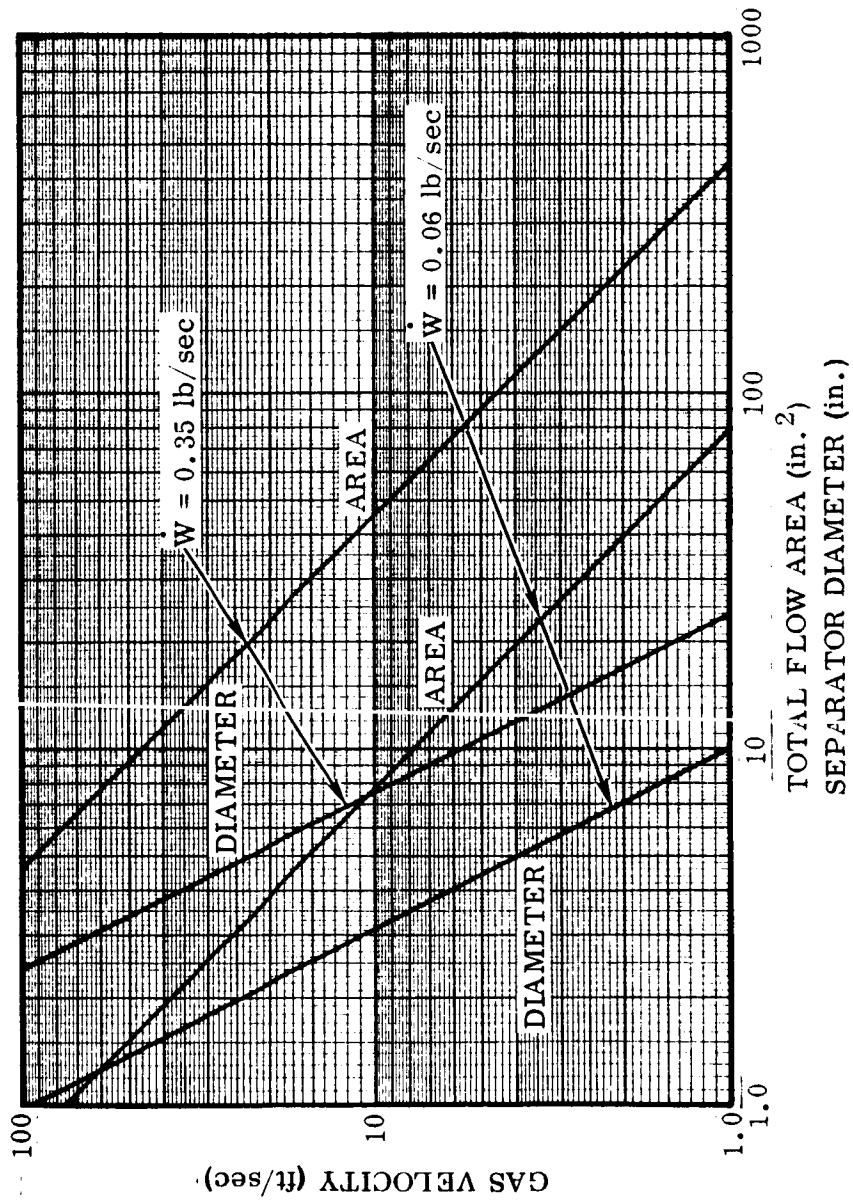


Figure C-4. Inlet Gas Velocity Versus Separator Diameter and Flow Area for Vent Gas Flow Rates of 0.35 lb/sec and 0.06 lb/sec

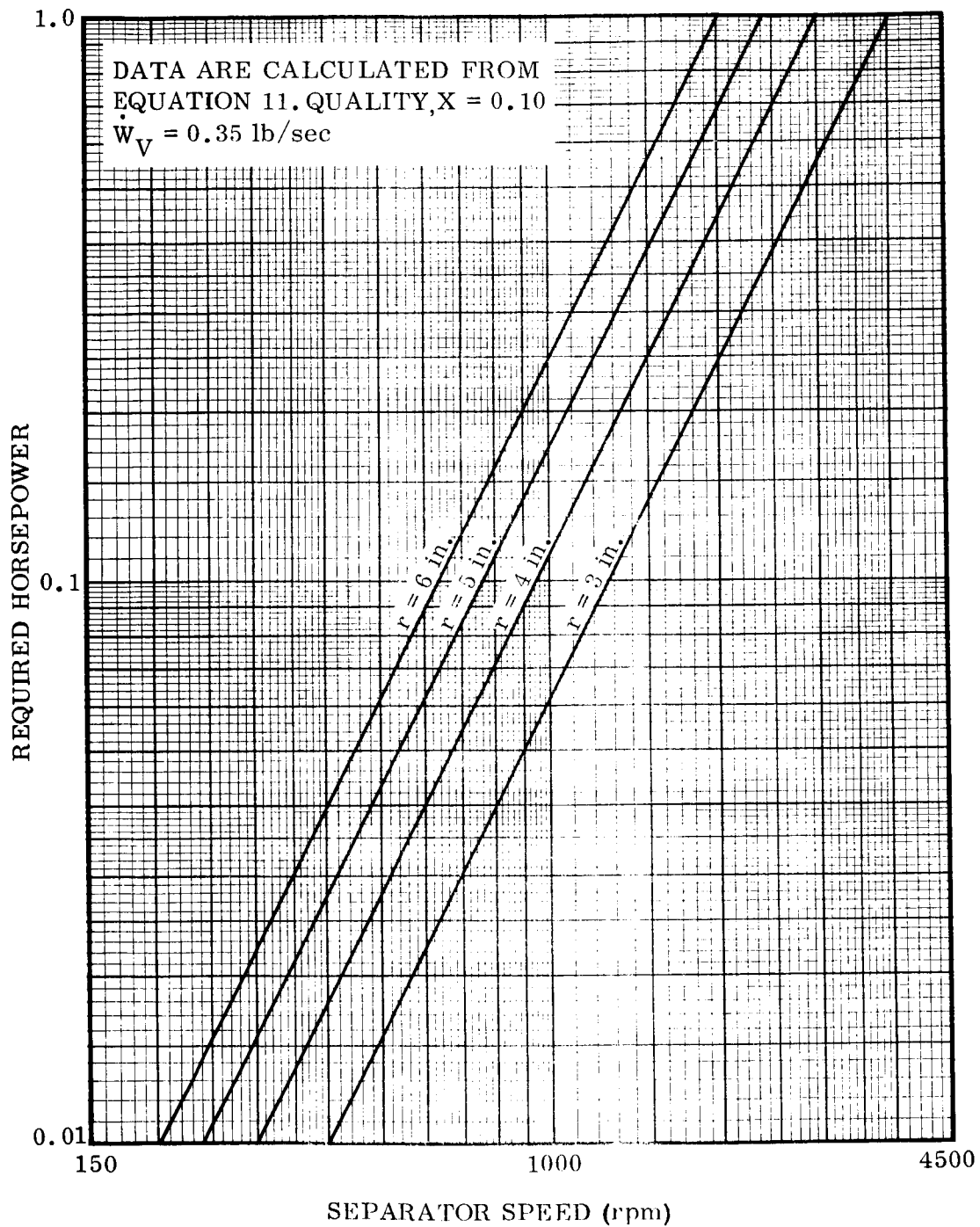


Figure C-5. Required Separator Horsepower Versus Separator Speed for Various Wheel Radii

All Liquid

$$P = 0.29 \frac{(\rho_L)}{(\rho_X)} + 0.1 = 1.48 \text{ hp}$$

$$\text{Torque} = 5.974 \text{ ft-lb}$$

All Gas

$$P = 0.29 \frac{(\rho_V)}{(\rho_X)} + 0.1 = 0.1357 \text{ hp}$$

$$\text{Torque} = 0.548 \text{ ft-lb}$$

Assuming the use of a 3-phase, 4-pole motor (synchronous speed = 12,000 rpm) and an 8:1 gear reduction with gear box efficiency of 95 percent, then

$$\text{Maximum Motor Torque (100-percent LH}_2) = \frac{5.974}{8 \times 0.95} \text{ ft-lb} = 0.785 \text{ ft-lbf}$$

$$\text{Minimum Motor Torque (GH}_2) = \frac{0.548}{8 \times 0.95} = 0.0721 \text{ ft-lbf}$$

$$\text{Design Operating Torque (90-percent liquid)} = \frac{1.574}{8 \times 0.95} = 0.2075 \text{ ft-lbf}$$

Performance curves for a standard type induction motor with 5- to 8-percent slip and meeting the present requirements are shown in Figure C-6. The motor is chosen such that the separator unit will operate at near rated speed (1300 rpm) when completely surrounded with LH₂ in order that the liquid can be effectively pumped away from the unit. The nominal rating of the motor is 0.887 horsepower or 0.4 ft-lbf at a speed of 11,600 rpm. With an 8:1 gear reduction the actual operating speed of the separator will be between 1300 and 1480 rpm.

From Figure C-6 the power input required at the 90-percent liquid point

$$P = \frac{(0.2075)(11,850)}{(5250)(0.825)} = 0.567 \text{ hp or 424 watts}$$

$$\text{Input power operating in liquid} = \frac{(0.785)(10,700)}{(5250)(0.87)} = 1.84 \text{ hp or 1373 watts}$$

$$\text{Input power operating in gas} = \frac{(0.072)(11,950)}{(5250)(0.65)} = 0.252 \text{ hp or 188 watts}$$

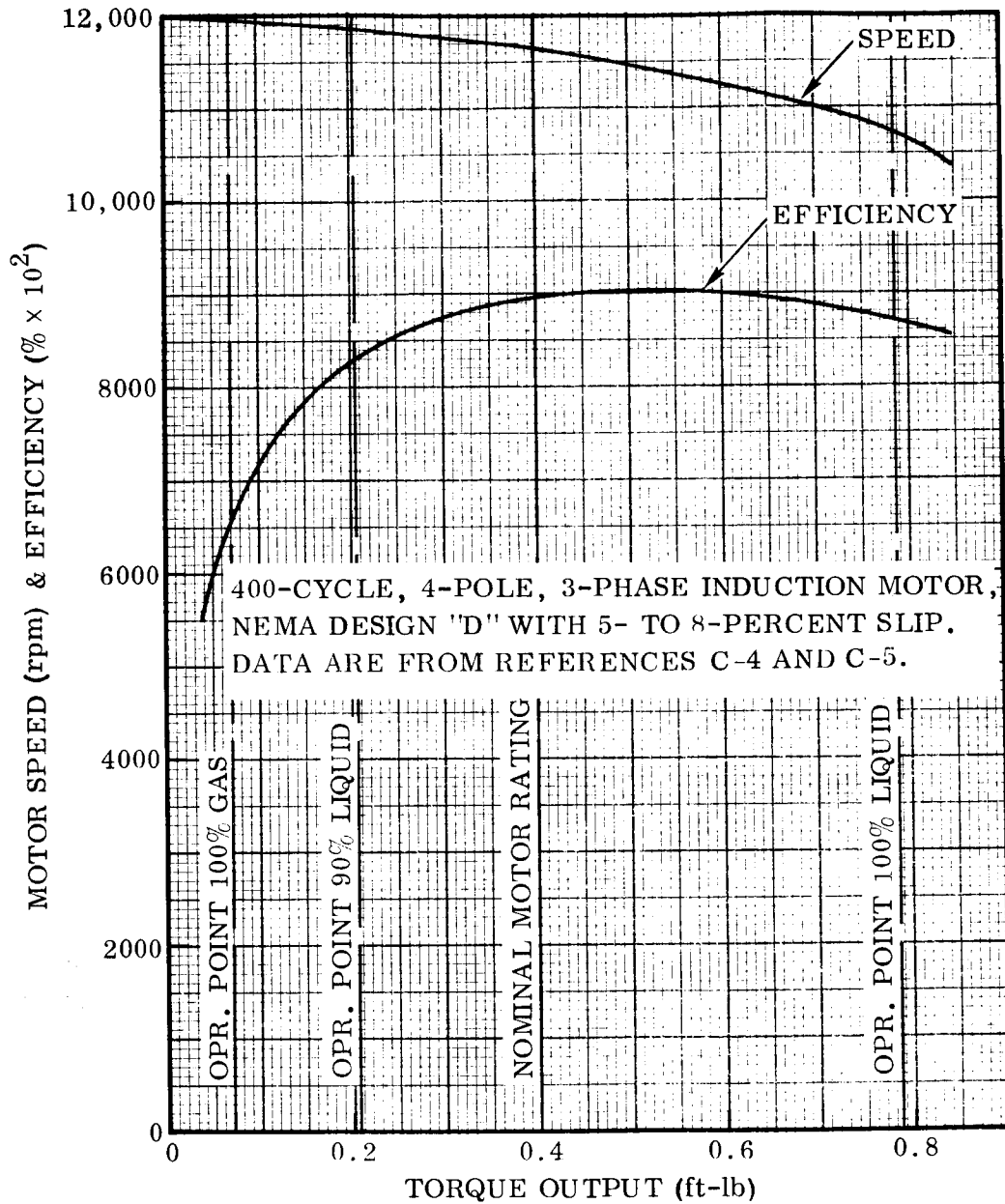


Figure C-6. Motor Operating Characteristics

For nominal operation with 420-watt input the increase in vent rate due to this added energy is

$$\Delta \dot{W} = \frac{P_{\text{input}}}{\Delta h_V} = \frac{(420)(3.42)}{(3600)(189)} = 0.00211 \text{ lb/sec}$$

A rough weight estimate of the unit is made as follows. The analysis is set up so that sizing and weight estimates can be made over a range of flow rates and operating conditions for the predesign model shown in Figure 3-3.

To determine the minimum flow passage diameter through the unit it is assumed that the maximum pressure drop through the unit is 1 psi.

Letting

$$\Delta p = \xi_T \frac{\rho_V (u_V)^2}{2g_0} = 1 \text{ psi}$$

and assuming two mitre-type 90-degree bends with $\xi = 1.2$ and an entrance with $\xi = 0.5$ and exit with $\xi = 1.0$ then $\xi_T \cong 4$ and

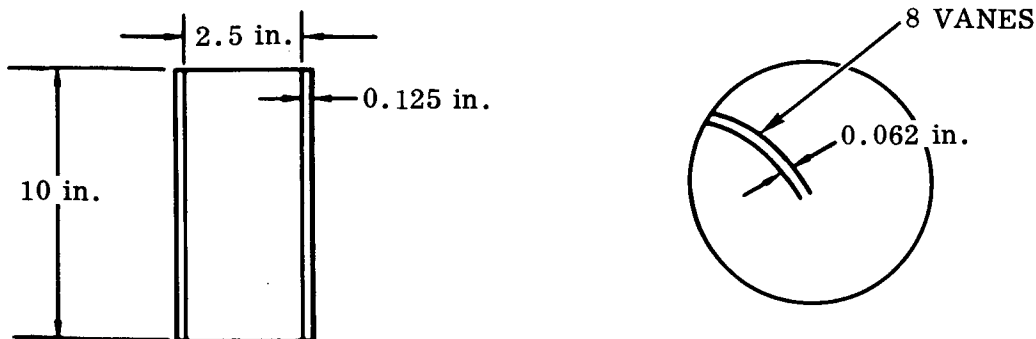
$$u_V = \sqrt{\frac{(1)(2)(32.2)(144)}{(4)(0.112)}} = 144 \text{ fps}$$

From the relation

$$\dot{W}_V = \rho_V A u_V$$

and for $\dot{W}_V = 0.35 \text{ lb/sec}$, $A = 3.12 \text{ in.}^2$ or a shaft diameter of 2 inches.

C.3.1 Weight of Separator Wheel



ALLUMINUM ALLOY
 $\rho = 0.1 \text{ lb/in.}^3$

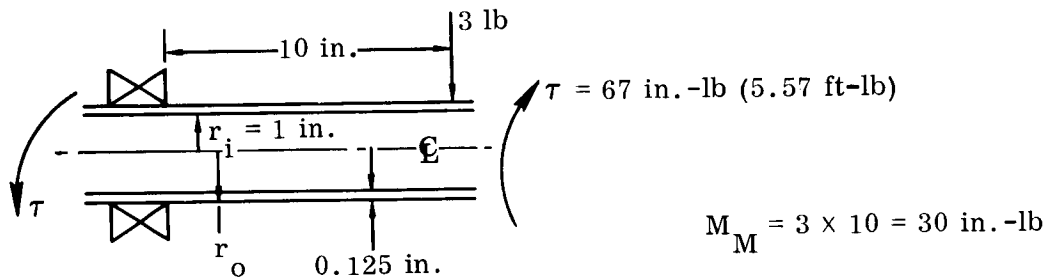
Basic weight = 2.58 lb

C.3.2 Weight of Connecting Shaft (Aluminum Alloy). Assuming the shaft to be 10-in. long with wall thickness of 0.125 inch

Basic weight = 0.785 lb

The following equation is used to check for torsional strength (Reference C-6).

$$(S_s)_{\max} = \frac{r_o}{\frac{\pi}{2}(r_o^4 - r_i^4)} \sqrt{(2M_M)^2 + (1.5\tau)^2}$$



$$S_{s \max} = 139 \text{ psi}$$

From this it is seen that the shaft design is conservative as to torsional strength.

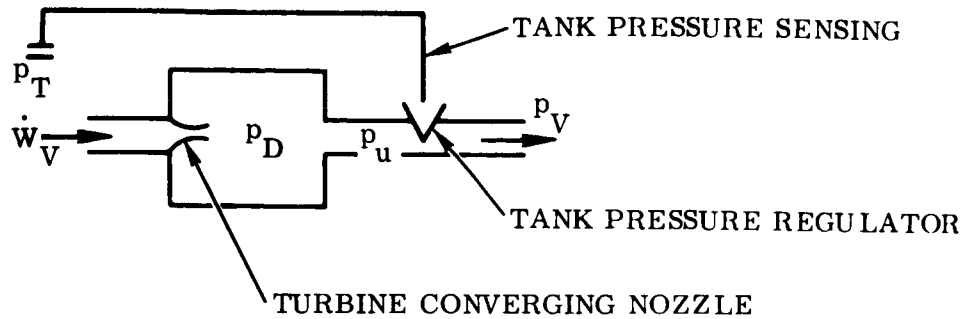
C.3.3 Weight of Drive Housing. The housing is sized to accommodate the motor and drive mechanism. The motor dimensions including gear box are estimated at 3-1/4-inch diameter by 5-inch length (Reference C-7). The drawing of Figure 3-3 is approximately one-fifth scale for the S-IVB application.

Housing weight = 5.10 lb

The total weight of the system excluding valving and electrical power supply is estimated to be 150 percent of the basic weights of separator, drive shaft, and housing to account for bearings, seals, etc. This agrees with data on units previously fabricated. Then the total weight = $(5.1 + 0.8 + 2.6) 1.5 = 12.8$ pounds. The motor and gear box weight is estimated from Reference C-7 to be 10 pounds.

As an alternate to the electric drive discussed above the use of a turbine operating on vent fluid is considered in the following paragraph.

C.3.4 Analysis of the Turbine Drive. It is assumed that the separation portion is the same as discussed in connection with the electric motor-driven unit. The power consumed by the separator is shown plotted in Figure C-7 as a function of speed for operation in all liquid and all gas as well as the 90 percent design point. Turbine output is also plotted showing operation of the system with vent flows of 0.35 lb/sec and 0.06 lb/sec. The basic flow schematic is shown in the sketch.



It is assumed that the regulator is sized for a maximum (wide open) flow rate of 0.35 lb/sec of gas and that actual flow through the regulator will vary from 0.35 down to 0.06 lb/sec. The following major assumptions are made.

- a. Single stage impulse type turbine.
- b. Efficiency of 50 percent at $u_b/u_o = 0.50$. Efficiency is plotted as a function of u_b/u_o in Figure C-8.
- c. Saturated hydrogen gas initially at 20 psia enters the turbine nozzle.

$$\text{Theoretical power} = (\Delta h_s) \dot{W}_V$$

Assuming Δp across the turbine of 2.5 psi ($\Delta h_s = 5$ Btu/lb) and

$$u_o = \sqrt{2g_o \Delta h_s} = 500 \text{ fps}$$

The theoretical power is 2.5 horsepower at a flow rate of 0.35 lb/sec. Assuming a 10-inch-diameter turbine rotating at 1300 rpm, then $u_b = \omega r = 56.6$ fps and $u_b/u_o = 0.1133$. Then from Figure C-8 the turbine efficiency is 20 percent and the available horsepower = $0.2 \times 2.5 = 0.5$ horsepower.

Similarly at

2000 rpm	$u_b/u_o = 0.1745$	Eff. = 29%	P = 0.725 hp
3000 rpm	$u_b/u_o = 0.262$	Eff. = 38.7%	P = 0.967 hp
1000 rpm	$u_b/u_o = 0.0872$	Eff. = 16%	P = 0.4 hp

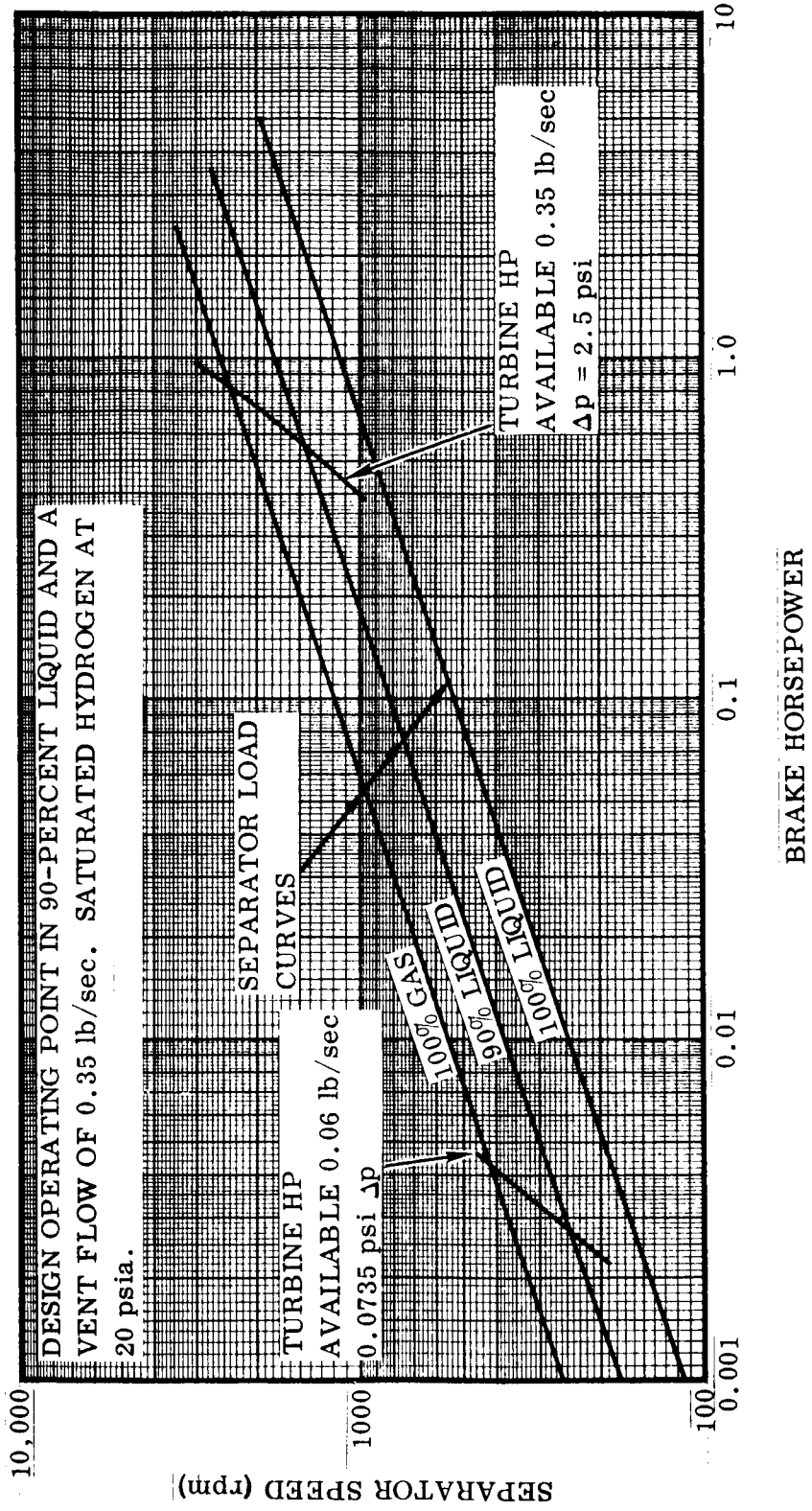
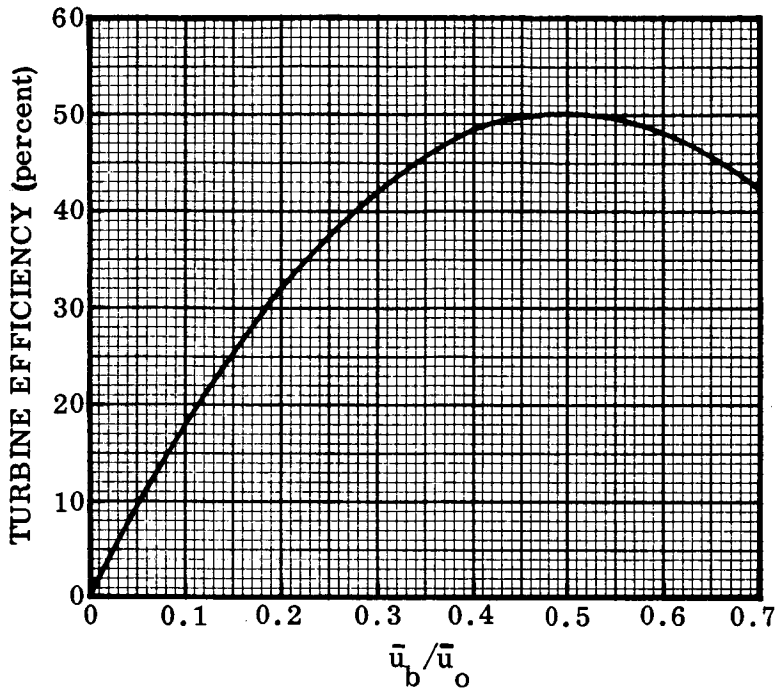


Figure C-7. Turbine-Driven Separator Performance Curves



MAXIMUM EFFICIENCY OF 50 PERCENT. THE SHAPE OF THE CURVE SHOWN IS TYPICAL OF A SINGLE-STAGE, FULL-ADMISSION-IMPULSE TURBINE (REFERENCE C-8).

Figure C-8. Turbine Performance Curve

These data are plotted in Figure C-7 showing an operating point in 90-percent liquid of 1480 rpm and 0.56 horsepower. Assuming the flow through the turbine nozzle is incompressible and governed by the following equation

$$\dot{W} = C_V A \sqrt{2g_o \rho \Delta P}$$

the turbine Δp at a flow rate of 0.06 lb/sec is

$$(\Delta p)_{0.06} = \left(\frac{0.06}{0.35}\right)^2 (2.5 \text{ psi}) = 0.0735 \text{ psi}$$

for a fixed area nozzle.

Since $\dot{W} = \rho A (u_o)$

$$(u_o)_{0.06} = \left(\frac{0.06}{0.35}\right)(u_o)_{0.35} \quad \text{and} \quad u_o = \sqrt{2g_o \Delta h_s}$$

then

$$(\Delta h_s)_{0.06} = \left(\frac{0.06}{0.35}\right)^2$$

and the theoretical power = $\Delta h_s \dot{W}_V$

or

$$(P)_{0.06} = \left(\frac{0.06}{0.35}\right)^3 P_{0.35} = 0.1715^3 (2.5) = 0.0126 \text{ hp}$$

and

$$(u_o)_{0.06} = 0.1715 \times 500 = 85.6 \text{ fps}$$

Then at

200 rpm	$u_b/u_o = 0.1019$	Eff. = 18.5%	P = 0.00233 hp
300 rpm	$u_b/u_o = 0.1528$	Eff. = 26%	P = 0.00327 hp
400 rpm	$u_b/u_o = 0.204$	Eff. = 32.6%	P = 0.0041 hp

These data are plotted in Figure C-7 showing a nominal operating speed of 250 rpm at 0.0028 horsepower for a vent flow of 0.06 lb/sec.

Referring to Equation 12 for the separator in question it is seen that the theoretical separation speed is proportional to \dot{W}_V or that for the flow rate of 0.06 lb/sec the required minimum separation speed is $\frac{(0.06)}{(0.35)} 1300 = 223 \text{ rpm}$.

The power transferred back to the tank fluid varies from 0.56 to 0.0028 horsepower as the flow varies from 0.35 to 0.06 lb/sec. This corresponds to a Δ vent flow rate of

$$(\Delta \dot{W})_{0.35} = \frac{0.56 \times 2545}{3600 \times 189} = 0.0021 \text{ lb/sec}$$

$$(\Delta \dot{W})_{0.06} = \frac{0.0028 \times 2545}{3600 \times 189} = 0.0000105 \text{ lb/sec}$$

The main disadvantage of the turbine-driven separator is that liquid is lost during start-up of the unit when submerged in liquid, and liquid operation of the turbine at reduced speeds might result in a fairly long time for the separator to clear itself of liquid. The efficiency of such units when surrounded with LH_2 is not well defined; however, from the testing that has been done it appears to be quite low.

C.4 CRYOGENIC SERVICE MODULE PREDESIGN CALCULATIONS

C.4.1 CSM Hydrogen Tank. These calculations are based on the following assumptions.

- a. Single tank containing 2500 pounds of hydrogen.
- b. Initial ullage of 5 percent.

- c. Maximum vent rate of 1 lb/hr.
- d. Minimum vent rate of 0.25 lb/hr.

From the relationship $v_X = v_L + X v_{fg}$ an equation relating quality to the volume fraction of gas $(VF)_V$ is derived as

$$X = \frac{1}{1 + \frac{\rho_L [1 - (VF)_V]}{\rho_V (VF)_V}} \quad (14)$$

and for 5-percent gas by volume

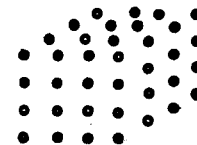
$$X = \frac{1}{1 + \frac{4.34 (0.95)}{0.114 (0.05)}} = 0.00138$$

For the large amounts of liquid present it is necessary to determine the effect of liquid entrainment or blockage on the separator design, and the following analysis is made.

From $v_X = v_L + X v_{fg}$ the volume fraction of liquid $(VF)_L$ is related to the quality by

$$(VF)_L = \frac{1}{1 + \frac{\rho_L X}{\rho_V (1 - X)}} \quad (15)$$

Further, assuming a uniform spacial distribution of liquid and gas as in the sketch, the area fraction of liquid $(AF)_L$ is shown to be approximately



$$(AF)_L = (VF)_L^{2/3} \quad (16)$$

For the 5-percent ullage case

$$(AF)_L = (0.95)^{2/3} = 0.9664$$

or

$$(AF)_V = 0.0336$$

Assuming the same separation model as for the S-IVB vehicle ($A = \frac{\pi D^2}{4}$), and maximum vent rate of 1 lb/hr the inlet velocity for a 2-inch-diameter wheel is

$$u_V = \frac{\dot{W}_V}{\rho_V A (AF)_V} = 3.395 \text{ fps}$$

and from Equation 8, the required separator speed $\omega = 1710$ rpm.

From Equation 11, assuming 50-percent separation efficiency the separation power required is 1.28×10^{-3} hp.

Assuming a 3-inch-diameter separator

$$\omega = 620 \text{ rpm}$$

$$P = 3.79 \times 10^{-4} \text{ hp}$$

Assuming a 4-inch disk

$$P = 1.6 \times 10^{-4} \text{ hp}$$

$$\omega = 302 \text{ rpm}$$

It is desirable in the present case to operate at fairly low speeds to promote efficient mixing of the propellant without large kinetic energy losses between the mixer impeller and the tank fluid. Therefore, the 4-inch-diameter separator is chosen for the present predesign.

In the absence of gravity it is assumed that a Weber number (ratio of inertia to surface-tension forces) of 100 is sufficient to maintain tank fluid circulation.

$$We = \frac{\rho L u^2}{\sigma}$$

where the characteristic length, L , is taken as the tank diameter. Then for $We = 100$,

$$u_{\text{avg}} = 0.107 \text{ fps}$$

The energy required to accelerate the total fluid (2500 pounds) to 0.1 fps

$$e = \frac{m u^2}{2 g_0} = 0.00057 \text{ Btu.}$$

Assuming the acceleration of the fluid to occur in 1 minute at 10-percent efficiency, the required mixing power = 1.34×10^{-4} hp.

In order to estimate power loss due to flow friction, assume velocity of 0.1 fps. With viscous flow, and flow diameter = 25 inches (1/4 of tank diameter), and length = 156 inches, then from Reference C-1 the head loss is

$$\frac{32 \mu (\text{length}) u}{\rho D^2} = \frac{32 (0.85 \times 10^{-5}) 156 (0.1) 12}{4.34 (25)^2 32.2} = 5.82 \times 10^{-7} \text{ ft}$$

Since

$$\dot{W} = \rho A u = \frac{\rho \pi D^2 u}{4} = \frac{4.34 \pi (25)^2 (0.1)}{4 (144)} = 1.48 \text{ lb/sec}$$

the power loss,

$$P = \frac{(5.82 \times 10^{-7}) (1.48)}{(550)} = \text{very small}$$

The efficiency of the flow at the pump in producing the desired average velocities would be the main consideration, and a mixing power of 1.34×10^{-4} horsepower would appear to be sufficiently conservative. Then, assuming the use of the 4-inch separator, the total power required = $1.34 \times 10^{-4} + 1.6 \times 10^{-4} = 2.94 \times 10^{-4}$ horsepower. Allowing 2.94×10^{-4} horsepower for bearings and seals (50-percent efficiency) the total output of the motor is 5.88×10^{-4} horsepower. For motor efficiency of 20 percent, the input to motor, $P = 2.940 \times 10^{-3}$ horsepower and the additional boiloff rate =

$$\frac{(2.94 \times 10^{-3})(2545)}{189} = 0.0396 \text{ lb/hr.}$$

C.4.2 CSM Oxygen Tank. The design is based on a single tank containing 12,500 pounds of LO_2 with a maximum heating rate of 90 Btu/hr and a minimum of one-fourth this value. The same basic analysis is made as for the hydrogen tank. The unit is sized to operate with a minimum ullage of 5 percent and a continuous vent of 1 lb/hr. Performance and configuration data are determined as follows. Assuming the tank contents to be completely mixed, for 5-percent ullage, from Equation 14,

$$\text{Quality } X_{\text{avg}} = \frac{1}{1 + \frac{70.8 \times 0.95}{0.378 \times 0.05}} = 0.0002805$$

Assuming a 2-inch-diameter separator the gas velocity into the separator, u_V , is 1.003 fps.

The pumping requirement, \dot{W}_L , is $\frac{1}{0.0002805} = 3560 \text{ lb/hr.}$

The required speed for separation, ω , is 24.05 rad/sec, or 230 rpm.

For separation,

$$P = \frac{(24.05)^2 (1) (3560)}{(32.2) (3600) (144) (550)} = 2.24 \times 10^{-4} \text{ hp}$$

For $We = 100$, the average required fluid velocity, u_{avg} , is 0.0724 fps where L is taken as the tank diameter. The energy required to accelerate the total mass of oxygen to this velocity is

$$\frac{m u^2}{2 g_o} = \frac{12,500 (0.0724)^2}{2 (32.2) 778} = 0.00131 \text{ Btu}$$

Assuming a 1-minute acceleration and a 10-percent pump efficiency, the required power for mixing is $\frac{(0.00131)(60)}{0.1(1)2545}$ or 3.09×10^{-4} horsepower. Assuming the power requirements are additive, the total pump/separator power required is $3.09 \times 10^{-4} + 2.24 \times 10^{-4}$ or 5.33×10^{-4} horsepower.

Assuming a 50-percent efficiency to account for bearings, seals, etc gives a motor output requirement of 1.066×10^{-3} horsepower. Assuming a motor efficiency of 20-percent, the motor power input is 5.330×10^{-3} horsepower. This corresponds to a nominal increase in vent rate of

$$\Delta \dot{W}_{\text{vent}} = \frac{(0.00533)(2545)}{(90)} = 0.151 \text{ lb/hr}$$

APPENDIX D

CALCULATION OF FRICTIONAL PRESSURE DROP FOR TWO-PHASE FLOW

The method described in References D-1 and D-2 was used to determine frictional pressure drops when the flowing fluid was a two-phase mixture of liquid and vapor. The method correlates two-phase pressure drop data with the pressure drop calculated from the conventional Fanning equation assuming only one of the fluids is flowing through the passage. The original test data were obtained with isothermal flow of constant mixtures of air and various liquids (Reference D-1). Data are presented for two flow conditions: a) liquid-turbulent, gas-turbulent and b) liquid-viscous, gas-turbulent. In the present study both liquid and vapor were assumed to be turbulent, and pressure drops were low enough that compressibility of the gas could be neglected. The method has been extended to conditions where heat transfer is occurring and the fluid quality changes along the flow path (Reference D-2). In this case, the average of inlet and outlet fluid qualities is used for the overall pressure drop calculation.

Some testing has been performed with hydrogen, and fairly good correlation with the Martinelli method was found (Reference D-3).

The equations used in the present study are listed below.

$$\Delta p_{\text{TPF}} = \Delta p_{\text{V}} (\Phi_{\text{Vtt}})^2 \quad (1)$$

$$\Delta p_{\text{TPF}} = \Delta p_{\text{L}} (\Phi_{\text{Ltt}})^2 \quad (2)$$

$$\chi_{\text{tt}} = \left(\frac{\rho_{\text{V}}}{\rho_{\text{L}}} \right)^{0.571} \left(\frac{\mu_{\text{L}}}{\mu_{\text{V}}} \right)^{0.143} \left(\frac{1}{X} - 1 \right) \quad (3)$$

where quality, $X = \frac{\dot{W}_{\text{V}}}{\dot{W}_{\text{V}} + \dot{W}_{\text{L}}}$ and average values of flow rates are used.

Δp_{V} = single component frictional pressure drop calculated by conventional means, assuming only the vapor fraction is flowing.

Δp_{L} = single component frictional pressure drop calculated by conventional means assuming only the liquid fraction is flowing.

χ_{tt} = two-phase flow modulus, defined by Equation 3, for mechanism in which flow of both liquid and gas is turbulent.

Φ_{Vtt} = function of χ_{tt} , obtained experimentally, correlating the two-phase frictional pressure drop to Δp_V . Values are plotted in Figure D-1.

Φ_{Ltt} = function of χ_{tt} , obtained experimentally, correlating the two-phase frictional pressure drop to Δp_L . Values are plotted in Figure D-1.

Δp_{TPF} = frictional pressure drop for two-phase flow.

Either Equation 1 or 2 can be used to calculate the two-phase frictional pressure drop. It was found to be convenient and most accurate to use Equation 1 when $\sqrt{\chi_{tt}}$ is less than one and Equation 2 when $\sqrt{\chi_{tt}}$ is greater than one.